Evaluation, Prediction, and Monitoring of Methane Emission from Oil and Gas Development

By

Yunpo Li

MS, Civil and Environmental Engineering, Stanford University, 2018
B.S.E., Environmental Science and Engineering, Shanghai Jiao Tong University, 2015

Submitted to the Department of Civil and Environmental Engineering in partial fulfillment of the requirements for the degree(s) of
Doctor of Philosophy
in
Civil and Environmental Engineering
at the

Massachusetts Institute of Technology

February 2024

Authored by: Yunpo Li
Department of Civil and Environmental Engineering
November 20, 2023

Certified by: Desirée L. Plata
Department of Civil and Environmental Engineering
Thesis supervisor

Accepted by: Heidi Nepf
Donald and Martha Harleman Professor of Civil and Environmental Engineering
Chair, Graduate Program Committee

Evaluation, Prediction, and Monitoring of Methane Emission from Oil and Gas Development

By

Yunpo Li

Submitted to the Department of Civil and Environmental Engineering on November 20, 2023 in partial fulfillment of the requirements for the degree(s) of
Doctor of Philosophy
in
Civil and Environmental Engineering

ABSTRACT

Human beings are experiencing man-made climate change due to the emission of greenhouse gases, among which methane is a highly potent one, with a 20-year global warming potential 80 times higher than that of carbon dioxide. A systematic approach is needed to evaluate, monitor, and mitigate methane emissions such as those from the oil and gas (O&G) industry (22% of total anthropogenic emissions). In this thesis, I addressed three critical challenges to control such emissions, namely, (i) the uncertainty in a potential O&G methane emission pathway via the groundwater system, (ii) the large population of potential leaking infrastructural elements making routine inspection inefficient and expensive, and (iii) the intermittent emissions that cannot be captured via periodic surveys. To address (i), groundwater samples were collected from more than 300 sites in O&G-producing Northern Appalachia. Dissolved methane concentration was negatively correlated with the distance to O&G well in one of our study regions, but such correlation was confounded by topographic variation. Furthermore, dissolved sulfate concentration was negatively correlated with methane concentration and with distance to coal mine, and these correlations were robust even when considering topographic confounding. In conclusion, groundwater methane could be attributed to natural geological sources and sulfate-mediated biogeochemical processes, rather than O&G development. To investigate (ii), Machine Learning (ML) models were used to predict O&G well integrity issues related to methane leakage to guide prioritized sensor allocation. Different ML models (e.g., Random Forrest, XGBoost, and Logistic Regression) were compared on a dataset consisting of 1,250 O&G wells, and a test F-1 score above 65% was achieved. Furthermore, the most important physical parameters for the prediction were identified, and the geospatial clustering of integrity issues was observed and analyzed. These findings could enable prioritized sensor allocation near O&G facilities with high emission risk and inform better design of future O&G wells. To study (iii), inexpensive continuous methane sensors are needed, but such sensors can suffer from signal interferences. Given such, an ML signal deconvolution strategy was proposed and an experimental apparatus, consisting of mass flow controllers, a gas chamber, and a data logging system, had been built to collect data for ML model training and testing. In addition, preliminary tests were conducted to study the influence of humidity and gas flow rate on the performance of the sensors. Lastly, the apparatus is being upgraded to integrate commercially available methane

sensors and temperature control system. Overall, the research of this thesis deepens our understanding of O&G methane emissions and enhances our capability to monitor and mitigate those contributions.

Thesis supervisor: Desirée L. Plata
Title: Associate Professor of Civil and Environmental Engineering

Acknowledgments

First, I want to thank the funding sources which supported my thesis work: the U.S. Environmental Protection Agency (EPA) supported the groundwater methane study (Chapter 2 & 3), the MIT Undergraduate Research Opportunities Program (UROP) and the MIT Energy Initiative (MITEI) supported many undergraduate students participating in the well integrity prediction study (Chapter 4), and the Advanced Research Projects Agency-Energy (ARPA-E) of the U.S. Department of Energy supported the methane sensor signal deconvolution study (Chapter 5). In addition, I appreciate the Louis Berger Fellowship and the CEE Cross-Disciplinary Seed Funds for their financial support of me.

During my PhD journey, I have received help and encouragement from many people. I want to first thank my student collaborators. For the groundwater methane study, Helen Siegel and Mario Soriano Jr. from Yale University gave me enormous help. Helen helped me with constructing the spatial metrics of oil and gas drilling and coal mining, and Mario helped me with topographical analysis and groundwater hydrology. I also want to thank Prof. James Saiers and Prof. Nicole Deziel at Yale for their guidance and support, as well as their group members for the field sampling efforts. For the methane sensor signal deconvolution study, I want to thank Haosheng Feng and Shao-Xiong Lennon Luo from the MIT Department of Chemistry for their work on the fabrication of chemiresistive methane sensors, and Ruifeng Song from Northeastern University for his help in setting up the electronics and temperature control system. Lastly, I want to thank the undergraduate researchers who participated in the groundwater methane study and the well integrity prediction study. They not only contributed to the scientific findings but also gave me the opportunity to learn to become a good mentor.

Next, I want to thank my fellow lab mates in the Plata group. They have provided so many great suggestions and feedback on my thesis work. For example, for well integrity prediction, Joules Provenzano inspired me to include data leakage prevention measures, and Glen Andrew de Vera inspired me to find better ways to organize the well casing information. There are many other scientific and technical questions that I couldn't realize by myself, but I was lucky enough because my lab mates would point them out and make suggestions on the solutions. Moreover, I am very grateful for their help and support in the experiments. Especially, Eric Johnson taught me how to use different instruments and helped me solve all sorts of technical issues, and Glen served as a wonderful lab manager to keep the lab clean and functioning well.

In addition, I want to express my appreciation to my wonderful thesis committee members for their feedback had pushed my work toward the right direction. Prof. Saurabh Amin provided me with valuable suggestions on choosing the most appropriate geospatial features for my Machine Learning models. Prof. Steven Wofsy taught me important statistical methods for environmental research, which were essential to most of the work described in this thesis. He also encouraged me to tackle the methane emission problem for my PhD study. Prof. Jesse Kroll taught me the fundamentals of atmospheric chemistry, which were indispensable for my understanding of the methane problem. He also discussed other research ideas with me, such as ambient methane removal, and I look forward to working on them in the future.

Most importantly, I feel a deep sense of gratitude to Prof. Desirée Plata, my PhD advisor. She is always caring, positive, and communicative. At the beginning of my PhD program, I was working on a project not related to methane. One day, I realized that anthropogenic methane emissions could have a significant global impact and was the type of problem I wanted to solve. Desirée was super supportive and encouraged me to shift my research focus, and this was the beginning of all the work that led to this thesis. Moreover, Desirée showed a great amount of love and care during the COVID-19 pandemic when she provided her office as a lunch space for the group and shipped snacks to everyone. Desirée always showed a positive attitude toward work and life, which greatly inspired me. She never said no to any research ideas but encouraged me to identify the important questions and make positive changes. Lastly, Desirée taught me how to communicate science to different audiences. She always emphasized the importance of making scientific results understandable to the general public, and it influenced me profoundly. With all the help from Desirée and the other people I mentioned, I was able to complete my Ph.D. study and write this thesis to address the oil and gas methane emission problem, which has significant implications in our fight against climate change.

Table of Contents

Chapter 1: Introduction and thesis overview *16*

ABSTRACT **17**

Climate and public health impact of oil and gas methane emission **17**

Research challenges **20**

Overview of challenges 20

Knowledge gap in methane emission via groundwater pathway 23

Difficulties in monitoring methane leaks from O&G facilities 27

Research questions addressed in this thesis **32**

Thesis overview **36**

References **41**

Chapter 2. Groundwater methane in Northeastern Pennsylvania attributable to thermogenic sources and hydrogeomorphologic migration pathways *47*

ABSTRACT **48**

Introduction **49**

Materials and methods **52**

Results and discussion **53**

Groundwater methane levels 53

Geochemical indicators 58

Geochemical fingerprinting of water masses 62

Comparison with predrilling records 69

Estimation of natural methane emission 72

Implications **73**

Acknowledgments **75**

References **76**

Supporting information for Chapter 2 ..... *81*

Geological setting of the study area **81**

Supplemental methods **82**

Sample locations 82

Sample collection 83

Dissolved hydrocarbon measurement 84

Converting headspace measurements to dissolved hydrocarbon concentrations 84

Dissolved ion species measurement and isotopic analysis 91

Spatial metrics and topographical information 92

Predrilling data collection and processing 93

Violation code for well integrity violations that could potentially lead to stray gas migration **94**

Calculating initial concentrations of biogenic methane undergoing microbial oxidation **97**

Dilution calculation and estimated methane solubility of deep Appalachian Basin Brine **98**

Estimation of methane emission from inland waters and O&G wells **99**

Supplemental figures **101**

References **111**

Chapter 3. Conventional fossil fuel extraction, associated biogeochemical processes, and topography influence methane groundwater concentrations in Appalachia ***114***

ABSTRACT **115**

Introduction **116**

Materials and methods **119**
Sample locations 119
Sample collection 120
Dissolved hydrocarbon measurement 120
Isotopic analysis and other dissolved species 121
Geospatial and topographical Information 121

Results and discussion **122**

Implications **138**

Acknowledgments **140**

References **140**

Supporting information for Chapter 3. ..... ***147***

Supplementary tables **147**

Supplementary figures **149**

References **168**

Chapter 4. Prediction of oil and gas well integrity using well construction physical parameters and geospatial metrics ***171***

ABSTRACT **172**

Introduction **173**

Methods **177**
Data collection and processing 177
Training and evaluation of ML models 178
Performance metrics of ML models 179

Results and discussion **180**
Prediction performance of ML models 180
Feature importance analysis 185
Geospatial clustering of well integrity issue 187

Implication **190**

Acknowledgment **193**

References **194**

Supporting information for Chapter 4 ..... ***197***

Supplementary methods **197**
Details of processing casing and cement information 197
Details of data cleaning and processing 198
Details of constructing geospatial metrics to avoid data leakage 199
Topography and geological folds 200

Supplementary tables **200**

Supplementary figures **206**
References **213**
Chapter 5. Methane sensor signal deconvolution - apparatus and preliminary results ***215***
ABSTRACT **216**
Introduction **216**
Material and method **218**
Concept of machine learning for signal deconvolution 218
Sensing material 220
Experimental set-up 220
Preliminary sensor test results **226**
Summary and implication of preliminary results **232**
Ongoing Investigations **233**
Future steps for ML signal deconvolution and expected outcomes **240**
References **242**
Chapter 6. Conclusions, criticisms, and opportunities ***244***
Conclusions **245**
Summary of thesis contributions 246
Criticisms and opportunities 253
Closing remarks and looking forward **256**
References **258**

List of Figures

Page Number

Chapter 1.

Figure 1. Global annual methane emissions from different sources averaged over 2008 to 2017 — 20

Figure 2. Potential methane migration pathways into groundwater aquifer and atmosphere under the influence of HDHF — 24

Chapter 2.

Figure 1. Dissolved methane concentrations in relation to the distances to the nearest UOG well and the nearest well integrity violation — 57

Figure 2. The methane carbon and hydrogen isotopic signatures of dissolved methane — 59

Figure 3. The C_1-to-$C_2 + C_3$ ratio vs. $\delta^{13}C$-CH_4 of high methane concentration samples — 62

Figure 4. Water type and topography of sampling location in relation to measured methane concentration — 64

Figure 5. The distribution of methane concentration among different water types and topographical groups — 65

Figure 6. Comparison between pre-drilling and post-drilling methane concentrations — 71

Figure S1. Yield tests for the measurement accuracy of dissolved concentration of methane, ethane, and propane — 89

Figure S2. The topographical map of the study region — 101

Figure S3. Methane concentration in relation to distance to the nearest HDU well, O&G well, and well violation — 102

Figure S4. Dissolved methane concentrations in relation to the counts of O&G wells and violations within selected radii centered at the water wells — 103

Figure S5. Dissolved methane concentration in relation to the violation status of the nearest UOG well and O&G well — 104

Figure S6. Error bars of dissolved methane concentrations versus distances to the nearest UOG well — 105

Figure S7. Subset of our sampling region that includes the sampling location of Llewellyn et al. in Sugar Run, Bradford County — 106

Figure S8. Sensitivity of inferred initial methane concentrations to different values of ϵ_C and initial $\delta^{13}C - CH_4$ if the detected dissolved methane originated from biogenic methane undergoing microbial oxidation 107

Figure S9. ^{13}C ratio of methane in relation to the distance to the nearest UOG well and dissolved methane concentration 108

Figure S10. Inorganic species of water samples show the fingerprints of Appalachian Basin Brine in our water samples 109

Figure S11. Number of sampled domestic wells falling in each topographical class, divided by household self-reported well-depth 111

Chapter 3.

Figure 1. Groundwater methane concentrations in Region I and Region II as a function of distance to the nearest UOG or O&G well 124

Figure 2. Groundwater dissolved methane and sulfate concentration as a function of the distance to the nearest active underground coal mine in Region II 126

Figure 3. Groundwater dissolved methane concentration increased as a function of topography 128

Figure 4. $\delta^{13}C$ vs. $\delta^{2}H$ and C1-to-C2 + C3 ratio vs. $\delta^{13}C$-CH_4 of groundwater methane collected in Region I and Region II 135

Figure S1. Geographical information of the study regions 150

Figure S2. Error bars of dissolved methane concentration versus distance to the nearest UOG well and distances to the nearest O&G well 151

Figure S3. Distribution of dissolved methane concentrations in each study region 152

Figure S4. Correlation between groundwater dissolved methane concentration and count of UOG wells within certain radii centered at the water sample 153

Figure S5. Correlation between groundwater dissolved methane concentration and count of all O&G wells within certain radii centered at the water sample 154

Figure S6. Methane concentration compared to the age of the nearest O&G well 155

Figure S7. Groundwater dissolved methane concentration in OH water in ration to sulfate concentration, and sulfate concentration in relation to the distance to the nearest abandoned underground coal mine and surface coal mine in OH 155

Figure S8. Groundwater dissolved methane concentration versus water types 158

Figure S9. Cl/Br ratio against Cl concentration for methane concentration and geochemical water source attribution 159

Figure S10. Geochemical water type of groundwater sample in correlation with topographical class of sample location among all water samples 160

Figure S11. Distribution of groundwater methane concentrations among different water types and different topographical locations within Region I and Region II 161

Figure S12. The distance to the nearest O&G well and to the nearest active underground coal mine of Region II samples from different topographical locations 162

Figure S13. The number of O&G wells within 1 km radius and the well age of the nearest O&G well of Region II samples from different topographical locations 164

Figure S14. The correlation between other redox agents and sulfate and methane concentration as well as active underground coal mine and O&G spatial metrics among Region II water samples 166

Figure S15. Comparing $\delta^{13}C - CH_4$ and distance to the nearest O&G well for the outlier data in Fig. 3 and Fig. S8 167

Chapter 4.

Figure 1. CV F-1 scores of different ML models 182

Figure 2. Proportions of test samples predicted as nonfaulty and faulty by the XGB model using all features or all features except the geospatial ones 184

Figure 3. Top 15 important features selected by SHAP values for XGB predictor using all features or all features excluding geospatial ones 187

Figure 4. Spatial clustering of faulty wells characterized by the Local Join Counts statistics 189

Figure S1. Distribution of the percentage of missing values among features 207

Figure S2. workflow of training and testing machine learning models 208

Figure S3. Clusters of high and low values of four important continuous features 209

Figure S4. Clustering of wells whose operators were not C 210

Figure S5. The clustering of faulty wells versus topographical variation 211

Figure S6. The locations of clustered faulty wells and geological folds in the study region 212

Figure S7. The distances to the nearest geological fold among clustered faulty wells, faulty wells, nonfaulty wells, and all wells 213

Chapter 5.

Figure 1. Concept of using advanced machine learning algorithms (e.g., Neural Network) to predict gas concentrations 219

Figure 2. Experimental set-up to collect data for ML signal deconvolution 222

Figure 3. Schematic of the test chamber design 225

Figure 4. Chemiresistive sensors installed inside the gas chamber 226

Figure 5. Change in sensors' resistances responsive to 0.5% methane at 2.5% RH 228

Figure 6. The influence of RH on chemiresistive sensors' responses to 0.5% methane 229

Figure 7. Sensor signals responsive to 0.5% methane at 37% relative humidity 230

Figure 8. The influence of total flow rate in the gas chamber on chemiresistive sensors' responses to 0.5% methane at <0.5% RH 232

Figure 9. The modified gas chamber to accommodate both prototype chemiresistive sensors and commercial sensors 237

Figure 10. Design diagram of gas temperature control system 239

Figure 11. Photo of the gas temperature control system 240

List of tables

Page Number

Chapter 1.

Table 1. Research challenges addressed in this thesis 23

Chapter 2.

Table S1. Fitted parameters for Henry's Law constant calculation 86

Table S2. Salt ion specific parameters 87

Table S3. Hydrocarbon specific parameters 87

Table S4. limit of detection and limit of quantification of hydrocarbons 91

Table S5. violation code related to well integrity issues that could potentially lead to stray gas migration 94

Table S6. Estimation of methane emission from active O&G wells in Bradford County 100

Chapter 3.

Table 1. Regression outputs for the prediction of methane concentration as a function of variables of interest and topography as a confounder 131

Table 2. Regression outputs for the prediction of sulfate concentration as a function of distance to coal mine and another potential confounding variable 131

Table S1. Data sources for geographical information 147

Table S2. Linear regression on the rank of methane concentration and O&G well count metrics in Region II 148

Table S3. Linear regression on the rank of methane concentration and age of the nearest O&G well in Region II 148

Table S4. Linear regressions on the rank of ion concentrations and O&G / coal spatial metrics in Region II 149

Chapter 4.

Table S1. List of feature names, data source, percentage of missing values, and note 200

Chapter 5.

Table 1. Commercial MQ-series sensors 234

List of Acronyms

Phrase	*Acronym*
Casing Vent Flow	CVF
Conventional Oil and Gas	COG
Cross-Validation	CV
Environmental Protection Agency's Greenhouse Gas Inventory	EPA GHGI
Exploration and Development Well Information Network	EDWIN
Flame Ionization Detection	FID
Gas Chromatograph	GC
Global Warming Potential	GWP
Greenhouse Gas	GHG
Horizontal Drilling with Hydraulic Fracturing	HDHF
Inductively Coupled Plasma - Optical Emission Spectrometry	ICP-OES
Inductively Coupled Plasma Mass Spectrometry	ICP-MS
Institutional Review Board	IRB
Ion Chromatography	IC
K-Nearest Neighbor	KNN
Leak Detection and Repair	LDAR
Limit of Detection	LOD
Limit of Quantification	LOQ
Logistic Regression	LR
Logistic Regression with Interaction	LR-IA
Machine Learning	ML
Mass Flow Controller Array for Nanostructure Growth Optimization	MANGO
Mass Flow Controller	MFC
Multi-Scale Topographic Position Index	mTPI
New York Department of Environmental Conservation	NYDEC
Northeastern Pennsylvania	NE PA
Northern West Virginia	N WV
Oil and Gas	O&G
Pennsylvania Department of Environmental Protection	PADEP
Pentypcene	Pentyp
Platinum-Polyoxometalate	Pt-POM
Poly(4-Vinylpyridine)	P4VP
Printed Circuit Board	PCB
Random Forrest	RF
Relative Humidity	RH
SHapley Additive exPlanations	SHAP
Single-Walled Carbon Nanotube	SWCNT

Southeastern Ohio	SE OH
Spirobifluorene	SBF
Support Vector Machine	SVM
Sustained Casing Pressure	SCP
Conference of Parties	COP
Thermal Conductivity Detector	TCD
Unconventional Oil and Gas	UOG
United States	US
XGBoost	XGB

Chapter 1: Introduction and thesis overview

By

Yunpo Li

ABSTRACT

Methane, a greenhouse gas absorbing 80 times more heat than carbon dioxide over 20 years, has short-term climate impact. Therefore, reducing methane would be one of the fastest ways to slow down climate change over the next decades. The oil and gas (O&G) industry is one of the biggest sources of methane emissions and reducing such emissions requires a systematic effort combining evaluation, prediction, and monitoring. This chapter outlines the climate and public health impact of methane emissions and then defines several major research challenges in addressing O&G methane emissions. These include: (1) knowledge gaps in emission pathways via the groundwater system, (2) the intractably large number of potential emitters to monitor, and (3) temporal intermittency of emissions. For (1), the potential climate and safety implications of groundwater methane emission are discussed. In **Chapter 2&3**, I leveraged field sample analyses to evaluate the influences of O&G extraction on groundwater methane. For (2) and (3), I proposed a proactive monitoring strategy to first predict high-risk emitters and then prioritize them for monitoring (**Chapter 4**). In addition, I proposed a machine learning-enabled signal deconvolution approach to improve the accuracy and selectivity of prototype chemiresistive sensors for continuous monitoring (**Chapter 5**). Finally, an overview of each chapter is provided together with a brief summary of the main conclusions and implications of the thesis.

Climate and public health impact of oil and gas methane emission

Human beings are experiencing man-made global warming due to the emission of greenhouse gases (GHGs), among which carbon dioxide is the biggest contributor.[1] Some suggested that the

window to restrain climate change requires full elimination of GHG emission by 2030 to avoid climate disasters.[2] Besides carbon dioxide, methane is a much more potent GHG, whose 20-year and 100-year global warming potential is around 80 times and 30 times higher than that of carbon dioxide.[3] Moreover, methane emissions by human activities (about half of total global methane emissions[4,5]) contributed to about 0.5 °C of global temperature rise comparing between 2010 -2019 and 1850 -1900, where the total temperature rise due to human activities was about 1 °C (considering the cooling effect of aerosols).[1] It has been estimated that up to 45% of man-made methane emissions can potentially be eliminated by 2030, which would avoid 0.3 °C global warming from 2040 to 2070 and serve as a cost-effective solution to meet the 1.5 °C goal of the Paris Agreement together with the reduction of other climate forcer emissions.[4] According to the Global Methane Pledge signed by 122 countries, methane emission reduction should become a prioritized task to slow climate change.[6,7]

In addition to its negative climate impact, methane poses a public health threat as a precursor of tropospheric ozone. Tropospheric ozone can cause damage to the human respiration system, causing issues such as coughing, chest pain, inflammation, and asthma.[8] The ozone production due to anthropogenic methane emission can cause approximately half a million premature deaths globally per year.[4] In addition, the produced ozone can suppress the growth of crops such as wheat, rice, maize, and soybeans thus threatening the global food security.[4] As such, reducing methane emissions could have great benefits in terms of public health and food security: a 45% reduction in global anthropogenic methane emission by 2030 would transfer to 255,000 avoided ozone-induced death, 775,000 avoided asthma related emergency room visits, 73 billion hours avoided work hour lost, and 26 Mt avoided crop lost per year.[4]

Around 128 teragrams (Tg; 1 Tg = 10^{12} g) methane was emitted from fossil fuel production and utilization (sum of Oil & Gas (O&G), Coal Mining, Industry, and Transport; bottom-up estimation; Fig. 1), which accounts for 35% of the 366 Tg / year total anthropogenic methane emissions, and O&G emitted around 80 Tg methane per year (over 60% of fossil fuel emissions) [5] In the US, O&G accounts for 67% of the total energy production and 68% of total energy consumption.[9,10] Since the early 2000s, unconventional oil and gas (UOG) production has been growing rapidly. Horizontal drilling with hydraulic fracturing (HDHF) have enabled 79% of dry natural gas production and 65% of crude oil production in the US.[11,12] Furthermore, the intermittency of solar and wind supplies along with other considerations currently necessitate the use of fossil energy *and this remains the case in the near term - the critical time horizon for climate action*. Thus, failure to reduce methane emissions and impacts associated with O&G production has a direct translation to delayed climate benefits. Fortunately, methane, the main component of natural gas, is a valuable commodity, so cutting methane leakage can recover revenue for O&G firms. Thus, unlike cutting CO_2 emissions, which typically requires time- and resource-consuming transition to clean energy or restricting economic growth, reducing O&G methane emissions are considered "lower hanging fruit" for climate mitigation. It was estimated that about 25% to 50% of O&G methane emissions can be reduced at a net profit.[4] In addition, the GHG benefit per unit carbon captured for methane is larger and the atmosphere responds more quickly than that for CO_2 controls. That is, cutting methane emission is the faster way to slow down the progress of global warming now and in the near future. Finally, because many methane leaks are poorly accounted, there is uncertainty surrounding the magnitude of GHG benefit that should come with a transition to natural gas.

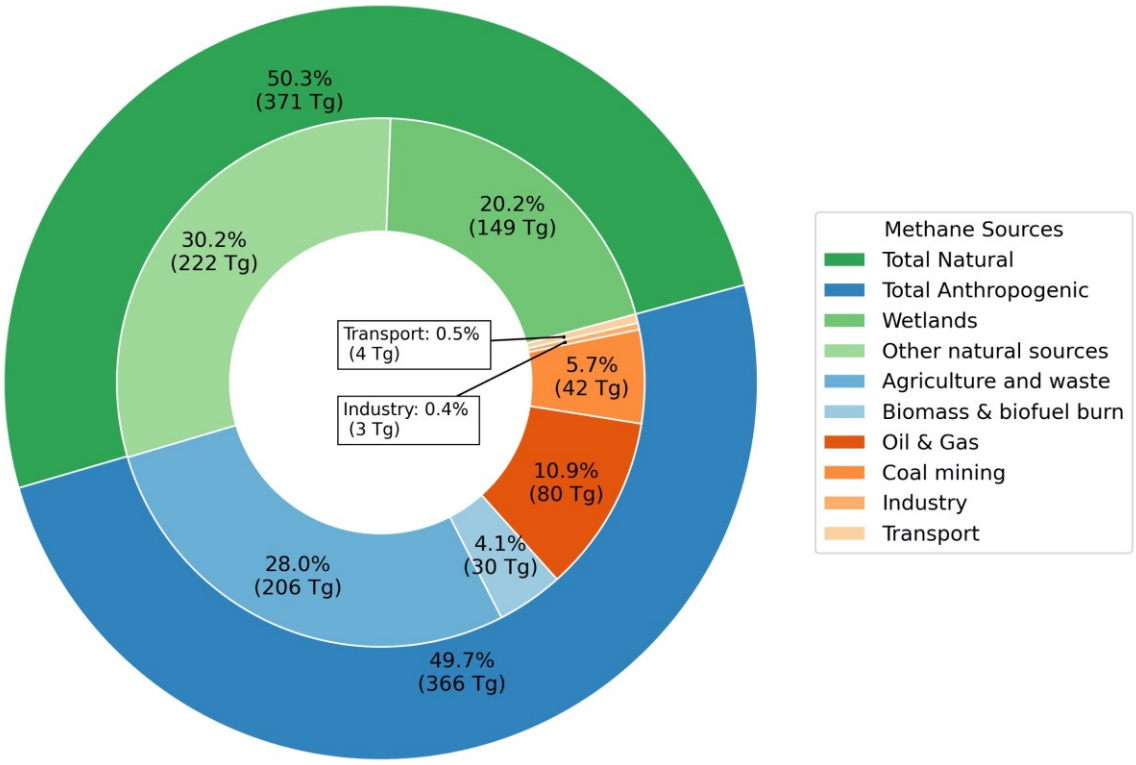

Figure 1. Global annual methane emissions from different sources averaged over 2008 to 2017 (bottom-up estimation).[5] The annual emission rate from each source is represented as percentage of the total emission rate, with their absolute value (Tg CH_4 $year^{-1}$) shown in the bracket.

Research challenges

Overview of challenges

To successfully reduce methane emissions from O&G infrastructures, a systematic approach is needed with three key components: (i) evaluating emission, (ii) monitoring emission, and (iii) mitigating emission. First, various pathways of methane emissions should be thoroughly evaluated as prerequisites for effective monitoring and mitigation. In the O&G industry, components that can leak methane include above-ground ones such as pipelines, compression stations, storage tanks, and well heads, and underground ones such as well casing and cementation. While the above-ground components directly release methane into the atmosphere, underground ones first release methane into environmental media such as groundwater and soil, and then this methane can transport across media and eventually reach the atmosphere. Estimating the scale, as well as spatial and temporal distribution of emission from both above- and underground pathways would serve as necessary preparation for the subsequent emission mitigation efforts. (Also note that at the start of this thesis, home owners living near O&G extraction were concerned about methane in their water exceeding warning level (i.e., 10 mg/L) [13], which I was able to explicitly evaluate). Second, methane emission monitoring aims at identifying the exact location and timing of emission events, and guiding the following fixation and mitigation measures. Methane plumes in the air are invisible to human eyes but can be detected by instruments such as infrared camera, open path laser sensors, and chemiresistive sensors based on catalytic oxidation of methane. In order to monitor methane migration in the underground environment, groundwater or soil samples can be collected so that the dissolved or adsorbed methane in these samples can be quantified by gas chromatography (GC). Third, after methane emission sources and their emission pathways are identified, mitigation measures should be taken to stop the emissions or reduce their rate. Such measures include fixing or replacing the leaky component (e.g., broken natural gas pipelines and faulty valves), improving

operational procedures (e.g., avoiding gas flaring), and methane removal or conversion (e.g., catalytic oxidation of methane to carbon dioxide). The last measure is suitable to mitigate emissions that are difficult to avoid and cannot be addressed by the first two measures, such as diluted methane below limit of flammability (i.e., 4%) released by O&G well pads, coal mines, and enteric fermentation of ruminant animals.

Although great advancements have been made in research and in practice to reduce methane emissions from O&G infrastructures in the past decade, there are still some key challenges in the first two steps of the evaluation-monitoring-mitigation chain, which have delayed the elimination (or minimization) of O&G methane emissions (Table 1). For the "evaluation" step, the understudied emission pathway via groundwater system may introduce uncertainty to our estimation of the total O&G emission rate. Numerous studies have focused on the above-ground methane emission, but few have characterized the potential methane transport from O&G wells to groundwater aquifer, and then to surface water body and eventually the atmosphere. If such a pathway was found to be substantive, then total O&G methane emissions would be underestimated. For the "monitoring" step, the large number of O&G facilities that can become potential methane emitters result in high cost of leak monitoring programs. Moreover, the temporal intermittency of methane leaks can cause underestimation by traditional leak detection programs, such as those conducted by hand-held sensors. Taken together, these challenges in understanding and monitoring methane emissions will ultimately affect our ability and efficiency in mitigating emissions. In the following sections, I will discuss the details of each challenge, and outline the key research questions that were addressed in this thesis.

Table 1. Research challenges addressed in this thesis

Topic	Key Challenges	Solutions	Corresponding Chapter
Evaluate emission	Large uncertainty in the methane emission pathway via groundwater	Analysis of groundwater methane field samples	2 & 3
Monitor emission	Intractably large number of potential methane leaking sources	Prediction of methane emission risk to guide prioritized monitoring	4
Monitor emission	Temporal intermittency of methane emissions	Continuous methane sensors with signal deconvolution (apparatus and preliminary results)	5

Knowledge gap in methane emission via groundwater pathway

1. Uncertainties in groundwater methane emission pathway

HDHF is an unconventional extraction technique that injects high pressure fluid to crack tight shales and release the natural gas and/or oil trapped in their pores. Such industrial processes raise concern that it may cause methane contamination in groundwater aquifer, and that wellbores might provide methane migration pathways (Fig. 2).[14–17] There has not been a consensus in literature regarding whether the HDHF process causes methane migration into groundwater aquifers. If such migration to groundwater is possible, and if this methane is ultimately released

into the air, there would be risk of accelerated climate change. Methane, after entering groundwater aquifer, can eventually reach the atmosphere following the natural hydrological circle: groundwater dissolved methane can be brought into surface water bodies such as lakes and streams by groundwater discharge (Fig. 2),[16,18] and then enter the atmosphere at the air-water interface.[19–22] In addition, groundwater extracted from aquifers for human use also releases dissolved methane to the air.[20,21,23] The first step of such potential groundwater methane emissions pathways would be the O&G induced intrusion of methane into the groundwater aquifers, which would alter the concentration and isotopic signatures of the groundwater-dissolved methane. Therefore, assessing how these properties of dissolved methane were or are influenced by O&G development is an important first step to evaluate the entire groundwater methane emission pathway.

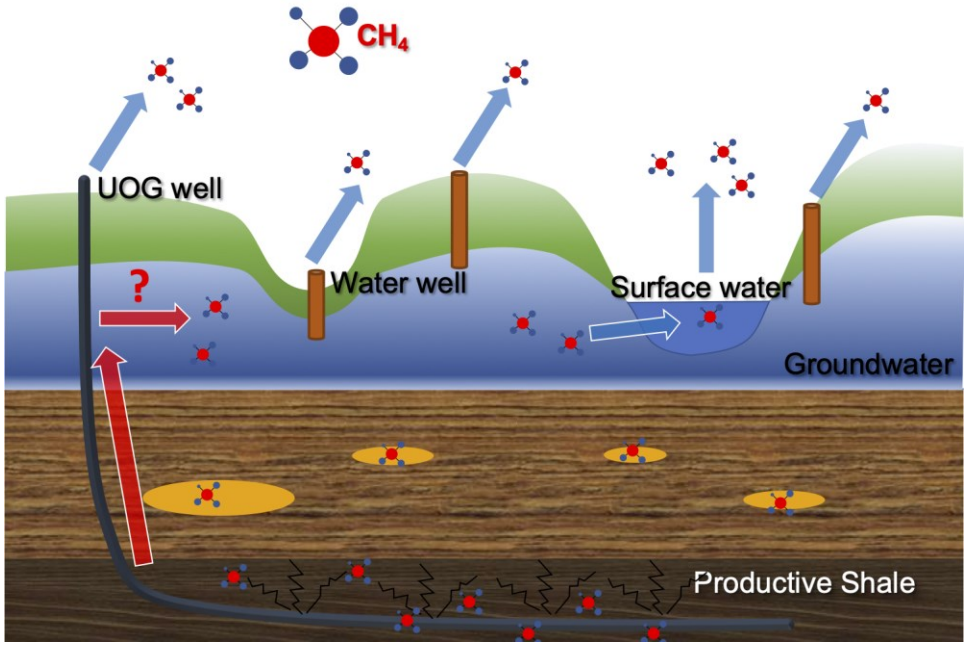

Figure 2. Potential methane migration pathways into groundwater aquifer and atmosphere under the influence of HDHF. UOG-induced methane migration pathways to groundwater aquifer were

uncertain (red arrows). Pathways from groundwater to surface water and subsequently to the atmosphere are confirmed pathways (blue arrows). Aboveground methane emissions at the UOG wells and water wells (i.e., by groundwater extraction and degassing) are also well-known source terms (blue arrows).

Whether or not UOG development introduced additional methane into groundwater aquifer has been debated over the last decade. On the one hand, earlier studies attributed elevated methane concentrations to UOG development based on spatial correlation and supporting isotopic signatures.[14,15] On the other hand, later studies did not observe such spatial correlation between groundwater methane concentration and UOG development, or only observed local correlation in small sub-regions. These latter studies were based on analyzing pre-drilling datasets whose sizes were much larger compared to those of the earlier works.[24–29] However, existing studies were limited by the timing of data collection or the comprehensiveness of their data, thus leaving uncertainty surrounding the question of UOG induced methane intrusion into groundwater. Such uncertainty would limit our understanding of the potential groundwater methane emission pathways and eventually lead to inefficiency in designing mitigation strategies for O&G methane emissions. Moreover, the regions of conventional fossil fuel extractions, including conventional oil and gas (COG, mostly with vertically drilled wells) and coal mining are typically overlapping the UOG development regions in the US. These conventional fossil fuel extractions are also potential sources of groundwater methane, and thus, they should be taken into account for groundwater methane source attribution. In addition, natural biogeochemical processes such as methanogenesis and anaerobic methane oxidation can also alter groundwater methane concentrations and these need to be evaluated as well. This thesis undertook a new study to give

an updated evaluation of the sources and migration of groundwater methane with rigorous methods and a holistic consideration of multiple anthropogenic and natural factors.

2. Climate and safety implication of groundwater methane

Several previous studies have estimated regional methane emission rates from groundwater.[20–23] For example, Gooddy and Darling estimated the maximum methane emission by groundwater abstraction from the four major aquifers of the United Kingdom to be 3.30×10^{-4} Tg CH_4/year.[21] The climate impact of such emission was equivalent to that of carbon dioxide emitted by about 6,000 passenger vehicles (assuming each vehicle emits 4.6 tons CO_2 per year,[30] and methane's 20-year global warming potential is used). Kulongoski and McMahon estimated the annual methane emission by ground water pumping from principal aquifers in the US to be 4.4×10^{-2} Tg CH_4 / year, and the global groundwater pumping methane emission to be 0.53 Tg CH_4 / year.[23] These numbers correspond to equivalent carbon dioxide emission from 800,000 and 9,000,000 passenger vehicles, respectively. It is worth noting that such calculation did not include the methane carried by groundwater discharge to surface water and eventually emitted to the air. Moreover, gas phase migration of methane (e.g., bubbles) in groundwater was not considered in these estimations. Previous studies have shown that gas phase methane could be released into groundwater by problematic O&G wells,[31–33] and omitting the gas phase migration would lead to underestimation of the total groundwater methane emission. Noticeably, gas phase methane could increase the dissolved methane concentration in the surrounding groundwater body by phase partitioning of methane molecules from gas to water. Therefore, gas phase

methane migration in groundwater should be indicated by elevated dissolved methane concentrations.

The public safety impact of groundwater dissolved methane is also important. The US Department of the Interior has set a warning level and immediate action level at 10 and 28 mg/L dissolved methane, respectively.[13] When the methane concentration exceeds the 10 mg/L warning level, residents should be warned and any ignition sources should be removed. When the methane concentration further exceeds the 28 mg/L immediate action level (equivalent to the methane solubility at 15 °C), there is immediate risk of fire or explosion due to degassing and immediate ventilation is needed. There are some reported cases of fire and explosions caused by groundwater dissolved methane in the O&G production regions in the US. For example, methane migrated along a water well caused explosion in the basement of a house in Chagrin Falls, Ohio.[34,35] The explosion cracked the house's foundation and peeled paint off its wall and the incident was attributed to the poorly cemented casing of a gas well. Note that while the impacts to the home are obvious, the impacts to the neighborhood property values are non-zero. Finally, although localized cases of O&G induced stray gas migration were linked to fire and explosion incidents, it has been unclear if O&G development systematically elevated groundwater methane concentration in regional scale (e.g., county level).

Difficulties in monitoring methane leaks from O&G facilities

1. Number and intermittency of methane emitters

The successful detection of above-ground fugitive emissions from leaky O&G infrastructures (e.g., well pads, compressor stations, and transmission pipelines) is the prerequisite for efficient leak fixation and will translate to improved safety, climate, and economics. In US states such as California[36] and Pennsylvania[37], quarterly leak detection and repair (LDAR) practice is required for O&G facilities, and such inspections are typically conducted using hand-held instruments such as infrared camera, thermal conductivity detector (TCD), or laser detector. Such manual inspections cost about $100 to $600 USD per well site per inspection,[38–40] and there are about one million producing O&G wells in the US.[41] Therefore, quarterly inspection of all wells can cost $400M to $2.4B per year, and such high cost could negatively affect O&G companies incentives to stop methane leaks. In addition, if each O&G well is treated equally during leak detection (e.g., deploying the same number of sensors or applying the same inspection frequency), the monitoring resources allocated to each well will be diffused and may be insufficient to effectively identify the leaks.

In addition to the large number of potential emitting facilities, the temporal intermittency of methane emissions is another major challenge for the emission monitoring efforts.[42–46] For example, the episodic activities such as manual liquid uploading can contribute to a significant portion of the total O&G methane emission,[45] and the traditional discontinuous survey methods can leave much of the emission undetected. As shown by a recent airborne methane emission study in California,[46] point source methane emitters often appear intermittently, with a mean persistence of about 30% (defined by the number of observed plumes divided by the number of overflights for a given emitter). This suggests that as many as 70% of point sources may be missed by a one-time screening. Given the low frequency of traditional LDAR program (i.e., every quarter), much of the intermittent sources could be undetected, and this would lead to

significant underestimation of the total emission rate and inefficiency to fix leaks. In recent years, remote sensing-based methane sensors, including airplane and satellite-mounted sensors, can screen large geospatial areas in a shorter period of time, increasing the frequency of leak monitoring.[47–49] However, the remote-sensing tools still cannot overcome the intermittency issue of emitters: screening by airplane (where revisit time depends on the mission logistics) and satellites (where revisit time ranges from several days to two weeks[50]) is discontinuous. Consequently, the methane emission events not captured by these visits would still be un-fixed. One possible solution to the intermittency challenge is to deploy continuously monitoring sensors in close distance to potential emitters. In order to make this strategy economically and technically feasible, two related strategies can be pursued: first, the total number of sensors could be reduced. The large number of O&G facilities would require an intractable number of sensors and huge cost of maintenance if we treat each facility as equally possible to emit methane. Thus, a prioritization strategy is needed to focus the sensor allocation on a subset of high-risk facilities, reducing the total number of sensors required and enhancing the monitoring efficiency. Second, continuous sensors with compact size, low cost, and low energy consumption should be developed. Existing continuous methane sensors such as infrared cameras, open path laser detectors, and cavity ring-down spectrometers are relatively expensive and consume large amount of energy. As such, they are not suitable for large-scale deployment among O&G facilities. Instead, very low cost, low power, compact chemiresistive methane sensors could become a better candidate for the tasks.

2. Proactive emission monitoring enabled by prediction of risky emitters

Given the intermittent occurrence and heterogeneous distribution of methane leaks, improved strategies to allocate the limited resources of leakage monitoring and fixation are required. So far, a reactive approach has been used to deal with methane leaks: leaks are first identified via inspection and screening, and then repairs can be made. However, if we could adapt a more proactive approach to predict those facilities (e.g., well pads) at higher risk of methane leakage, we could concentrate our sensing resources to this subset of facilities. This would increase the efficiency in detecting methane leaks. In particular, one could increase fly-over frequency of airplanes and satellites for a subset of high-risk emitters and deploy stationary sensors near those emitters that suggest a need for continuous monitoring, or even repair/replace vulnerable components before leaks occur. Moreover, the number of sensors and the fly-over frequency allocated to emitters with lower risk could be reduced, decreasing the total monitoring cost. Fortunately, the recent advancement in machine learning (ML), especially supervised learning algorithms, opens opportunities for predicting the risk of methane leakage from a given facility. My research will explore different ML algorithms for such prediction task.

The main challenges to predict methane emission risk are (i) to find an appropriate target variable (y) which captures the emission risk of a given facility, (ii) to find features (X) that are predictive of y, and (iii) to find efficient predicting algorithms. For (i), GHG emission inventories such as the U.S. Environmental Protection Agency's Greenhouse Gas Inventory (EPA GHGI) were first considered. These inventories apply unified emission factors for each component of the same type (e.g., valves and pipelines), but lack explicit measurements of emission rate for each individual emitter (or group of emitters). As such, they could not provide the target variable (y) for ML training. In addition, the inventories can largely underestimate the

total emission compared to estimations based on bottom-up measurements of facility-scale emissions.[51] A second potential source of the target variable could be remote sensing measurement data. Although numerous remote sensing measurements of methane emissions have been published,[46,52,53] the discontinuous nature of such measurements prevents them from correctly capturing all emissions thus leads to underestimation of the emission risk. Moreover, the remote sensing tools have difficulty to distinguish emission plumes from nearby emitters especially under complex metrological conditions, which largely limits the data's value as ML target variable. As such, an ideal target variable should be specific to individual facility, stable over time (i.e., having small temporal intermittency), and reflecting the underlying physical phenomenon relevant to the emission. For (ii), basic information of O&G well has been published in several states, including well completion date, surface elevation, well orientation and so on.[54–57] However, such public data does not contain rich physical information on how the wells are constructed. Thus, these have limited predictive power for physical mechanisms leading to methane leakage. More detailed physical data, especially on well casing and cement is needed to make the models predictive of integrity failures. For (iii), multiple state-of-the-art ML models should be compared in order to achieve the best performance in predicting methane emission risk.

3. Novel chemiresistive methane sensor: selectivity issue

Recently, researchers reported a compact, low-cost, and low-power prototype chemiresistive methane sensor which operates at room temperature.[58] This prototype sensor has a small size (about 2.5 cm long and 1.5 cm wide), which allows it to be deployed in various types of

environments. Moreover, the material cost of each sensor is below $10, and the power consumption can be smaller than 0.1 mW. This gives the sensor a distinct advantage over other continuous sensors such as infrared cameras, open path laser detectors, and cavity ring-down spectrometers, whose costs are typically well above $1,000 and power input above 5 W. The method of fabricating the novel chemiresistive sensor has been reported previously:[58] briefly, researchers combined single-walled carbon nanotubes (SWCNTs) with poly(4-vinylpyridine) (P4VP), and then added a platinum-polyoxometalate (Pt-POM) catalyst for methane oxidation. The catalytic methane oxidation reaction changes the resistance of the material and, thus, a signal can be detected using a potential stat applying fixed potential or fixed current. However, one critical drawback of this prototype sensor, and many sensors, is the interference from other gas species. Besides methane, the sensor can be responsive to species like water vapor and hydrogen sulfide (H_2S). In other words, this signal is a combination of responses to different species when they are all present in the environment. Given that water vapor is always present in ambient air, and H_2S can co-occur in natural gas before refining, the interferences cannot be avoided for the sensor. Therefore, data science or ML tools[59] can be used to extract the signal of methane from the combined signal of all species (i.e., signal deconvolution). Such signal deconvolution is a necessary step before the prototype sensor can be used for real-world methane emission detection. Here, I note that there is broad utility of this approach for a wide array of sensor modalities.

Research questions addressed in this thesis

Research Question I: *Does UOG development increase groundwater dissolved methane concentration?*

If UOG development is leaking methane into the groundwater aquifer, it can lead to environmental and climate consequences. The stray methane migration, either from stimulated shale or from problematic wellbores into the groundwater aquifer, would serve as the first step of a complete methane emission pathway (i.e., methane enters an aquifer and then migrates to surface water prior to atmospheric release). Therefore, finding evidence for groundwater methane contamination caused by UOG development would be an important first step to evaluate this emission pathway. Moreover, various natural factors can also shape the distribution of groundwater methane concentration thus require examination I have answered the following sub-questions to address Research Question I:

- Is there spatial correlation between groundwater methane concentration and location of UOG extraction?
- What does the isotopic signature imply about the origin of groundwater methane?
- What is the relationship between geochemistry of bulk groundwater and dissolved methane concentration?
- How does topography variation affect groundwater methane concentration?
- Are there changes in groundwater methane concentrations before and after nearby UOG drilling takes place?

These questions are addressed in Chapter 2.

Research Question II: *What are the contributions of traditional fossil fuel extraction, including COG and coal mining, and of natural biogeochemical processes to groundwater methane concentration?*

Traditional fossil fuel extraction activities, including COG and coal mining, have a long history and often overlap UOG activities over productive shales in the US. It is important to include traditional fossil fuel extractions in groundwater methane source attribution study. In addition, biogeochemical cycles of methane, involving methanogenesis and anaerobic methane oxidation, can alter groundwater methane concentration, and possibly interact with the fossil fuel extraction processes. To understand how traditional fossil fuel extraction and biogeochemical processes affect groundwater methane concentration, I have investigated the following sub-questions:

- What is the contribution of COG to the distribution of groundwater methane concentration?
- Does coal mining influence groundwater methane concentration?
- How does microbial methanogenesis and methanotroph alter groundwater methane concentration and interact with fossil fuel extraction activities?

These questions are addressed in Chapter 3.

Research Question III: *How can ML predict the risk of fugitive methane emission from O&G facilities?*

The complete programming pipeline to make prediction on emission risk will require three key components: the target variable, the predictors, and the ML estimators. Interpretation of the prediction results may provide insights into some important questions such as what factors have the strongest impact on emission risk, and whether emission risk is geospatially correlated. I break down Research Question III into the following sub-questions:

- What is the appropriate target variable to capture methane emission risk from a given O&G facility (e.g., well pad)?
- What physical information of O&G facilities can serve as predictors of the target variable?
- What ML models can achieve the most accurate prediction of the target variable?
- Is there geospatial correlation between facilities with high risk of methane emission? If yes, what factors drive such geospatial correlation?
- How can the prediction results inform prioritized allocation of methane sensors?
- How can future O&G operators and regulators learn from the prediction results to improve O&G well quality and design policy for emission reduction?

These questions are addressed in Chapter 4.

Research Question IV: *What is the concept and experimental set-up for chemiresistive methane sensor signal deconvolution?*

A ML framework is used to pave the way for addressing the signal deconvolution challenge. The ultimate goal of this work is to predict the true concentrations of gas species

(including methane and other interfering species) given the sensor readings as input. This thesis focused on the experimental set up for collecting the data for ML training and testing, while some preliminary results of sensor characterization were also obtained. However, it is beyond the scope of the thesis to fully execute the ML training and optimization program. Nevertheless, the following sub-questions were addressed:

- What is the experimental apparatus to collect data for training and testing ML models?
- What is the influence of relative humidity on chemiresistive sensors' ability to detect methane?
- What is the influence of flow rate on chemiresistive sensors' ability to detect methane?

These questions were addressed in Chapter 5.

Thesis overview

This thesis aims at providing a better understanding to the problem of methane emissions from the O&G industry and developing tools to facilitate the monitoring of such emissions. Reducing O&G methane emissions requires a systematic approach combining evaluation, prediction, and monitoring. First, there is a knowledge gap on methane emission pathways other than the direct air emission. For example, the pathway through groundwater system was very uncertainty and needed to be carefully evaluated before this work commenced. My evaluation of this pathway relies on answering whether groundwater methane concentration is elevated by O&G drilling, as opposed to other natural or anthropogenic factors. Second, a new proactive strategy of

monitoring methane emissions requires the prediction of methane emission risk associated with specific facilities and the improvement on chemiresistive methane sensors for continuous monitoring. I addressed these questions in the following chapters:

In Chapter 2, I analyzed water samples collected from 94 domestic wells or springs in Northeastern Pennsylvania. I measured the concentration of dissolved methane, ethane, and propane using a head-space extraction method followed by GC quantification. The spatial correlation between methane concentrations and the locations of UOG wells was computed to examine possible impact of UOG development. Moreover, I leveraged the $\delta^{13}C$ and $\delta^{2}H$ isotopic signatures of methane as well as the ratio of methane concentration over the sum of ethane and propane concentrations to determine the origin of measured groundwater methane. To further assess the likelihood of UOG induced contamination, the isotopic signatures of measured methane were compared to those of production gas samples, and the methane concentrations were compared to their pre-drilling levels. As an alternative to UOG-induced migration pathway, a pathway controlled by topography and geology was used to explain the observed distribution of groundwater methane concentration. Finally, the methane emission rate by groundwater discharge in the study region was estimated.

In Chapter 3, 217 domestic wells and springs were sampled in Ohio and West Virginia, where intense COG development and coal mining accompanied UOG extraction. I analyzed these additional samples to include the potential impact of traditional fossil fuel extraction in my analysis framework. Geospatial metrics, including proximity and site density, were used to evaluate the influence of fossil fuel extraction on groundwater methane concentration. In

addition, correlations between the concentration of methane and important biogeochemical indicators such as sulfate were studied to delineate the contribution of microbial activities on methane concentration. I analyzed isotopic signatures of these new methane samples to serve as evidence for the possible biogeochemical processes. Lastly, the influences of confounding factors such as topography on the observed correlations between methane concentration and fossil fuel extractions were examined.

In Chapter 4, I demonstrated how ML could predict the occurrences of O&G well integrity failures as proxy of the risk of fugitive methane emissions. Physical parameters of O&G well casing and cement were manually extracted from well completion reports to serve as basic predictors, and geospatial metrics capturing the integrity statuses of neighboring wells were used as additional predictors. I built a complete programming pipeline for ML training and testing, whose steps include data preprocessing, feature selection, hyperparameter and model selection, and final evaluation using test set. Different ML algorithms were explored to select for the best prediction performance, and feature importance was studied to gain physical insights of well integrity failures. Furthermore, I examined the geospatial correlations between integrity failures and explored different factors that could drive such correlations. Finally, recommendations were given regarding prioritized sensor placement, better data reporting practice, and strategies to reduce well integrity failures.

In Chapter 5, I introduced the concept and experimental apparatus for methane sensor signal deconvolution using ML. First, multiple chemiresistve sensors were fabricated (by collaborators) and each sensor underwent different treatments so that they had different selectivity toward the

same gas species (e.g., CH_4, H_2O, and H_2S). Second, these sensors were installed in a custom-made gas chamber where the gas composition could be controlled via mass flow control array and automated experimentation. Third, the signals of each sensor responsive to the current gas compositions were recorded. Lastly, the experiment was repeated for different gas compositions. The signals recorded for each sensor (predictors) and the true gas composition inside the chamber (target variable) will be used to train and test ML models. A gas-tight chamber was built to accommodate the chemiresistive sensors, and the specific gas composition inside the chamber could be controlled by mass flow controllers. The sensors' responses were recorded by a potential stat and exported as data in .csv format. Using this apparatus, I tested the chemiresistive sensors' tolerance to relative humidity and gas flow rate (i.e., above which humidity level and flow rate did the sensors stop responding to methane). At the time of this writing, the experimental set-up is also being upgraded to accommodate additional commercial methane sensors, and allow the internal temperature inside the chamber to be adjustable. This work will be continued by a colleague. The preliminary work here provides a platform to generate data upon which ML models will be trained and tested to achieve signal deconvolution of chemiresistive methane sensors.

Through the work presented in the above chapters, I was able to shed light on the motivating research question of my thesis. Principle findings included: (1) There was no systematic correlation between groundwater methane concentration and UOG development over our study regions in Pennsylvania, Ohio, and West Virginia. Instead, correlations between methane concentration and natural topographical and geochemical features suggested a natural migration mechanism of groundwater methane. (2) Groundwater methane concentration was higher closer

to COG well, but such correlation was confounded by topography variation. Moreover, lower methane concentration was observed with higher sulfate concentration, which was associated with closer distance to coal mine. I hypothesized that that methanogenesis was suppressed and methanotroph was facilitated by groundwater sulfate likely introduced by coal mining. (3) O&G well integrity failures were predictable by physical parameters of well casing and cement, and the most important parameters for the prediction were identified. Moreover, there existed significant geospatial correlation among well integrity failures. (4) A complete experimental set-up, including mass flow controllers, a gas tight chamber, and a data logging system were built. Preliminary data on the chemiresistive sensors' tolerance on humidity and flow rate were collected. To better understand, predict, monitor, and mitigate methane emission, the following products were generated during my dissertation work:

1. A framework to predict what groundwater is more vulnerable to natural methane intrusion. This can be used to distinguish natural methane migration from potential methane contamination caused by O&G drilling or coal mining.
2. A dataset of O&G well casing and cement physical parameters, which can be leveraged to further study the physical mechanisms driving integrity failures and become part of a larger training dataset for prediction of integrity failures.
3. Trained ML models for predicting O&G well integrity failures. These models can be used by O&G operators to predict which wells would have integrity issues related to fugitive methane emission, and prioritize them for emission monitoring. The number of sensors can be reduced, and the detection efficiency can be improved by taking this proactive monitoring approach.

4. An experimental apparatus for testing different types of chemiresistive methane sensors responding to controlled gas composition. This can be a useful tool for either evaluating, validating, and calibrating sensors, or collecting data for ML applications including signal deconvolution. Future researchers can also use this platform for their customized research projects.

References

(1) Masson-Delmotte, V.; Zhai, P.; Pirani, A.; Connors, S. L.; Péan, C.; Berger, S.; Caud, N.; Chen, Y.; Goldfarb, L.; Gomis, M. I.; Huang, M.; Leitzell, K.; Lonnoy, E.; Matthews, J. B. R.; Maycock, T. K.; Waterfield, T.; Yelekçi, O.; Yu, R.; Zhou, B. *Summary for Policymakers. In: Climate Change 2021: The Physical Science Basis. Contribution of Working Group I to the Sixth Assessment Report of the Intergovernmental Panel on Climate Change*; 2021. https://doi.org/10.1017/9781009157896.001.

(2) Lamontagne, J. R.; Reed, P. M.; Marangoni, G.; Keller, K.; Garner, G. G. Robust Abatement Pathways to Tolerable Climate Futures Require Immediate Global Action. *Nature Climate Change*. 2019, *9* (4), 290–294. https://doi.org/10.1038/s41558-019-0426-8.

(3) Forster, P.; Storelvmo, T.; Armour, K.; Collins, W.; Dufresne, J.-L.; Frame, D.; Lunt, D. J.; Mauritsen, T.; Palmer, M. D.; Watanabe, M.; Wild, M.; Zhang, H. *The Earth's Energy Budget, Climate Feedbacks, and Climate Sensitivity. In Climate Change 2021: The Physical Science Basis. Contribution of Working Group I to the Sixth Assessment Report of the Intergovernmental Panel on Climate Change*; Cambridge, United Kingdom and New York, NY, USA, 2021. https://doi.org/10.1017/9781009157896.009.

(4) United Nations Environment Programme and Climate and Clean Air Coalition. *Global Methane Assessment: Benefits and Costs of Mitigating Methane Emissions.*; Nairobi, 2021.

(5) Saunois, M.; Stavert, A.; Poulter, B.; Bousquet, P.; Canadell, J.; Jackson, R.; Raymond, P.; Dlugokencky, E.; Houweling, S.; Patra, P.; Ciais, P.; Arora, V.; Bastviken, D.; Bergamaschi, P.; Blake, D.; Brailsford, G.; Bruhwiler, L.; Carlson, K.; Carrol, M.; Castaldi, S.; Chandra, N.; Crevoisier, C.; Crill, P.; Covey, K.; Curry, C.; Etiope, G.; Frankenberg, C.; Gedney, N.; Hegglin, M.; Höglund-Isaksson, L.; Hugelius, G.; Ishizawa, M.; Ito, A.; Janssens-Maenhout, G.; Jensen, K.; Joos, F.; Kleinen, T.; Krummel, P.; Langenfelds, R.; Laruelle, G.; Liu, L.; Machida, T.; Maksyutov, S.; McDonald, K.; McNorton, J.; Miller, P.; Melton, J.; Morino, I.; Müller, J.; Murguia-Flores, F.; Naik, V.; Niwa, Y.; Noce, S.; O'Doherty, S.; Parker, R.; Peng, C.; Peng, S.; Peters, G.; Prigent, C.; Prinn, R.; Ramonet, M.; Regnier, P.; Riley, W.; Rosentreter, J.; Segers, A.; Simpson, I.; Shi, H.; Smith, S.; Steele, L. P.; Thornton, B.; Tian, H.; Tohjima, Y.; Tubiello, F.;

Tsuruta, A.; Viovy, N.; Voulgarakis, A.; Weber, T.; van Weele, M.; van der Werf, G.; Weiss, R.; Worthy, D.; Wunch, D.; Yin, Y.; Yoshida, Y.; Zhang, W.; Zhang, Z.; Zhao, Y.; Zheng, B.; Zhu, Q.; Zhu, Q.; Zhuang, Q. The Global Methane Budget 2000–2017. *Earth Syst. Sci. Data* **2020**, *12* (3), 1561–1623. https://doi.org/10.5194/essd-12-1561-2020.

(6) Nesbit, J. The new Global Methane Pledge can buy time while the world drastically reduces fossil fuel use https://www.pbs.org/newshour/science/the-new-global-methane-pledge-can-buy-time-while-the-world-drastically-reduces-fossil-fuel-use (accessed Aug 31, 2022).

(7) Homepage | Global Methane Pledge https://www.globalmethanepledge.org/ (accessed Oct 4, 2022).

(8) United States Environmental Protection Agency. Health Effects of Ozone Pollution https://www.epa.gov/ground-level-ozone-pollution/health-effects-ozone-pollution (accessed Jul 18, 2023).

(9) U.S. Energy Information Administration. U.S. energy facts explained https://www.eia.gov/energyexplained/us-energy-facts/data-and-statistics.php (accessed Aug 31, 2022).

(10) U.S. Energy Information Administration. Monthly Energy Review - August 2022. **2022**.

(11) U.S. Energy Information Administration. Frequently Asked Questions (FAQs) - How much shale gas is produced in the United States? https://www.eia.gov/tools/faqs/faq.php?id=907&t=8 (accessed Sep 1, 2022).

(12) U.S. Energy Information Administration. Frequently Asked Questions (FAQs) - How much shale (tight) oil is produced in the United States? https://www.eia.gov/tools/faqs/faq.php?id=847&t=6 (accessed Sep 1, 2022).

(13) Eltschlager, K. K.; Hawkins, J. W.; Ehler, W. C.; Baldassare, F. J. Technical Measures for the Invetigation and Mitigation of Fugitive Methane Hazards in Areas of Coal Mining, U.S. Department of the Interior, Office of Surface Mining. **2001.**

(14) Osborn, S. G.; Vengosh, A.; Warner, N. R.; Jackson, R. B. Methane Contamination of Drinking Water Accompanying Gas-Well Drilling and Hydraulic Fracturing. *Proc. Natl. Acad. Sci.* **2011**, *108* (20), 8172–8176. https://doi.org/10.1073/pnas.1100682108.

(15) Jackson, R. B.; Vengosh, A.; Darrah, T. H.; Warner, N. R.; Down, A.; Poreda, R. J.; Osborn, S. G.; Zhao, K.; Karr, J. D. Increased Stray Gas Abundance in a Subset of Drinking Water Wells near Marcellus Shale Gas Extraction. *Proc. Natl. Acad. Sci. U. S. A.* **2013**, *110* (28), 11250–11255. https://doi.org/10.1073/pnas.1221635110.

(16) Heilweil, V. M.; Grieve, P. L.; Hynek, S. A.; Brantley, S. L.; Solomon, D. K.; Risser, D. W. Stream Measurements Locate Thermogenic Methane Fluxes in Groundwater Discharge in an Area of Shale-Gas Development. *Environ. Sci. Technol.* **2015**, *49* (7), 4057–4065. https://doi.org/10.1021/es503882b.

(17) Woda, J.; Wen, T.; Oakley, D.; Yoxtheimer, D.; Engelder, T.; Clara Castro, M.; Brantley, S. L. Detecting and Explaining Why Aquifers Occasionally Become Degraded near Hydraulically Fractured Shale Gas Wells. *Proc. Natl. Acad. Sci. U. S. A.* **2018**, *115* (49), 12349–12358. https://doi.org/10.1073/pnas.1809013115.

(18) Woda, J.; Wen, T.; Lemon, J.; Marcon, V.; Keeports, C. M.; Zelt, F.; Steffy, L. Y.; Brantley, S. L. Methane Concentrations in Streams Reveal Gas Leak Discharges in Regions of Oil, Gas, and Coal Development. *Sci. Total Environ.* **2020**, 140105. https://doi.org/10.1016/j.scitotenv.2020.140105.

(19) Stanley, E. H.; Casson, N. J.; Christel, S. T.; Crawford, J. T.; Loken, L. C.; Oliver, S. K.

The Ecology of Methane in Streams and Rivers: Patterns, Controls, and Global Significance. *Ecol. Monogr.* **2016**, *86* (2), 146–171. https://doi.org/10.1890/15-1027.
(20) Pinti, D. L.; Gelinas, Y.; Moritz, A. M.; Larocque, M.; Sano, Y. Anthropogenic and Natural Methane Emissions from a Shale Gas Exploration Area of Quebec, Canada. *Sci. Total Environ.* **2016**, *566–567*, 1329–1338. https://doi.org/10.1016/j.scitotenv.2016.05.193.
(21) Gooddy, D. C.; Darling, W. G. The Potential for Methane Emissions from Groundwaters of the UK. *Sci. Total Environ.* **2005**, *339* (1–3), 117–126. https://doi.org/10.1016/j.scitotenv.2004.07.019.
(22) Crawford, J. T.; Striegl, R. G.; Wickland, K. P.; Dornblaser, M. M.; Stanley, E. H. Emissions of Carbon Dioxide and Methane from a Headwater Stream Network of Interior Alaska. *J. Geophys. Res. Biogeosciences* **2013**, *118* (2), 482–494. https://doi.org/10.1002/jgrg.20034.
(23) Kulongoski, J. T.; McMahon, P. B. Methane Emissions from Groundwater Pumping in the USA. *npj Clim. Atmos. Sci.* **2019**, *2* (1), 1–8. https://doi.org/10.1038/s41612-019-0068-6.
(24) Molofsky, L. J.; Connor, J. A.; Farhat, S. K.; Wylie, A. S.; Wagner, T. Methane in Pennsylvania Water Wells Unrelated to Marcellus Shale Fracturing. *Oil Gas J.* **2011**, *109* (19).
(25) Molofsky, L. J.; Connor, J. A.; Wylie, A. S.; Wagner, T.; Farhat, S. K. Evaluation of Methane Sources in Groundwater in Northeastern Pennsylvania. *GroundWater* **2013**, *51* (3), 333–349. https://doi.org/10.1111/gwat.12056.
(26) Siegel, D. I.; Azzolina, N. A.; Smith, B. J.; Perry, A. E.; Bothun, R. L. Methane Concentrations in Water Wells Unrelated to Proximity to Existing Oil and Gas Wells in Northeastern Pennsylvania. *Environ. Sci. Technol.* **2015**, *49* (7), 4106–4112. https://doi.org/10.1021/es505775c.
(27) Wen, T.; Niu, X.; Gonzales, M.; Zheng, G.; Li, Z.; Brantley, S. L. Big Groundwater Data Sets Reveal Possible Rare Contamination Amid Otherwise Improved Water Quality for Some Analytes in a Region of Marcellus Shale Development. *Environ. Sci. Technol.* **2018**, *52* (12), 7149–7159. https://doi.org/10.1021/acs.est.8b01123.
(28) Li, Z.; You, C.; Gonzales, M.; Wendt, A. K.; Wu, F.; Brantley, S. L. Searching for Anomalous Methane in Shallow Groundwater near Shale Gas Wells. *J. Contam. Hydrol.* **2016**, *195*, 23–30. https://doi.org/10.1016/j.jconhyd.2016.10.005.
(29) Li, Z.; You, C.; Gonzales, M.; Wendt, A. K.; Wu, F.; Brantley, S. L. Corrigendum to "Searching for Anomalous Methane in Shallow Groundwater near Shale Gas Wells" (J. Contam. Hydrol. (2016) 195 (23–30) (S0169772216300985) (10.1016/j.Jconhyd.2016.10.005)). *Journal of Contaminant Hydrology*. Elsevier B.V. December 1, 2017, pp 50–51. https://doi.org/10.1016/j.jconhyd.2017.09.009.
(30) United States Environmental Protection Agency. Greenhouse Gas Emissions from a Typical Passenger Vehicle https://www.epa.gov/greenvehicles/greenhouse-gas-emissions-typical-passenger-vehicle#:~:text=including the calculations.-,How much tailpipe carbon dioxide (CO2) is emitted from,of CO2 per mile. (accessed Jul 19, 2023).
(31) Darrah, T. H.; Vengosh, A.; Jackson, R. B.; Warner, N. R.; Poreda, R. J. Noble Gases Identify the Mechanisms of Fugitive Gas Contamination in Drinking-Water Wells Overlying the Marcellus and Barnett Shales. *Proc. Natl. Acad. Sci. U. S. A.* **2014**, *111* (39), 14076–14081. https://doi.org/10.1073/pnas.1322107111.
(32) Lackey, G.; Rajaram, H.; Sherwood, O. A.; Burke, T. L.; Ryan, J. N. Surface Casing

Pressure As an Indicator of Well Integrity Loss and Stray Gas Migration in the Wattenberg Field, Colorado. *Environ. Sci. Technol.* **2017**, *51* (6), 3567–3574. https://doi.org/10.1021/acs.est.6b06071.
(33) Lackey, G.; Rajaram, H.; Bolander, J.; Sherwood, O. A.; Ryan, J. N.; Shih, C. Y.; Bromhal, G. S.; Dilmore, R. M. Public Data from Three US States Provide New Insights into Well Integrity. *Proc. Natl. Acad. Sci. U. S. A.* **2021**, *118* (14). https://doi.org/10.1073/PNAS.2013894118.
(34) Engelder, T.; Zevenbergen, J. F. Analysis of a Gas Explosion in Dimock PA (USA) during Fracking Operations in the Marcellus Gas Shale. *Process Saf. Environ. Prot.* **2018**, *117*, 61–66. https://doi.org/10.1016/j.psep.2018.04.004.
(35) Bair, S.; Tomastik, T.; Benko, T.; Hill, T. Geologic AndHydrogeologic FactorsControlling How Stray Gas from the English #1 Well Invaded Residences in Geauga County, Ohio, Causing an In- House Explosion. In *Groundwater Protection Council Stray Gas Incidence & Response Forum*; Cleveland, OH, 2012.
(36) California Air Resources Board. CARB ' s Oil and Gas Methane Regulation 2019 Annual LDAR Summary. **2022**.
(37) Pennsylvania Department of Environmental Protection. *Comparison of Pennsylvania Requirements , EPA Rules , and CSSD Requirements for Methane & VOC Emission Reduction for the Oil & Gas Industry Effective August 8 , 2018*; 2018.
(38) Environmental Defense Fund. *Finding, Fixing Leaks Is a Cost-Effective Way to Cut Oil and Gas Methane Emissions*; 2016.
(39) Saunier, S.; Haugland, T.; Pederstad, A. *Quantifying Cost-Effectiveness of Systematic Leak Detection and Repair Programs Using Infrared Cameras*; 2014.
(40) Kemp, C. E.; Ravikumar, A. P. New Technologies Can Cost Effectively Reduce Oil and Gas Methane Emissions, but Policies Will Require Careful Design to Establish Mitigation Equivalence. *Environ. Sci. Technol.* **2021**, *55* (13), 9140–9149. https://doi.org/10.1021/acs.est.1c03071.
(41) U.S. Energy Information Administration. US Oil and Gas Wells by Production Rate https://www.eia.gov/petroleum/wells/ (accessed Dec 27, 2022).
(42) Vaughn, T. L.; Bell, C. S.; Pickering, C. K.; Schwietzke, S.; Heath, G. A.; Pétron, G.; Zimmerle, D. J.; Schnell, R. C.; Nummedal, D. Temporal Variability Largely Explains Top-down/Bottom-up Difference in Methane Emission Estimates from a Natural Gas Production Region. *Proc. Natl. Acad. Sci. U. S. A.* **2018**, *115* (46), 11712–11717. https://doi.org/10.1073/PNAS.1805687115/VIDEO-1.
(43) Allen, D. T.; Cardoso-Saldaña, F. J.; Kimura, Y. Variability in Spatially and Temporally Resolved Emissions and Hydrocarbon Source Fingerprints for Oil and Gas Sources in Shale Gas Production Regions. *Environ. Sci. Technol.* **2017**, *51* (20), 12016–12026. https://doi.org/10.1021/acs.est.7b02202.
(44) Nathan, B. J.; Golston, L. M.; O'Brien, A. S.; Ross, K.; Harrison, W. A.; Tao, L.; Lary, D. J.; Johnson, D. R.; Covington, A. N.; Clark, N. N.; Zondlo, M. A. Near-Field Characterization of Methane Emission Variability from a Compressor Station Using a Model Aircraft. *Environ. Sci. Technol.* **2015**, *49* (13), 7896–7903. https://doi.org/10.1021/acs.est.5b00705.
(45) Schwietzke, S.; Pétron, G.; Conley, S.; Pickering, C.; Mielke-Maday, I.; Dlugokencky, E. J.; Tans, P. P.; Vaughn, T.; Bell, C.; Zimmerle, D.; Wolter, S.; King, C. W.; White, A. B.; Coleman, T.; Bianco, L.; Schnell, R. C. Improved Mechanistic Understanding of Natural

Gas Methane Emissions from Spatially Resolved Aircraft Measurements. *Environ. Sci. Technol.* **2017**, *51* (12), 7286–7294. https://doi.org/10.1021/acs.est.7b01810.
(46) Duren, R. M.; Thorpe, A. K.; Foster, K. T.; Rafiq, T.; Hopkins, F. M.; Yadav, V.; Bue, B. D.; Thompson, D. R.; Conley, S.; Colombi, N. K.; Frankenberg, C.; McCubbin, I. B.; Eastwood, M. L.; Falk, M.; Herner, J. D.; Croes, B. E.; Green, R. O.; Miller, C. E. California's Methane Super-Emitters. *Nature* **2019**, *575* (7781), 180–184. https://doi.org/10.1038/s41586-019-1720-3.
(47) Jacob, D. J.; Varon, D. J.; Cusworth, D. H.; Dennison, P. E.; Frankenberg, C.; Gautam, R.; Guanter, L.; Kelley, J.; McKeever, J.; Ott, L. E.; Poulter, B.; Qu, Z.; Thorpe, A. K.; Worden, J. R.; Duren, R. M. Quantifying Methane Emissions from the Global Scale down to Point Sources Using Satellite Observations of Atmospheric Methane. *Atmos. Chem. Phys.* **2022**, *22* (14), 9617–9646. https://doi.org/10.5194/acp-22-9617-2022.
(48) Sawyer, W.; Genina, I.; Brenneis, R.; Feng, H.; Li, Y.; Lennon Luo, S.-X. Methane Emissions and Global Warming: Mitigation Technologies, Policy Ambitions, and Global Efforts. *MIT Sci. Policy Rev.* **2022**, *3*, 73–84. https://doi.org/10.38105/spr.8u4spgvc0e.
(49) Nisbet, E. G.; Fisher, R. E.; Lowry, D.; France, J. L.; Allen, G.; Bakkaloglu, S.; Broderick, T. J.; Cain, M.; Coleman, M.; Fernandez, J.; Forster, G.; Griffiths, P. T.; Iverach, C. P.; Kelly, B. F. J.; Manning, M. R.; Nisbet-Jones, P. B. R.; Pyle, J. A.; Townsend-Small, A.; Al-Shalaan, A.; Warwick, N.; Zazzeri, G. Methane Mitigation: Methods to Reduce Emissions, on the Path to the Paris Agreement. *Reviews of Geophysics*. John Wiley & Sons, Ltd March 1, 2020, p e2019RG000675. https://doi.org/10.1029/2019RG000675.
(50) Sherwin, E. D.; Rutherford, J. S.; Chen, Y.; Aminfard, S.; Kort, E. A.; Jackson, R. B.; Brandt, A. R. Single-Blind Validation of Space-Based Point-Source Detection and Quantification of Onshore Methane Emissions. *Sci. Reports 2023 131* **2023**, *13* (1), 1–10. https://doi.org/10.1038/s41598-023-30761-2.
(51) Alvarez, R. A.; Zavala-Araiza, D.; Lyon, D. R.; Allen, D. T.; Barkley, Z. R.; Brandt, A. R.; Davis, K. J.; Herndon, S. C.; Jacob, D. J.; Karion, A.; Kort, E. A.; Lamb, B. K.; Lauvaux, T.; Maasakkers, J. D.; Marchese, A. J.; Omara, M.; Pacala, S. W.; Peischl, J.; Robinson, A. L.; Shepson, P. B.; Sweeney, C.; Townsend-Small, A.; Wofsy, S. C.; Hamburg, S. P. Assessment of Methane Emissions from the U.S. Oil and Gas Supply Chain. *Science (80-.).* **2018**, *361* (6398), 186–188. https://doi.org/10.1126/science.aar7204.
(52) Varon, D. J.; McKeever, J.; Jervis, D.; Maasakkers, J. D.; Pandey, S.; Houweling, S.; Aben, I.; Scarpelli, T.; Jacob, D. J. Satellite Discovery of Anomalously Large Methane Point Sources From Oil/Gas Production. *Geophys. Res. Lett.* **2019**, *46* (22), 13507–13516. https://doi.org/10.1029/2019GL083798.
(53) Heimburger, A. M. F.; Harvey, R. M.; Shepson, P. B.; Stirm, B. H.; Gore, C.; Turnbull, J.; Cambaliza, M. O. L.; Salmon, O. E.; Kerlo, A. E. M.; Lavoie, T. N.; Davis, K. J.; Lauvaux, T.; Karion, A.; Sweeney, C.; Brewer, W. A.; Hardesty, R. M.; Gurney, K. R. Assessing the Optimized Precision of the Aircraft Mass Balance Method for Measurement of Urban Greenhouse Gas Emission Rates through Averaging. *Elementa* **2017**, *5*. https://doi.org/10.1525/elementa.134.
(54) Pennsylvania Department of Environmental Protection. Oil Gas Locations - Unconventional https://newdata-padep-1.opendata.arcgis.com/datasets/oil-gas-locations-unconventional?geometry=-81.196%2C40.740%2C-74.247%2C42.181 (accessed Mar 24,

2020).
(55) Pennsylvania Department of Environmental Protection. Oil Gas Locations - Conventional https://newdata-padep-1.opendata.arcgis.com/datasets/oil-gas-locations-conventional (accessed Mar 24, 2020).
(56) Ohio Department of Natural Resources. Oil and Gas Data https://ohiodnr.gov/discover-and-learn/safety-conservation/about-odnr/oil-gas/oil-gas-resources/featured-content-3 (accessed Feb 1, 2022).
(57) West Virginia Department of Environmental Protection. Oil and Gas Production Data https://dep.wv.gov/oil-and-gas/databaseinfo/Pages/default.aspx (accessed Dec 1, 2020).
(58) Bezdek, M. J.; Luo, S. X. L.; Ku, K. H.; Swager, T. M. A Chemiresistive Methane Sensor. *Proc. Natl. Acad. Sci. U. S. A.* **2021**, *118* (2), 1–6. https://doi.org/10.1073/pnas.2022515118.
(59) Snauffer, A. M.; Chauhan, U.; Cogert, K.; Winkler, M. K. H.; Mueller, A. V. Data Fusion for Environmental Process Control: Maximizing Useful Information Recovery under Data Limited Constraints. *IEEE Sensors Lett.* **2019**, *3* (1), 2019–2022. https://doi.org/10.1109/LSENS.2018.2889274.

Chapter 2. Groundwater methane in Northeastern Pennsylvania attributable to thermogenic sources and hydrogeomorphologic migration pathways

By

[1]Yunpo Li, [1]Nathalie A. Thelemaque, [2]Helen G. Siegel, [3]Cassandra J. Clark, [3]Emma Ryan, [1]Rebecca J. Brenneis, [2]Kristina M. Gutchess, [2]Mario A. Soriano Jr., [1]Boya Xiong, [3]Nicole C. Deziel, [2]James E. Saiers, [1]Desiree L. Plata

[1]Massachusetts Institute of Technology, Department of Civil and Environmental Engineering, Parsons Laboratory, 15 Vassar Street, Cambridge, Massachusetts 02139, USA

[2]Yale University, the School of the Environment, 195 Prospect Street, New Haven, Connecticut 06511, USA

[3]Yale University, Yale School of Public Health, Department of Environmental Health Sciences, 60 College St., New Haven, Connecticut 06512, USA

Reprinted (adapted) with permission from Li, Y., Thelemaque, N. A., Siegel, H. G., Clark, C. J., Ryan, E. C., Brenneis, R. J., ... & Plata, D. L. (2021). Groundwater methane in northeastern Pennsylvania attributable to thermogenic sources and hydrogeomorphologic migration pathways. *Environmental Science & Technology*, *55*(24), 16413-16422.

ABSTRACT

Conflicting evidence exists as to whether or not unconventional oil and gas (UOG) development has enhanced methane transport into groundwater aquifers over the past 15 years. In this study, recent groundwater samples were collected from 90 domestic wells and 4 springs in Northeastern Pennsylvania located above the Marcellus Shale after more than a decade of UOG development. No statistically significant correlations were observed between groundwater methane level and various UOG geospatial metrics, including proximity to UOG wells and well violations, as well as number of UOG wells and violations within particular radii. The $\delta^{13}C$ and methane-to-higher chain hydrocarbon signatures suggested that the elevated methane levels were not attributable to UOG development, nor could they be explained by simple biogenic-thermogenic end-member mixing models. Instead, groundwater methane levels were significantly correlated with geochemical water type and topographical location. Comparing a subset of contemporary methane measurements to their co-located pre-drilling records (n = 64 at 49 distinct locations) did not indicate systematic increases in methane concentration, but did reveal several cases of elevated concentration (n=12) across a spectrum of topographies. Multiple lines of evidence suggested that the high-concentration groundwater methane could have originated from shallow thermogenic methane that migrated upward into groundwater aquifers with Appalachian Basin Brine.

Keywords: groundwater, unconventional oil and gas, methane, hydraulic fracturing, geochemistry

SYNOPSIS STATEMENT
Geochemical evidence illustrated elevated concentrations of groundwater methane associated with topographical lows, Appalachian Basin Brine, and shallow thermogenic methane.

Introduction

The fast growth of unconventional oil and gas (UOG) development in the United States has provided reliable domestic energy, but there is persistent concern regarding the impacts of the extraction process on groundwater. A unique feature of the UOG boom in the United States is that it is often collocated within residential areas, which has created a concern for chemical impacts, such as explosion risk if groundwaters become impacted by fugitive methane (accumulating above 10 mg/L[1]). Considering that natural gas is playing an important role in meeting society's energy needs today and is projected to remain so through at least 2050[2], efforts to understand and mitigate environmental impacts from natural gas extraction are imperative.

The impact of UOG development on groundwater methane levels has been debated for over a decade. Following the onset of rapid UOG growth (circa 2007), Osborn et al.[3] (n=68) and Jackson et al.[4] (n=141) found that groundwater samples in proximity to gas wells in Northeastern Pennsylvania (NE PA) contained elevated methane concentrations and used isotopic tracing to suggest that such methane likely originated from thermogenic sources. Ultimately, these studies attributed those elevated groundwater methane concentrations to UOG extraction from the Marcellus Shale. Nevertheless, several later investigations contradicted those findings based on analyses of large amounts of pre-drilling measurements. Here, "pre-drilling" means measurements made before a specific proposed conventional or unconventional gas well was

drilled near the groundwater sample location, but likely with some older gas wells already drilled in the vicinity due to the long history of drilling in PA extending back to circa 1850. Thus, while there is no undisturbed baseline data available, it is possible to analyze impacts associated with local drilling. Molofsky et al.[5,6] (sample size over 1,000) and Siegel et al.[7] (sample size greater than 10,000) found no statistically significant correlation between dissolved methane concentrations in groundwater and the distance to gas wells in NE PA. Li et al.[8,9] and Wen et al.[10] applied sliding window data mining techniques on large pre-drilling datasets (n over 1,000 and 10,000, respectively) and found that methane concentrations were primarily influenced by geologic features (i.e., faults and anticlines) as well as surface topography in NE PA, except in a few cases where UOG proximity exerted influence. Another study by Wen et al.[11] identified no regional systematic impact of UOG development on groundwater methane concentrations using a machine learning model. Unfortunately, many of these large-scale, pre-drilling analyses lacked the methane isotopic information essential for source apportionment.

Considering the reliance on pre-drilling datasets[5–10] or relatively early analyses[3,4], the possibility remains that sufficient UOG activity and/or transport times had not passed in order to observe systematic effects on groundwater composition. More than a decade has passed since the onset of UOG extraction activities, allowing time for possible subsurface transport of methane and other geochemical indicators related to UOG development to adjacent groundwaters. In addition, intense expansion of gas extraction has taken place over this time period; of the 5533 UOG wells permitted in Bradford, PA and surrounding counties, 2705 were drilled between 2007 and 2011, and 2780 were drilled 2011-2018.[12] As such, impacts on groundwater methane associated with the oil and gas boom warrant renewed exploration.

In addition to providing insights of geochemical mechanisms, accounting for methane migration to groundwater can inform health and climatological risk assessments. Health concerns derive from exceedances of warning levels, which are set at 10 mg/L by the US Department of the Interior[1] as the threshold where warning should be provided to the well owner that there is a risk for flammability. In addition, shale gas extraction in Appalachian basin could have climate impacts.[13] Climate impacts are seldom estimated in groundwater transport schemes, but could be important. Natural gas utilization that offsets coal or oil combustion confers a greenhouse gas (GHG) benefit on a region or corporation's emissions inventory[14–16], but fugitive emissions of methane via the groundwater system associated with gas extraction are poorly accounted in those budgets. After entering an aquifer, methane could migrate to surface water bodies such as streams, rivers, and lakes via groundwater discharge[17,18] and subsequently release into the atmosphere[19–22]. In addition, groundwater extraction by human activities also results in methane degassing.[20,21,23] Thus, identifying potentially enhanced methane transport into groundwater aquifers from UOG is an important first step to understand methane emissions via hydrogeological pathways and determine the true GHG benefit of natural gas utilization.

The objectives of this study were to understand the sources and migration pathways of groundwater dissolved methane in NE PA, evaluate the potential impacts of UOG development on groundwater methane level, and move toward better understanding of the environmental, safety, and climatic impacts of shale gas extraction. In this investigation, we collected a large number of groundwater samples in NE PA (90 domestic water wells and 4 springs; Fig. S2), over one of the most productive shale plays in the United States (US), the Marcellus Shale. Methane

levels, isotopic signatures, and higher-chain hydrocarbons were evaluated to reveal potential methane sources. These analyses were complemented with geochemical characteristics, including major ion and trace metal concentrations. In combination with topographical information, these data revealed potential migration mechanisms of methane. These important indicators were examined alongside geospatial indicators, such as distance to nearest UOG well or UOG violation, as well as UOG well intensity within particular radii about a groundwater well. Finally, each measured methane concentration was compared with its pre-drilling concentration(s) from the same location, in cases where the latter was available. Using these multiple lines of evidence, we determined the dominant origin and transport mechanisms of groundwater methane in these samples in NE PA and extended the analysis to constrain the potential contributions of UOG development to groundwater methane emissions over gas-rich shale formations.

Materials and methods

Water samples for dissolved hydrocarbon (methane, ethane, and propane) analysis were collected from 90 domestic wells and 4 springs (89 in Bradford County and 5 in Tioga County) in NE PA as part of the Yale Water and Energy Resources Study (see various refernces[24–27]). Sample locations were the outcome of recruitment efforts (semi-random), election to participation (which is impossible to fully randomize), and eligibility. First, we applied multiple recruitment methods, including newspaper advertisements, flyers posted at local businesses, social media, and mailed informational postcards to zip codes in the study region to reach a broad population. Then, prospective participants who responded to these solicitations were

deemed eligible for the study based on these criteria: (1) they were the head of house older than 21; (2) they spoke English (a requirement for participation considering the interview and onsite access needs); and (3) they lived in a home served by private groundwater well or spring. Thus, we made every effort to recruit a broad pool of participants.

Water samples were collected upstream of any residential water treatment devices, filled into serum bottles with sodium azide added for sample preservation, and sealed with rubber stoppers and crimpers (see SI methods for extensive sample collection details). Dissolved hydrocarbon species were accessed using a headspace extraction method and analyzed using an SRI 8610C Gas Chromatography with a Flame Ionization Detector (see SI methods for details on hydrocarbon quantification and yield test). Methane isotopes were analyzed by UC Davis Stable Isotope Facility. The measurement of dissolved ion species, the construction of spatial metrics and topographical classes, and the collection of pre-drilling data are also discussed in the SI and presented in other publications[24–27]. Any referenced pre-drilling data were acquired from the Shale Network database[10,28] and matched with our sampling locations, or provided by the homeowners.

Results and discussion

Groundwater methane levels

The majority of groundwater samples contained low levels of dissolved methane, while about 5% of samples were above the 10 mg/L warning level recommended by U.S. Department of the

Interior[1] (Fig. 1). Methane levels ranged from 3.9 x 10^{-5} to 32 mg/L, where the mean concentration was 1.5 mg/L (n=94) and seven samples were below detectable limits (2.3 × 10^{-5} mg/L; limit of detection (LOD)). The correlation between dissolved methane concentrations and distances to the nearest UOG well borehole (drilled on or before sampling campaign start date) was not statistically significant (Fig. 1A, Spearman correlation $\rho = 0.026$, p-value = 0.80). Distances to vertical boreholes instead of horizontal wellbore segments were considered because previous studies have documented stray gas migration through improperly cased or cemented vertical sections of the borehole (i.e., in accidents or violations)[6,29–31], whereas evidence for long-distance vertical methane migration directly from production shale depths to shallower groundwater aquifers is lacking[31]. Our analysis included any UOG well; the insignificant correlation persisted for horizontally-drilled UOG wells (i.e., a subset of all UOG) (Fig S3A) and when all oil and gas (O&G) wells (UOG and conventional) were included (Fig S3B). The finding that there is no statistically significant correlation between distance to nearest UOG well and groundwater methane levels stands in contrast with earlier work from Osborn et al.[3] and Jackson et al.[4], but is consistent with these conclusions of later studies by Molofsky et al.[5,6], Siegel et al.[7], and Wen et al.[10]. There are two possible explanations for the apparent disparity of our work and earlier studies: first, the spatiotemporal variability in samples could have given rise to apparently distinct findings. In particular, the observation of elevated methane near gas extraction wells could have been temporally transient or a happenstance consequence of the spatial distribution of study participant wells and dissolved methane content at those particular loci. Later studies leveraged very large sample sizes associated with state-mandated pre-drilling methane assessments, and these studies would not have been as sensitive to the stochastic spatiotemporal variability (due to sheer number and broad distribution). Second, possible analytical errors giving

rise to disproportionately elevated methane in the highest-methane samples (e.g., from a dilution and/or calculation error) could have resulted in a false positive correlation with proximity to nearest UOG well reported in the earlier studies[3,4]. It is difficult to validate this possibility due to scarcity of experimental details, but it is noteworthy that the earlier observations included several samples that had methane concentrations well over the methane saturation limit (about 22 mg/L at 25 °C), up to approximately 70 mg/L. Such values are not impossible; one can super-saturate a water via methane over-pressurization in the subsurface. Nevertheless, if these values were affected by a quantification error, especially one disproportionately affecting highest-methane samples, it may have given rise to the surprisingly high levels of methane observed in the near-gas-well region. If erroneous, those skewed-high values would have contributed to a finding that methane levels were statistically higher within a kilometer of hydraulic fracturing wells. Our results (with rigorous quality assurances; see SI) stand in contrast to this earlier finding. Last, we emphasize that if all the data are trustworthy, then the Jackson et al.[4] and Osborn et al.[3] findings considered in light of our more recent investigation would imply temporal transience in methane releases to groundwaters, underscoring the importance of frequent evaluation and/or deeper understanding of transport mechanisms driving transience.

To evaluate the possibility that well integrity violations could augment methane migration, we investigated the correlation between the distance to such violations (inspected on or before sampling campaign start date) and groundwater methane levels. Our analysis showed no statistically significant correlation between methane concentration and the distance to the nearest well integrity violations (Fig. 1B, Spearman correlation $\rho = -0.078$, p-value = 0.45) and the insignificant correlation persisted when violations of all kinds, including spillage of flowback

water, were included (Fig. S3C). Extending this analysis to other geospatial metrics yielded the same conclusion: there was no statistically significant correlation between methane levels in groundwater and the O&G or UOG well or violation intensity within radii of 1km, 2km, 5km or 10km centered at the sampled water well (Fig. S4). Furthermore, the nearest gas well having integrity violation, other violation, or no violation did not result in statistically significant difference in dissolved methane levels of water wells (Fig. S5).

The lack of a significant correlation between methane levels and UOG spatial metrics either indicates the deficiency of using spatial metrics to anticipate UOG-related impacts *or* provides evidence for a lack of systematic contamination events derived from the extraction wells themselves. In any scenario, there is a need for more detailed geochemical analysis to elucidate methane migration pathways to the high methane-containing groundwater wells.

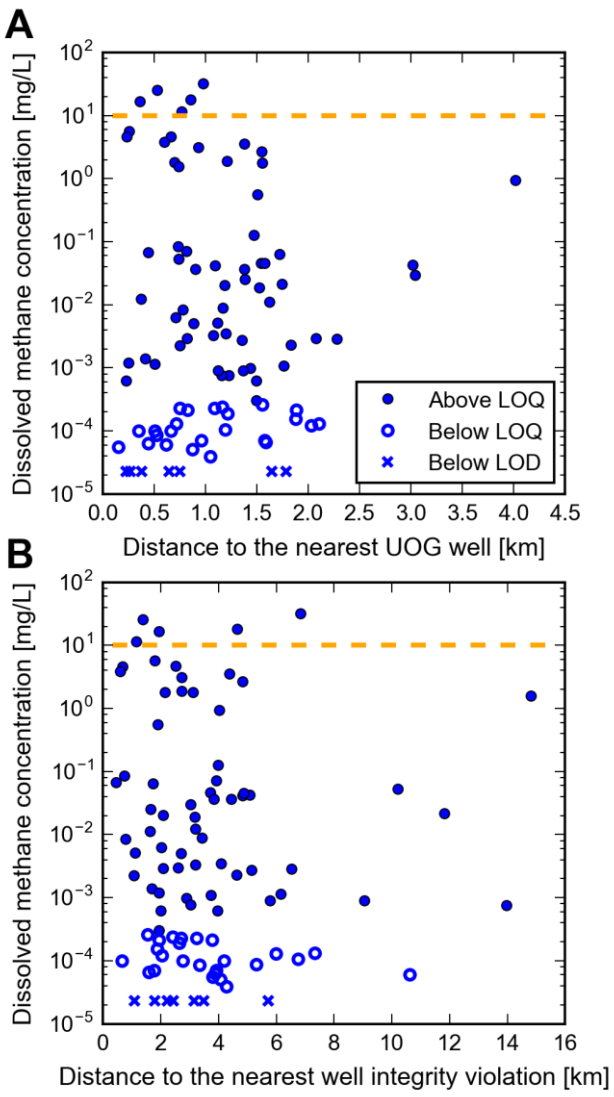

Figure 1. Dissolved methane concentrations and distances to (A) the nearest UOG well and (B) the nearest well integrity violation lack statistically significant correlation. The warning level recommended by the U.S. Department of the Interior[1] is shown (10 mg/L, dashed line). The symbols represent methane concentrations above the limit of quantification (LOQ) (filled circles, n=62; LOQ = 2.7 × 10^{-4} mg/L, the lowest concentration at which a calibration standard was run); concentrations below LOQ but above the limit of detection (LOD) (open circles, n=25; LOD = 2.3 × 10^{-5} mg/L); concentrations below LOD (crosses, n=7; see SI for detail on LOQ and LOD). All are the average of duplicate samples (except three); error bars are omitted for clarity and can be found in Fig. S6.

Geochemical indicators

While UOG proximity and intensity metrics do not support a UOG-derived methane source, isotopic tracers may help delineate the origins of the methane. Thermogenic methane generated by decomposition of organic matter is relatively enriched in heavier isotopes and exhibits higher $\delta^{13}C$ and $\delta^{2}H$ signatures, whereas biogenic methane produced by anaerobic methanogenesis is depleted in heavier isotopes and exhibits lower $\delta^{13}C$ and $\delta^{2}H$ signatures. Among our samples with the highest methane concentrations (n=18 over 0.5 mg/L), the majority (n=14) had isotopic signatures consistent with thermogenic methane ranges (delineated by literature[29,32]), whereas one sample fell in the CO_2 reduction biogenic region, and a few samples showed signs of mixed biogenic and thermogenic sources (Fig. 2). Of note, most groundwater samples were isotopically more depleted than previous groundwater samples reported in Sugar Run, Bradford County[29] and Dimock, Susquehanna County[30] (Fig. 2). These earlier analyses suggested that groundwater samples were impacted by drilling based on dissolved methane $\delta^{2}H$-$\delta^{13}C$ signatures reflecting signatures of nearby annular gas. This was attributed to stray gas migration due to improper cementation and excessive annular pressure in several nearby gas wells.[29] While we did not sample those same locations, groundwater samples within 4 km of the earlier Sugar Run study[29] (marked A and B in Fig. 2 and Fig. S7) had much lighter $\delta^{13}C$ values and did not reflect direct impacts from annular gas methane. In response to PADEP's citation in 2011, the gas company remediated the problematic Sugar Run gas wells (e.g., cement squeezes and plugs)[29] and the apparent disparity between our analyses and the earlier measurements could result from multiple spatial, temporal, or geochemical factors. Only one groundwater methane sample from our study

enriched in $\delta^{13}C$ (-31.9 ‰, as one might expect from thermogenic annular gas) but exhibited heavily enriched $\delta^{2}H$ (-76.9 ‰), outside the range of typical thermogenic sources. We postulate that this sample underwent significant microbial oxidation based on the large enrichment of $\delta^{2}H$, as microbial oxidation is known to increase $\delta^{2}H$-CH_4[33,34].

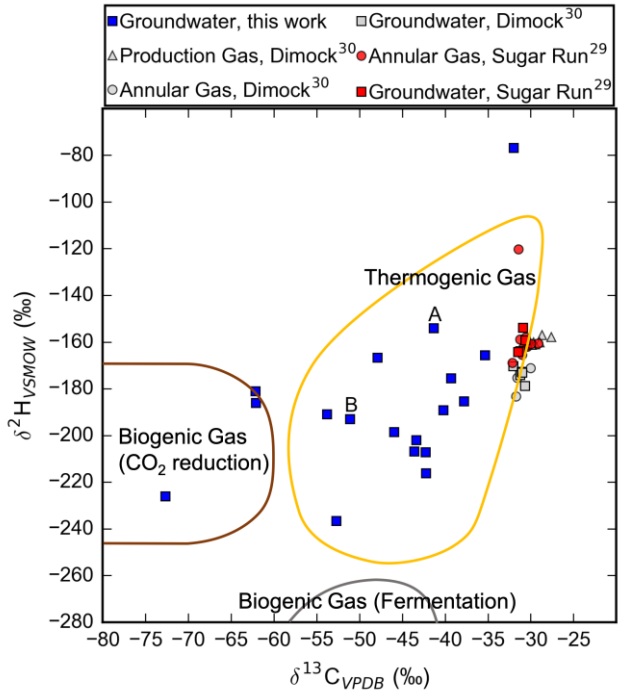

Figure 2. The methane carbon and hydrogen isotopic signatures of dissolved methane. For the majority of samples assayed in this study (blue squares), the methane $\delta^{13}C$ and $\delta^{2}H$ signatures were depleted relative to the production/annular gas and impacted water dissolved gas from previous studies (all other symbols). The symbols represent groundwater samples with dissolved methane concentration greater than 0.5 mg/L (n = 18) collected in Bradford and Tioga County in 2018 (this study; blue squares); previous production gas (light gray triangles), annular gas (light gray circles), and impacted groundwater (light gray squares) collected in Dimock, Susquehanna County, PA in 2009[30]; and previous annular gas (red circles) and impacted groundwater (red squares) collected in Sugar Run, Bradford County from 2010 to 2012[29]. The approximate isotope ranges for microbial gases (CO_2 reduction in brown outline, fermentation in gray outline) and thermogenic gas (yellow outline) are adapted from literature[29,32].

Samples A and B were collected near the sampling locations of prior Sugar Run samples[29] (see Fig. S7). VSMOW stands for Vienna Standard Mean Ocean Water and VPDB stands for Vienna Pee Dee Belemnite, the standard materials against which the isotopic values were measured.

It is possible that the $\delta^{13}C$ and $\delta^{2}H$ of groundwater methane fall in the thermogenic range due to post-genic alteration of biogenic methane by microbial oxidation. Starting with previously reported average $\delta^{13}C$ of biogenic methane by marine CO_2 reduction or freshwater fermentation ($\delta^{13}C_{VPDB}$ = -68‰ or -59‰, respectively;)[35], we calculated that median initial methane concentrations would have to be 27 g/L or 1.4 g/L, respectively, in order for microbial oxidative fractionation of methane to account for the observed $\delta^{13}C_{VPDB}$ values (see SI). These numbers are outside the realm of known maximum dissolved methane concentrations for over 10,000 pre-drilling groundwater records in Bradford County (max 72.1 mg/L)[10]. A sensitivity analysis over reasonable ranges of initial $\delta^{13}C$ and kinetic isotopic fractionation factors, ϵ, confirmed that unreasonably high initial methane concentrations would be necessary to explain the observed isotopic values (Fig. S8). Thus, the paired $\delta^{13}C$ and $\delta^{2}H$ suggest a source of dissolved methane that was thermogenic or mixture of biogenic and thermogenic in origin (possibly with moderate degree of microbial oxidation), rather than purely biogenic methane undergoing microbial oxidation.

Since microbial methanogenesis selectively produces methane (C_1) over ethane and propane ($C_2 + C_3$), biogenic gas has high molar ratios of C_1 -to- $C_2 + C_3$. In comparison, thermogenic gas contains higher levels of higher chain hydrocarbons (e.g., ethane and propane) and consequently lower C_1-to-$C_2 + C_3$ ratios (Fig. 3). All of samples with elevated ethane and/or propane (n = 8 above LOQ, Fig. 3) had enriched methane $\delta^{13}C$ values and also high C_1-to-$C_2 + C_3$ ratios. That

is, these indicators did not imply distinctly thermogenic or biogenic methane sources. Mixing lines connecting thermogenic and biogenic extremes (corners of shaded areas, Fig. 3) could not explain the observations, suggesting that mixing between biogenic and thermogenic gases was not responsible for the apparently conflicting $\delta^{13}C$ values and C_1-to-$C_2 + C_3$ ratios. Reconciling the relatively enriched $\delta^{13}C$ values with elevated C_1-to-$C_2 + C_3$ ratios of our gas samples compared to the range of typical thermogenic gas (Fig. 3) requires a mechanism that results in preferential enrichment of methane (relative to ethane and propane) without affecting the $\delta^{13}C$-CH_4 values substantially. Gas-water fractionation has small impacts on $\delta^{13}C$-CH_4 values (on the order of a few permil), but can influence molar ratios of molecules. Indeed, others have invoked equilibrium partitioning fractionation to explain increases in the hydrocarbon ratios,[36,37] but this model is difficult to justify experimentally and especially in the absence of supporting noble gas data. The observation of high C_1-to-$C_2 + C_3$ ratios have been reported by other researchers working in the Northern Appalachian Basin ($\delta^{13}C$ between -30 and -50 ‰ while C_1-to-C_{2+} above 1,000)[4,36–38]. As such, it is possible that the relatively high hydrocarbon ratios could also be a distinguishing characteristic of the formations themselves.

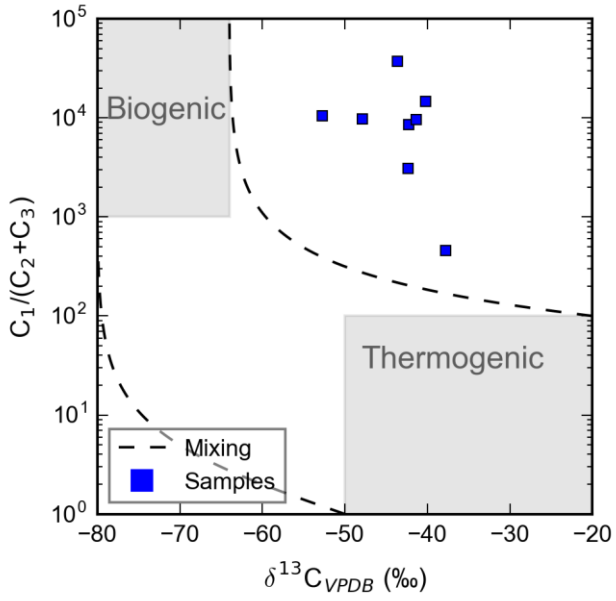

Figure 3. The C_1-to-C_2 + C_3 ratio vs. $\delta^{13}C$-CH_4 of high methane concentration samples. The shaded areas represent typical biogenic and thermogenic gas ranges adapted from literature[4,39]. High-methane groundwater samples with dissolved ethane or propane concentration above LOQ (n = 8, blue squares) and calculated mixing lines (dashed lines) are illustrated.

Reexamining the dissolved methane $\delta^{13}C$ signatures (-53.8 to -35.3 ‰, excluding the microbially oxidized outlier) in this context, we find these values were similar to those of Upper Devonian gases from Catskill and Lockhaven formations overlying the Marcellus shale (n = 238, mean = -42.1 ± 6.3 ‰)[39], which were depleted compared to the Middle Devonian Marcellus production gases (-30.0 to -27.6 ‰)[30]. Further, the dissolved methane $\delta^{13}C$ signatures were not correlated with distances to the nearest UOG well or concentrations of dissolved methane (Fig. S9). Taken together, the evidence presented here is consistent with groundwater dissolved methane originating from the Upper Devonian thermogenic gas.

Geochemical fingerprinting of water masses

To further understand the origin of groundwater dissolved methane in the context of fluid transport, we leveraged an inorganic geochemical fingerprinting framework developed by Warner et al.[40]. In this framework, low-salinity Water Types A and B were defined by Cl concentration lower than 20 mg/L; among samples with Cl concentration greater or equal to 20mg/L, Type C was defined by low Br-to-Cl molar ratios (Br/Cl below 0.001), while Type D waters contained high Br-to-Cl ratios (Br/Cl greater than or equal to 0.001) and low Na-to-Cl ratios (Na/Cl below 5). Br-to-Cl ratios have served as important indicators for the source of groundwater salinity. For example, Br-to-Cl ratios less than or equal to 0.001 suggest

anthropogenic sources (e.g., road salts, sewage and animal waste),[41] whereas Br-to-Cl ratios greater than or equal to 0.001 are consistent with Appalachian Basin Brine[40]. Applying this classification scheme, the water type with the highest dissolved methane concentrations was Type D water (n = 12), followed by Type C (n = 6), and then Type A and B (n=75; Fig. 5A), where the methane concentrations were statistically distinguishable. A Welch's ANOVA test and Games-Howell post-hoc tests confirmed the statistically significant differences between population means of log-transformed methane concentrations within water types AB and D (assuming methane concentrations within each water type followed lognormal distribution; Welch's ANOVA p-value = 2.3×10^{-4}; post hoc pairwise adjusted p-values were: 2.7×10^{-5} (Type AB and D), 0.12 (Type C and D), and 0.76 (Type AB and C)).

Topographical location plays an important role in groundwater transport phenomenon and the influence from deeper formation water signatures, and these have a corresponding impact on methane concentrations in groundwater.[5,6,10,42] Classifying groundwater sampling locations as associated with either peaks (n = 1), upper slopes (n = 32), lower slopes (n = 33), or valleys (n = 28), we found that Type D water samples were located mostly in topographical lows (i.e., valleys and lower slopes) (Fig. 4) and methane concentrations were generally higher in valleys as compared to upper slope topographies (Fig. 5B). These results were statistically robust: population means of log-transformed methane concentrations between valley and upper slope, and between lower slope and upper slope, were statistically different (Welch's ANOVA test on log-transformed concentrations had p-value of 6.7×10^{-4}, where peaks were excluded due to insufficient sample size; Post hoc pairwise adjusted p-values were: 1×10^{-3} (valley and upper slope), 2.2×10^{-2} (lower slope and upper slope), and 3.3×10^{-1} (valley and lower slope)).

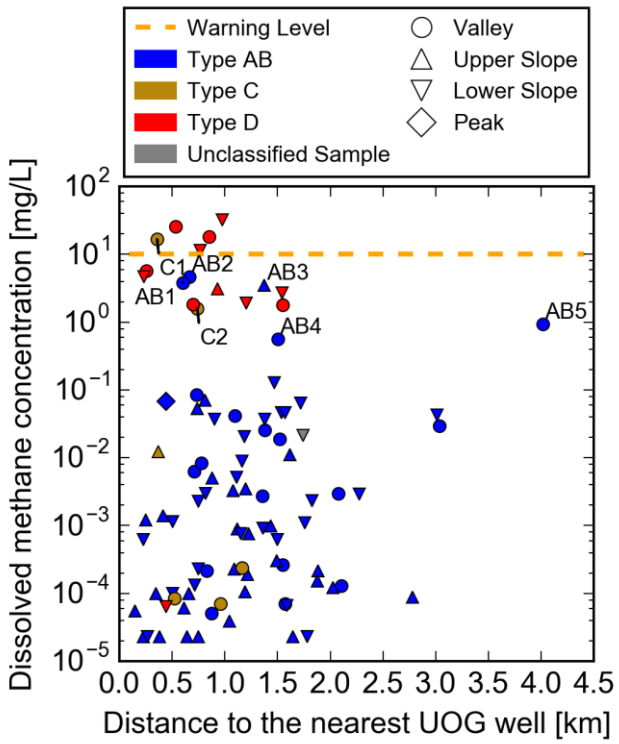

Figure 4. Water type and topography of sampling location are related to measured methane concentration. Type D water has the highest methane concentration among water types and is mostly occurring in topographically lower locations (i.e., valley and lower slope). Symbol colors distinguish groundwater samples of Type AB (blue), Type C (deep yellow) and type D (red), where there is one unclassified sample (grey). The samples labeled with letters and numbers are discussed in detail in the text. Topographical distinction of valley (circle), upper slope (upward triangle), lower slope (downward triangle), and peak (diamond) is indicated. Warning level set by the U.S. Department of the Interior is shown (dashed line; 10 mg/L).

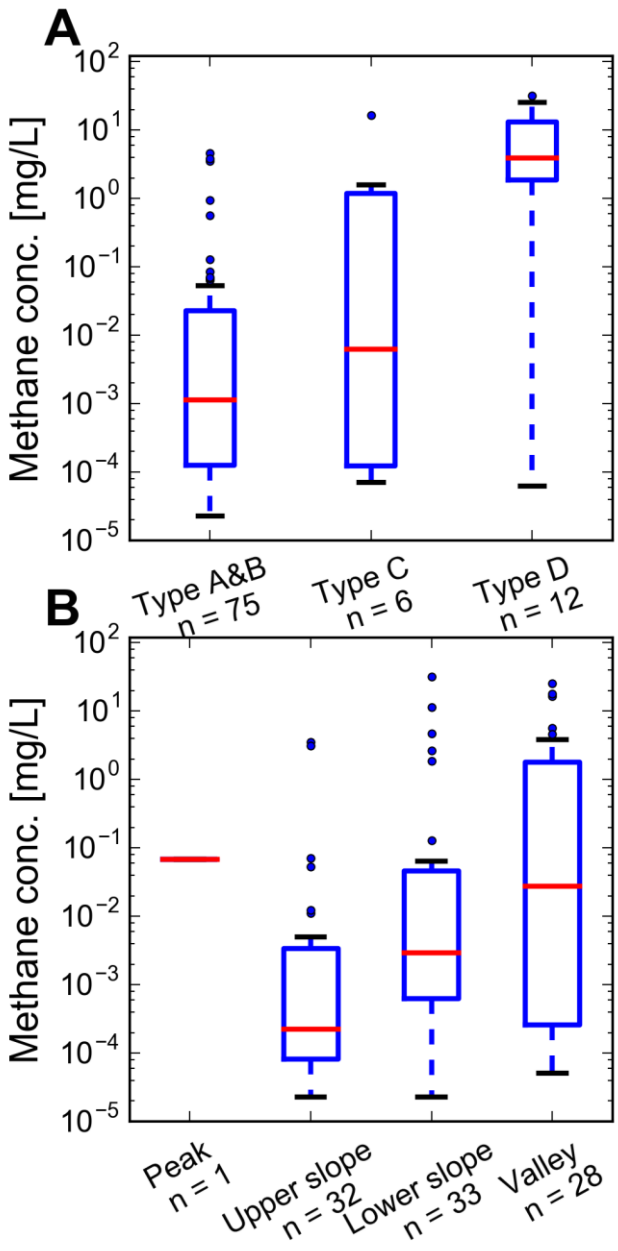

Figure 5. The distribution of methane concentration among different (A) water types and (B) topographical groups. Each box extends from the lower quartile (Q1) to the upper quartile (Q3) of the data, the horizontal bar is the median, and flier points are data that extend past the whiskers. Median methane concentrations increase from low saline water type (AB) to high saline and Br/Cl ratio water type (D) and increase with lowering topographical location (from upper slope to valley).

The co-occurrence of high groundwater dissolved methane concentration, saline Type D groundwater, and low topographical feature can be explained by the upward migration of thermogenic methane and deep Appalachian Basin Brine. Warner et al. previously illustrated that the saline Type D water reflects fingerprints of Appalachian Basin Brine, especially that from Middle Devonian and lower formations;[40] we confirmed this in the inorganic signatures of our water samples (Fig. S10). These brine fingerprints are a consequence of phenomena that occur over geological time, facilitated by the specific geology of NE PA.[10,40,42,43] Although the relatively shallow thermogenic methane and deep Appalachian Basin Brine originated from different geological formations, geological features (e.g., bedding plane partings, faults, and joints), can serve as preferential pathways for the upward migration of methane,[10,29] as well the deep brine to shallow groundwater aquifers. Those geological features have increased density under topographical lows or valleys,[44–48] and this potentially explains the co-enrichment of Type D water fingerprints and groundwater methane in those loci. Others have postulated additional potential mechanisms, such as groundwater discharging flow from uplands to valleys converging methane and brine tracers to topographical lows,[10,46] and shorter vertical distances between the valley water well bottoms and the underlying brine and thermogenic methane[46,49]. Such mechanisms could also explain the co-occurrence of Upper Devonian gas with Appalachian Basin Brine at topographical lows.

The association of Type D water, reflective of Appalachian Basin Brine, with elevated methane levels does not necessarily indicate those methane levels were derived from dissolved methane in deep formation fluids alone. Indeed, dilution factor analysis (based on median Cl^- levels) indicated a more than 1200-fold dilution of formation brine to generate Type D groundwaters.

This would correspond to brine formation fluids with methane concentrations on the order of 5,000 and 40,000 mg/L (median and maximum, respectively; note this calculation assumes groundwater methane originated from brine fluid alone, excluding shallow sources of biogenic methane). However, methane solubility of the lower Appalachian Basin Brine is estimated to be on the order of 1,100 mg/L (see SI; bottom hole temperature of 37 °C and pressure of 124 bars[50]), so diluted lower Appalachian Basin Brine alone cannot explain the elevated methane levels in Type D water samples. Instead, other methane sources such as Upper Devonian thermogenic gases and/or biogenic gases must also contribute to groundwater methane levels in NE PA. In addition, gas phase migration (e.g., gas bubbles) could also be a contributor to the groundwater methane.

There were several Type AB and Type C water samples (AB1 – AB5, C1 and C2; Fig. 4) that had relatively high methane concentrations (around or above 1 mg/L) but were not classified as brine-impacted water. Four of the Type AB samples (AB1, AB2, AB4, and AB5) were located in valleys and had relatively high Cl concentrations (10.2, 11.9, 14.4, and 16.1 mg/L, respectively, compared with median of 4.4 mg/L). Moreover, the Br/Cl ratio for AB1, AB2, and AB5 (0.001, 0.006, and 0.004, respectively) were all greater than the 0.001 threshold for Type D water. (We note that AB4 had non-detectable Br concentration). Thus, although these four samples were classified as Type AB water by the 20mg/L Cl concentration cut-off value defined by Warner et al.[40], they were still likely impacted by the same lower brine as in the Type D water based on their Br-to-Cl signature. Two saline Type C water samples (C1 and C2) with high methane concentrations were also located in valleys, which increased their vulnerability to be impacted by natural methane and brine migration. Both C1 and C2 had 50-150 feet (15 to 46 meters) self-

reported depth, which was relatively shallow among all sampled wells (Fig. S11). If correct, this shallow well depth might increase the probability of contamination by surface salinity source (e.g., road salt and animal waste), which could decrease their Br/Cl ratios down to the Type C range. Somewhat anomalously, sample AB3 had a relatively low Cl concentration (3.0 mg/L), high methane concentration (3.5 mg/L), an upper slope topography, and a relatively enriched isotope values ($\delta^{13}C$ of -39.32‰ and $\delta^{2}H$ of -175.4‰). This combination of characteristics is inconsistent with the natural methane migration mechanism explained by brine traces and topography. However, there is a relatively large distance between sample AB3 and the nearest O&G well and the nearest violation (1.4 km and 2.3 km, respectively). One possible explanation could be that the methane in sample AB3 originated from a shallow gas-bearing formation connected with fresh groundwater cycle and independent from brine migration. However, it is not entirely clear why sample AB3 has a high methane level, and this may underscore the importance of explicit measurement in addition to topographical or hydrogeological, or geochemical prediction alone.

In spite of such unusual occurrences, surface topography plays an important role in *where* groundwater characteristics, such as elevated methane or signatures of deep formation brines, can be observed. The sampling size, distribution of samples, and analysis of a large suite of geochemical indicators are necessary to deconvolute these controlling factors of methane level, and this may explain why debate has persisted on the origins of methane in this region, even after decades of study. Here, our near comprehensive geochemical analysis allows us to uncover dominant methane transport mechanisms and prioritize regions of risk near and about UOG activities.

Comparison with predrilling records

Comparing pre-industrial- and post-industrial-activity groundwater composition can provide compelling evidence of direct industrial impacts where they exist.[51] While there are no groundwater methane records predating all oil and gas extraction in Pennsylvania (onset circa 1850s), there are ample methane records before nearby proposed UOG wells were drilled (i.e., pre-drilling records). We accessed 64 pre-drilling methane measurements made between 2009 and 2016 at 49 locations which were again sampled as part of our 2018 sampling effort. The pre-drilling data were acquired from the Shale Network database[10,28] and matched with our sampling locations, or provided by the homeowners. Comparing the pre- and post-drilling methane levels indicated there was no systematic or statistically significant increase following installation and operation of UOG wells (Fig. 6; p-value = 0.17; Welch's t-test between log-transformed above-LOD pre-drilling concentrations (n=23) and the corresponding post-drilling concentrations). Some locations (n = 12) experienced a degree of increase from pre-drilling to post-drilling methane concentration, but such increases were mostly within a factor of two (e.g., 10.7 to 18.0 or 25.2 to 32.1 mg/L, Fig. 6B). Here, it is important to note the possibility that quantitative differences are a consequence of the variable measurement techniques or natural temporal fluctuations of methane level[51]. Notably, the water well with the highest post-drilling concentration (32.1 mg/L in 2018) was sampled in November 2010 and contained no detectable methane (presumably below 0.02 or 0.03 mg/L methane, marked as "2010-11", Fig. 6A). However, only two months later, the concentration was recorded at 25.2 mg/L (marked as "2011-01", Fig. 6A). Interestingly, this groundwater well belongs to lower slope topographic class and

had a Type D geochemical signature in our analysis, which could make it more vulnerable to elevated methane irrespective of industrial activity. Overall, a comparison between the recent methane concentration measurements and historical pre-drilling measurements of a subset of sampled locations supported that methane occurrence was a natural phenomenon in NE PA that largely predates the UOG installations in this region.

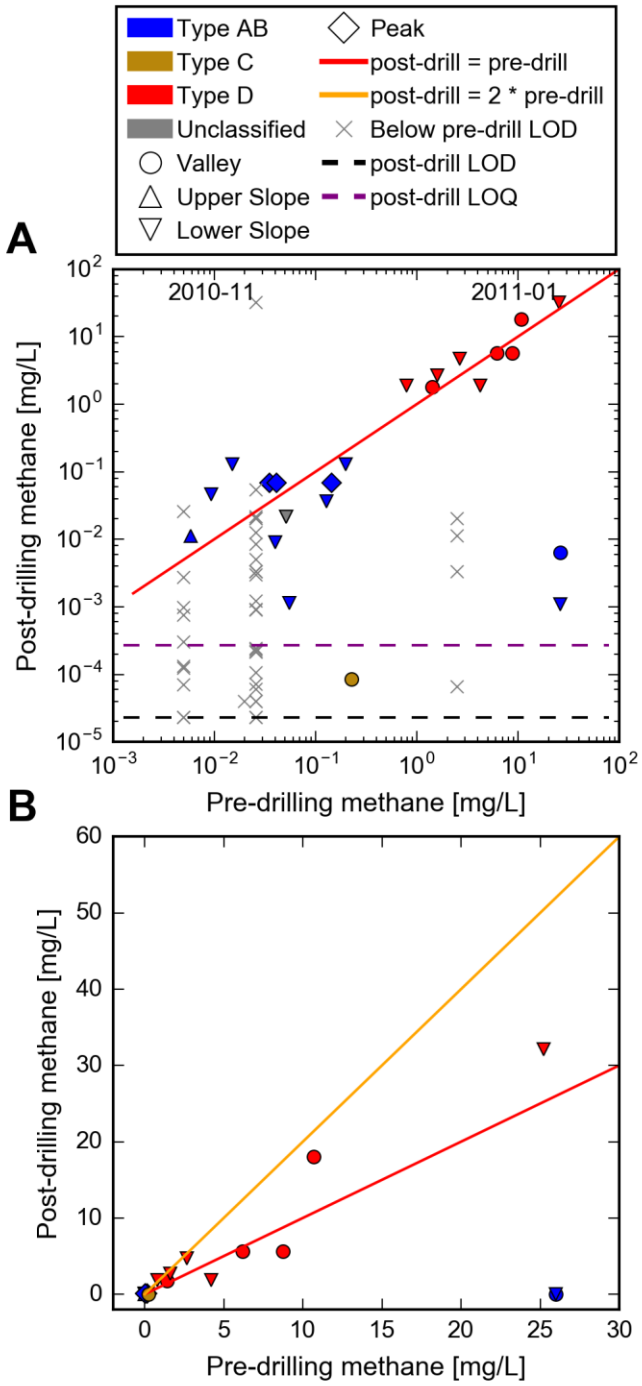

Figure 6. Comparison between pre-drilling and post-drilling methane concentrations. (A) Log-scale pre- and post-drilling methane measurements (n=64 at 49 distinct locations). These pre-drilling measurements were from the years of 2009 (n=3), 2010 (n=16), 2011 (n=35), 2012 (n=7), 2014 (n=1), and 2016 (n=1), with one measurement missing a date. Post-drilling measurements' LOD and LOQ (this

study, 2018 samples) are indicated with black and purple horizontal dashed lines, respectively; LODs of pre-drilling analyses were not always explicit but might be evident as vertically aligned values (below-LOD pre-drilling measurements are shown as gray crosses aligned on four vertical lines at 0.005, 0.02, 0.026 and 2.5 mg/L, see SI for the treatment of pre-drilling measurements below LODs). Above-LOD pre-drilling measurements are marked by colors and shapes the same as in Fig. 4 (water type: type AB in blue, type C in deep yellow, type D in red, and unclassified type in grey; topography: valley in circle, upper slope in upward triangle, lower slope in downward triangle, and peak in diamond). (B) Linear scale plot reflecting samples above LOD only. Post-drilling concentration equaling one and two times of pre-drilling concentration are represented by the red and orange line, respectively.

Estimation of natural methane emission

Methane emissions associated with groundwater discharge represents a potential contribution to GHG over geological time. Thus, we sought to estimate the methane emission caused by discharge of methane-containing groundwater to surface-water bodies in NE PA to bound the contribution of this understudied source term. Using the long-term mean groundwater recharge rate in Bradford County (0.198 m/year)[52,53] and assuming this represents total groundwater discharge (including extraction), the area of Bradford County (2972 km^2)[54], and the median measured dissolved methane concentration of 2.8×10^{-3} mg/L (or $1.4 \times 10^{-4} – 5.2 \times 10^{-2}$ mg/L, representing the 25th and 75th percentile of the concentration distribution, respectively; n= 94), we estimated groundwater discharge methane emission in this one county to be on the order of 2 (or 0.08 – 30) tonnes CH_4 /year. As a comparison, the median dissolved methane concentration in Bradford County reported by Wen et al.[10] (more than 10,000 pre-drilling values) was 0.026 mg/L, which equaled one of the detection limits in the pre-drilling dataset. Using this

groundwater methane limit, the county-level groundwater discharge emission was estimated to be around 15 tonnes CH_4/year. For further comparison, methane emission from non-wetland surface water bodies in Bradford County was estimated to be on the order of 1000 (200 – 2500) tonnes CH_4 / year. (This number reflects an estimate derived from considering areal methane fluxes from inland waters[55] and the total area of inland waters in Bradford County[56], see SI). As another reference, the total bottom-up estimation of methane emission (fugitive and engineered vent emission) by active O&G wells in Bradford County was on the order of 400 tonnes CH_4/year. (Briefly, this estimate is based on PA statewide emission rate averages per gas well, derived by Ingraffea et al. from measured annulus flow rates,[57] and the number and type of active gas wells in Bradford County; see SI). Noticeably, the estimated groundwater discharge methane emission was much smaller than the estimated non-wetland surface water emission or O&G well emission. While methane emissions through groundwater releases (i.e., discharge to surface water) in these methane-rich areas could help delineate a more rigorous construction of the global methane budget, more important terms may occur in regions where groundwater withdrawals are dominated by human population development, including industrial groundwater withdrawals. In these cases, there may be value in assessing the presence of an unanticipated methane emission source to the atmosphere.

Implications

Since the 2005 Energy Policy Act, domestic natural gas extraction in the US has disrupted the global energy economy, dramatically changed the US electricity source portfolio, and allowed the US to become a net exporter of oil and gas. Furthermore, in accounting of GHG budgets,

natural gas utilization that displaces coal or oil-derived hydrocarbons comes with a GHG credit. This higher energy-per-unit CO_2 equivalent of the energy source - rather than a sweeping transition from fossil energy to renewable solar or wind-derived energy- is dominantly responsible for the US' progress toward meeting Paris Agreement targets. However, fugitive emissions from methane associated with natural gas extraction are not included in this credit. Howarth et al.[58] and others sounded an early warning to encourage constraint of the contribution of fugitive methane emissions from gas extraction processes to the atmosphere that might reduce the net climate benefits of natural gas utilization. Osborn et al.[3] and Jackson et al.[4] highlighted early concerns that gas extraction might augment releases of methane into groundwater and also identified the need to protect the domestic water supply with respect to flammability limits.
In this work, we revisited those considerations following an intensified installation of gas extraction wells and allowing for longer temporal evolution to alleviate kinetic limitations on observing the impacts of gas extraction in field-based groundwater samples. Here, based on a large groundwater sample size (n=94) of methane and important geochemical indicators, we analyzed a combination of various UOG geospatial metrics, topographical information, and pre- and post-drilling comparison of same locations. We demonstrated that methane transport to groundwater over the Marcellus Shale is arguably natural and has not been systematically augmented by unconventional oil and gas extraction, although localized incidents of UOG-induced methane migration do occur (e.g., the stray gas migration incident in Sugar Run, Bradford County)[29].

Importantly, even if through natural processes, our finding that groundwater methane levels are sometimes elevated has important implications. In particular, topographical features and

underlying geological structures can influence the likelihood that thermogenic methane will accumulate in groundwaters. This information can be used to prioritize regions of investigation, but also underscores the need of evaluating methane in groundwater on a shale-by-shale basis. Indeed, it is not at all clear groundwater impacts will scale uniformly across entire shale plays and certainly not between different plays. Thus, evaluating methane migration in a heterogeneous suite of geographies is necessary to constrain methane fluxes writ large and understand the role of domestic gas extraction on the global climate.

IRB Information

The study protocol was approved by the Institutional Review Board (IRB) of Yale University (HIC # 2000021809) and the US Environmental Protection Agency (#HSR-001162). All participants provided informed consent prior to any data collection activities.

Supporting Information

Methodology details including hydrocarbon and dissolved ion measurements, construction of spatial metrics and topographical classes, and the collection of pre-drilling data; additional figures and tables are available in the Supporting Information.

Acknowledgments

The authors want to thank UC Davis Stable Isotope Facility for providing isotopic analysis, and Julie Plano and Keli Sorrentino for their support in data management and processing. This publication was developed under Assistance Agreement No. CR839249 awarded by the U.S. Environmental Protection Agency to Yale University. It has not been formally reviewed by EPA.

The views expressed in this document are solely those of the authors and do not necessarily reflect those of the Agency. EPA does not endorse any products or commercial services mentioned in this publication.

References

(1) Eltschlager, K. K.; Hawkins, J. W.; Ehler, W. C.; Baldassare, F. J. Technical Measures for the Invetigation and Mitigation of Fugitive Methane Hazards in Areas of Coal Mining, U.S. Department of the Interior, Office of Surface Mining. **2001**.

(2) U.S. Energy Information Administration. *Annual Energy Outlook 2021 Chart Library*; Washington, DC, 2021.

(3) Osborn, S. G.; Vengosh, A.; Warner, N. R.; Jackson, R. B. Methane Contamination of Drinking Water Accompanying Gas-Well Drilling and Hydraulic Fracturing. *Proc. Natl. Acad. Sci.* **2011**, *108* (20), 8172–8176. https://doi.org/10.1073/pnas.1100682108.

(4) Jackson, R. B.; Vengosh, A.; Darrah, T. H.; Warner, N. R.; Down, A.; Poreda, R. J.; Osborn, S. G.; Zhao, K.; Karr, J. D. Increased Stray Gas Abundance in a Subset of Drinking Water Wells near Marcellus Shale Gas Extraction. *Proc. Natl. Acad. Sci. U. S. A.* **2013**, *110* (28), 11250–11255. https://doi.org/10.1073/pnas.1221635110.

(5) Molofsky, L. J.; Connor, J. A.; Farhat, S. K.; Wylie, A. S.; Wagner, T. Methane in Pennsylvania Water Wells Unrelated to Marcellus Shale Fracturing. *Oil Gas J.* **2011**, *109* (19).

(6) Molofsky, L. J.; Connor, J. A.; Wylie, A. S.; Wagner, T.; Farhat, S. K. Evaluation of Methane Sources in Groundwater in Northeastern Pennsylvania. *GroundWater* **2013**, *51* (3), 333–349. https://doi.org/10.1111/gwat.12056.

(7) Siegel, D. I.; Azzolina, N. A.; Smith, B. J.; Perry, A. E.; Bothun, R. L. Methane Concentrations in Water Wells Unrelated to Proximity to Existing Oil and Gas Wells in Northeastern Pennsylvania. *Environ. Sci. Technol.* **2015**, *49* (7), 4106–4112. https://doi.org/10.1021/es505775c.

(8) Li, Z.; You, C.; Gonzales, M.; Wendt, A. K.; Wu, F.; Brantley, S. L. Searching for Anomalous Methane in Shallow Groundwater near Shale Gas Wells. *J. Contam. Hydrol.* **2016**, *195*, 23–30. https://doi.org/10.1016/j.jconhyd.2016.10.005.

(9) Li, Z.; You, C.; Gonzales, M.; Wendt, A. K.; Wu, F.; Brantley, S. L. Corrigendum to "Searching for Anomalous Methane in Shallow Groundwater near Shale Gas Wells" (J. Contam. Hydrol. (2016) 195 (23–30) (S0169772216300985) (10.1016/j.Jconhyd.2016.10.005)). *Journal of Contaminant Hydrology*. Elsevier B.V. December 1, 2017, pp 50–51. https://doi.org/10.1016/j.jconhyd.2017.09.009.

(10) Wen, T.; Niu, X.; Gonzales, M.; Zheng, G.; Li, Z.; Brantley, S. L. Big Groundwater Data Sets Reveal Possible Rare Contamination Amid Otherwise Improved Water Quality for Some Analytes in a Region of Marcellus Shale Development. *Environ. Sci. Technol.* **2018**, *52* (12), 7149–7159. https://doi.org/10.1021/acs.est.8b01123.

(11) Wen, T.; Liu, M.; Woda, J.; Zheng, G.; Brantley, S. L. Detecting Anomalous Methane in

Groundwater within Hydrocarbon Production Areas across the United States. *Water Res.* **2021**, *200*, 117236. https://doi.org/10.1016/j.watres.2021.117236.
(12) Pennsylvania Department of Environmental Protection. Oil Gas Locations - Unconventional https://newdata-padep-1.opendata.arcgis.com/datasets/oil-gas-locations-unconventional?geometry=-81.196%2C40.740%2C-74.247%2C42.181 (accessed Mar 24, 2020).
(13) Mayfield, E. N.; Cohon, J. L.; Muller, N. Z.; Azevedo, I. M. L.; Robinson, A. L. Cumulative Environmental and Employment Impacts of the Shale Gas Boom. *Nat. Sustain.* **2019**, *2* (12), 1122–1131. https://doi.org/10.1038/s41893-019-0420-1.
(14) U.S. Environmental Protection Agency. GHG Inventory Development Process and Guidance https://www.epa.gov/climateleadership/ghg-inventory-development-process-and-guidance (accessed Nov 1, 2021).
(15) U.S. Environmental Protection Agency. *GHG Emission Factors Hub*; 2021.
(16) U.S. Environmental Protection Agency. Emissions & Generation Resource Integrated Database (eGRID) https://www.epa.gov/egrid (accessed Nov 1, 2021).
(17) Heilweil, V. M.; Grieve, P. L.; Hynek, S. A.; Brantley, S. L.; Solomon, D. K.; Risser, D. W. Stream Measurements Locate Thermogenic Methane Fluxes in Groundwater Discharge in an Area of Shale-Gas Development. *Environ. Sci. Technol.* **2015**, *49* (7), 4057–4065. https://doi.org/10.1021/es503882b.
(18) Woda, J.; Wen, T.; Lemon, J.; Marcon, V.; Keeports, C. M.; Zelt, F.; Steffy, L. Y.; Brantley, S. L. Methane Concentrations in Streams Reveal Gas Leak Discharges in Regions of Oil, Gas, and Coal Development. *Sci. Total Environ.* **2020**, 140105. https://doi.org/10.1016/j.scitotenv.2020.140105.
(19) Stanley, E. H.; Casson, N. J.; Christel, S. T.; Crawford, J. T.; Loken, L. C.; Oliver, S. K. The Ecology of Methane in Streams and Rivers: Patterns, Controls, and Global Significance. *Ecol. Monogr.* **2016**, *86* (2), 146–171. https://doi.org/10.1890/15-1027.
(20) Pinti, D. L.; Gelinas, Y.; Moritz, A. M.; Larocque, M.; Sano, Y. Anthropogenic and Natural Methane Emissions from a Shale Gas Exploration Area of Quebec, Canada. *Sci. Total Environ.* **2016**, *566–567*, 1329–1338. https://doi.org/10.1016/j.scitotenv.2016.05.193.
(21) Gooddy, D. C.; Darling, W. G. The Potential for Methane Emissions from Groundwaters of the UK. *Sci. Total Environ.* **2005**, *339* (1–3), 117–126. https://doi.org/10.1016/j.scitotenv.2004.07.019.
(22) Crawford, J. T.; Striegl, R. G.; Wickland, K. P.; Dornblaser, M. M.; Stanley, E. H. Emissions of Carbon Dioxide and Methane from a Headwater Stream Network of Interior Alaska. *J. Geophys. Res. Biogeosciences* **2013**, *118* (2), 482–494. https://doi.org/10.1002/jgrg.20034.
(23) Kulongoski, J. T.; McMahon, P. B. Methane Emissions from Groundwater Pumping in the USA. *npj Clim. Atmos. Sci.* **2019**, *2* (1), 1–8. https://doi.org/10.1038/s41612-019-0068-6.
(24) Soriano, M. A.; Siegel, H. G.; Gutchess, K. M.; Clark, C. J.; Li, Y.; Xiong, B.; Plata, D. L.; Deziel, N. C.; Saiers, J. E. Evaluating Domestic Well Vulnerability to Contamination From Unconventional Oil and Gas Development Sites. *Water Resour. Res.* **2020**, *56* (10), 1–24. https://doi.org/10.1029/2020WR028005.
(25) Soriano, M. A.; Siegel, H. G.; Johnson, N. P.; Gutchess, K. M.; Xiong, B.; Li, Y.; Clark, C. J.; Plata, D. L.; Deziel, N. C.; Saiers, J. E. Assessment of Groundwater Well Vulnerability to Contamination through Physics-Informed Machine Learning. *Environ.*

Res. Lett. **2021**, *16* (8), 084013. https://doi.org/10.1088/1748-9326/AC10E0.
(26) Clark, C. J.; Xiong, B.; Soriano, M. A.; Gutchess, K.; Siegel, H. G.; Ryan, E. C.; Johnson, N. P.; Cassell, K.; Elliott, E. G.; Li, Y.; Cox, A. J.; Bugher, N.; Glist, L.; Brenneis, R. J.; Sorrentino, K. M.; Plano, J.; Ma, X.; Warren, J. L.; Plata, D. L.; Saiers, J. E.; Deziel, N. C. Assessing Unconventional Oil and Gas Exposure in the Appalachian Basin: Comparison of Exposure Surrogates and Residential Drinking Water Measurements. *Environ. Sci. Technol.* **2022**, *56* (2), 1091–1103. https://doi.org/10.1021/acs.est.1c05081.
(27) Xiong, B.; Soriano, M. A.; Gutchess, K. M.; Hoffman, N.; Clark, C. J.; Siegel, H. G.; De Vera, G. A. D.; Li, Y.; Brenneis, R. J.; Cox, A. J.; Ryan, E. C.; Sumner, A. J.; Deziel, N. C.; Saiers, J. E.; Plata, D. L. Groundwaters in Northeastern Pennsylvania near Intense Hydraulic Fracturing Activities Exhibit Few Organic Chemical Impacts. *Environ. Sci. Process. Impacts* **2022**, 24 (2), 252–264. https://doi.org/10.1039/d1em00124h.
(28) Brantley, S. L. Shale Network Database, Consortium for Universities for the Advancement of Hydrologic Sciences, Inc. (CUAHSI) https://doi.org/10.4211/his-data-shalenetwork (accessed Nov 19, 2018).
(29) Llewellyn, G. T.; Dorman, F.; Westland, J. L.; Yoxtheimer, D.; Grieve, P.; Sowers, T.; Humston-Fulmer, E.; Brantley, S. L. Evaluating a Groundwater Supply Contamination Incident Attributed to Marcellus Shale Gas Development. *Proc. Natl. Acad. Sci. U. S. A.* **2015**, *112* (20), 6325–6330. https://doi.org/10.1073/pnas.1420279112.
(30) Hammond, P. A. The Relationship between Methane Migration and Shale-Gas Well Operations near Dimock, Pennsylvania, USA. *Hydrogeol. J.* **2016**, *24* (2), 503–519. https://doi.org/10.1007/s10040-015-1332-4.
(31) Darrah, T. H.; Vengosh, A.; Jackson, R. B.; Warner, N. R.; Poreda, R. J. Noble Gases Identify the Mechanisms of Fugitive Gas Contamination in Drinking-Water Wells Overlying the Marcellus and Barnett Shales. *Proc. Natl. Acad. Sci. U. S. A.* **2014**, *111* (39), 14076–14081. https://doi.org/10.1073/pnas.1322107111.
(32) Coleman, D.; Liu, C.; Hackley, K.; Benson, L. Identification of Landfill Methane Using Carbon and Hydrogen Isotope Analysis. In *Proceedings of the Sixteenth International Madison Waste Conference*; Univ Wisconsin, Madison WI, 1993; pp 303–314.
(33) Coleman, D. D.; Risatti, J. B.; Schoell, M. Fractionation of Carbon and Hydrogen Isotopes by Methane-Oxidizing Bacteria. *Geochim. Cosmochim. Acta* **1981**, *45* (7), 1033–1037. https://doi.org/10.1016/0016-7037(81)90129-0.
(34) Schout, G.; Hartog, N.; Hassanizadeh, S. M.; Griffioen, J. Impact of an Historic Underground Gas Well Blowout on the Current Methane Chemistry in a Shallow Groundwater System. *Proc. Natl. Acad. Sci. U. S. A.* **2017**, *115* (2), 296–301. https://doi.org/10.1073/pnas.1711472115.
(35) Whiticar, M. J.; Faber, E.; Schoell, M. Biogenic Methane Formation in Marine and Freshwater Environments: CO2 Reduction vs. Acetate Fermentation-Isotope Evidence. *Geochim. Cosmochim. Acta* **1986**, *50* (5), 693–709. https://doi.org/10.1016/0016-7037(86)90346-7.
(36) Harkness, J. S.; Darrah, T. H.; Warner, N. R.; Whyte, C. J.; Moore, M. T.; Millot, R.; Kloppmann, W.; Jackson, R. B.; Vengosh, A. The Geochemistry of Naturally Occurring Methane and Saline Groundwater in an Area of Unconventional Shale Gas Development. *Geochim. Cosmochim. Acta* **2017**, *208*, 302–334. https://doi.org/10.1016/j.gca.2017.03.039.
(37) Darrah, T. H.; Jackson, R. B.; Vengosh, A.; Warner, N. R.; Whyte, C. J.; Walsh, T. B.;

Kondash, A. J.; Poreda, R. J. The Evolution of Devonian Hydrocarbon Gases in Shallow Aquifers of the Northern Appalachian Basin: Insights from Integrating Noble Gas and Hydrocarbon Geochemistry. *Geochim. Cosmochim. Acta* **2015**, *170*, 321–355. https://doi.org/10.1016/j.gca.2015.09.006.

(38) Révész, K. M.; Breen, K. J.; Baldassare, A. J.; Burruss, R. C. Carbon and Hydrogen Isotopic Evidence for the Origin of Combustible Gases in Water-Supply Wells in North-Central Pennsylvania. *Appl. Geochemistry* **2010**, *25* (12), 1845–1859. https://doi.org/10.1016/j.apgeochem.2010.09.011.

(39) Baldassare, F. J.; McCaffrey, M. A.; Harper, J. A. A Geochemical Context for Stray Gas Investigations in the Northern Appalachian Basin: Implications of Analyses of Natural Gases from Neogene-through Devonian-Age Strata. *Am. Assoc. Pet. Geol. Bull.* **2014**, *98* (2), 341–372. https://doi.org/10.1306/06111312178.

(40) Warner, N. R.; Jackson, R. B.; Darrah, T. H.; Osborn, S. G.; Down, A.; Zhao, K.; White, A.; Vengosh, A. Geochemical Evidence for Possible Natural Migration of Marcellus Formation Brine to Shallow Aquifers in Pennsylvania. *Proc. Natl. Acad. Sci.* **2012**, *109* (30), 11961–11966. https://doi.org/10.1073/pnas.1121181109.

(41) Mullaney, J. R.; Lorenz, D. L.; Arntson, A. D. Chloride in Groundwater and Surface Water in Areas Underlain by the Glacial Aquifer System , Northern United States Scientific Investigations Report 2009 – 5086. *US Geol Surv Sci Invest Rep* **2009**, *5086*, 41.

(42) Siegel, D. I.; Smith, B.; Perry, E.; Bothun, R.; Hollingsworth, M. Pre-Drilling Water-Quality Data of Groundwater Prior to Shale Gas Drilling in the Appalachian Basin: Analysis of the Chesapeake Energy Corporation Dataset. *Appl. Geochemistry* **2015**, *63*, 37–57. https://doi.org/10.1016/j.apgeochem.2015.06.013.

(43) Williams, J. H.; Taylor, L. E.; Low, D. J. Hydrogeology and Groundwater Quality of the Glaciated Valleys of Bradford, Tioga, and Potter Counties, Pennsylvania. *Pennsylvania Geol. Surv. 4th ser. Water Resource Report 68*. **1998**.

(44) Mason, G. Structurally Related Migration Of Hydrocarbons in the Central Appalachian Basin of Eastern Ohio. *AAPG Search Discov. Artic. #50733* **2012**.

(45) Taylor, L. E. Groundwater Resources of the Upper Susquehanna River Basin, Pennsylvania. *Pennsylvania Geol. Surv. 4th ser. Water Resource Report 58.* **1984**.

(46) Heisig, P. M.; Scott, T.-M. Occurrence of Methane in Groundwater of South-Central New York State, 2012- Systematic Evaluation of a Glaciated Region by Hydrogeologic Setting. *Sci. Investig. Rep.* **2013**, *2013–5190*. https://doi.org/10.3133/sir20135190.

(47) Ferguson, H. F.; Hamel, J. V. Valley Stress Relief in Flat-Lying Sedimentary Rocks. *Weak rock soft, Fract. Weather. rock. Proc. Symp. Tokyo, Sept. 1981. Vol. 2* **1981**, 1235–1240.

(48) Wyrick, G. G.; Borchers, J. W. Hydrologic Effects of Stress-Relief Fracturing in an Appalachian Valley. *US Geol. Surv. Water Supply Pap.* **1981**. https://doi.org/10.3133/wsp2177.

(49) Williams, J. H. Evaluation of Well Logs for Determining the Presence of Freshwater, Saltwater, and Gas above the Marcellus Shale in Chemung, Tioga, and Broome Counties, New York. *New York Sci. Investig. Rep. 2010-5224, 27* **2010**.

(50) Sumner, A. J.; Plata, D. L. Exploring the Hydraulic Fracturing Parameter Space: A Novel High-Pressure, High-Throughput Reactor System for Investigating Subsurface Chemical Transformations. *Environ. Sci. Process. Impacts* **2018**, *20* (2), 318–331. https://doi.org/10.1039/c7em00470b.

(51) Barth-Naftilan, E.; Sohng, J.; Saiers, J. E. Methane in Groundwater before, during, and after Hydraulic Fracturing of the Marcellus Shale. *Proc. Natl. Acad. Sci.* **2018**, *115* (27), 6970–6975. https://doi.org/10.1073/pnas.1720898115.
(52) Reitz, M.; Sanford, W. E.; Senay, G. B.; Cazenas, J. Annual Estimates of Recharge, Quick-Flow Runoff, and Evapotranspiration for the Contiguous U.S. Using Empirical Regression Equations. *J. Am. Water Resour. Assoc.* **2017**, *53* (4), 961–983. https://doi.org/10.1111/1752-1688.12546.
(53) Reitz, M.; Sanford, W. E.; Senay, G. B.; Cazenas, J. Annual estimates of recharge, quick-flow runoff, and ET for the contiguous US using empirical regression equations, 2000-2013 https://doi.org/10.5066/F7PN93P0 (accessed Mar 14, 2021).
(54) U.S. Census Bureau QuickFacts: Bradford County, Pennsylvania https://www.census.gov/quickfacts/bradfordcountypennsylvania (accessed Mar 14, 2021).
(55) Rosentreter, J. A.; Borges, A. V; Deemer, B. R.; Holgerson, M. A.; Liu, S.; Song, C.; Melack, J.; Raymond, P. A.; Duarte, C. M.; Allen, G. H.; Olefeldt, D.; Poulter, B.; Battin, T. I.; Eyre, B. D. Half of Global Methane Emissions Come from Highly Variable Aquatic Ecosystem Sources. *Nat. Geosci.* **2021**, *14* (4), 225–230. https://doi.org/10.1038/s41561-021-00715-2.
(56) U.S. Fish & Wildlife Service National Wetlands Inventory https://www.fws.gov/wetlands/data/data-download.html (accessed May 14, 2021).
(57) Ingraffea, A. R.; Wawrzynek, P. A.; Santoro, R.; Wells, M. Reported Methane Emissions from Active Oil and Gas Wells in Pennsylvania, 2014-2018. *Environ. Sci. Technol.* **2020**, *54* (9), 5783–5789. https://doi.org/10.1021/acs.est.0c00863.
(58) Howarth, R. W.; Ingraffea, A.; Engelder, T. Natural Gas: Should Fracking Stop? *Nature*. Nature Publishing Group September 15, 2011, pp 271–273. https://doi.org/10.1038/477271a.

Supporting information for Chapter 2

Geological setting of the study area

The geological strata underlaying Bradford County and the surrounding Northeastern Pennsylvania (NE PA) area can be summarized as follows[1–3]: the surface geology is mainly characterized by unconsolidated glacial drift deposits (glacial till and outwash) and postglacial deposits (Quaternary alluvium). The postglacial deposit forms the Alluvium aquifer which consists of materials such as sands, gravel and silts. This deposit layer is generally thicker in valleys than in uplands.[1,2] The surface stratum is underlain by Pennsylvanian through Upper Devonian age rock formations, among which the Upper Devonian Catskill and Lock Haven formations are the two most common bedrock aquifers. These two aquifers mainly consist of sandstone, siltstone or shale and are the major water source for local water wells. Network of faults, joints and fractures existing in the Upper Devonian formations enhance the bedrock permeability as they serve as conduits for groundwater flow. Throughout the geologic history, the fracturing intensity has been enhanced by stress-relief and isostatic rebound effect caused by the glaciation-deglaciation cycles.[3] Beneath the Upper Devonian formations, the Middle Devonian formations include the Tully limestone, the Mahantango formation and the Marcellus Shale. The Marcellus Shale, which is the main target of shale gas development in the region, is approximately 1,500 to 2,500 m deep below the surface.[2] Formations in different strata are likely inter-connected by geological pathways such as joints and thrust faults.[3] Furthermore, the gentle folding of the underlying strata is expressed on the surface by the alternating synclines and anticlines.[3]

Supplemental methods

Sample locations

Water samples were collected from 90 domestic wells and 4 springs (89 in Bradford County and 5 in Tioga County with their zip codes intersecting with Bradford County) in NE PA (Fig S2). The study area was Bradford County, which had the second highest number of unconventional oil and gas (UOG) wells and the highest number of "water supply determination letters" (i.e., PA DEP determines a water supply to be impacted by O&G drilling) in NE PA upon sampling began.[4,5] We applied a participant-recruitment strategy for the determination of sampling locations. In order to maximize the number of participants, we applied multiple recruiting approaches, which included newspaper advertisements, flyers at local businesses, social media postings, and mailed informational postcards. We screened interested residents who responded to our recruitment methods based on the criteria that an eligible participant should be a head of household at least 21 years old, should speak English (for the necessity of collecting informed consent and completing interview-based questionnaires), and should live in a home served by private groundwater well or spring. Among the resulted 94 participating homes (Fig. S2), the minimum, mean, and maximum distance to the nearest UOG wells were 0.1 km, 1.1 km, and 4.0 km respectively; and the minimum, mean, and maximum count of UOG wells within a radius of 1 km centered at each home were 0, 1.8, and 22 respectively.

Sample collection

Water samples were collected upstream of any residential water treatment devices. The well spigot was purged to reach stabilized pH, dissolved oxygen, temperature, and specific conductance in three consecutive measurements at 3 min time intervals (measured by YSI 556 Handheld Multiparameter Instrument or YSI Pro Plus & flow cell) before sample collection. Water samples for dissolved hydrocarbon (methane, ethane, and propane) analysis were collected using either small (volume equals 57 mL with septum installed) or large (volume equals 157 mL with septum installed) serum bottles (Wheaton). Sodium azide tablets (from Sigma Aldrich, each tablet consists of 8 mg sodium azide and 92 mg sodium chloride) were added to the serum bottles before sample collection (2 tablets for small bottle or 5 tablets for large bottle). The serum bottle was filled with water sample and then capped with rubber stopper and sealed with a crimper. We stored the serum bottles at room temperature for analysis. For each drinking water well, we collect a triplicate of water samples for hydrocarbon (methane, ethane, and propane) analysis: two were used for gas chromatography (GC) measurement of dissolved concentrations, while the other one was reserved for isotope analysis. Water samples for measuring geochemical indicators, including major anion, major cation and trace metal, were filtered with a 0.45 μm filter and collected in HDPE bottles pre-washed with HCl and HNO_3. Major anion samples were frozen immediately after collection for preservation, while major cation and trace metal samples were acidified with 3 mL of 50% v/v hydrochloric acid and stored on ice or at 4 °C until analysis. We also collected field blanks for each type of samples using MilliQ water on each sampling day.

Dissolved hydrocarbon measurement

For measuring dissolved hydrocarbon concentrations, we used a simple headspace extraction method adapted from Magen et al.[6]. To create a headspace in the water-filled serum bottle, we first pierced through its septum using two 17-gauge needles (Hamilton Company) connected to two 10 mL gas-tight syringes with shut-off valve (SGE). One syringe was filled with 8 mL ultra-high purity helium gas (UHP300 HE, Air Gas), while the other syringe was empty (plunger pushed to the end). The helium gas was pushed into the serum bottle while the same volume of water was simultaneously withdrawn. The serum bottle was then inverted and stored overnight.

Before headspace extraction, additional 8 mL of helium gas was injected to the serum bottle to increase the headspace pressure, which allowed us to extract enough volume of headspace gas easily. The serum bottle was then vigorously shaken for 2 min to reach equilibrium between the water and gas phase. We then extracted 8 mL of headspace gas using a gas-tight syringe. The collected headspace gas was analyzed using an SRI 8610C FID Gas Chromatography. Five-point calibration (with one point being a repeat) was performed daily before sample analysis using calibration gas standards (MESA, Inc.).

Converting headspace measurements to dissolved hydrocarbon concentrations

Headspace concentrations can be converted to dissolved concentrations of a compound, *i* (i.e., methane, ethane, or propane), according to the following equations:

$$C_{w,i}^{0} V_w = C_{w,i} V_w + C_{hs,i} V_{hs} \quad \text{(equation 1)}$$

where $C_{w,i}^{0}$ is the initial dissolved concentration before phase equilibrium; $C_{w,i}$ is the water phase concentration after equilibrium; V_w is the volume of water after headspace creation; $C_{hs,i}$ is the gas phase concentration in the headspace after equilibrium; and V_{hs} is the volume of headspace. We can derive the dissolved concentration of compound *i* as follows:

$$C_{w,i}^{0} = \frac{C_{w,i} V_w + C_{hs,i} V_{hs}}{V_w} \quad \text{(equation 2)}$$

And we define $K_{aw,i}$ as the dimensionless headspace-water partitioning constant for compound i:

$$K_{aw,i} = \frac{C_{hs,i}}{C_{w,i}} \quad \text{(equation 3)}$$

By substituting equation 3 into equation 2 we obtain:

$$C_{w,i}^{0} = \frac{\frac{C_{hs,i}}{K_{aw,i}} V_w + C_{hs,i} V_{hs}}{V_w} \quad \text{(equation 4)}$$

And we can rearrange equation 4 to derive:

$$C_{w,i}^{0} = C_{hs,i} \frac{\frac{1}{K_{aw,i}} V_w + V_{hs}}{V_w}$$

$$= C_{hs,i}\left(\frac{1}{K_{aw,i}} + r_{hs/w}\right) \quad \text{(equation 5)}$$

where $r_{hs/w} = \frac{V_{hs}}{V_w}$ is the ratio of headspace volume to water volume. Using equation 5 we can calculate $C^0_{w,i}$ given $C_{hs,i}$ (measured by GC), $K_{aw,i}$ (based on literature, see below) and $r_{hs/w}$ (pre-determined).

The dimensionless headspace-water partitioning constant $K_{aw,i}$ can be derived from the well-known Henry's law constant (H[M/atm]) by a unit conversion:

$$K_{aw,i} = \frac{10^5[\frac{Pa}{atm}]}{H\left[\frac{M}{atm}\right]*R*T[K]*10^3\ [L/m^3]} \qquad \text{(equation 6)}$$

The Henry's Law constant under different temperature T is given by the fitted relationship[7]:

$\ln(H^O\ [M/atm]) = A + B/T + C\ \ln(T)$ (equation 7)

where H^O represent Henry's Law constant not influenced by salinity (i.e., of pure water). A, B, and C are fitted parameters, their values are shown in table S1:

Table S1. Fitted parameters for Henry's Law constant calculation[7]

Compound	A	B	C
CH_4	-194.7	9750	27.274
C_2H_6	-240.2	12420	33.744
C_3H_8	-281.1	14510	39.652

In order to adjust the Henry's law constant H to account for salinity, we have the following relationship[8]:

$$\mathrm{Log}(H^{O}/H) = \Sigma\,(h_s + h_i)\,c_s \qquad \text{(equation 8)}$$

$$h_i = h_{i,0} + h_{i,T}\,(T - 298.15K) \qquad \text{(equation 9)}$$

In equation 8, h_s is the parameter capturing the contributions of salt ions, while h_i is specific to hydrocarbon species. In equation 9, $h_{i,T}$ is the hydrocarbon specific temperature effect coefficient. For simplification, we assume the salinity of water samples were dominated by sodium chloride introduced by the azide tablets (92% sodium chloride and 8% sodium azide), which we assume is 100% sodium chloride. The tablets added over 2,900 mg/L sodium chloride to our samples while the explicitly measured sodium and chloride concentrations in our samples (without adding tablet) had maximum values of 290 mg/L and 385 mg/L, thus rendering our assumption acceptable. The values of these parameters are summarized in Table S2 and S3:

Table S2 Salt Ion Specific Parameters[8]

Species	h_s ($m^3\ kmol^{-1}$)
Na+	0.1143
CI-	0.0318

Table S3 Hydrocarbon Specific Parameters[8]

Hydrocarbon	$h_{i,0}$ ($m^3\ kmol^{-1}$)	10^3 x $h_{i,T}$ $m^3\ kmol^{-1}\ K^1$
CH_4	0.0022	-0.524
C_2H_6	0.0120	-0.601
C_3H_8	0.0240	-0.702

Yield test for dissolved hydrocarbon measurement

In order to test the accuracy of our experimental method and apparatus for $C_{w,i}^0$ measurements, we made a series of artificial water samples containing known dissolved concentrations of all three hydrocarbons (methane, ethane, and propane). Then, we measured their concentrations using our described method and compare the calculated C_w^0 with their expected values. We created the artificial samples from serial dilution of hydrocarbon-saturated water. Specifically, 7 g sodium chloride was dissolved in 2000 mL MiliQ water to simulate the salinity introduced by sodium azide tablet. This solution was then purged by ultra-high purity helium for 3 hours to remove any dissolved gases. Then, 500 mL of the solution was purged with a 98% methane, 1% ethane, and 1% propane mixture gas (from Airgas) for 2 hours at steady bubble-forming rate to achieve hydrocarbon saturation. This hydrocarbon-saturated solution was then serially diluted for eight times to give decreasing concentrations by repeating these steps: 8 mL of hydrocarbon solution was injected into a 57-mL serum bottle which was pre-filled with helium-purged water but left with an 8 mL helium headspace. The 8 mL headspace helium was pushed out simultaneously. The serum bottle was then vigorously shaken for 1 min to fully mix the solution so that the injected solution was diluted by a factor of 57/8. Then, we injected 8 mL helium into the serum bottle to recreate its headspace, which facilitated the following GC analysis, and simultaneously collected 8 mL of diluted hydrocarbon solution to be used for the next dilution cycle. We made triplicates of artificial water samples for each dilution level. The results of the yield test are shown in Figure S1.

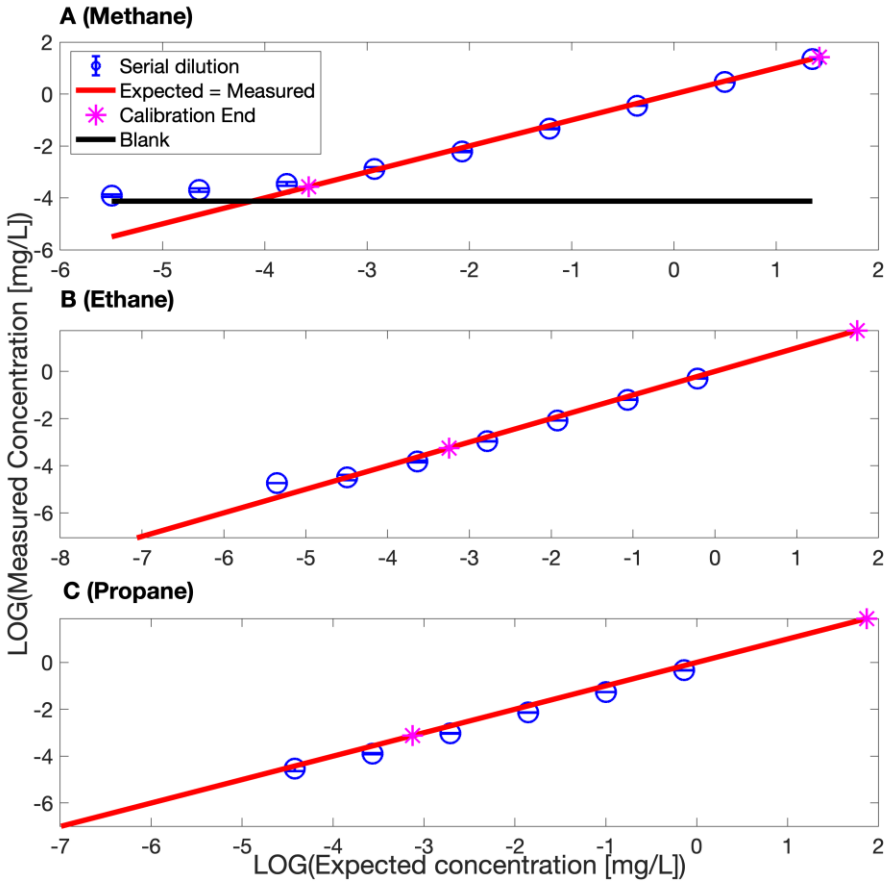

Figure S1. Yield tests demonstrated high measurement accuracy of dissolved concentration of (A) methane, (B) ethane, and (C) propane. Symbols represent: artificial water sample triplicates (blue circles, error bars represent standard errors of mean); measurement equaling expected values (solid red line); and the lower and higher end of the range of equivalent dissolved concentrations of our GC calibration standards (pink stars).

Accurate measurement of dissolved methane, ethane, and propane concentrations were achieved over wide concentration ranges (Fig. S1). For methane and ethane measurements, the measured concentrations were greater than expected values when the concentrations were very low. This might inform the method's limit of quantification (LOQ), which will be discussed below.

Although some detectable propane measurements were slightly lower than expected values, the differences were generally within one order of magnitude. In addition, propane was rarely detected in this study (only four out of 94 water samples contained small amount of detectable propane < 0.0001 mg/L), thus had minimum influence on the results of our analysis. Overall, these yield test results were deemed acceptable.

In addition to the measurement accuracy of our method, we can also derive our method's limit of detection (LOD) from the yield test results. For ethane, the left-most blue circle (Fig. S1B) corresponds to expected concentration of 4.5×10^{-6} mg/L (its x-coordinate). The next (further diluted) expected concentration was set to be 6.2×10^{-7} mg/L, but the triplicates had no detectable ethane. Thus, we selected 4.5×10^{-6} mg/L as the LOD for ethane. Similarly, the LOD for propane was set to be the expected concentration (x-coordinate) of the left-most blue circle (Fig. S1C), which was 3.8×10^{-5}mg/L (concentrations lower than that were not detected).

For methane, the lowest expected concentration in the serial dilution was detected, which was 3.2×10^{-6} mg/L. However, we suspected that the GC analysis was possibly affected by the low-concentration atmospheric methane: a tiny amount of ambient air containing methane (around 2 ppm) could escape into the GC column when we made a sample injection, which could result in a tiny methane peak even if the sample itself didn't contain methane. This was reflected by the mean methane concentration resulted from testing the MilliQ water blanks (7.6×10^{-5} mg/L, black horizontal line, Fig. S1A). Because the lowest measured concentration in the serial dilution was close to the water blank concentration, it's possible that the former actually reflected

atmospheric methane contamination. Thus, the second lowest expected concentration in the serial dilution was accepted as the LOD for methane, which was 2.3×10^{-5} mg / L.

The limit of quantification (LOQ) is a different concept from LOD: it's the minimum dissolved concentration above which the measurements are accurate to the true values. Reflected in the Figure S1, all blue circles above the LOQ should fall close to the 1:1 red line (measured = expected). Another convention is to use the lower end of the range of equivalent dissolved concentrations of GC calibration standards (lower purple stars, Fig. S1) as the LOQ. Since the blue circles above the lower purple stars were close to the red line, we used the lower purple stars' concentrations as our LOQs (2.7×10^{-4} mg/L, 5.6×10^{-4} mg/L, and 7.5×10^{-4} mg/L for methane, ethane, and propane, respectively). The LODs and LOQs are summarized in table S4.

Table S4 limit of detection (LOD) and limit of quantification (LOQ) of hydrocarbons

Hydrocarbon	Limit of detection [mg/L]	Limit of Quantification [mg/L]
Methane	2.3×10^{-5}	2.7×10^{-4}
Ethane	4.5×10^{-6}	5.6×10^{-4}
Propane	3.8×10^{-5}	7.5×10^{-4}

Dissolved ion species measurement and isotopic analysis

We used ion chromatography (IC) and inductively coupled plasma mass spectrometry (ICP-MS) to measure major anions and trace metals, respectively, at the Yale Analytical and Stable Isotope Center (YASIC). Meanwhile, we measured major cations and iron by inductively coupled

plasma - optical emission spectrometry (ICP-OES) at the Cary Institute for Environmental Sciences. $^{13}C\text{-}CH_4$ and $^{2}H\text{-}CH_4$ were analyzed by the UC Davis Stable Isotope Facility. Samples were prepared by transferring equilibrated headspace into an evacuated 12 mL exetainer (Labco, Model 839W), resulting in slight over-pressure. The results were reported in the form of $\delta^{13}C_{VPDB}\text{-}CH_4$ (‰) and $\delta^{2}H_{VSMOW}\text{-}CH_4$ (‰).

Spatial metrics and topographical information

The locations of O&G wells (including both conventional and unconventional wells) in Bradford County and five neighboring counties in Pennsylvania (Lycoming, Sullivan, Susquehanna, Toga, and Wyoming) were obtained from the Pennsylvania Department of Environmental Protection database (PADEP)[4,9]. O&G well locations in four New York State counties neighboring our study region (Steuben, Chemung, Tioga, and Broome) were obtained from the New York Department of Environmental Conservation (NYDEC)[10]. Only O&G wells drilled on or before the start date of our field campaign (SPUD date on or earlier than 2018-07-29) were considered. The number of conventional and unconventional wells included are 397 and 5481 respectively in the Pennsylvania counties, and 1840 and 52 respectively in the New York counties. Pennsylvania well violation reports (inspection date from 2000-01-01 to 2018-07-29) were from the Oil and Gas Compliance database of PADEP[11], and we filter for well integrity violations, especially those related to well casing and cementation issues, that could potentially lead to stray gas migration using a list of violation code (Table S5). Each Pennsylvania violation record included an American Petroleum Institute (API) number which mapped the violation to an O&G well. No violation records from New York State had been included in this study so far. The distances

between water samples and O&G wells in all ten Pennsylvania and New York State counties, and the distances between water samples and O&G wells associated with reported violations in six Pennsylvania counties were calculated based on longitude/latitude coordinates using the Haversine formula, and the number of wells and violations whose distance to water samples were smaller than certain radii (i.e., 1, 2, 5, and 10 km) were counted. Topographical position was adapted from the landform classification system of Theobald et al.[12] that is based on the multi-scale topographic position index (mTPI) derived from the 10-m resolution National Elevation Dataset. The system distinguishes four positions along the hillslope: summits (ridges, peaks), upper slopes (shoulders), lower slopes (foot slopes), and valleys (toe slopes).

Predrilling data collection and processing

Domestic groundwater wells sampled in 2018 were paired with industry-collected pre-drill geochemistry data for the same wells released by the PADEP and published online by Penn State University's Shale Network[13] using Generate Near Table (Analysis) in ArcGIS 10.4. Each pairing of groundwater wells (this study and pre-drill samples) was confirmed or invalidated manually using aerial imagery and the coordinates of the two wells (via Google Earth Pro, 2018). Additional geochemistry corresponding to pre-drill measurements was provided by homeowners for select wells.

When plotting Fig 5, we assigned below-LOD pre-drilling methane concentrations to be the values of the corresponding LODs and marked them with gray crosses. For records with methane concentration fields being '< 2.5' and '< 0.02' in the pre-drilling dataset, we assigned them

values of 2.5 and 0.02 mg/L, respectively. In the pre-drilling dataset, many records shared methane concentration values of 0.005 and 0.026 mg/L, and we inferred these values to indicate their LODs. We treated all pre-drilling methane measurement of 0.005 and 0.026 mg/L as below-LOD. Furthermore, we assigned 0.026 mg/L to pre-drilling records saying 'ND' (methane was not detected but LOD was unknown), since 0.026 mg/L was a frequently used LOD.

Violation code for well integrity violations that could potentially lead to stray gas migration

We collected all violation codes associated with violated wells in five Northeastern Pennsylvania (NE PA) counties (Bradford, Lycoming, Sullivan, Susquehanna, Toga, and Wyoming) from PADEP[11]. Then we used key words "cement", "cas" (standing for case or casing), "water", "pressure", "gas", and "integrity" to search through every code and determine if it could potentially lead to stray gas migration into groundwater aquifers. The resulted violation codes are shown in Table S5.

Table S5 violation code related to well integrity issues that could potentially lead to stray gas migration

Index	**violation_code** (source: PADEP[11])
1	"78a81(a)2 - CASING AND CEMENTING - GENERAL PROVISIONS - Operator conducted casing and cementing activities that failed to prevent migration of gas or other fluids into sources of fresh groundwater."
2	"78.85(a)5 - CASING AND CEMENTING - CEMENT STANDARDS - The operator failed prevent gas flow in the annulus. In areas of known shallow gas producing zones gas block additives and low fluid loss slurries shall be used."

3	“78.83COALCSG - Improper coal protective casing and cementing procedures”
4	“78.86_ - CASING AND CEMENTING - DEFECTIVE CASING OR CEMENTING - Operator failed to plug a well under 25 Pa. Code Sections 78.91 and 78.98 after the defect could not be corrected or an alternate method was not approved by the Department.”
5	“78.86 - CASING AND CEMENTING - DEFECTIVE CASING OR CEMENTING - Operator failed to report defect in a well that has defective insufficient or improperly cemented casing to the Department within 24 hours of discovery. Operator failed to correct defect or failed to submit a plan to correct the defect for approval by the Department within 30 days.”
6	“78a86 - CASING AND CEMENTING - DEFECTIVE CASING OR CEMENTING - Operator failed to report defect in a well that has defective insufficient or improperly cemented casing to the Department within 24 hours of discovery. Operator failed to correct defect or failed to submit a plan to correct the defect for approval by the Department within 30 days.”
7	“78.81D2 - Failure to case and cement properly through storage reservoir or storage horizon”
8	“78a85(a)5 - CASING AND CEMENTING - CEMENT STANDARDS - Operator failed to prevent gas flow in the annulus and use gas block additives and low fluid loss slurries in areas of known shallow gas producing zones.”
9	“78.83(c) - CASING AND CEMENTING - SURFACE AND COAL PROTECTIVE CASING AND CEMENTING PROCEEDURES - Operator failed to drill to approximately 50 feet below the deepest fresh groundwater or at least 50 feet into consolidated rock whichever is deeper and immediately set and permanently cement a string of surface casing to that depth.”
10	“207B - Failure to case and cement to prevent migrations into fresh groundwater”
11	“78.86* - Failure to report defective insufficient or improperly cemented casing w/in 24 hrs or submit plan to correct w/in 30 days”
12	“78a85(a)4 - CASING AND CEMENTING - CEMENT STANDARDS - Operator failed to protect the casing from corrosion from and degradation by the geochemical lithologic and physical conditions of the surrounding wellbore while cementing surface or coal protective casing.”
13	“OGA3217(B) - PROTECTION OF FRESH GROUNDWATER AND CASING REQUIREMENTS - CASING -Failure to prevent migration of gas or fluids into sources of fresh water causing pollution or diminution. Failure to properly case and cement well through a fresh water-bearing strata in regulated manner or depth.”
14	“78a85(c)2 - CASING AND CEMENTING - CEMENT STANDARDS - After casing cement was placed and cementing operations were completed the operator disturbed casing within 8 hours by nippling up on or in conjunction to the casing.”

15	“78.81(a)3 - CASING AND CEMENTING - GENERAL PROVISIONS - Operator conducted casing and cementing activities that failed to prevent pollution or diminution of fresh groundwater.”
16	“78a85(c)4 - CASING AND CEMENTING - CEMENT STANDARDS - After casing cement was placed and cementing operations were completed operator disturbed casing within 8 hours by running drill pipe or other mechanical devices into or out of the wellbore.”
17	“78a81(a)3 - CASING AND CEMENTING - GENERAL PROVISIONS - Operator conducted casing and cementing activities that failed to prevent pollution or diminution of fresh groundwater.”
18	“78.81(a)2 - CASING AND CEMENTING - GENERAL PROVISIONS - Operator conducted casing and cementing activities that failed to prevent migration of gas or other fluids into sources of fresh groundwater.”
19	“78.85 - Inadequate insufficient and/or improperly installed cement”
20	“78.81(b) - CASING AND CEMENTING - GENERAL PROVISIONS - The operator failed to drill through fresh groundwater zones with diligence and as efficiently as practical to minimize drilling disturbance and commingling of groundwaters.”
21	“78.83GRNDWTR - Improper casing to protect fresh groundwater”
22	“78.73(c) - GENERAL PROVISION FOR WELL CONSTRUCTION AND OPERATION - Operator failed to prevent excessive surface shut-in pressure and surface producing back pressure inside the surface casing or coal protective casing after a well has been completed recompleted reconditioned or altered.”
23	“78.84 - Insufficient casing strength thickness and installation equipment”
24	“78.73(b) - GENERAL PROVISION FOR WELL CONSTRUCTION AND OPERATION - Operator failed to prevent gas oil brine completion and servicing fluids and any other fluids or materials from below the casing seat from entering fresh groundwater and prevent pollution or diminution of fresh groundwater.”
25	“78.73B - Excessive casing seat pressure”
26	“78a73(b) - GENERAL PROVISION FOR WELL CONSTRUCTION AND OPERATION - Operator failed to prevent gas oil brine completion and servicing fluids and any other fluids or materials from below the casing seat from entering fresh groundwater and prevent pollution or diminution of fresh groundwater.”
27	“78.81D1 - Failure to maintain control of anticipated gas storage reservoir pressures while drilling through reservoir or protective area”
28	“78.73A - Operator shall prevent gas and other fluids from lower formations from entering fresh groundwater.”
29	“78a73(a) - GENERAL PROVISION FOR WELL CONSTRUCTION AND OPERATION - Operator failed to construct and operate the well in accordance with 25

	Pa. Code Chapter 78a and ensure that the integrity of the well is maintained and health safety environment and property are protected."
30	"78.73(a) - GENERAL PROVISION FOR WELL CONSTRUCTION AND OPERATION - Operator failed to construct and operate the well in accordance with 25 Pa. Code Chapter 78 and ensure that the integrity of the well is maintained and health safety environment and property are protected."

Calculating initial concentrations of biogenic methane undergoing microbial oxidation

If we assume that the dissolved methane detected in each water sample is the product of biogenic methane being oxidized by anaerobic microbial activity, then the resulted ^{13}C enrichment can be expressed by the following equation[14]:

$$^{13}\delta_t = {}^{13}\delta_i - \epsilon_C \ln(f) \quad \text{(equation 10)}$$

where $^{13}\delta_t$ is the $\delta^{13}C$ signature of methane after oxidation (i.e., detected methane in water samples), and $^{13}\delta_i$ is the signature of methane before oxidation (i.e., initial biogenic methane). ϵ_C is the kinetic isotopic fractionation factor, and f stands for the residual methane fraction. We can rewrite equation 10 to equation 11 and calculate f:

$$f = \exp\left[\frac{^{13}\delta_t - {}^{13}\delta_i}{-\epsilon_C}\right] \quad \text{(equation 11)}$$

The kinetic ^{13}C fractionation factor under anaerobic condition ϵ_C = 3 was reported in literature.[14] For sensitivity analysis, we varied ϵ_C from 0.3 to 30, and varied $^{13}\delta_i$ over the typical range of

biogenic methane (-80 to -55‰ adapted from literature[14]). Note, for any sample whose $^{13}\delta_t$ is smaller than $^{13}\delta_i$, we treat it as not being oxidized thus its residual fraction f equals 100%. Finally, we divided the observed methane concentration by the corresponding residual fraction f to obtain the initial methane concentration.

Dilution calculation and estimated methane solubility of deep Appalachian Basin Brine

The median Cl concentrations of type D water samples (n = 12; red circles in Fig S10) and of Middle Devonian and lower brine samples (n = 69 with Cl concentration available; orange diamonds in Fig. S10) are 58 mg/L and 7.3×10^4 mg/L respectively, rendering a dilution factor of 1252. If the dissolved methane in type D water came from diluted dissolved methane in the brine, we could multiply the methane concentrations of type D water (median = 3.9 mg/L; max = 32.1 mg/L) by this dilution factor to obtain that the dissolved methane concentrations of the corresponding brine were expected to have median of around 4.9×10^3 mg/L and maximum of around 4.0×10^4 mg/L.

To test if such expected dissolved methane concentrations were realistic for the deep Appalachian Basin Brine, we estimated the methane solubility of the brine. The median O&G well bottom hole temperature (37 °C) and the estimated median bottom hole pressure (124 bars or 122 atm) in the Appalachian Basin[15] were used as the surrogates for the shale in-situ temperature and pressure. The NaCl concentration of deep brine was assumed to equal the median Cl concentration of Middle Devonian and lower brine samples (7.3×10^4 mg/L). Based

on the temperature and NaCl concentration, the local Henry's law constant was estimated by equation 7, 8, and 9 to be 5.8×10^{-4} M/atm. Then, based on the 122 atm pressure (assuming pure methane in the gas phase), the methane solubility of brine (i.e., dissolved methane concentration in equilibrium with the gas phase) was calculated to be on the order of 1.1×10^{3} mg/L. The methane solubility was smaller than the expected methane concentrations above, suggesting that the expected concentrations were unrealistically high for the deep Appalachian Basin Brine.

Estimation of methane emission from inland waters and O&G wells

Methane emission by non-wetland inland surface water bodies within Bradford County can be estimated by multiplying the methane flux from a water body type and the area of that type, and then summing over all types of water bodies. The global methane fluxes of different surface water bodies (mg CH_4 $m^{-2}d^{-1}$, median (lower quartile – upper quartile)) are: 21.6 (7.9 – 81.1) for rivers and streams, 46.4 (11.7-129.0) for lakes, and 136.1 (12.7 – 247.5) for freshwater aquaculture ponds.[16] The areas of corresponding water bodies within Bradford County (km^2) are: 41.7 for riverine, 6.1 for lake, and 11.2 for freshwater pond.[17] The estimated total emission was 986.84 (198.16 – 2531.14) tonne CH_4 / year. Note that this estimation didn't include emission from freshwater wetlands, which could account for about half of the total inland water methane emission on the global scale[16].

The PA-statewide average methane emission rates for different types of active O&G wells (the second column of table S6) were estimated by Ingraffea et al.[18] based on extrapolation of operator-reported flow rates from annuli and wellheads of a subset of active wells. Ingraffea et

al. assumed a gas composition of 83.5% methane and methane density of 656 g/m^3.[18] We multiplied the average emission rates by the number of active wells (not plugged nor in regulatory inactive status) in Bradford County under each well type and calculated the total emission to be on the order of 400 t CH4/year. Ingraffea et al. reported that the methane emission estimated by this component-based (bottom-up) method could be much smaller than the total emission measured by top-down approach due to factors such as super emitters that are not fully accounted in the bottom up approach.[18,19]

Table S6. Estimation of methane emission from active O&G wells in Bradford County

Well Type	Avg. flow (m^3/year per well)[18]	Bradford well count	Total Emission (t CH_4/year)
Conventional gas	828.8	10	4.54
Unconventional gas	588.0	1285	413.88
Conventional combined oil & gas	540.0	2	0.59
Unconventional combined oil & gas	638.3	1	0.35
Sum			419.36

Supplemental figures

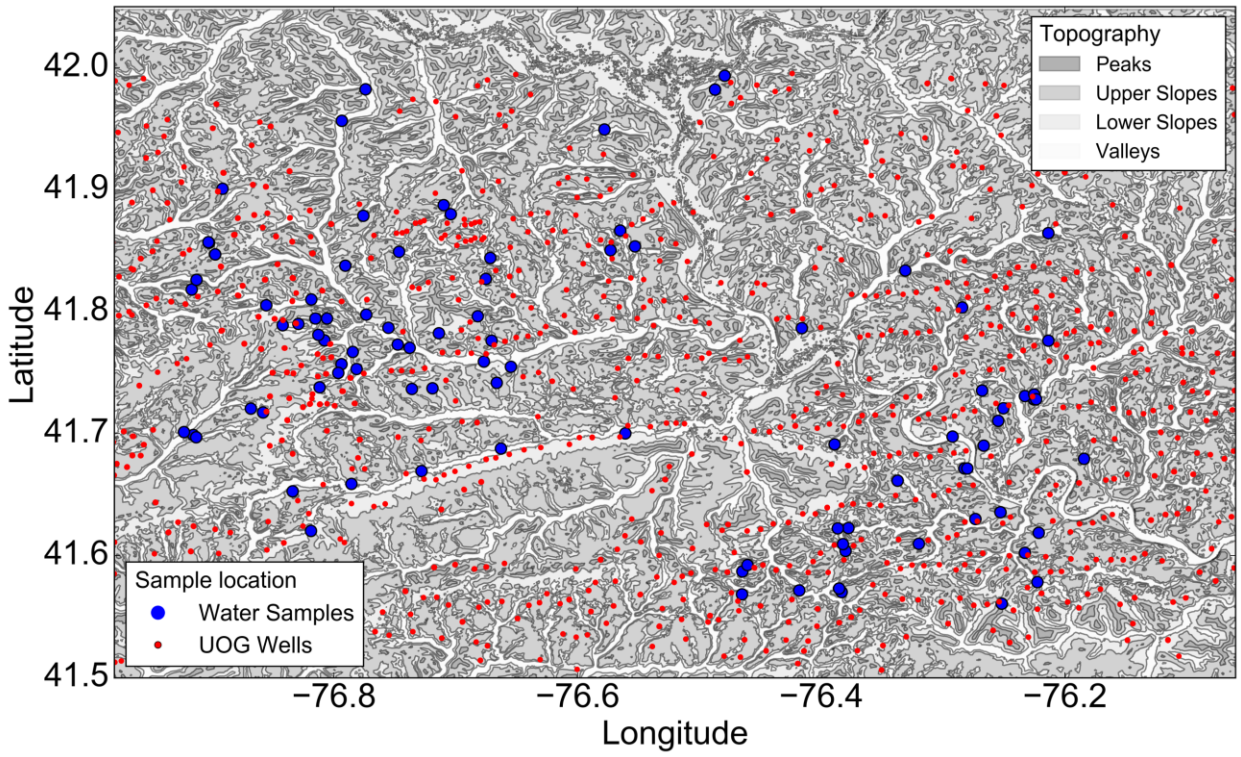

Figure S2. The topographical map of the study region. Symbols represent: sampled water wells or springs (blue circles) and UOG wells (red dots). Note that multiple UOG wells on the same well pad may not be distinguished from each other due to close distances. Topography is shown with shaded color, where darker shades indicate higher topographical features.

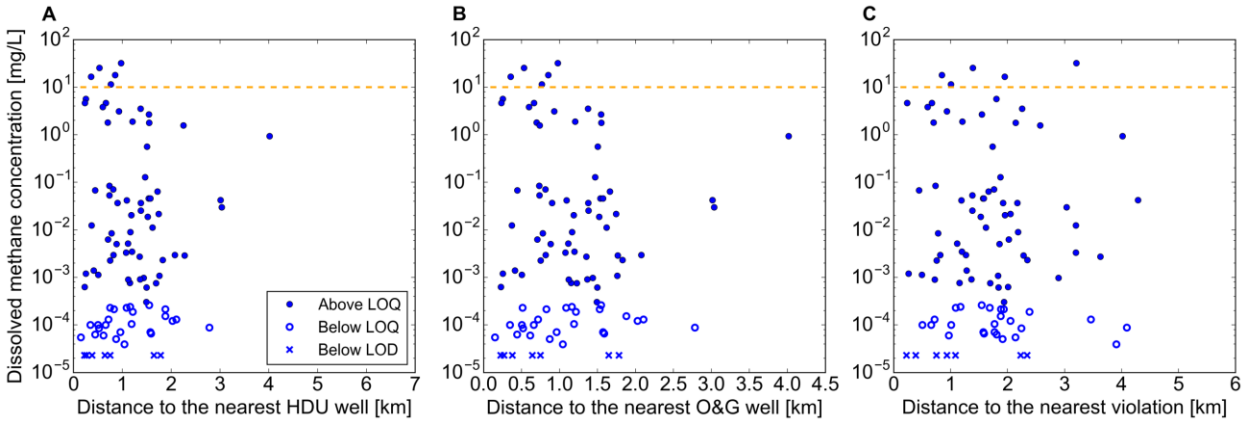

Figure S3. Spearman tests indicated the lack of correlation between methane concentration and (A) distance to the nearest horizontally drilled unconventional (HDU) well (a subset of unconventional well; $\rho = 0.049$, p-value = 0.64), (B) distance to the nearest O&G well (either conventional or unconventional; $\rho = 0.033$, p-value = 0.76) and (C) distance to the nearest well violation (can be any type of violation; $\rho = -0.013$, p-value = 0.90). Symbols represent: samples above LOQ (filled circles); samples below LOQ but above LOD (open circles); samples below LOD (crosses); and the 10 mg/L warning level by the US Department of the Interior[20] (yellow dashed line) (as in Figure 1).

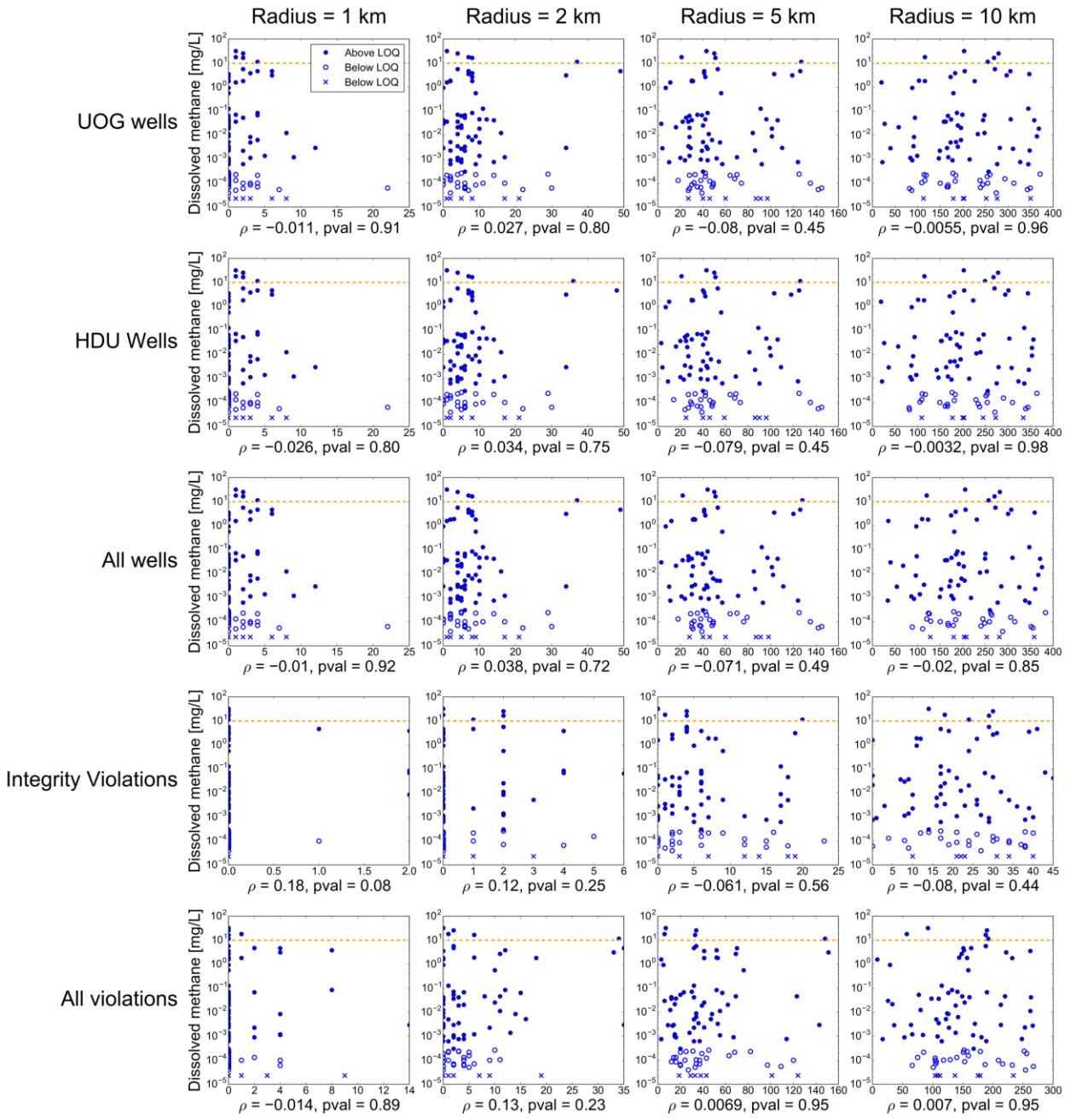

Figure S4. Spearman tests indicated the insignificant correlations between dissolved methane concentrations (y-axes) and counts of O&G wells or violations (x-axes) within selected radii centered at the water wells. The rows, from top to bottom, represent the counts of unconventional O&G wells, horizontally drilled unconventional (HDU) O&G wells, all O&G wells, well integrity violations, and all type of violations, respectively. The columns, from left to right, represent counting within the radius of 1km, 2km, 5km, and 10km centered at the water well, respectively. The Spearman correlation

coefficient (ρ) and p-value (pval) for each correlation are printed below the sub-figures. Symbols represent: samples above LOQ (filled circles); samples below LOQ but above LOD (open circles); samples below LOD (crosses); and the 10 mg/L warning level by the US Department of the Interior[20] (yellow dashed line) (as in Fig. 1).

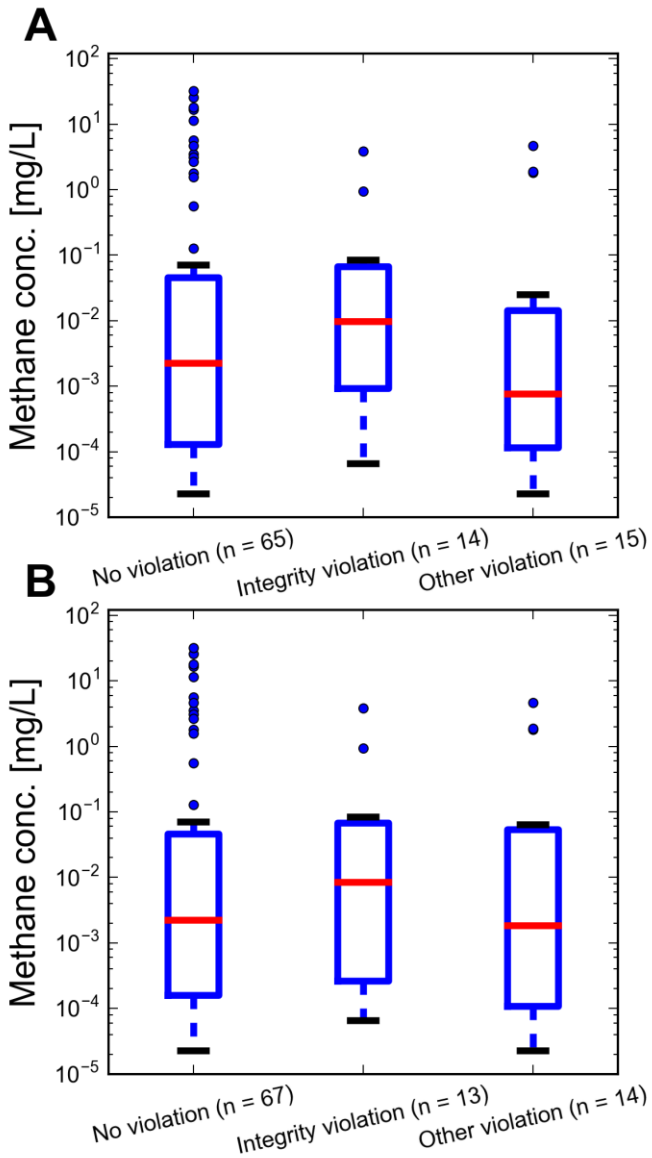

Figure S5. Dissolved methane concentration was not impacted by whether there was violation in the nearest (A) UOG well or (B) O&G well (either conventional or unconventional) to the water sample. The methane concentration distribution for samples whose nearest gas well had no violation, had

well integrity violation, or had other types of violation were represented by box plots. Each box extends from the lower quartile (Q1) to the upper quartile (Q3) of the data, the horizontal bar is the median, the lower whisker is at the lowest datum above Q1 – 1.5 × (Q3 - Q1), the upper whisker is at the highest datum below Q3 + 1.5 × (Q3 - Q1), and flier points are data that extend past the whiskers. The population means of log-transformed methane concentrations in different violation scenarios were not statistically distinguishable (p-values: 0.64 (A) and 0.87 (B); Welch's ANOVA on log-transformed concentrations)

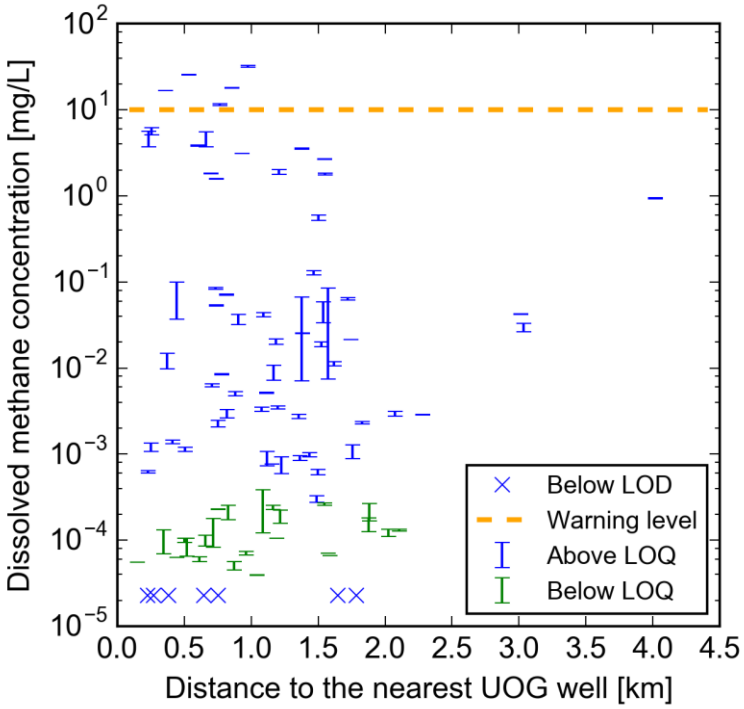

Figure S6. Error bars of dissolved methane concentrations versus distances to the nearest UOG well. Error bar represents minimum and maximum concentration measured for each water sample. One sample was measured in triplicate, and two samples only had single measurement, while the rest were measured in duplicate, so most error bars essentially show the values of the two measurements. The error bar heights for samples with higher methane concentrations (>0.1 mg/L) are very small or negligible.

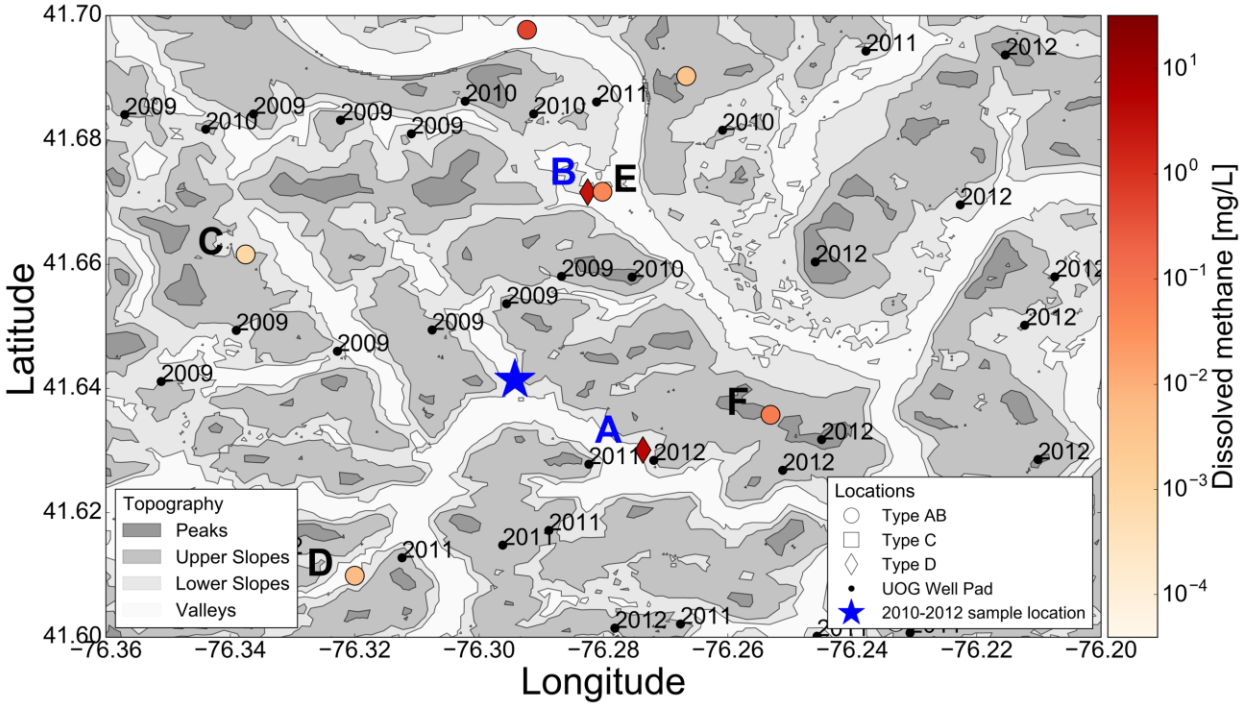

Figure S7. Subset of our sampling region that includes the sampling location of Llewellyn et al. in Sugar Run, Bradford County[21]**.** Symbols represent: the approximate location of the center of the water well clusters sampled by Llewellyn et al. during 2010 to 2012[21] (blue star); water type AB (circles); water type C (square); water type D (thin diamond); and UOG well pad locations (black dots; with black numbers being the earliest SPUD years among all individual wells drilled on the same well pad). The color scale indicates methane concentrations, and topography is shown with shaded color, where darker shades indicate higher topographical features.

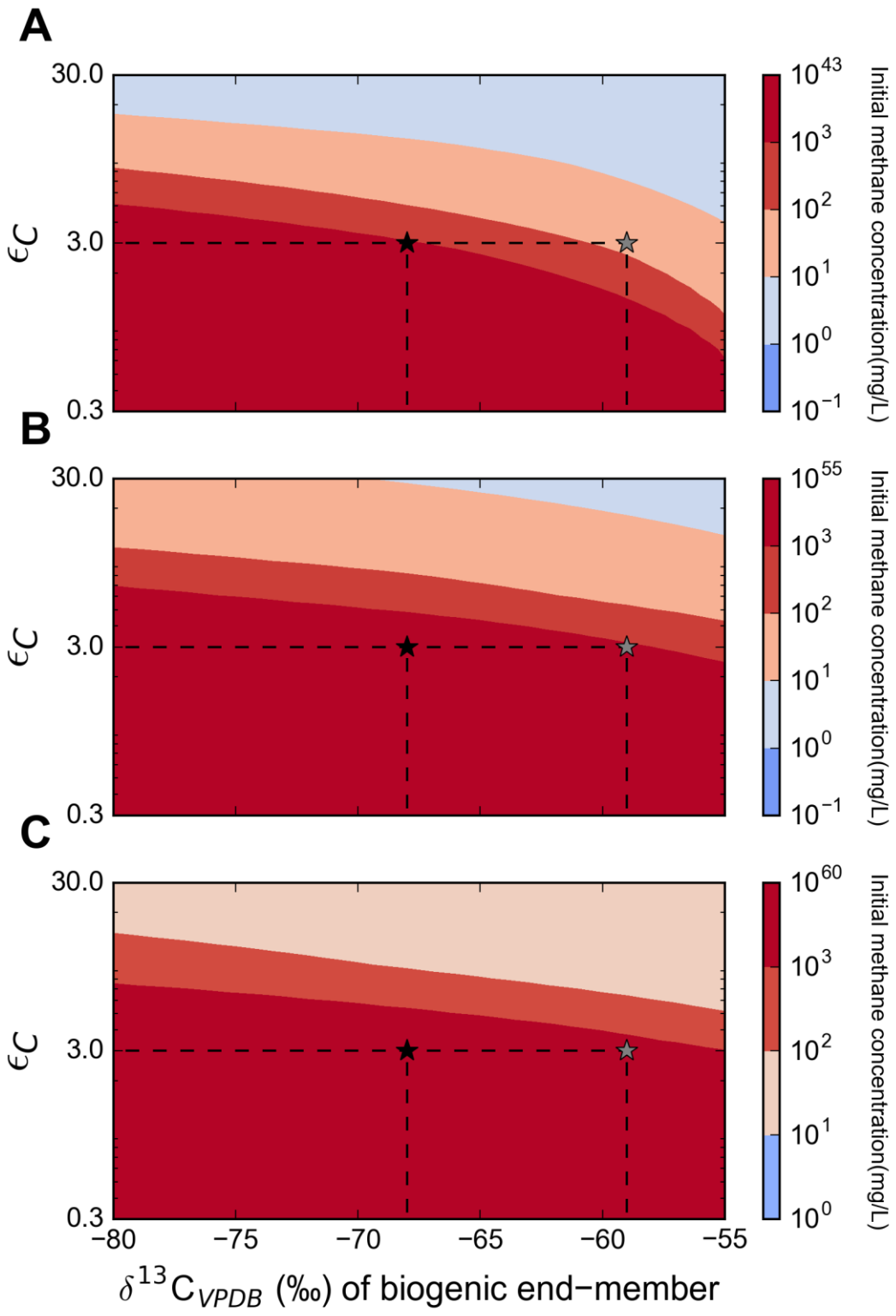

Figure S8. Sensitivity of inferred initial methane concentrations to different values of ϵ_C and initial $\delta^{13}C - CH_4$, if the detected dissolved methane originated from biogenic methane undergoing

microbial oxidation. (A) The 25th percentile of inferred initial methane concentrations, (B) the median of inferred initial methane concentrations, and (C) the 75th percentile of inferred initial methane concentrations. Average $\delta^{13}C_{VPDB}$ signature of marine (-68‰) and freshwater (-59‰) biogenic methane[22] (used as starting point of microbial oxidation) are shown as black and grey star, respectively, at the reported ϵ_C value (ϵ_C = 3) in literature[14].

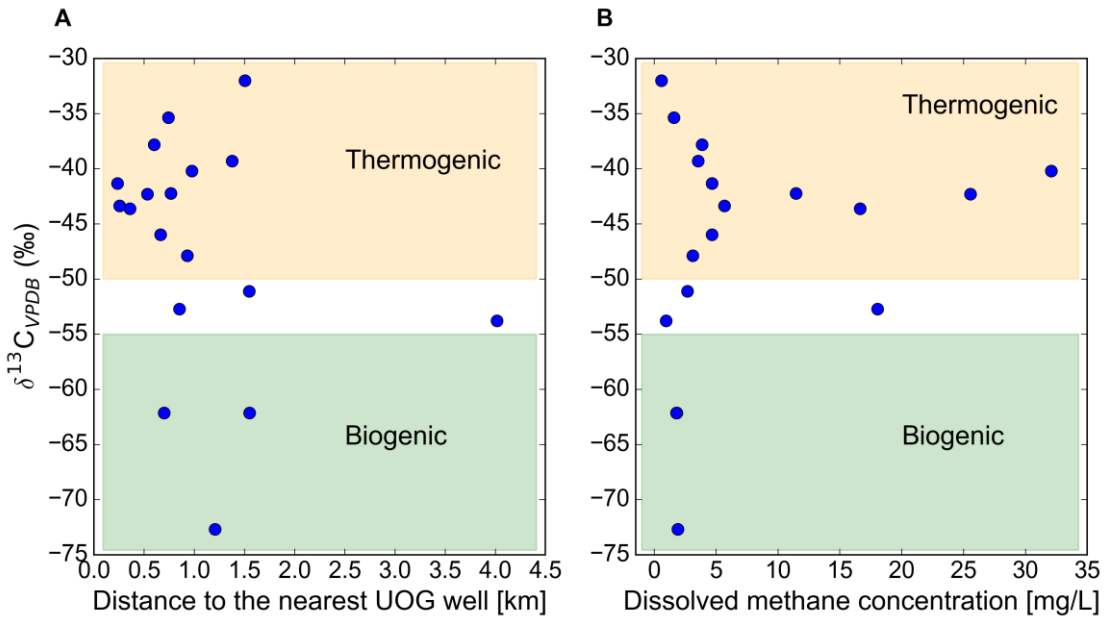

Figure S9. Spearman tests indicated a lack of significant correlation between ^{13}C ratio of methane and (A) distance to the nearest UOG well (ρ = -0.26, p-value = 0.29) and (B) dissolved methane concentration (ρ = 0.14, p-value = 0.57). High methane concentration (> 0.5 mg/L) samples are represented by blue circles, and samples falling in the yellow and green shaded areas are within the $\delta^{13}C_{VPDB}$ ranges of thermogenic methane and biogenic methane, respectively.

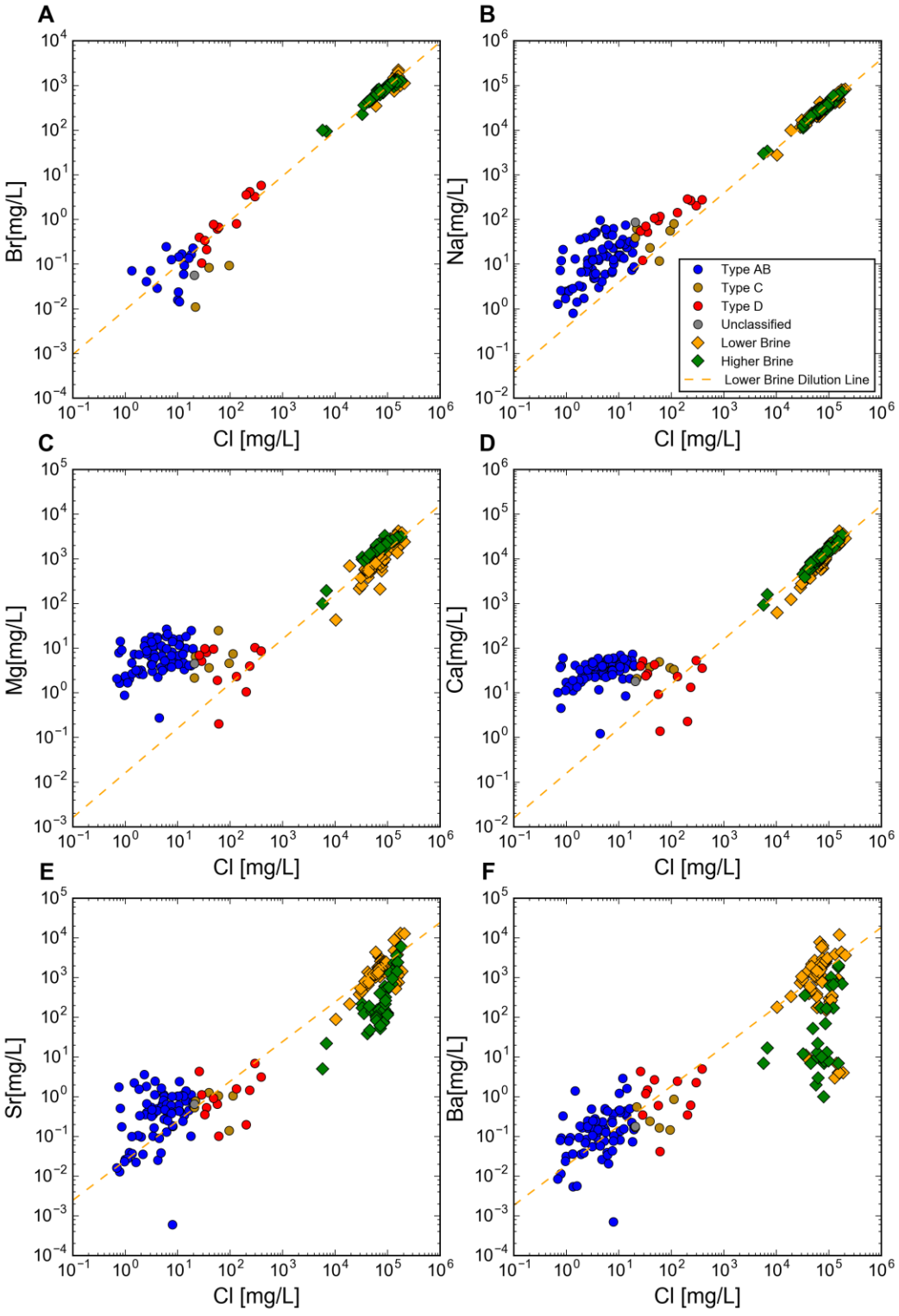

Figure S10. Inorganic species of water samples show the fingerprints of Appalachian Basin Brine in our water samples. The inorganic ratios are shown as (A)Br, (B)Na, (C)Mg, (D)Ca, (E)Sr, and (F)Ba

versus Cl. Symbols represent: water type AB (blue circles); water type C (deep yellow circles); water type D (red circles); unclassified water type (grey circles); and brine samples from Middle Devonian and lower formations (i.e., Middle Devonian, Lower Devonian, Lower Silurian, and Ordovician; orange diamond) as well as Upper Devonian and higher formations (i.e., Upper Devonian and Lower Mississippian; green diamonds)[1]. Linear regressions (with intercept equaling zero) on Middle Devonian and lower formation brine data points (orange diamonds) were performed to serve as their dilution lines (orange lines). Compared with other water types, the Br/Cl, Na/Cl, Mg/Cl, and Ca/Cl ratios of type D water samples were more similar to those of the Appalachian Basin Brine (sub-figure A through D), therefore type D water samples were the groups containing the most abundant Appalachian Basin Brine tracers. Moreover, type D water samples' Sr/Cl and Ba/Cl ratios were more similar to the ratios of brine from Middle Devonian and lower formations (orange diamonds) than those of brine from Upper Devonian and higher formations (green diamonds) (sub-figure E and F), indicating that the former was more likely to be the source of observed brine tracers in type D water samples.

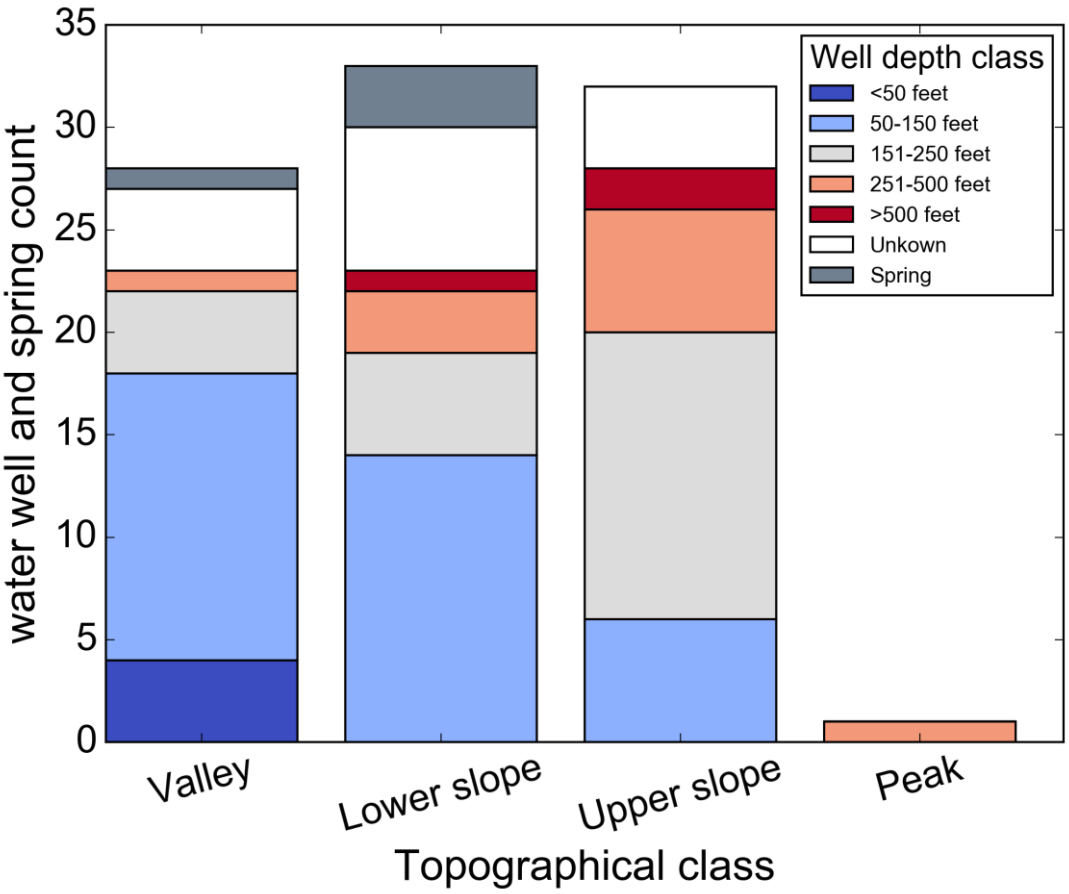

Figure S11. Number of sampled domestic wells falling in each topographical class, divided by household self-reported well-depth. Depths of springs were not reported. According to the self-reported well depths, upper slope had larger percentage of deep wells (> 150 feet) than valley. However, the well depths self-reported by homeowners might have large uncertainty, and it is not clear that the well depth in valleys were systematically smaller than the well depths in upper slopes in our study.

References

(1) Warner, N. R.; Jackson, R. B.; Darrah, T. H.; Osborn, S. G.; Down, A.; Zhao, K.; White, A.; Vengosh, A. Geochemical Evidence for Possible Natural Migration of Marcellus Formation Brine to Shallow Aquifers in Pennsylvania. *Proc. Natl. Acad. Sci.* **2012**, *109* (30), 11961–11966. https://doi.org/10.1073/pnas.1121181109.

(2) Molofsky, L. J.; Connor, J. A.; Farhat, S. K.; Wylie, A. S.; Wagner, T. Methane in

Pennsylvania Water Wells Unrelated to Marcellus Shale Fracturing. *Oil Gas J.* **2011**, *109* (19).
(3) Wen, T.; Niu, X.; Gonzales, M.; Zheng, G.; Li, Z.; Brantley, S. L. Big Groundwater Data Sets Reveal Possible Rare Contamination Amid Otherwise Improved Water Quality for Some Analytes in a Region of Marcellus Shale Development. *Environ. Sci. Technol.* **2018**, *52* (12), 7149–7159. https://doi.org/10.1021/acs.est.8b01123.
(4) Pennsylvania Department of Environmental Protection. Oil Gas Locations - Unconventional https://newdata-padep-1.opendata.arcgis.com/datasets/oil-gas-locations-unconventional?geometry=-81.196%2C40.740%2C-74.247%2C42.181 (accessed Mar 24, 2020).
(5) Pennsylvania Department of Environmental Protection. Water Supply Determination Letters https://files.dep.state.pa.us/OilGas/BOGM/BOGMPortalFiles/OilGasReports/Determination_Letters/Regional_Determination_Letters.pdf (accessed Sep 26, 2021).
(6) Magen, C.; Lapham, L. L.; Pohlman, J. W.; Marshall, K.; Bosman, S.; Casso, M.; Chanton, J. P. A Simple Headspace Equilibration Method for Measuring Dissolved Methane. *Limnol. Oceanogr. Methods* **2014**, *12* (SEP), 637–650. https://doi.org/10.4319/lom.2014.12.637.
(7) Burkholder, J. B.; Sander, S. P.; Abbatt, J.; Barker, J. R.; Huie, R. E.; Kolb, C. E.; Kurylo, M. J.; Orkin, V. L.; Wilmouth, D. M.; Wine, P. H. *Chemical Kinetics and Photochemical Data for Use in Atmospheric Studies*; 2015. https://doi.org/10.1002/kin.550171010.
(8) Weisenberger, S.; Schumpe, A. Estimation of Gas Solubilities in Salt Solutions at Temperatures from 273 K to 363 K. *AIChE J.* **1996**, *42* (1), 298–300. https://doi.org/10.1002/aic.690420130.
(9) Pennsylvania Department of Environmental Protection. Oil Gas Locations - Conventional https://newdata-padep-1.opendata.arcgis.com/datasets/oil-gas-locations-conventional (accessed Mar 24, 2020).
(10) New York State Department of Environmental Conservation. Downloadable Well Data http://www.dec.ny.gov/energy/1603.html (accessed Jul 6, 2020).
(11) Pennsylvania Department of Environmental Protection. Oil and Gas Compliance Report http://www.depreportingservices.state.pa.us/ReportServer/Pages/ReportViewer.aspx?/Oil_Gas/OG_Compliance (accessed Mar 24, 2020).
(12) Theobald, D. M.; Harrison-Atlas, D.; Monahan, W. B.; Albano, C. M. Ecologically-Relevant Maps of Landforms and Physiographic Diversity for Climate Adaptation Planning. *PLoS One* **2015**, *10* (12), e0143619. https://doi.org/10.1371/journal.pone.0143619.
(13) Brantley, S. L. Shale Network Database, Consortium for Universities for the Advancement of Hydrologic Sciences, Inc. (CUAHSI) https://doi.org/10.4211/his-data-shalenetwork (accessed Nov 19, 2018).
(14) Schout, G.; Hartog, N.; Hassanizadeh, S. M.; Griffioen, J. Impact of an Historic Underground Gas Well Blowout on the Current Methane Chemistry in a Shallow Groundwater System. *Proc. Natl. Acad. Sci. U. S. A.* **2017**, *115* (2), 296–301. https://doi.org/10.1073/pnas.1711472115.
(15) Sumner, A. J.; Plata, D. L. Exploring the Hydraulic Fracturing Parameter Space: A Novel High-Pressure, High-Throughput Reactor System for Investigating Subsurface Chemical Transformations. *Environ. Sci. Process. Impacts* **2018**, *20* (2), 318–331.

https://doi.org/10.1039/c7em00470b.
(16) Rosentreter, J. A.; Borges, A. V; Deemer, B. R.; Holgerson, M. A.; Liu, S.; Song, C.; Melack, J.; Raymond, P. A.; Duarte, C. M.; Allen, G. H.; Olefeldt, D.; Poulter, B.; Battin, T. I.; Eyre, B. D. Half of Global Methane Emissions Come from Highly Variable Aquatic Ecosystem Sources. *Nat. Geosci.* **2021**, *14* (4), 225–230. https://doi.org/10.1038/s41561-021-00715-2.
(17) U.S. Fish & Wildlife Service National Wetlands Inventory https://www.fws.gov/wetlands/data/data-download.html (accessed May 14, 2021).
(18) Ingraffea, A. R.; Wawrzynek, P. A.; Santoro, R.; Wells, M. Reported Methane Emissions from Active Oil and Gas Wells in Pennsylvania, 2014-2018. *Environ. Sci. Technol.* **2020**, *54* (9), 5783–5789. https://doi.org/10.1021/acs.est.0c00863.
(19) Omara, M.; Sullivan, M. R.; Li, X.; Subramian, R.; Robinson, A. L.; Presto, A. A. Methane Emissions from Conventional and Unconventional Natural Gas Production Sites in the Marcellus Shale Basin. *Environ. Sci. Technol.* **2016**, *50* (4), 2099–2107. https://doi.org/10.1021/acs.est.5b05503.
(20) Eltschlager, K. K.; Hawkins, J. W.; Ehler, W. C.; Baldassare, F. J. Technical Measures for the Invetigation and Mitigation of Fugitive Methane Hazards in Areas of Coal Mining, U.S. Department of the Interior, Office of Surface Mining. **2001**
(21) Llewellyn, G. T.; Dorman, F.; Westland, J. L.; Yoxtheimer, D.; Grieve, P.; Sowers, T.; Humston-Fulmer, E.; Brantley, S. L. Evaluating a Groundwater Supply Contamination Incident Attributed to Marcellus Shale Gas Development. *Proc. Natl. Acad. Sci. U. S. A.* **2015**, *112* (20), 6325–6330. https://doi.org/10.1073/pnas.1420279112.
(22) Whiticar, M. J.; Faber, E.; Schoell, M. Biogenic Methane Formation in Marine and Freshwater Environments: CO2 Reduction vs. Acetate Fermentation-Isotope Evidence. *Geochim. Cosmochim. Acta* **1986**, *50* (5), 693–709. https://doi.org/10.1016/0016-7037(86)90346-7.

Chapter 3. Conventional fossil fuel extraction, associated biogeochemical processes, and topography influence methane groundwater concentrations in Appalachia

By

[1]Yunpo Li, [2]Helen G. Siegel, [1]Nathalie A. Thelemaque, [1]Kathleen R. Bailey, [1]Priya Moncrieffe, [1]Timothy Nguyen, [3]Cassandra J. Clark, [3]Nicholaus P. Johnson, [2]Mario A. Soriano Jr., [3]Nicole C. Deziel, [2]James E. Saiers, [1]Desiree L. Plata

[1]Massachusetts Institute of Technology, Department of Civil and Environmental Engineering, Parsons Laboratory, 15 Vassar Street, Cambridge, Massachusetts 02139, USA

[2]Yale University, the School of the Environment, 195 Prospect Street, New Haven, Connecticut 06511, USA

[3]Yale University, Yale School of Public Health, Department of Environmental Health Sciences, 60 College St., New Haven, Connecticut 06512, USA

Reprinted (adapted) with permission from Li, Y.; Siegel, H. G.; Thelemaque, N. A.; Bailey, K. R.; Moncrieffe, P.; Nguyen, T.; Clark, C. J.; Johnson, N. P.; Soriano Jr., M. A.; Deziel, N. C.; Saiers, J. E.; Plata, D. L. (2023). Conventional Fossil Fuel Extraction, Associated Biogeochemical Processes, and Topography Influence Methane Groundwater Concentrations in Appalachia. *Environmental Science & Technology.* https://doi.org/10.1021/acs.est.3c01862.

ABSTRACT

The production of fossil fuels, including oil, gas, and coal, retains a dominant share in US energy production and serves as a major anthropogenic source of methane, a greenhouse gas with a high warming potential. In addition to directly emitting methane into the air, fossil fuel production can release methane into groundwater, and that methane may eventually reach the atmosphere. In this study, we collected 311 water samples from an unconventional oil and gas (UOG) production region in Pennsylvania, and an oil and gas (O&G) and coal production region across Ohio and West Virginia. Methane concentration was negatively correlated to distance to the nearest O&G well in the second region, but such a correlation was shown to be driven by topography as a confounding variable. Furthermore, sulfate concentration was negatively correlated with methane concentration and with distance to coal mining in the second region, and these correlations were robust even when considering topography. We hypothesized that coal-mining enriched sulfate in groundwater, which in turn inhibited methanogenesis and enhanced microbial methane oxidation. Thus, this study highlights the complex interplay of multiple factors in shaping groundwater methane concentrations, including biogeochemical conversion, topography, and conventional fossil extraction.

Keywords: methane, groundwater, oil and gas, coal, emissions, sulfate

Synopsis Statement

Apparent relationships between higher groundwater methane concentration and conventional oil and gas development are shown to be confounded by topographic variation, while

biogeochemical processes associated with coal mining lowered groundwater methane in Northern Appalachia.

Introduction

Methane is a highly potent greenhouse gas whose global warming potential is instantaneously 120 times stronger than CO_2's.[1] The climatic impact of anthropogenic methane release has received broad attention both in the United States (US) and around the world. The recent Inflation Reduction Act imposes a waste emission charge of methane for oil and gas (O&G) producers, which starts at $900 per metric ton of methane in 2024 and grows to $1,500 by 2026.[2] At the Conference of Parties (COP) 26 meeting in November 2021, the Global Methane Pledge was issued to prioritize methane emission reduction to slow climate change;[3] to date, it has been signed by 122 countries.[4]

Roughly 35% of anthropogenic methane emission comes from fossil fuel production and utilization (or 17% of total emissions; based on bottom-up estimation from 2008 to 2017).[5] In the US, O&G accounts for 67% of total energy production and 68% of total energy consumption.[6,7] Since the shale gas boom in the early 2000s, unconventional oil and gas production (UOG; i.e., tight O&G development typically enabled by horizontal drilling with hydraulic fracturing) has been growing rapidly and is now the main driving force of US fossil energy production (79% of dry natural gas production and 65% of crude oil production).[8,9] Coal mining has had a declining share in the US energy portfolio, but its contribution remains nontrivial (12% of total energy production, 11% of total energy consumption, and 8% of total energy export).[6,10] However, coal

is experiencing a recent surge due to global energy shifts.[11] Based on the important roles O&G and coal mining are playing in the US, minimizing methane release from these sources is a key step to slow down climate change in the next decade. Numerous studies have focused on detecting and quantifying the aboveground fugitive methane emissions directly into the atmosphere from O&G infrastructures and coal mining sites.[12–14] Similarly, elevated groundwater methane concentrations have been reported near dominantly UOG wells above the Marcellus Shale and raised concerns of groundwater methane contamination by UOG extraction.[15,16] Dissolved methane in groundwater could enter surface water bodies (e.g., streams and lakes) through groundwater discharge and subsequently enter the atmosphere by mass transport at the water-air interface.[17–23] Earlier work from Li et al. (2021) suggested that this contribution was comparatively small in Northeastern Pennsylvania (NE PA).[23] More expansively, Northern Appalachia has other legacy and active fossil fuel extraction technologies that may introduce additional methane into groundwater. For example, coal mining could be an important contributor of dissolved methane in streams in these regions.[18] Thus, understanding the origins and fundamental controls on groundwater methane across regions of Northern Appalachia that have multiple possible methane mobilization activities is valuable for identifying methane mitigation strategies.

There is some debate regarding the impact of shale gas extraction on groundwater dissolved methane in literature: earlier studies by Osborn et al. and Jackson et al. reported that groundwater methane concentration increased with shorter distance to the nearest gas well in NE PA.[15,16] However, several later studies found no statistically significant correlation between groundwater methane concentration and distance to gas wells[24] or no significant difference in methane

concentration between samples closer or farther than 1 km from the nearest gas well,[25,26] based on large datasets of predrilling groundwater samples (i.e., samples taken before certain nearby proposed gas wells were drilled, but possibly with other gas wells already drilled in the surrounding area). Using a similar approach, others found methane concentration increased near gas wells only in some small sub regions.[27–29] Such studies are often limited by the nature of the predrilling dataset (lack of isotopic information, and lack of direct postdrilling comparison). An analysis of 94 recently collected water samples in NE PA showed that groundwater methane concentration was not systematically correlated with UOG extraction[23] and was instead dominantly controlled by natural migration processes driven by topography (e.g., topographical lowlands had higher groundwater methane concentration), consistent with several previous studies in the region.[25,26,29–32] However, it is unclear if this finding holds across various geographies or if distinct local geography, geobiology, and anthropogenic activities can lead to different outcomes. Thus, a study with wider geographical coverage and a broader variety of extraction processes is needed. Specifically, few prior studies have evaluated coal mining's impact on groundwater methane in Northern Appalachia,[33] and many of the previous studies focused on regions where the number of UOG wells largely outnumbered that of conventional oil and gas (COG) wells or lacked substantial coal mining activities (e.g., NE PA). Additionally, biogeochemical processes such as anaerobic methane oxidation have been found to alter groundwater methane concentrations,[34,35] and such factors (e.g., oxidant levels) can be influenced by fossil fuel extraction activities themselves.

In this analysis, we evaluated the distribution of groundwater methane in two study regions across Northern Appalachia. Region I was located in NE PA where UOG was the dominant type

of fossil fuel extraction, while Region II was located across Southeastern Ohio (SE OH) and Northern West Virginia (N WV) where UOG coexisted with a substantial amount of COG extraction as well as coal mining. Correlations between methane concentrations and geochemical and topographical indicators as well as spatial metrics of UOG, COG, and coal mine were analyzed, and isotopic signatures were measured to inform source attribution. Such work enables the delineation of methane mobilization routes and suggests fundamental mechanisms of methane biogeochemistry that can inform important environmental responses.

Materials and methods

Sample locations

A total of 311 groundwater samples (Figure S1; 279 collected from domestic wells; 31 collected from springs; 1 sample undetermined) were collected across the North Appalachian region. Of these, 94 samples were located in Region I (majority in Bradford County, PA, collected from July to September 2018) and 217 samples were located in Region II (Belmont and Monroe Counties, OH, collected from May to August 2019; and Marshall, Wetzel, Tyler, Ritchie, and Doddridge County, WV, collected in October 2020). Region I was dominated by UOG development (about 1500 UOG wells and 60 COG wells), while Region II had significant numbers of both UOG and COG wells (about 4,000 and 50,000, respectively), as well as coal mining. Thus, the contrast was suitable for evaluating the combined impact of UOG, COG, and coal extraction. Note that the regions of study (PA, OH, and WV) were selected to represent a distribution across Appalachia and were grouped as Region I and Region II following data interpretation (i.e., the importance of UOG, COG, and coal was made evident by the data

analysis and was not a foregone conclusion or study design element). The methods for recruiting participant households were described in Li et al.;[23] briefly, we advertised the study via flyers, newspaper advertisements, postcards, and social media and accepted applicants who lived in our study areas, were head of households older than 21, spoke English, and had water supplied by private groundwater wells or springs.

Sample collection

Methods for sample collection were detailed in Li et al.[23] Briefly, water samples were collected upstream of any domestic water treatment equipment. Samples for dissolved hydrocarbon (methane, ethane, and propane) measurements were sealed in serum bottles (Wheaton, 57 or 157 mL) with rubber stoppers and crimp caps. Triplicate samples were preserved by sodium azide tablets (Sigma-Aldrich) and stored at room temperature. All samples were analyzed for dissolved hydrocarbons in at least duplicate (except for n = 4 out of 311 samples with lost or wasted bottles), whereas the third sample was sometimes reserved for isotopic analysis. The collection and analysis of other geochemical indicators (e.g., major anion, major cation, and trace metal) was detailed in Li et al.[23]

Dissolved hydrocarbon measurement

The approach for measuring dissolved hydrocarbons was detailed previously[23] following Magen et al.[36] Briefly, headspace was created in a serum bottle by removing 8 mL of water and simultaneously injecting the same volume of ultrahigh-purity helium gas (Air Gas) using gastight syringes. After storing the serum bottle overnight, another 8 mL of helium gas was injected into the headspace (i.e., to create overpressure in the headspace) and the bottle was shaken vigorously

for 2 min. Finally, 8 mL of equilibrated headspace gas was extracted with a syringe and analyzed via an SRI 8610C Gas Chromatograph (GC) with flame ionization detection (FID) to quantify methane, ethane, and propane. We performed GC calibration using analytical gas standards (MESA, Inc.) each day when we analyzed water samples. The limits of detection (LODs; lowest observable concentration in serial-dilution yield test) in the dissolved phase were 2.3×10^{-5}, 0.45×10^{-5}, and 3.8×10^{-5} mg/L for methane, ethane, and propane, respectively, while the limits of quantification (LOQs, the minimum concentration in calibration standards) for dissolved gases were 2.7×10^{-4}, 5.6×10^{-4}, and 7.5×10^{-4} mg/L for methane, ethane, and propane, respectively. Equations and further details are available in Li et al.[23]

Isotopic analysis and other dissolved species

See Li et al.[23] and Siegel et al.[37] for the measurement of other geochemical indicators (e.g., major anion, major cation, and trace metal). Isotopic analysis (^{13}C-CH_4 and ^{2}H-CH_4) was conducted at the UC Davis Stable Isotope Facility for selected samples collected from headspace gas into 12-mL exetainers (Labco, model 839W).

Geospatial and topographical Information

We obtained the geographical location information on O&G wells and coal mining extents from publicly available data sources documented in Table S1. We filtered the underground coal mining extents based on mine status indicator or permit information for active underground coal mining extents. We also filtered the datasets to only include O&G wells drilled before our sample collection and coal mine extents added before sample collection. Note that the coal mining extents represented the entire permitted areas and did not necessarily reflect the actual

longwall (i.e., working face) mining sections at a given point of time. Topographical categories (i.e., peaks, upper slopes, lower slopes, and valleys) of groundwater sample locations were adapted from the classification system of Theobald et al.[38] based on multi-scale topographic position index (mTPI).

Results and discussion

Across the Northern Appalachian region, 311 groundwater samples were analyzed, including 94 previously discussed samples in Region I (NE PA)[23] and 217 in Region II [SE OH (n=161) and N WV(n=56)) (Fig. S1). Most measured dissolved methane concentrations were below the 10 mg/L warning level given by the U.S. Department of the Interior,[39] in spite of the expansive fossil energy extraction in these regions (Fig. 1, Fig. S2). There were some exceedances above the warning level (4% of all samples), which presents a flammability risk rather than a toxicological concern.[39] The 50th, 75th and 90th percentiles of methane concentrations in all samples ranged over several orders of magnitude from 0.00066, 0.050, to 1.9 mg/L, respectively, and the median methane concentration within Region I (2.8×10^{-3} mg/L) was nearly one order of magnitude higher than that within Region II (3.5×10^{-4} mg/L; a histogram of concentration distribution for each region is available in Fig. S3). There was no statistically significant correlation (Spearman test) between methane concentration and distance to the nearest UOG well (Fig. 1A) or UOG well density (i.e., the number of UOG wells within a given radius of a groundwater sample (Fig. S4); this finding held in both study regions independently and in combination. This is consistent with prior results suggesting that linear transport distance to gas well in the UOG-dominated NE PA is not predictive of dissolved methane concentration.[24–29] As noteworthy counterexamples, Osborn et al.[15] and Jackson et al.[16] did find a negative correlation

between methane concentration and distance to gas well with n = 68 and n = 141 in 2011 and 2013, respectively, in NE PA. The contrast between these select earlier findings and this investigation could reflect a difference in temporal evolution of methane with increased time since the onset of UOG (ca. 2008), changes in gas well construction stemming, in part, from the tightening of regulations, or stochastic sampling effects associated with sample size and spatial distribution.

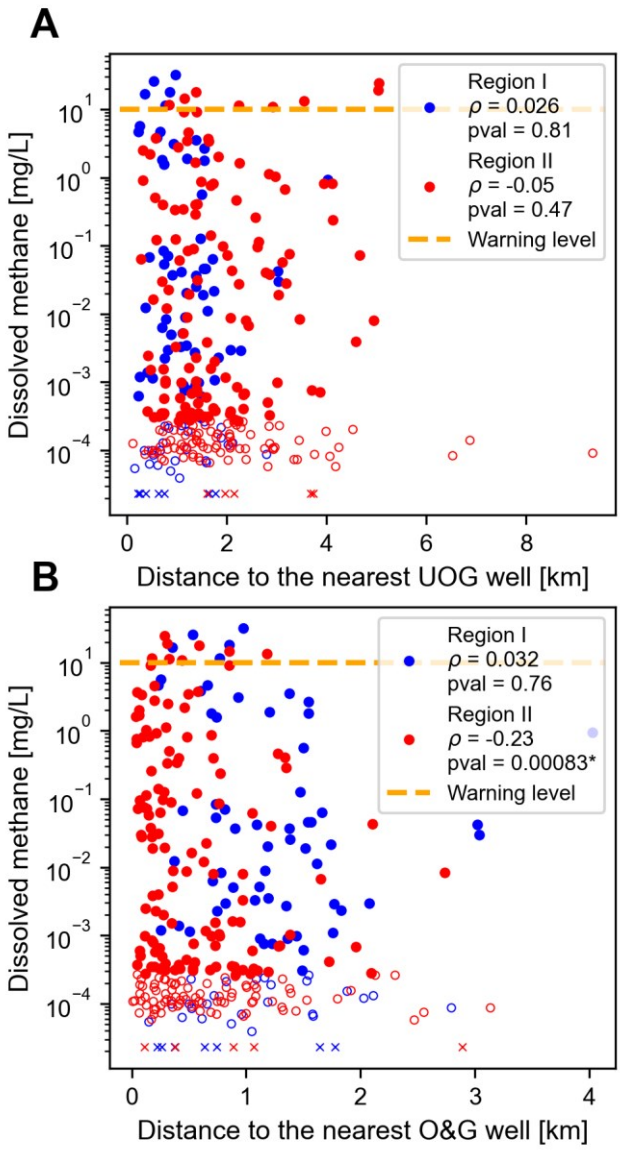

Figure 1. Groundwater methane concentrations in Region I (NE PA) and Region II (SE OH and N WV) as a function of distance to the nearest (A) UOG or (B) O&G well (i.e., conventional and unconventional). The warning level set by the U.S. Department of the Interior is 10 mg/L methane (dashed line).[39] Average groundwater methane from Region I (blue) and Region II (red) above the LOQ of 2.7×10^{-4} mg/L (filled symbols), between the LOQ and the LOD of 2.3×10^{-5} mg/L (open symbols), or below the LOD (crosses) are shown, where error bars on these measures are given in Fig. S2. For UOG only, Spearman correlations were not significant in either region (coefficients of 0.026, -0.050, and -0.037 and p-values of 0.81, 0.47, and 0.51 for Region I, Region II, and both regions combined, respectively). For O&G wells (UOG and conventional wells), Spearman correlations were significant for Region II only (coefficients of 0.032, -0.23, and -0.099 with p-values of 0.76, 0.00083, and 0.082 for Region I, Region II, and both regions combined, respectively). Note that confounding factors, such as topography, may be important drivers for these relationships.

The expansive coverage of this study enabled investigation of the impact of COG extraction on groundwater methane. Compared to the UOG-dominated Region I (around 60 COG wells and 1,500 UOG), Region II had a larger proportion of COG wells (around 50,000 COG wells and 4,000 UOG wells). In Region I, methane concentration was not correlated with distance to the nearest O&G well (conventional and unconventional wells; p=0.76; Fig. 1B), or the count of O&G wells within different radii (Fig. S5). In contrast, Region II methane concentrations were negatively correlated to the distance to the nearest O&G well with statistical significance (i.e., methane concentration was higher with closer distance to the well; p=0.00083; Fig. 1B) and positively correlated to the count of O&G wells within different radii with statistical significance (Fig. S5). Combining Region I and Region II data gave a near significant negative correlation between methane concentration and distance to O&G well (p=0.082, Fig. 1B), and significant

positive correlations between methane concentration and count of O&G wells within radius of 2 km (Fig. S5), reflecting the influence of Region II's high proportion of COG well composition. These findings suggest that the large number of COG wells in Region II could have introduced additional methane into the groundwater aquifer and emphasized the importance of evaluating COG activities alongside UOG activities; critically, it is possible that the apparent relationships between fossil energy development and enhanced groundwater methane concentration are the consequence of confounding factors such as topography (see later discussion). Furthermore, many COG wells in Region II are old (e.g., drilled in the 1920s), and well integrity issues have been reported to worsen with age (e.g., faulty well casing and annular cementation) in a previous study[40] but the effect was unclear in another,[41] and these issues could lead to stray gas migration that augmented groundwater methane in aquifers.[42–44] Indeed, methane concentration was positively correlated with the age of the nearest O&G well in Region II ($p = 0.002$), while the correlation was not statistically significant in Region I ($p = 0.26$, Fig. S6); confounding factors, such as topography, must also be considered (see later discussion). Further efforts may be needed to inspect COG wells (abandoned and active), identify key strategies for prioritizing those inspections, and eliminate associated methane emissions.

Other fossil energy extraction activities were prevalent in Region II, such as coal mining, which could influence groundwater methane via the mobilization of coal seam methane. Perhaps counterintuitively, groundwater methane was *less* abundant in proximity to active underground coal mining activities (Fig 2A). Exploring other geochemical indicators revealed that sulfate concentrations were elevated near coal mines (i.e., negatively correlated to the distance to active

underground coal mines). Note that distances to both surface and abandoned underground coal mines show a persistent negative correlation with groundwater sulfate concentrations (Fig. S7).

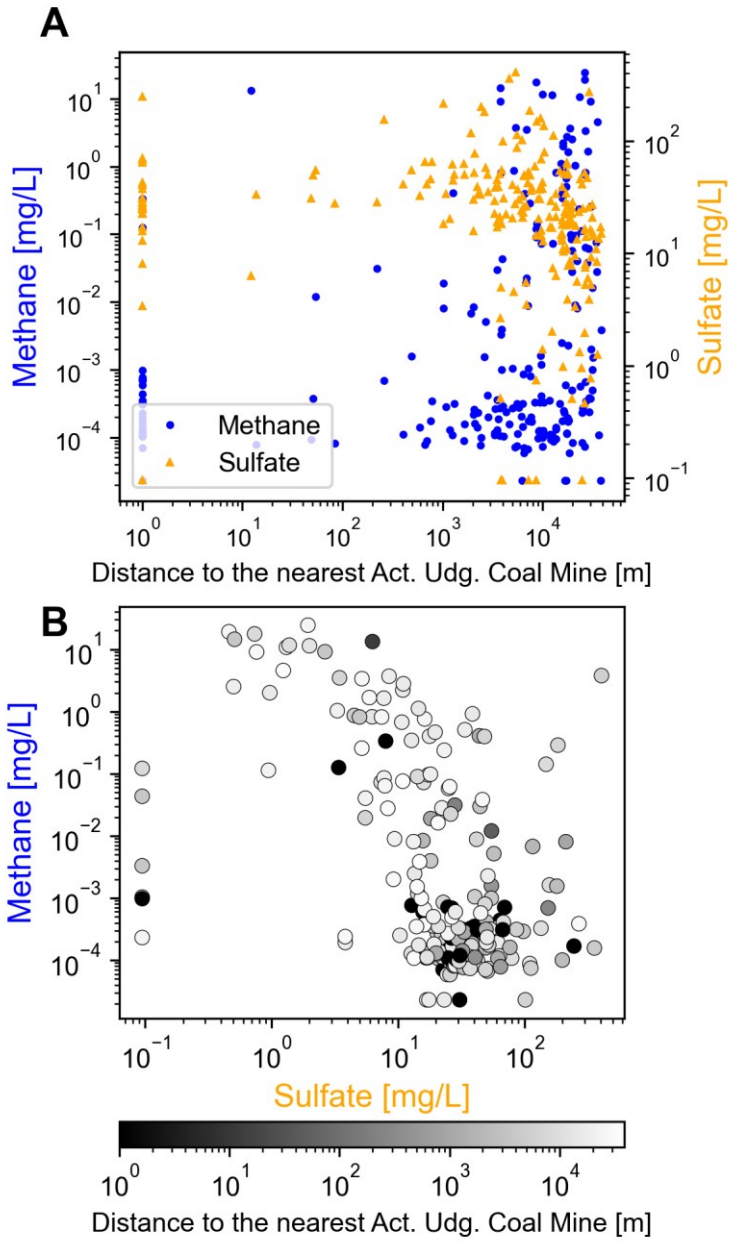

Figure 2. (A) In Region II, groundwater dissolved methane concentration (blue circles, left axis) increased while sulfate concentration (orange triangles, right axis) decreased with increasing distance to the nearest active underground coal mine. The Spearman correlation coefficients between

methane concentration and distance, between sulfate concentration and distance, and between methane concentration and sulfate concentration were 0.29 (p-value of 1.1×10^{-5}), -0.38 (p-value of 7.3×10^{-9}), and -0.46 (p-value of 1.4×10^{-12}), respectively. In order to show distance = 0 (i.e., sample overlapping with coal mines) in the logscale, distances equal to or smaller than 1 m were treated as 1 m. **(B) Correlation between dissolved methane and sulfate concentrations in Region II. The** distance to the coal mine is represented by the color of each marker.

Simultaneously, dissolved methane concentrations were correlated to the topographical location of the groundwater well (Fig. 3). The median methane concentration increased with lower topographical position [i.e., peaks had the lowest median methane, followed by upper slopes, lower slopes, and the highest methane concentrations in valleys; Welch's ANOVA p-value of 1.8×10^{-11}, and pairwise adjusted p-values by Games-Howell post-hoc test were significant between lower slope and upper slope (4.0×10^{-3}), lower slope and valley (5.2×10^{-5}), peak and valley (2.6×10^{-4}), and upper slope and valley (9.1×10^{-14})]. Also, high salinity and high Br-to-Cl ratio waters (type D and unclassified; see Fig. S8, Fig. S9, and SI text) were associated with high dissolved methane concentration (Fig. S8) and had a stronger tendency to appear in valleys than samples of other water types (Fig. S10), and the correlation between the water type and topographical class was confirmed to be statistically significant by a chi-squared test (simulated p-value of 1×10^{-3} based on 2,000 replicates). These correlations between methane concentration, topography, and water type hold in each study region (Fig. S11).

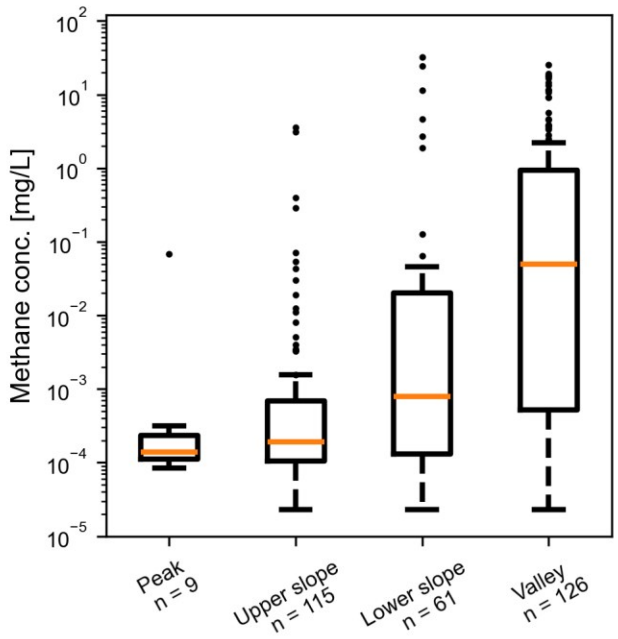

Figure 3. Groundwater dissolved methane concentration increased in topographical lows. Each rectangular box represents the distribution of methane concentrations within a certain topographical class, where the orange horizontal bar gives the median, and the upper and lower edges of the box represent the upper and lower quartiles (e.g., 75th and 25th percentile, respectively). The whiskers indicate variability outside the quartiles and individual datum (black dots) are only visible in the extrema outside these ranges.

The elevated dissolved methane concentration associated with valley topography and brine-impacted water type may be explained by the enhanced connectivity between the groundwater aquifer and underlying geological strata through fracture networks,[29,31,42] which have enhanced density beneath valleys. Valley topography often corresponds to higher density of underlying geological fractures than surrounding uplands because fractures such as faults, joints, and bedding partings generated by basement movement can increase lithologic weakness, which facilitate the formation of valleys by corrosion.[32,45,46] Further, existing valleys can accelerate the

formation of fractures. For example, river erosion of rocks releases horizontal stress in a valley wall and vertical stress in the valley bottom, causing deformation that increases the fracture density.[47,48] The secondary permeability created by these fractures may form pathways for the localized upward migration of methane and possibly Appalachian brine into the groundwater aquifer under valley topography,[29,42,45,49] explaining the occurrence of high methane concentration in brine-type groundwaters. Besides increased fracture density, other theories on the elevated methane concentration in valleys include: (i) the topographically driven groundwater flow from hilltop to valley entraining the migrating methane and brine into the valley bottom[29,32] and (ii) valley bottoms have the deepest incision into the bedrock and the smallest vertical distance to the buried thermogenic methane as well as the subterranean boundary between fresh groundwater and brine-impacted groundwater.[32]

Incidentally, the topographic location of the groundwater samples was correlated with the sample location's distance to the nearest O&G well and distance to the nearest active underground coal mine in Region II (Fig. S12), where samples in the valleys had smaller distances to O&G wells and larger distances to coal mines, compared to samples on the slopes. Thus, apparent correlations between methane levels and distances to coal mine or O&G well may be driven by topography as a confounding factor. To evaluate this possibility, we performed multiple linear regressions to predict groundwater methane concentration, $C_{methane}$, as a function of the key variables ($d_{O\&G}$, distance to the nearest O&G well; d_{coal}, distance to the nearest active underground coal mine; and $C_{sulfate}$, sulfate concentration) and topography ($T_{topography}$, converted to integers 1-4 for the valley, lower slope, upper slope, and peak, respectively) (Eqn 1; Table 1).

$$C_{methane} = aA_{variable} + bT_{topography} + c, \quad \text{(Eqn 1)}$$

where $A_{variable}$ was $d_{O\&G}$, d_{coal}, or $C_{sulfate}$, the distance to the nearest O&G well, distance to the nearest active underground coal mine, or sulfate concentration, respectively. The linear models were fitted on the ranks of the variables (rank increases with variable value) to account for the nonlinearity in their correlations and standardize the variable spans. After adding topography to the model, associations between methane concentration and distance to the nearest O&G well and distance to the nearest active underground coal mine were no longer statistically significant, while the association between methane concentration and topography was significant. Similarly, samples located in valleys had more O&G wells within a 1 km radius, and the age of the nearest O&G well was older compared to samples on the slopes (Fig. S13). After accounting for topography as a confounding factor, the associations of methane concentration to the count of O&G wells within different radii (Table S2), and to the age of the nearest O&G well (Table S3) were not statistically significant. Taken together, these analyses indicate that the correlation between methane concentration and O&G extraction depended on the topographical variation in Region II, rather than the causal relationship between gas drilling and elevated methane level. Interestingly, higher sulfate concentration was still a significant predictor of lower methane concentration with topography present. Note that a shorter distance to a coal mine was a significant predictor of higher sulfate concentration when topography or methane concentration was considered as a potential confounder (Eqn 2, Table 2).

$$C_{sulfate} = aA_{variable} + bd_{coal} + c, \quad \text{(Eqn 2)}$$

where $A_{variable}$ was $T_{topography}$ or $C_{methane}$, the topographical designation or the methane concentration, respectively. Higher sulfate concentrations were reliably related to the distance to the nearest coal mine, even when including topography or methane concentration as potential confounder. These results are consistent with a mechanism in which groundwater sulfate

concentration affects methane concentration and in which coal mining elevates sulfate concentration.

Table 1. Regression outputs for the prediction of methane concentration as a function of variables of interest and topography as a confounder (Eqn 1).

$A_{variable}$	*a*	*p-value of a*	*b*	*p-value of b*	*c*
$d_{O\&G}$	-0.083	0.16	-0.57	$<2 \times 10^{-16}$*	180
d_{coal}	0.056	0.38	-0.57	2.1×10^{-14}*	165
$C_{sulfate}$	-0.29	2.2×10^{-6}*	-0.48	2.2×10^{-12}*	192

*statistically significant at the 5% threshold.

Table 2. Regression outputs for the prediction of sulfate concentration as a function of distance to coal mine and another potential confounding variable (Eqn 2).

$A_{variable}$	*a*	*p-value of a*	*b*	*p-value of b*	*c*
$T_{topography}$	0.30	9.0×10^{-5}*	-0.26	2.2×10^{-4}*	105
$C_{methane}$	-0.38	2.8×10^{-9}*	-0.27	1.6×10^{-5}*	180

*statistically significant at the 5% threshold.

To interpret the negative correlation between sulfate and the distance to the nearest coal mine (Fig. 2A) and the negative correlation between sulfate and methane (Fig. 2B), we note that groundwater can be enriched in sulfate due to coal mining (e.g., via acid mine drainage[50,51]) and acknowledge the known importance of sulfate in geo-biochemical methane cycling.[34,52,53] Increased sulfate concentrations can lower methane concentrations in groundwater through two

possible mechanisms: (i) inhibiting methanogenesis and (ii) methane oxidation coupled with sulfate reduction. First, in order for methanogenesis to occur, carbonate can serve as an electron acceptor for organic matter oxidation, producing methane (Reaction 1). However, sulfate is often a thermodynamically preferred electron acceptor due to both the favorable energy gain (larger $|\Delta G^0|$) and abundance of sulfate (i.e., the organic matter is oxidized without the production of methane; Reaction 2). Second, in anaerobic environments, sulfate can promote methane oxidation via microbial reactions (e.g., by methanotrophs and sulfate reducing bacteria), thereby reducing methane abundance (Reaction 3).[52] As such, recognizing that coal mining often mobilizes dissolved sulfate provides multiple mechanistic pathways that ultimately reduce dissolved methane concentrations. (See SI Fig. S14, Table S4, and associated text for further discussion of dissolved Fe and Mn concentrations that support the importance of sulfate cycling in these groundwaters).

$CH_3COO^- + HCO_3^- + H_2O \rightarrow CH_4 + 2\ HCO_3^-$, ΔG^0 = -14.7 kJ mol^{-1}

(Reaction 1, Methanogenesis[54])

$CH_3COO^- + SO_4^{2-} \rightarrow HS^- + 2\ HCO_3^-$, ΔG^0 = -47.4 kJ mol^{-1}

(Reaction 2, Sulfate reduction with organic matter oxidation[54])

$CH_4 + SO_4^{2-} \rightarrow HCO_3^- + HS^- + H_2O$, ΔG^0 = -16.6 kJ mol^{-1}

(Reaction 3, Sulfate reduction with methane oxidation[55])

Isotopic characterization (e.g., $\delta^{13}C$ and $\delta^{2}H$) can provide some further indication of the biogeochemical processes of methane formation and conversion. Specifically, methane generated by thermal decomposition of organic matter buried deep underground (i.e., thermogenic methane) typically has enriched ^{13}C and ^{2}H relative to methane generated by methanogenesis (i.e., biogenic methane). This is due to a difference in the activation energies of light and heavy isotopologues, where the reaction of light isotopologues has a lower energetic barrier; this effect is more pronounced in enzymatically catalyzed biological processes (i.e., due to enzymatic stabilization of the transition state).[56,57] Similarly, microbial oxidation of methane can result in enriched $\delta^{13}C$ and $\delta^{2}H$ signatures of the residual methane (e.g., apparently more thermogenic), and the enrichment in $\delta^{2}H$ is usually much greater than that in $\delta^{13}C$.[35,58]

In Region I, the majority of dissolved methane samples fell within the thermogenic $\delta^{13}C$ - $\delta^{2}H$ range, whereas in Region II, a few samples were classified as thermogenic or CO_2 reduction biogenic gas (Fig. 4A). More than half of the Region II samples fell close to or outside the traditionally defined thermogenic or biogenic ranges. Some Region II samples had $\delta^{13}C$ ratios similar to those of Region I samples, but with elevated $\delta^{2}H$ ratios. This was consistent with the effect of microbial oxidation, supporting the hypothesis of anaerobic methane oxidation coupled with sulfate reduction in Region II. Further, the $\delta^{13}C$ isotopic ratios of thermogenic methane in Region I were relatively depleted compared to Marcellus production gas, annular gas, and dissolved gas in shale gas drilling-impacted groundwater collected from Sugar Run, Bradford County[42] and Dimock, Susquehanna County[43] in PA (see detailed discussion in Li et al.[23]), but similar to those of Upper Devonian gases from Catskill and Lockhaven formations above the Marcellus shale ($\delta^{13}C$ mean = -42.1 ± 6.3 ‰ of 238 samples, error bars in Fig. 4A)[59]. This

suggested that the sampled methane did not originate from shale gas drilling and was consistent with the lack of correlation between methane concentration and proximity to UOG wells observed in Region I. In addition, the isotopic ratios of groundwater methane in Region II were depleted relative to production gas samples from Ordovician age formations (to which the Utica Shale belongs) in Cottontree field, Roane County, WV,[60,61] supporting the influence of other processes on methane groundwater concentrations in the region. Lastly, for high-methane outliers in each topography and geochemical groups (black dots beyond the whiskers in Fig. 3 and Fig. S8), the $\delta^{13}C$ ratios varied between -30 to -90 ‰ and distance to the nearest gas well varied between 0 to 4 km (Fig. S15), and neither the $\delta^{13}C$ nor the proximity were significantly enhanced compared to the median values of the groups (when the number of outliers exceeded 5). Therefore, it was unlikely for these outliers to be affected by O&G gas derived methane contamination.

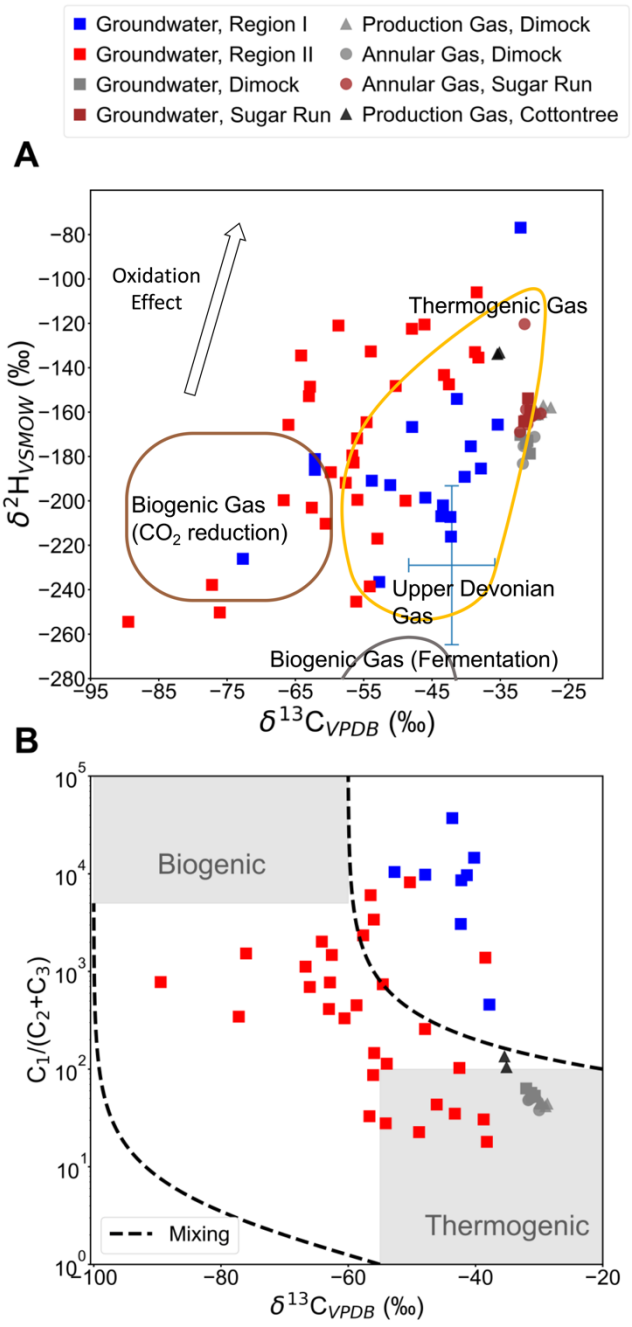

Figure 4. (A) $\delta^{13}C$ and $\delta^{2}H$ signatures of groundwater methane collected in Region I and Region II and of reference samples. The $\delta^{13}C$ and $\delta^{2}H$ signatures of methane are expressed in $\delta^{13}C_{VPDB}$ (‰) and $\delta^{2}H_{VSMOW}$ (‰), where VPDB indicates Vienna Pee Dee Belemnite and VSMOW indicates Vienna Standard Mean Ocean Water. Groundwater samples (squares) with high methane concentrations (> 0.5 mg/L) were selected for isotopic analysis and are shown for Region I (blue) and Region II (red). Samples

collected near reported stray gas contamination sites (light gray symbols in Dimock, Susquehanna County, PA,[43] brown symbols in Sugar Run, Bradford County, PA,[42] and black symbols in Cottontree field, Roane County, WV[60,61]) are shown for comparison. The isotopic ranges of Upper Devonian methane (for $\delta^{13}C$, mean = -42.1‰, standard deviation = 6.3‰; for $\delta^{2}H$, mean = -229.0‰, standard deviation = 35.8‰) are shown (error bars centered at means showing standard deviations).[59] The approximate methane isotopic ranges of thermogenic gas (orange outline), CO_2 reduction biogenic gas (brown outline), and fermentation biogenic gas (gray outline) were adapted from literature.[42,66] The effect of microbial oxidation is shown by the arrow. (B) **C1-to-C2 + C3 ratio vs. $\delta^{13}C$-CH_4 of groundwater samples.** Groundwater samples with $\delta^{13}C$-CH_4 analyzed and above-LOQ ethane or propane concentration are shown. The typical extents of biogenic and thermogenic gas (gray shaded areas) are adapted from literature.[67] The mixing between typical biogenic and thermogenic gases is represented by the dashed lines. Reference gas samples (light gray symbols in Dimock and black symbols in Cottontree field) are also shown.

Methanogens primarily produce methane without higher-chain hydrocarbons (e.g., ethane and propane), resulting in high ratios of methane concentration to the sum of ethane and propane concentration ("C1-to-C2+C3" ratio) in biogenic gas. Thermogenic gas has a larger proportion of higher-chain hydrocarbons and correspondingly lower C1-to-C2+C3 ratios. In Region II, the methane $\delta^{13}C$ ratios and dissolved gas compositions of some samples fell within the thermogenic range, while the rest were explained by mixing biogenic and thermogenic gas (Fig. 4B). The Region I samples indicated a thermogenic $\delta^{13}C$ profile (-30 to -55 ‰) but were depleted in C2 and C3 hydrocarbons (C1-to-C2+C3 ratios greater than 100). This phenomenon was previously observed in PA,[16,62,63] and researchers have proposed equilibrium partitioning fractionation (albeit with some tenuous assumptions) to explain the higher hydrocarbon ratio.[62] Similarly,

others have suggested preferential C2 and C3 oxidation that might explain elevated C1 to C2+C3 ratios,[64,65] but there is little evidence to support this claim. It is possible that the unique and reproducible signature could simply be characteristic of the local geological formations.[23]

Based on the observed correlation between methane concentration and topographical, geochemical, and geobiological indicators, we propose that the following mechanisms governed the spatial distribution of groundwater methane: first, the fracture network beneath valley topography enhanced the secondary permeability and facilitated the migration of thermogenic methane from reservoirs overlying the producing shales (e.g., Upper Devonian reservoirs) upward to groundwater aquifers. The Appalachian basin brine could originate from much deeper formations than the methane and migrated on different time scales, and it is uncertain whether the brine shared the same migration pathway as methane. Nevertheless, brine tracers (e.g., type D water) were observed in valleys coincident with the enriched methane. Second, sulfate released by coal mining operations entered groundwater aquifers, and the data are consistent with the oxidation of organic matter using sulfate as an electron acceptor outcompeting the utilization of organic matter by methanogenesis, thus reducing biogenic methane production. The microbial oxidation of existing biogenic or thermogenic methane in the groundwater coupled with microbial sulfate reduction could also reduce the dissolved methane concentration. Taken together, dissolved methane concentration was lower closer to coal mining regions and elevated in topographical lows influenced by brine intrusion; this indicates that there will be a great deal of complexity in predicting vulnerability to methane intrusion to domestic wells associated with colocated fossil energy extraction.

Implications

This large (n=311) groundwater study across Northern Appalachia revealed the contribution of a variety of fossil fuel extraction technologies, natural biogeochemical factors, and topographical features on the groundwater methane distribution. In order to evaluate the climatic impact of the observed groundwater methane, we approximated the total methane emission rate of groundwater discharge in Region II by multiplying the mean groundwater recharge rate (0.20 m/year[68,69]) by the geographical area (9,400 km^2), and then by the median dissolved methane concentration of 3.5×10^{-4} mg/L (or 1.3×10^{-4} - 4.3×10^{-2} mg/L, representing the 25th and 75th percentile of the concentration distribution, respectively) to be on the order of 0.7 (or 0.2 - 80) tonnes CH_4 / year. This estimation assumed that the groundwater recharge rate was equivalent to the discharge rate over the annual time scale and that all dissolved methane eventually degassed into the atmosphere. Using the same approach, the total emission rate in Region I was previously estimated to be on the order of 2 (or 0.08 - 30) tonnes CH_4 /year.[23] For comparison, *each* active unconventional gas well in PA leaked 588 m^3 natural gas / year on average by fugitive emission or engineered venting,[70] which equates to 0.35 tonnes CH_4 /year assuming the composition of natural gas is 83.5% methane. Considering there are approximately 1,500 O&G wells across Region I, the estimated groundwater emission rates are small compared to losses at the well head.

There are several important environmental implications of this study's findings. First, methane emissions from O&G development via the groundwater pathway should have a relatively small climate impact. The correlation between groundwater methane concentration and the distance to

O&G well was not significant in Region I and, after controlling for the confounding effect of topography in Region II, was not significant there. Therefore, it was unlikely that O&G development systematically altered groundwater methane concentrations in the study region. Moreover, the estimated total emission from groundwater discharge was small. Future efforts to reduce O&G methane emissions should focus on the above-ground methane emissions from well pads or pipelines using monitoring measures such as satellite or aerial survey (note that this study didn't explicitly evaluate extreme events such as well blow-outs, which could be large methane sources).[35] Second, this work provided a framework for predicting the public health and safety risks associated with elevated groundwater methane concentrations in regions with fossil fuel production. For example, residents living in valleys may have a higher risk of methane exposure. Residents living closer to O&G wells may also see higher methane in their groundwater (despite the fact that proximity to O&G is not necessarily the *cause* of high methane). Third, the interaction between groundwater methane and groundwater sulfate likely emitted by coal mining exemplified the complex influences of industrial processes on local biogeochemistry. A future study could leverage additional information such as $\delta^{34}S - SO_4^{2-}$, $\delta^{18}O - SO_4^{2-}$, and $\delta^{13}C$ – DIC isotopic signatures and HS^- concentration to gain deeper insight into the proposed biogeochemical processes. Finally, there is an important role of topography in affecting the correlations among geochemical indicators, illustrating the important interplay between biology, chemistry, and physics in environmental systems. As such, confounding factors are implicit in all environmental studies, and computational tools to address this complexity are important for a fundamental understanding of the relative contributions of each.

Supporting Information: data sources of geographical information, maps of the study regions, and supplementary information such as figures and text on additional geospatial and geochemical analyses.

Competing Interest Statement: The authors declare no competing financial interest.

Acknowledgments: This publication was developed under Assistance Agreement No. CR839249 awarded by the U.S. Environmental Protection Agency (EPA) to Yale University. It has not been formally reviewed by EPA. The views expressed in this document are solely those of the authors and do not necessarily reflect those of the Agency. EPA does not endorse any products or commercial services mentioned in this publication. The authors thank Keli Sorrentino and Julie Plano for support in logistics and data management, Barathkumar Baskaran for TOC graphic preparation, as well as the UC Davis Stable Isotope Facility for isotopic analysis, and anonymous reviewers for critical improvements to the manuscript.

References

(1) Myhre, G.; Shindell, D.; Bréon, F.; Collins, W.; Fuglestvedt, J.; Huang, J.; Koch, D.; Lamarque, J.; Lee, D.; Mendoza, B.; Nakajima, T.; Robock, A.; Stephens, G.; Takemura, T.; Zhan, H. Anthropogenic and Natural Radiative Forcing: In Climate Change 2013: The Physical Science Basis. Contribution of Working Group I to the Fifth Assessment Report of the Intergovernmental Panel on Climate Change. *Cambridge Univ. Press. Cambridge, United Kingdom New York, NY, USA* **2013**, 659–740. https://doi.org/10.1017/CBO9781107415324.018.

(2) Ramseur, J. L. *Inflation Reduction Act Methane Emissions Charge: In Brief*; 2022.

(3) Nesbit, J. The new Global Methane Pledge can buy time while the world drastically reduces fossil fuel use https://www.pbs.org/newshour/science/the-new-global-methane-pledge-can-buy-time-while-the-world-drastically-reduces-fossil-fuel-use (accessed Aug 31, 2022).

(4) Homepage | Global Methane Pledge https://www.globalmethanepledge.org/ (accessed Oct 4, 2022).
(5) Saunois, M.; Stavert, A.; Poulter, B.; Bousquet, P.; Canadell, J.; Jackson, R.; Raymond, P.; Dlugokencky, E.; Houweling, S.; Patra, P.; Ciais, P.; Arora, V.; Bastviken, D.; Bergamaschi, P.; Blake, D.; Brailsford, G.; Bruhwiler, L.; Carlson, K.; Carrol, M.; Castaldi, S.; Chandra, N.; Crevoisier, C.; Crill, P.; Covey, K.; Curry, C.; Etiope, G.; Frankenberg, C.; Gedney, N.; Hegglin, M.; Höglund-Isaksson, L.; Hugelius, G.; Ishizawa, M.; Ito, A.; Janssens-Maenhout, G.; Jensen, K.; Joos, F.; Kleinen, T.; Krummel, P.; Langenfelds, R.; Laruelle, G.; Liu, L.; Machida, T.; Maksyutov, S.; McDonald, K.; McNorton, J.; Miller, P.; Melton, J.; Morino, I.; Müller, J.; Murguia-Flores, F.; Naik, V.; Niwa, Y.; Noce, S.; O'Doherty, S.; Parker, R.; Peng, C.; Peng, S.; Peters, G.; Prigent, C.; Prinn, R.; Ramonet, M.; Regnier, P.; Riley, W.; Rosentreter, J.; Segers, A.; Simpson, I.; Shi, H.; Smith, S.; Steele, L. P.; Thornton, B.; Tian, H.; Tohjima, Y.; Tubiello, F.; Tsuruta, A.; Viovy, N.; Voulgarakis, A.; Weber, T.; van Weele, M.; van der Werf, G.; Weiss, R.; Worthy, D.; Wunch, D.; Yin, Y.; Yoshida, Y.; Zhang, W.; Zhang, Z.; Zhao, Y.; Zheng, B.; Zhu, Q.; Zhu, Q.; Zhuang, Q. The Global Methane Budget 2000–2017. *Earth Syst. Sci. Data* **2020**, *12* (3), 1561–1623. https://doi.org/10.5194/essd-12-1561-2020.
(6) U.S. Energy Information Administration. U.S. energy facts explained https://www.eia.gov/energyexplained/us-energy-facts/data-and-statistics.php (accessed Aug 31, 2022).
(7) U.S. Energy Information Administration. Monthly Energy Review - August 2022. **2022**.
(8) U.S. Energy Information Administration. Frequently Asked Questions (FAQs) - How much shale gas is produced in the United States? https://www.eia.gov/tools/faqs/faq.php?id=907&t=8 (accessed Sep 1, 2022).
(9) U.S. Energy Information Administration. Frequently Asked Questions (FAQs) - How much shale (tight) oil is produced in the United States? https://www.eia.gov/tools/faqs/faq.php?id=847&t=6 (accessed Sep 1, 2022).
(10) U.S. Energy Information Administration. *Annual Energy Outlook 2022 Chart Library*; Washington, DC, 2022.
(11) Murtaugh, D.; Stringer, D. Coal Was Meant to Be History. Instead, Its Use Is Soaring https://www.bloomberg.com/news/articles/2022-11-04/most-polluting-fossil-fuel-finds-new-life-with-world-burning-more-coal-for-power?leadSource=uverify wall (accessed Jan 8, 2023).
(12) Duren, R. M.; Thorpe, A. K.; Foster, K. T.; Rafiq, T.; Hopkins, F. M.; Yadav, V.; Bue, B. D.; Thompson, D. R.; Conley, S.; Colombi, N. K.; Frankenberg, C.; McCubbin, I. B.; Eastwood, M. L.; Falk, M.; Herner, J. D.; Croes, B. E.; Green, R. O.; Miller, C. E. California's Methane Super-Emitters. *Nature* **2019**, *575* (7781), 180–184. https://doi.org/10.1038/s41586-019-1720-3.
(13) Alvarez, R. A.; Zavala-Araiza, D.; Lyon, D. R.; Allen, D. T.; Barkley, Z. R.; Brandt, A. R.; Davis, K. J.; Herndon, S. C.; Jacob, D. J.; Karion, A.; Kort, E. A.; Lamb, B. K.; Lauvaux, T.; Maasakkers, J. D.; Marchese, A. J.; Omara, M.; Pacala, S. W.; Peischl, J.; Robinson, A. L.; Shepson, P. B.; Sweeney, C.; Townsend-Small, A.; Wofsy, S. C.; Hamburg, S. P. Assessment of Methane Emissions from the U.S. Oil and Gas Supply Chain. *Science (80-.).* **2018**, *361* (6398), 186–188. https://doi.org/10.1126/science.aar7204.
(14) Omara, M.; Sullivan, M. R.; Li, X.; Subramian, R.; Robinson, A. L.; Presto, A. A.

Methane Emissions from Conventional and Unconventional Natural Gas Production Sites in the Marcellus Shale Basin. *Environ. Sci. Technol.* **2016**, *50* (4), 2099–2107. https://doi.org/10.1021/acs.est.5b05503.

(15) Osborn, S. G.; Vengosh, A.; Warner, N. R.; Jackson, R. B. Methane Contamination of Drinking Water Accompanying Gas-Well Drilling and Hydraulic Fracturing. *Proc. Natl. Acad. Sci.* **2011**, *108* (20), 8172–8176. https://doi.org/10.1073/pnas.1100682108.

(16) Jackson, R. B.; Vengosh, A.; Darrah, T. H.; Warner, N. R.; Down, A.; Poreda, R. J.; Osborn, S. G.; Zhao, K.; Karr, J. D. Increased Stray Gas Abundance in a Subset of Drinking Water Wells near Marcellus Shale Gas Extraction. *Proc. Natl. Acad. Sci. U. S. A.* **2013**, *110* (28), 11250–11255. https://doi.org/10.1073/pnas.1221635110.

(17) Heilweil, V. M.; Grieve, P. L.; Hynek, S. A.; Brantley, S. L.; Solomon, D. K.; Risser, D. W. Stream Measurements Locate Thermogenic Methane Fluxes in Groundwater Discharge in an Area of Shale-Gas Development. *Environ. Sci. Technol.* **2015**, *49* (7), 4057–4065. https://doi.org/10.1021/es503882b.

(18) Woda, J.; Wen, T.; Lemon, J.; Marcon, V.; Keeports, C. M.; Zelt, F.; Steffy, L. Y.; Brantley, S. L. Methane Concentrations in Streams Reveal Gas Leak Discharges in Regions of Oil, Gas, and Coal Development. *Sci. Total Environ.* **2020**, 140105. https://doi.org/10.1016/j.scitotenv.2020.140105.

(19) Stanley, E. H.; Casson, N. J.; Christel, S. T.; Crawford, J. T.; Loken, L. C.; Oliver, S. K. The Ecology of Methane in Streams and Rivers: Patterns, Controls, and Global Significance. *Ecol. Monogr.* **2016**, *86* (2), 146–171. https://doi.org/10.1890/15-1027.

(20) Pinti, D. L.; Gelinas, Y.; Moritz, A. M.; Larocque, M.; Sano, Y. Anthropogenic and Natural Methane Emissions from a Shale Gas Exploration Area of Quebec, Canada. *Sci. Total Environ.* **2016**, *566–567*, 1329–1338. https://doi.org/10.1016/j.scitotenv.2016.05.193.

(21) Gooddy, D. C.; Darling, W. G. The Potential for Methane Emissions from Groundwaters of the UK. *Sci. Total Environ.* **2005**, *339* (1–3), 117–126. https://doi.org/10.1016/j.scitotenv.2004.07.019.

(22) Crawford, J. T.; Striegl, R. G.; Wickland, K. P.; Dornblaser, M. M.; Stanley, E. H. Emissions of Carbon Dioxide and Methane from a Headwater Stream Network of Interior Alaska. *J. Geophys. Res. Biogeosciences* **2013**, *118* (2), 482–494. https://doi.org/10.1002/jgrg.20034.

(23) Li, Y.; Thelemaque, N. A.; Siegel, H. G.; Clark, C. J.; Ryan, E. C.; Brenneis, R. J.; Gutchess, K. M.; Soriano, M. A.; Xiong, B.; Deziel, N. C.; Saiers, J. E.; Plata, D. L. Groundwater Methane in Northeastern Pennsylvania Attributable to Thermogenic Sources and Hydrogeomorphologic Migration Pathways. *Environ. Sci. Technol.* **2021**, *55* (24), 16413–16422. https://doi.org/10.1021/acs.est.1c05272.

(24) Siegel, D. I.; Azzolina, N. A.; Smith, B. J.; Perry, A. E.; Bothun, R. L. Methane Concentrations in Water Wells Unrelated to Proximity to Existing Oil and Gas Wells in Northeastern Pennsylvania. *Environ. Sci. Technol.* **2015**, *49* (7), 4106–4112. https://doi.org/10.1021/es505775c.

(25) Molofsky, L. J.; Connor, J. A.; Farhat, S. K.; Wylie, A. S.; Wagner, T. Methane in Pennsylvania Water Wells Unrelated to Marcellus Shale Fracturing. *Oil Gas J.* **2011**, *109* (19).

(26) Molofsky, L. J.; Connor, J. A.; Wylie, A. S.; Wagner, T.; Farhat, S. K. Evaluation of Methane Sources in Groundwater in Northeastern Pennsylvania. *GroundWater* **2013**, *51*

(3), 333–349. https://doi.org/10.1111/gwat.12056.
(27) Li, Z.; You, C.; Gonzales, M.; Wendt, A. K.; Wu, F.; Brantley, S. L. Searching for Anomalous Methane in Shallow Groundwater near Shale Gas Wells. *J. Contam. Hydrol.* **2016**, *195*, 23–30. https://doi.org/10.1016/j.jconhyd.2016.10.005.
(28) Li, Z.; You, C.; Gonzales, M.; Wendt, A. K.; Wu, F.; Brantley, S. L. Corrigendum to "Searching for Anomalous Methane in Shallow Groundwater near Shale Gas Wells" (J. Contam. Hydrol. (2016) 195 (23–30) (S0169772216300985) (10.1016/j.Jconhyd.2016.10.005)). *Journal of Contaminant Hydrology*. Elsevier B.V. December 1, 2017, pp 50–51. https://doi.org/10.1016/j.jconhyd.2017.09.009.
(29) Wen, T.; Niu, X.; Gonzales, M.; Zheng, G.; Li, Z.; Brantley, S. L. Big Groundwater Data Sets Reveal Possible Rare Contamination Amid Otherwise Improved Water Quality for Some Analytes in a Region of Marcellus Shale Development. *Environ. Sci. Technol.* **2018**, *52* (12), 7149–7159. https://doi.org/10.1021/acs.est.8b01123.
(30) Warner, N. R.; Jackson, R. B.; Darrah, T. H.; Osborn, S. G.; Down, A.; Zhao, K.; White, A.; Vengosh, A. Geochemical Evidence for Possible Natural Migration of Marcellus Formation Brine to Shallow Aquifers in Pennsylvania. *Proc. Natl. Acad. Sci.* **2012**, *109* (30), 11961–11966. https://doi.org/10.1073/pnas.1121181109.
(31) Woda, J.; Wen, T.; Oakley, D.; Yoxtheimer, D.; Engelder, T.; Clara Castro, M.; Brantley, S. L. Detecting and Explaining Why Aquifers Occasionally Become Degraded near Hydraulically Fractured Shale Gas Wells. *Proc. Natl. Acad. Sci. U. S. A.* **2018**, *115* (49), 12349–12358. https://doi.org/10.1073/pnas.1809013115.
(32) Heisig, P. M.; Scott, T.-M. Occurrence of Methane in Groundwater of South-Central New York State, 2012- Systematic Evaluation of a Glaciated Region by Hydrogeologic Setting. *Sci. Investig. Rep.* **2013**, *2013–5190*. https://doi.org/10.3133/sir20135190.
(33) Wen, T.; Woda, J.; Marcon, V.; Niu, X.; Li, Z.; Brantley, S. L. Exploring How to Use Groundwater Chemistry to Identify Migration of Methane near Shale Gas Wells in the Appalachian Basin. *Environ. Sci. Technol.* **2019**, *53* (15), 9317–9327. https://doi.org/10.1021/acs.est.9b02290.
(34) Villa, C. A. Identification of the Causes and Extent of Elevated Methane Concentrations in the Groundwater of Eastern Kentucky, University of Kentucky, 2020. https://doi.org/https://doi.org/10.13023/etd.2020.486.
(35) Schout, G.; Hartog, N.; Hassanizadeh, S. M.; Griffioen, J. Impact of an Historic Underground Gas Well Blowout on the Current Methane Chemistry in a Shallow Groundwater System. *Proc. Natl. Acad. Sci. U. S. A.* **2017**, *115* (2), 296–301. https://doi.org/10.1073/pnas.1711472115.
(36) Magen, C.; Lapham, L. L.; Pohlman, J. W.; Marshall, K.; Bosman, S.; Casso, M.; Chanton, J. P. A Simple Headspace Equilibration Method for Measuring Dissolved Methane. *Limnol. Oceanogr. Methods* **2014**, *12* (SEP), 637–650. https://doi.org/10.4319/lom.2014.12.637.
(37) Siegel, H. G.; Soriano, M. A.; Clark, C. J.; Johnson, N. P.; Wulsin, H. G.; Deziel, N. C.; Plata, D. L.; Darrah, T. H.; Saiers, J. E. Natural and Anthropogenic Processes Affecting Domestic Groundwater Quality within the Northwestern Appalachian Basin. *Environ. Sci. Technol.* **2022**, *56* (19), 13761–13773. https://doi.org/10.1021/acs.est.2c04011.
(38) Theobald, D. M.; Harrison-Atlas, D.; Monahan, W. B.; Albano, C. M. Ecologically-Relevant Maps of Landforms and Physiographic Diversity for Climate Adaptation Planning. *PLoS One* **2015**, *10* (12), e0143619.

https://doi.org/10.1371/journal.pone.0143619.
(39) Eltschlager, K. K.; Hawkins, J. W.; Ehler, W. C.; Baldassare, F. J. Technical Measures for the Invetigation and Mitigation of Fugitive Methane Hazards in Areas of Coal Mining, U.S. Department of the Interior, Office of Surface Mining. **2001.**
(40) Brufatto, C.; Cochran, J.; Conn, L.; Power, D.; El-Zeghaty, S. Z. A. A.; Fraboulet, B.; Griffin, T.; James, S.; Munk, T.; Justus, F.; Levine, J. R.; Montgomery, C.; Murphy, D.; Pfeiffer, J.; Pornpoch, T.; Rishmani, L. From Mud to Cement - Building Gas Wells. *Oilf. Rev.* **2003**, *15* (3), 62–76.
(41) Watson, T. L.; Bachu, S. Evaluation of the Potential for Gas and CO2 Leakage along Wellbores. In *SPE Drilling and Completion*; Society of Petroleum Engineers, 2009; Vol. 24, pp 115–126. https://doi.org/10.2118/106817-PA.
(42) Llewellyn, G. T.; Dorman, F.; Westland, J. L.; Yoxtheimer, D.; Grieve, P.; Sowers, T.; Humston-Fulmer, E.; Brantley, S. L. Evaluating a Groundwater Supply Contamination Incident Attributed to Marcellus Shale Gas Development. *Proc. Natl. Acad. Sci. U. S. A.* **2015**, *112* (20), 6325–6330. https://doi.org/10.1073/pnas.1420279112.
(43) Hammond, P. A. The Relationship between Methane Migration and Shale-Gas Well Operations near Dimock, Pennsylvania, USA. *Hydrogeol. J.* **2016**, *24* (2), 503–519. https://doi.org/10.1007/s10040-015-1332-4.
(44) Darrah, T. H.; Vengosh, A.; Jackson, R. B.; Warner, N. R.; Poreda, R. J. Noble Gases Identify the Mechanisms of Fugitive Gas Contamination in Drinking-Water Wells Overlying the Marcellus and Barnett Shales. *Proc. Natl. Acad. Sci. U. S. A.* **2014**, *111* (39), 14076–14081. https://doi.org/10.1073/pnas.1322107111.
(45) Mason, G. Structurally Related Migration Of Hydrocarbons in the Central Appalachian Basin of Eastern Ohio. *AAPG Search Discov. Artic. #50733* **2012**.
(46) Taylor, L. E. Groundwater Resources of the Upper Susquehanna River Basin, Pennsylvania. *Pennsylvania Geol. Surv. 4th ser. Water Resource Report 58.* **1984**.
(47) Ferguson, H. F.; Hamel, J. V. Valley Stress Relief in Flat-Lying Sedimentary Rocks. *Weak rock soft, Fract. Weather. rock. Proc. Symp. Tokyo, Sept. 1981. Vol. 2* **1981**, 1235–1240.
(48) Wyrick, G. G.; Borchers, J. W. Hydrologic Effects of Stress-Relief Fracturing in An Appalachian Valley. *US Geol. Surv. Water Supply Pap.* **1981**. https://doi.org/10.3133/wsp2177.
(49) Llewellyn, G. T. Evidence and Mechanisms for Appalachian Basin Brine Migration into Shallow Aquifers in NE Pennsylvania, USA. *Hydrogeol. J.* **2014**, *22* (5), 1055–1066. https://doi.org/10.1007/s10040-014-1125-1.
(50) Gammons, C. H.; Brown, A.; Poulson, S. R.; Henderson, T. H. Using Stable Isotopes (S, O) of Sulfate to Track Local Contamination of the Madison Karst Aquifer, Montana, from Abandoned Coal Mine Drainage. *Appl. Geochemistry* **2013**, *31*, 228–238. https://doi.org/10.1016/j.apgeochem.2013.01.008.
(51) Galhardi, J. A.; Bonotto, D. M. Hydrogeochemical Features of Surface Water and Groundwater Contaminated with Acid Mine Drainage (AMD) in Coal Mining Areas: A Case Study in Southern Brazil. *Environ. Sci. Pollut. Res.* **2016**, *23* (18), 18911–18927. https://doi.org/10.1007/s11356-016-7077-3.
(52) Bhattarai, S.; Cassarini, C.; Lens, P. N. L. Physiology and Distribution of Archaeal Methanotrophs That Couple Anaerobic Oxidation of Methane with Sulfate Reduction. *Microbiol. Mol. Biol. Rev.* **2019**, *83* (3). https://doi.org/10.1128/mmbr.00074-18.

(53) Erhardt, A.; Alvarez, C.; Fichtner, V.; Parris, T.; Zhu, J.; Fryar, A.; Webb, S.; Munizzi, J. Using Sulfate and Methane Isotopes to Track Methane Sources in Eastern Kentucky Groundwater. In *AGU Fall Meeting 2021*; New Orleans, LA, 2021.
(54) Ozuolmez, D.; Na, H.; Lever, M. A.; Kjeldsen, K. U.; Jørgensen, B. B.; Plugge, C. M. Methanogenic Archaea and Sulfate Reducing Bacteria Co-Cultured on Acetate: Teamwork or Coexistence? *Front. Microbiol.* **2015**, *6* (MAY), 492. https://doi.org/10.3389/FMICB.2015.00492/ABSTRACT.
(55) Meulepas, R. J. W.; Jagersma, C. G.; Khadem, A. F.; Stams, A. J. M.; Lens, P. N. L. Effect of Methanogenic Substrates on Anaerobic Oxidation of Methane and Sulfate Reduction by an Anaerobic Methanotrophic Enrichment. *Appl. Microbiol. Biotechnol.* **2010**, *87* (4), 1499. https://doi.org/10.1007/S00253-010-2597-0.
(56) Stolper, D. A.; Martini, A. M.; Clog, M.; Douglas, P. M.; Shusta, S. S.; Valentine, D. L.; Sessions, A. L.; Eiler, J. M. Distinguishing and Understanding Thermogenic and Biogenic Sources of Methane Using Multiply Substituted Isotopologues. *Geochim. Cosmochim. Acta* **2015**, *161*, 219–247. https://doi.org/10.1016/j.gca.2015.04.015.
(57) Elsner, M. Stable Isotope Fractionation to Investigate Natural Transformation Mechanisms of Organic Contaminants: Principles, Prospects and Limitations. *J. Environ. Monit.* **2010**, *12* (11), 2005–2031. https://doi.org/10.1039/c0em00277a.
(58) Coleman, D. D.; Risatti, J. B.; Schoell, M. Fractionation of Carbon and Hydrogen Isotopes by Methane-Oxidizing Bacteria. *Geochim. Cosmochim. Acta* **1981**, *45* (7), 1033–1037. https://doi.org/10.1016/0016-7037(81)90129-0.
(59) Baldassare, F. J.; McCaffrey, M. A.; Harper, J. A. A Geochemical Context for Stray Gas Investigations in the Northern Appalachian Basin: Implications of Analyses of Natural Gases from Neogene-through Devonian-Age Strata. *Am. Assoc. Pet. Geol. Bull.* **2014**, *98* (2), 341–372. https://doi.org/10.1306/06111312178.
(60) Burruss, R. C.; Laughrey, C. D. Carbon and Hydrogen Isotopic Reversals in Deep Basin Gas: Evidence for Limits to the Stability of Hydrocarbons. *Org. Geochem.* **2010**, *41* (12), 1285–1296. https://doi.org/10.1016/J.ORGGEOCHEM.2010.09.008.
(61) Román-Colón, Y. A.; Ruppert, L. F. *Central Appalachian Basin Natural Gas Database: Distribution, Composition, and Origin of Natural Gases U.S. Geological Survey Open-File Report 2014-1207*; 2014. https://doi.org/10.3133/ofr20141207.
(62) Darrah, T. H.; Jackson, R. B.; Vengosh, A.; Warner, N. R.; Whyte, C. J.; Walsh, T. B.; Kondash, A. J.; Poreda, R. J. The Evolution of Devonian Hydrocarbon Gases in Shallow Aquifers of the Northern Appalachian Basin: Insights from Integrating Noble Gas and Hydrocarbon Geochemistry. *Geochim. Cosmochim. Acta* **2015**, *170*, 321–355. https://doi.org/10.1016/j.gca.2015.09.006.
(63) Révész, K. M.; Breen, K. J.; Baldassare, A. J.; Burruss, R. C. Carbon and Hydrogen Isotopic Evidence for the Origin of Combustible Gases in Water-Supply Wells in North-Central Pennsylvania. *Appl. Geochemistry* **2010**, *25* (12), 1845–1859. https://doi.org/10.1016/j.apgeochem.2010.09.011.
(64) Ragsdale, S. W. A Microbe That Eats Ethane under the Sea. *Nature* **2019**, *568*, 40–41.
(65) James, A. T.; Burns, B. J. Microbial Alteration of Subsurface Natural Gas Accumulations. *Am. Assoc. Pet. Geol. Bull.* **1984**, *68* (8), 957–960. https://doi.org/10.1306/ad46169c-16f7-11d7-8645000102c1865d.
(66) Coleman, D.; Liu, C.; Hackley, K.; Benson, L. Identification of Landfill Methane Using Carbon and Hydrogen Isotope Analysis. In *Proceedings of the Sixteenth International*

Madison Waste Conference; Univ Wisconsin, Madison WI, 1993; pp 303–314.
(67) Harkness, J. S.; Darrah, T. H.; Warner, N. R.; Whyte, C. J.; Moore, M. T.; Millot, R.; Kloppmann, W.; Jackson, R. B.; Vengosh, A. The Geochemistry of Naturally Occurring Methane and Saline Groundwater in an Area of Unconventional Shale Gas Development. *Geochim. Cosmochim. Acta* **2017**, *208*, 302–334. https://doi.org/10.1016/j.gca.2017.03.039.
(68) Reitz, M.; Sanford, W. E.; Senay, G. B.; Cazenas, J. Annual Estimates of Recharge, Quick-Flow Runoff, and Evapotranspiration for the Contiguous U.S. Using Empirical Regression Equations. *J. Am. Water Resour. Assoc.* **2017**, *53* (4), 961–983. https://doi.org/10.1111/1752-1688.12546.
(69) Reitz, M.; Sanford, W. E.; Senay, G. B.; Cazenas, J. Annual estimates of recharge, quick-flow runoff, and ET for the contiguous US using empirical regression equations, 2000-2013 https://doi.org/10.5066/F7PN93P0 (accessed Mar 14, 2021).
(70) Ingraffea, A. R.; Wawrzynek, P. A.; Santoro, R.; Wells, M. Reported Methane Emissions from Active Oil and Gas Wells in Pennsylvania, 2014-2018. *Environ. Sci. Technol.* **2020**, *54* (9), 5783–5789. https://doi.org/10.1021/acs.est.0c00863.

Supporting information for Chapter 3.

Supplementary tables

Table S1. Data sources for geographical information

Dataset	Sub-region	Data Source	References
Location of Oil and Gas wells	PA	Pennsylvania Department of Environmental Protection	1,2
	OH	Ohio Department of Natural Resources	3
	WV	West Virginia Department of Environmental Protection	4
Coal Mine Extent - Active Underground Mine	OH	Ohio Department of Natural Resources	5
	WV	West Virginia Geological and Economic Survey and West Virginia Department of Environmental Protection	6 7
Coal Mine Extent - Abandoned Underground Mine	OH	Ohio Department of Natural Resources	5
	WV	Not included due to lack of complete public dataset	
	OH	Ohio Department of Natural Resources	5

Coal Mine Extent - Surface Mine	WV	West Virginia Geological and Economic Survey (No WV surface mine extents within 10 km away from the boundary of our sampling counties)	6

Table S2. Linear regression on the rank of methane concentration and O&G well count metrics in Region II (Eqn S1)

$C_{methane} = aN_{OGxrad} + bT_{topography} + c,$ (Eqn S1)

where N_{OGxrad} is the number of O&G wells within an *x* kilometer radius.

N_{OGxrad}	***a***	***p-value of a***	***b***	***p-value of b***	***c***
N_{OG1rad}	0.061	0.30	-0.58	$<2 \times 10^{-16}$*	166
N_{OG2rad}	0.097	0.099	-0.57	$<2 \times 10^{-16}$*	161
N_{OG5rad}	0.12	0.051	-0.56	5.7×10^{-16}*	158
$N_{OG10rad}$	0.10	0.087	-0.57	$<2 \times 10^{-16}$*	160

*statistically significant at the 5% threshold.

Table S3. Linear regression on the rank of methane concentration and age of the nearest O&G well in Region II (Eqn S2)

$C_{methane} = aAge + bT_{topography} + c,$ (Eqn S2)

where Age is the age of the nearest O&G well.

Age	***a***	***p-value of a***	***b***	***p-value of b***	***c***

Age	0.071	0.34	-0.54	4.3×10^{-10}*	113

*statistically significant at the 5% threshold.

Table S4. Linear regressions on the rank of ion concentrations and O&G / coal spatial metrics in Region II (Eqn S3)

$C_i = aA_{variable} + bT_{topography} + c,$ (Eqn S3)

where C_i is the concentration of a species, *i*, and $A_{variable}$ is $d_{O\&G}$ or d_{coal}, the distance to the nearest O&G well, or distance to the nearest active underground coal mine, respectively.

i	$A_{variable}$	***a***	***p-value of a***	***b***	***p-value of b***	***c***
Fe	d_{coal}	0.23	5.8×10^{-4}*	-0.36	6.1×10^{-7}*	124
Fe	$d_{O\&G}$	-0.098	0.11	-0.44	2.2×10^{-10}*	168
Mn	d_{coal}	-0.037	0.61	-0.38	1.8×10^{-6}*	154
Mn	$d_{O\&G}$	0.066	0.32	-0.38	2.5×10^{-7}*	143
NO_3^-	d_{coal}	-0.064	0.36	0.39	9.9×10^{-7}*	74
NO_3^-	$d_{O\&G}$	0.024	0.72	0.41	2.7×10^{-8}*	62

Supplementary figures

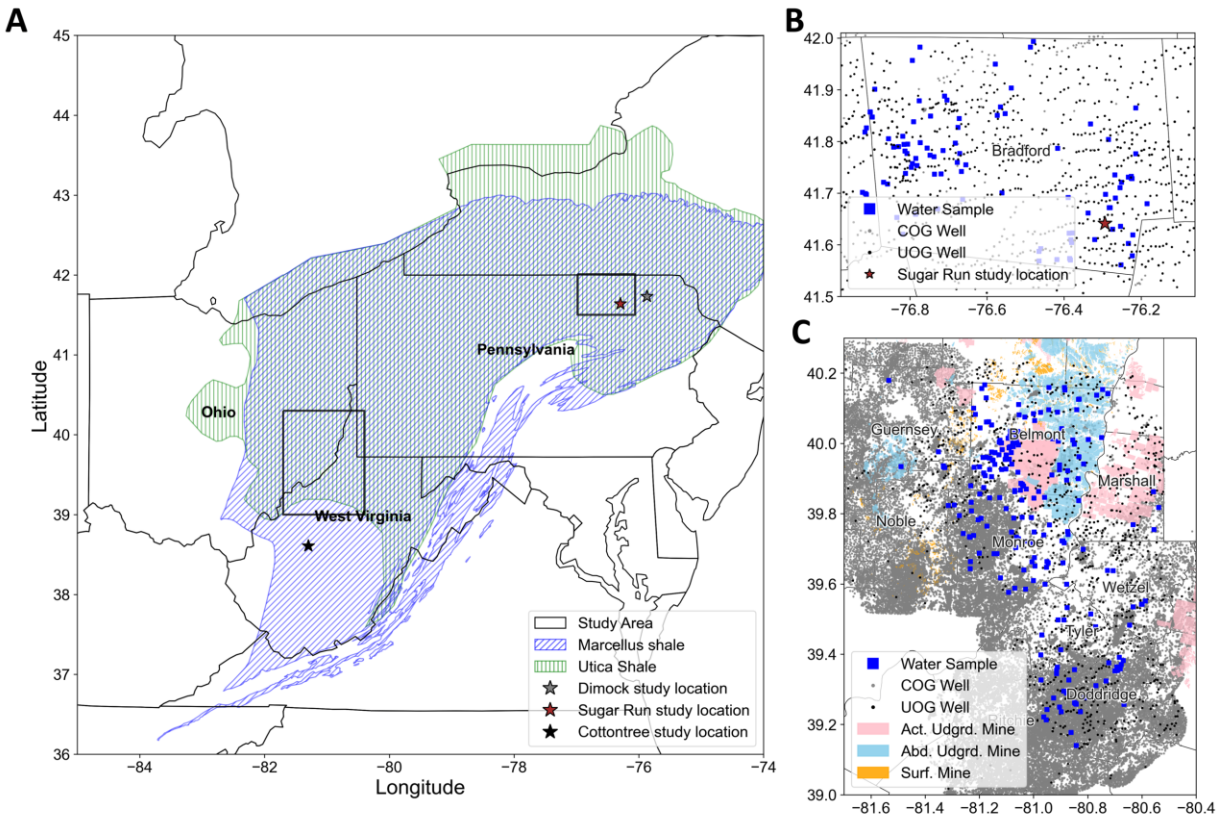

Figure S1. Geographical information of (A) the extent of Marcellus and Utica Shale; (B) Region I (NE PA); and (C) Region II (OH and WV). Boundaries of study areas are outlined by black frames in (A). Approximate locations of previous studies where isotopic information of production gas, annular gas, or dissolved gas was collected were marked by stars (gray star: Dimock, PA;[8] brown star: Sugar Run, PA;[9] black star: Cottontree field, WV[10,11]); Water samples, UOG wells, and COG wells' locations are shown in blue squares, black dots, and grey dots, respectively. Extent of active underground coal mines, abandoned underground coal mines, and surface coal mines are shaded in pink, blue, and orange, respectively. In Region II, we only include O&G wells and coal mine extents within 10 km away from the boundary of our sampling counties. There were not any eligible surface coal mine extents in WV within this distance range. Abandoned underground coal mines in WV were also not included due to lack of complete and updated public data.

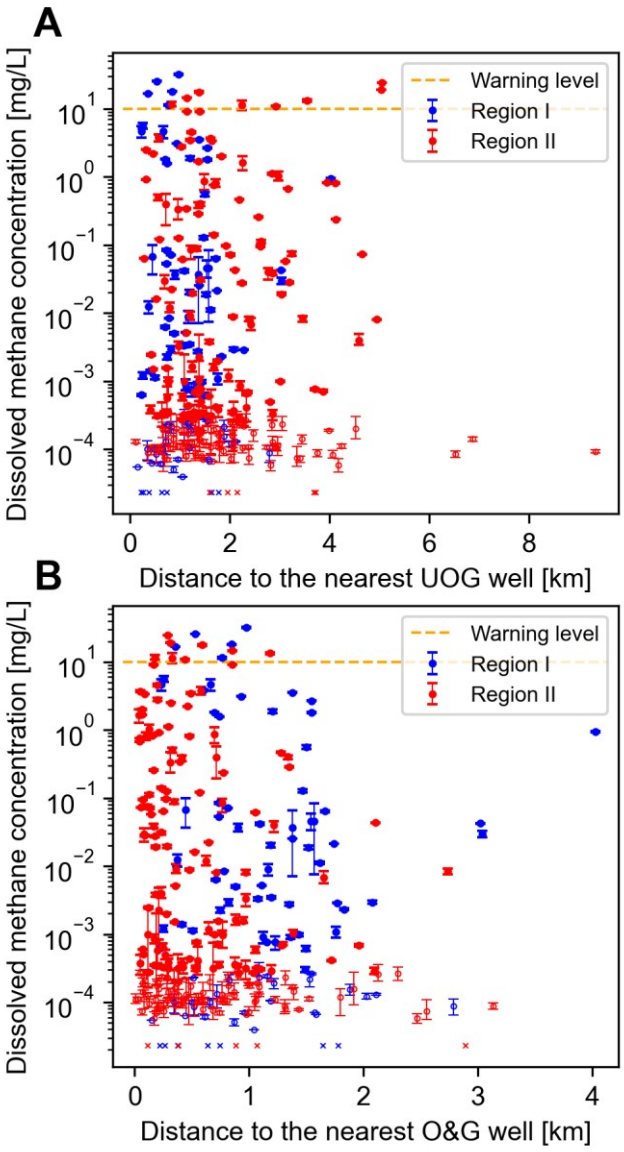

Figure S2. Error bars of dissolved methane concentration versus (A) distance to the nearest UOG well and (B) distances to the nearest O&G well. Error bar represents minimum and maximum concentration measured for each water sample, while the marker (filled symbol for concentration above LOQ, open symbol for concentration between LOQ and LOD, and cross for concentration below LOD) is placed at the mean concentration. All samples were analyzed for dissolved methane concentration in at least duplicate (except for n < 10 out of 311 samples with lost or wasted bottles), whereas the third sample was sometimes reserved for isotopic analysis.

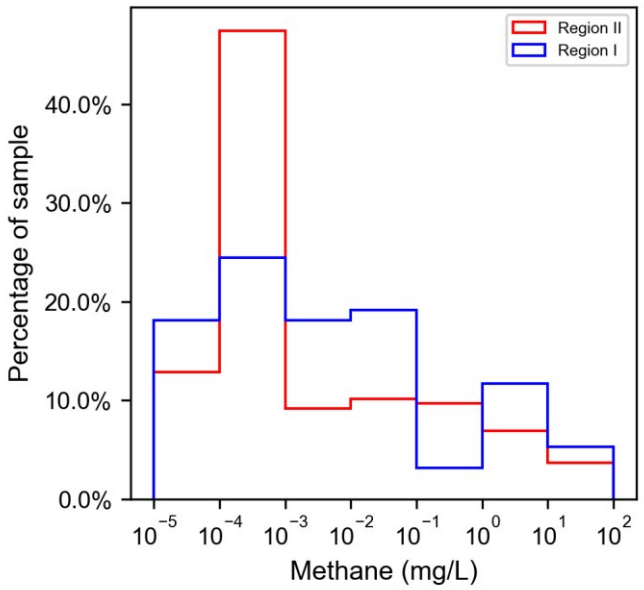

Figure S3. Distribution of dissolved methane concentrations in each study region

To examine the effect of UOG well density, methane concentrations were compared to the number of UOG wells within a radius of 1, 2, 5, or 10 km centered at the sample. The maximum number of UOG wells within increasing radii across both study regions was 22, 49, 145, and 371, respectively. In spite of this drilling intensity, there was no statistically significant correlation between methane concentration and UOG well density (Fig. S4).

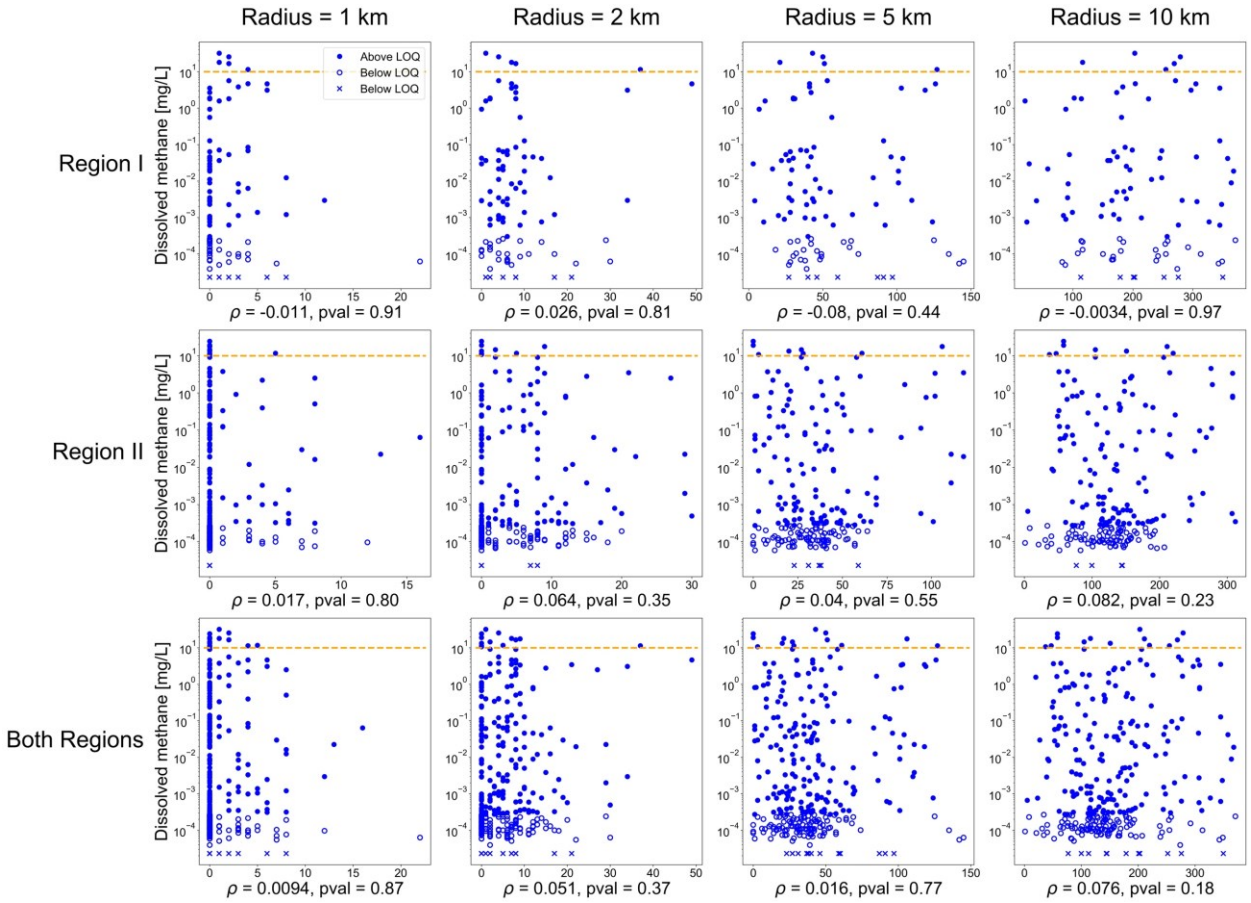

Figure S4. Correlation between groundwater dissolved methane concentration and count of UOG wells within certain radii centered at the water sample. The rows represent water samples collected in Region I, Region II, and both regions combined, while the columns represent radii applied: 1 km, 2 km, 5 km, and 10km. Spearman correlation coefficients (ρ) and p-values are shown below each subplot. The warning level (10 mg/L, dashed line) provided by the U.S. Department of the Interior[12] is also shown.

When counting O&G wells (UOG and COG) within the same radii, groundwater methane concentration in Region I was not statistically correlated with the O&G well count (Fig. S5). In Region II, methane concentration was statistically higher with higher well count for all radii, and the correlation conserved when considering Region I and Region II together for radius = 2 km

(Fig. S5). The maximum counts of O&G wells within increasing radii across both study regions were 86, 434, 1309, and 3565, respectively.

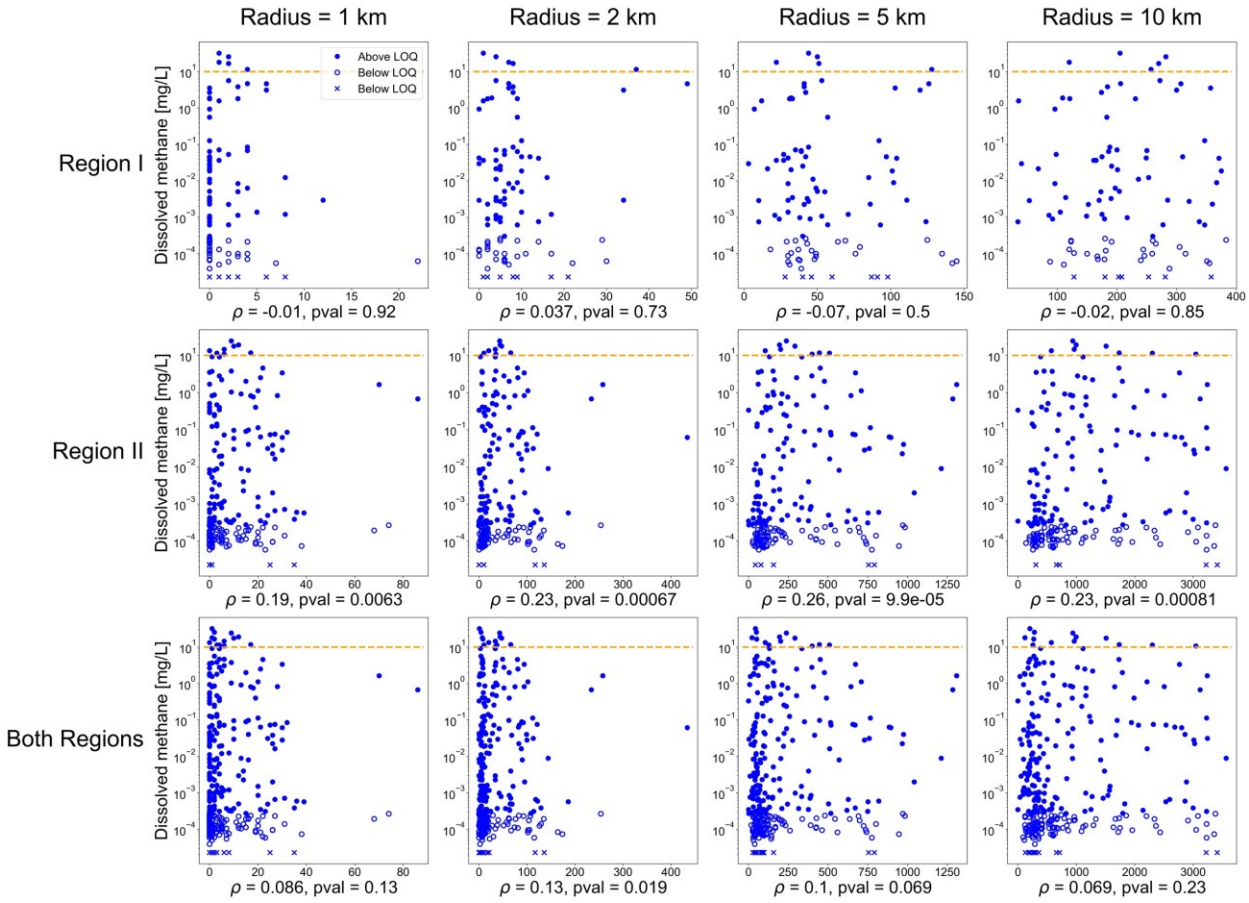

Figure S5. Correlation between groundwater dissolved methane concentration and count of all O&G wells (conventional and unconventional) within certain radii centered at the water sample. The rows represent water samples collected in Region I, Region II, and both regions combined, while the columns represent radii applied: 1 km, 2 km, 5 km, and 10km. Spearman correlation coefficients (ρ) and p-values are shown below each subplot. The warning level (10 mg/L, dashed line) provided by the U.S. Department of the Interior[12] is also shown.

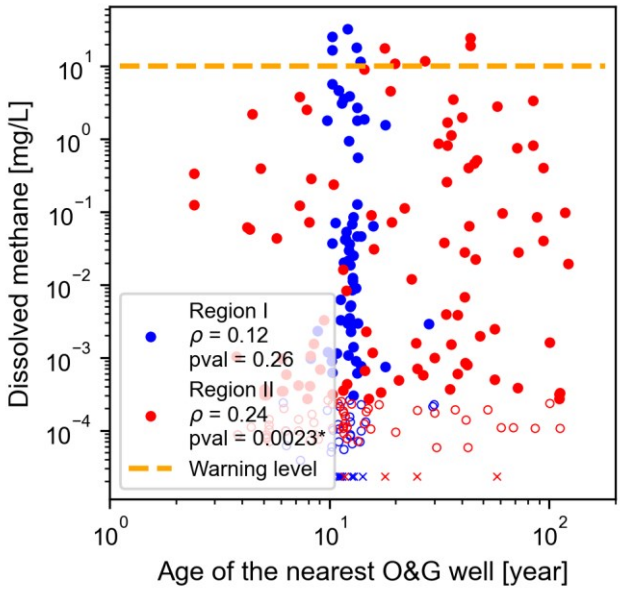

Figure S6. Methane concentration compared to the age of the nearest O&G well. Groundwater methane concentrations from Region I (blue) and Region II (red) above the limit of quantification (LOQ) of 2.7×10^{-4} mg/L (filled symbols), between the LOQ and the limit of detection (LOD) of 2.3×10^{-5} mg/L (open symbols), or below the LOD (crosses) are shown. The well age was calculated as the difference between the permit issue date of each well and a chosen date (Jan 1st, 2023).

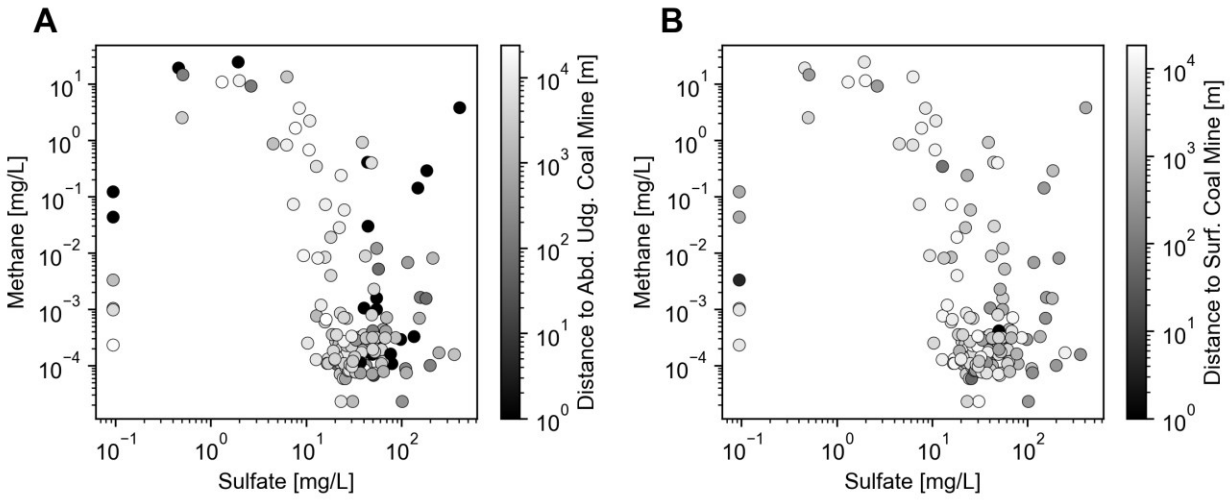

Figure S7. Groundwater dissolved methane concentration in OH water samples decreased with increasing sulfate concentration, and sulfate concentration increased with decreasing distance to

the nearest (A) abandoned underground coal mine and (B) surface coal mine in OH. Distance to the coal mine is represented by the color of each marker. In order to show samples with distance = 0 (i.e., overlapping with coal mines) in the logscale color bar, distances equal to or smaller than 1 m were treated as 1 m in color mapping. For both subplots, the spearman correlation coefficient between methane concentration and sulfate concentration was -0.25 (p-value = 1.2×10^{-3}). For (A), the coefficient between sulfate concentration and distance was -0.45 (p-value = 2.3×10^{-9}) and that between methane concentration and distance was 0.047 (p-value = 0.56); for (B) the coefficient between sulfate concentration and distance was -0.33 (p-value = 2.4×10^{-5}) and that between methane concentration and distance was 0.022 (p-value = 0.78). Due to the incomplete dataset of abandoned coal mines in WV and the lack of eligible WV surface coal mines near our study area, these mines and water samples in WV were not included in the analyses.

To understand the origin of bulk fluid migration and associated dissolved methane, we used geochemical indicators (i.e., conservative tracers), classifying water according to the criteria given by Warner et al.[13]: groundwaters with dissolved chloride (Cl) less than 20 mg/L were classified as type A and B; those with dissolved Cl greater than or equal to 20 mg/L and molar Br-to-Cl ratio smaller than 0.001 were classified as type C; and those with Cl greater than 20 mg/L, Br-to-Cl ratio larger than or equal to 0.001, and Na-to-Cl ratio smaller than 5 were classified as type D. (Note that groundwaters with Cl greater than or equal to 20 mg/L, Br-to-Cl larger than or equal to 0.001,and Na-to-Cl greater than or equal to 5 were not explicitly classified by Warner et al.). In this classification framework, Cl concentration serves as an indicator of the salinity of water samples. The low-salinity type AB water represents dilute groundwater which is less likely to be influenced by natural and anthropogenic salinity sources. Among the high-salinity water samples, there are generally two possible sources of salinity: first, contamination

by anthropogenic salinity sources such as road salt, animal waste, and domestic sewage which result in low Br-to-Cl ratio (type C water);[14] second, intrusion of deep Appalachian brine into shallow groundwater, which result in high Br-to-Cl ratio (type D and unclassified water).[13] The occurrence of brine tracers in groundwater is a natural phenomenon.[13,15–17] Water typing can also be compared on a Cl/Br vs. Cl plot (Fig. S9B) and this is consistent with the Warner classification analysis: type AB samples closely matched the signatures of dilute groundwater, type C samples indicated mixing between diluted groundwater, halite, and domestic sewage, and type D samples (including unclassified samples) indicated mixing between basin brine and dilute groundwater (with influence of sewage).

Among tested water samples from both study regions, high salinity and high Br-to-Cl ratio waters (type D and unclassified type) contained the highest dissolved methane concentration (Fig. S8). The difference in dissolved methane concentrations among water types was statistically significant (Welch's ANOVA test; p-value = 4.5×10^{-14}, test performed on log-transformed concentrations), and Games-Howell post-hoc tests (pairwise adjusted p-values were significant for between type AB and type D (4.0×10^{-10}), type AB and unclassified type (1.3×10^{-6}), type C and type D (1.2×10^{-10}), and type C and unclassified type (9.7×10^{-9}); tests performed on log-transformed concentrations). Thus, samples containing enriched methane were associated with intrusion of Appalachian brines in shallow groundwater (and this holds for both study regions; Fig. S11).

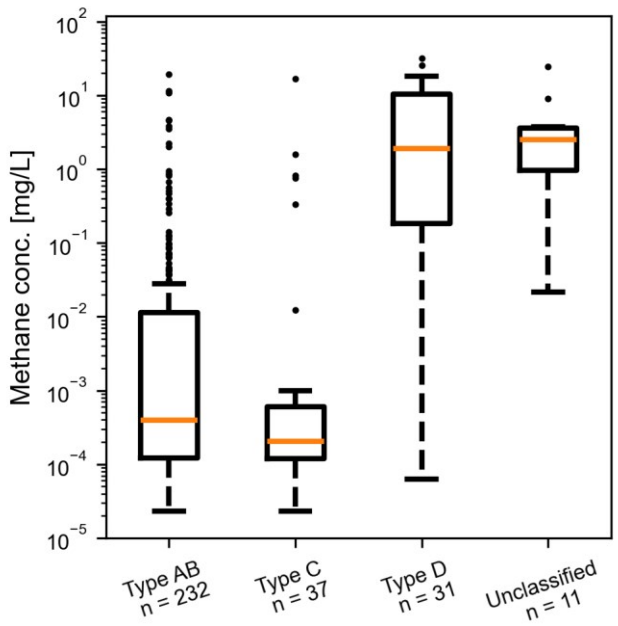

Figure S8. Groundwater dissolved methane concentration increased in water types influenced by Appalachian brine intrusion Each rectangular box represents the distribution of methane concentrations within a certain water type, where the orange horizontal bar gives the median, and the upper and lower edges of the box represent the upper and lower quartiles (e.g., 75th and 25th percentile, respectively). The whiskers indicate variability outside the quartiles and individual datum (black dots) are only visible in the extrema outside these ranges. See Figure S9 for alternative brine representation.

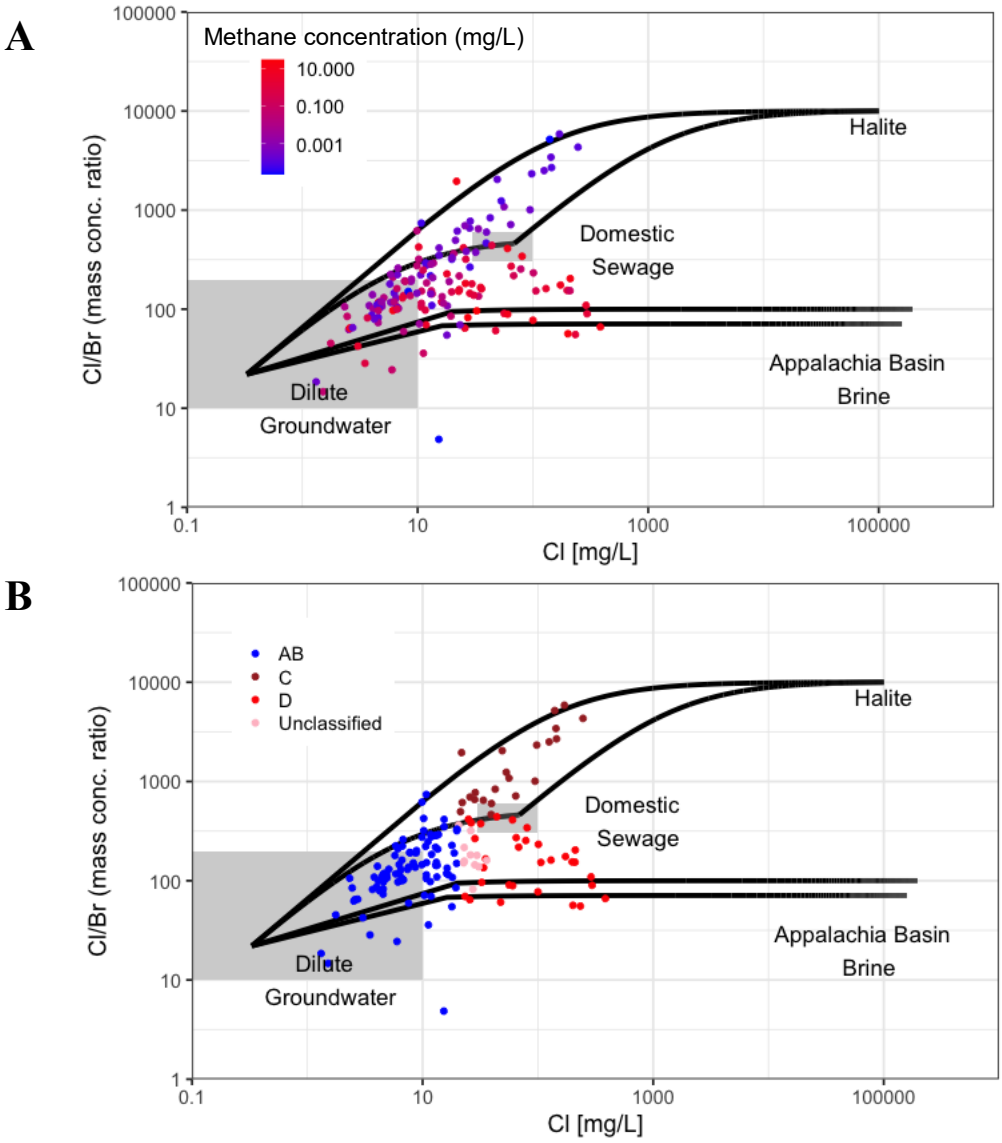

Figure S9. Cl/Br ratio against Cl concentration for methane concentration (A) and geochemical water source attribution (B). For (A) water samples with both Cl and Br concentrations measured above detection limits are shown in colors representing their methane concentrations. For (B), the same water samples are shown in colors representing their water types (blue for type AB, brown for type C, red for type D, and pink for unclassified). Reference range of dilute groundwater and domestic sewage are shown in grey shaded areas.[18] The endmembers used for constructing the mixing lines include: diluted groundwater endmember (a

water sample collected by this study, Cl/Br = 22, Cl = 0.33 mg/L), domestic sewage endmember from Jagucki and Darner, 2001,[18] halite endmember from Mullaney et al., 2009,[14] and Appalachia Basin Brine lower and upper bound endmember from Poth, 1962.[19]

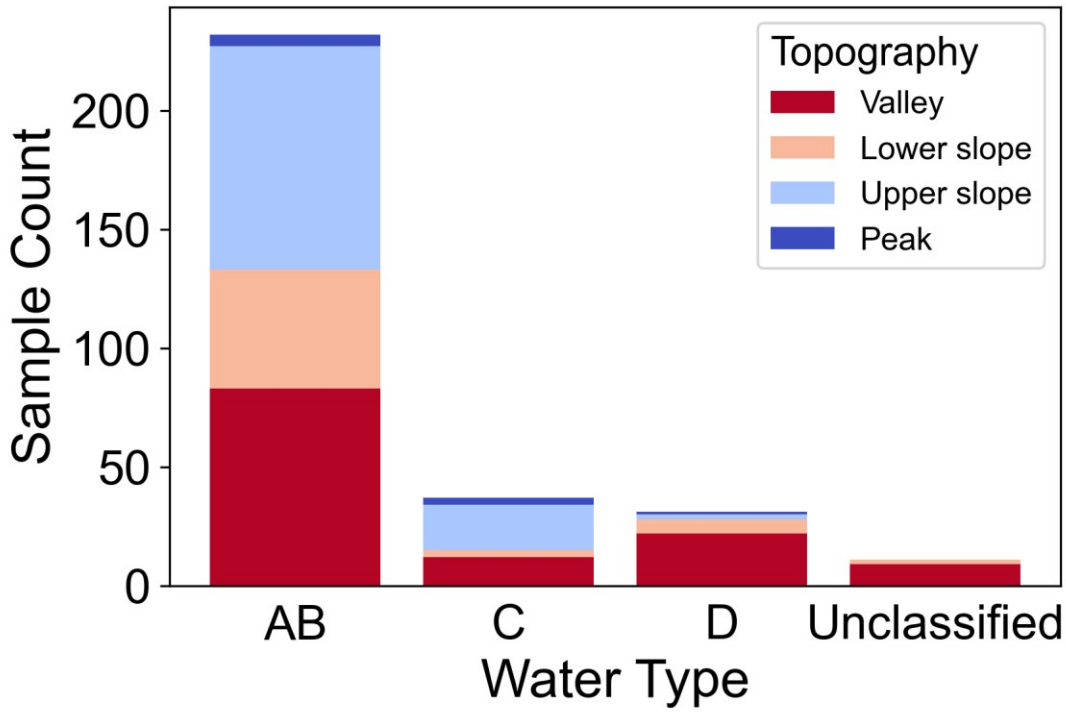

Figure S10. Geochemical water type of groundwater sample in correlation with topographical class of sample location among all water samples. Number of samples falling in each water type is represented by the height of each column. Within each column, the number of samples whose location belong to a specific topographical class is represented by the height of the color block: red for valley, pink for lower slope, light blue for upper slope, and blue for peak.

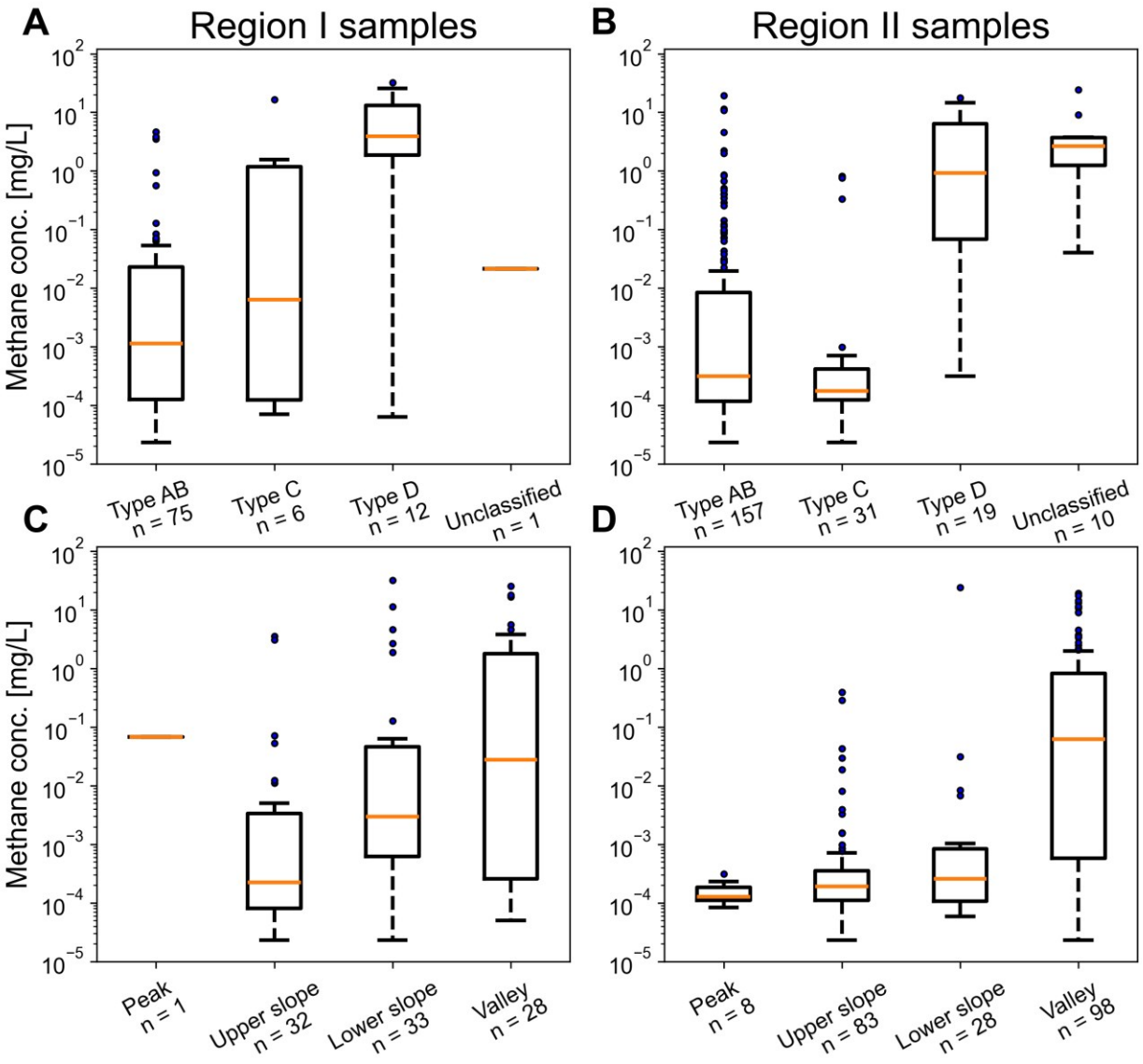

Figure S11. Distribution of groundwater methane concentrations among different water types and different topographical locations within Region I (A and C) and Region II (B and D) separately. The Welch's ANOVA p-value for each subplot was (A) 2.4×10^{-4} (unclassified type excluded), (B) 6.2×10^{-14}, (C) 6.5×10^{-4} (peak excluded), and (D) $< 2.2 \times 10^{-16}$.

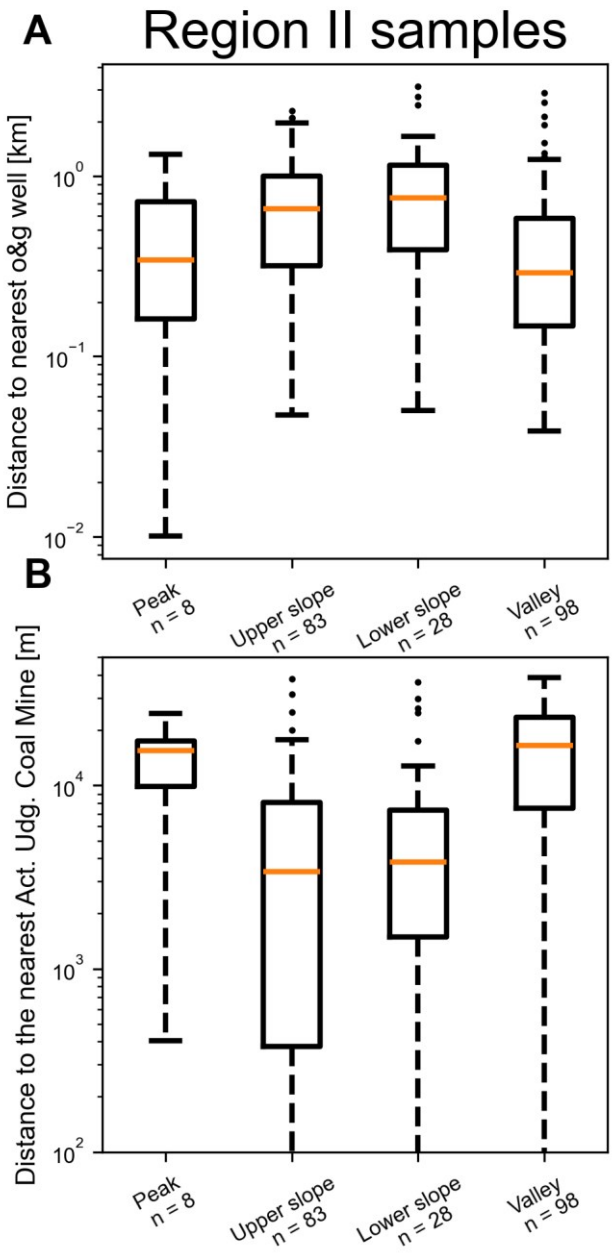

Figure S12. Region II samples collected from valley topography had (A) smaller distance to the nearest O&G well but (B) larger distance to the nearest active underground coal mine, when compared to slope topography samples. For (A), Welch's ANOVA p-value = 0.0044, and pairwise adjusted p-values by Games-Howell post-hoc test were significantly different between valley and lower slope (0.030) and valley and upper slope (0.004). For (B), Welch's ANOVA p-value = 8.1×10^{-8}, and pairwise adjusted p-values by Games-Howell post-hoc test were significant between valley and lower

slope (1.0×10^{-3}) and valley and upper slope (2.3×10^{-13}). Each rectangular box represents the distribution of distances for samples from a certain topographical class, where the orange horizontal bar gives the median, and the upper and lower edges of the box represent the upper and lower quartiles (e.g., 75th and 25th percentile, respectively). The whiskers indicate variability outside the quartiles and individual datum (black dots) are only visible in the extrema outside these ranges.

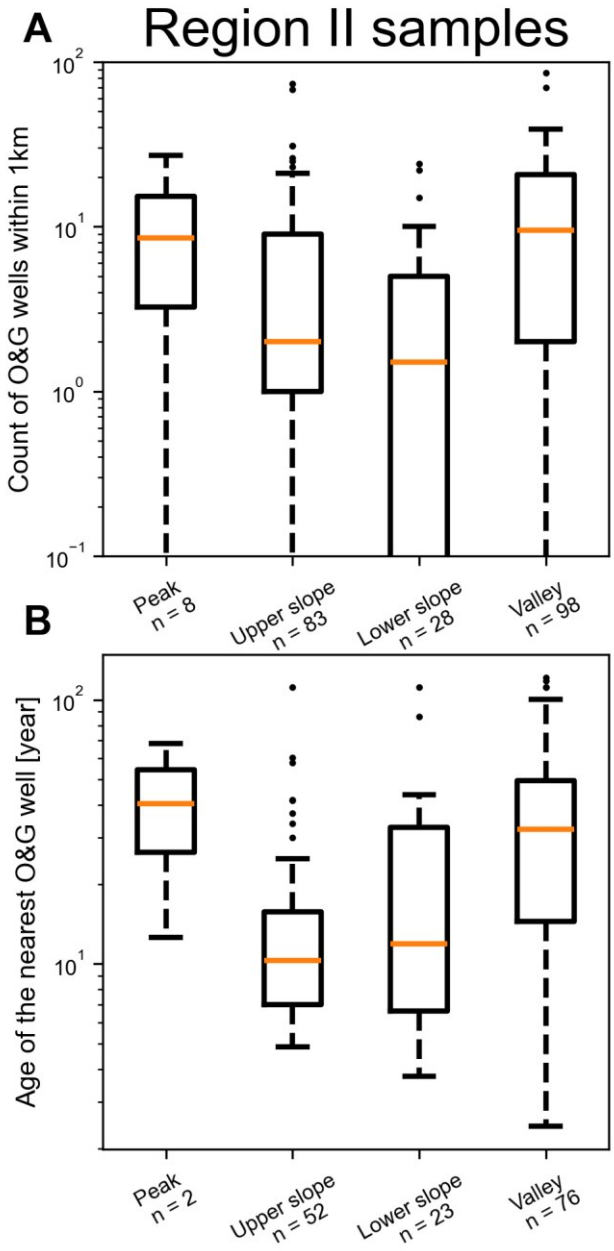

Figure S13. Samples collected from valley topography had (A) higher number of O&G wells within 1 km radius and (B) older well age for the nearest O&G well compared to samples on the slopes in Region II. For (A), Welch's ANOVA p-value = 5.3×10^{-4}, and pairwise adjusted p-values by Games-Howell post-hoc test were significant between valley and lower slope (2.8×10^{-5}) and valley and upper slope (0.021). For (B), Welch's ANOVA p-value = 6.6×10^{-5} (with the Peak class excluded for insufficient sample size), and pairwise adjusted p-value by Games-Howell post-hoc test was significant between valley and upper slope (1.4×10^{-5}). The well age is calculated as the difference between the permit issue date of each well and a chosen date (Jan 1st, 2023). Note that the permit issue data information is not available for some of the nearest wells, resulting in a smaller sample size n for each box in (B).

In addition to sulfate, other electron acceptors in the groundwater, including the oxide of iron and manganese[20–23] as well as nitrate,[24] can be coupled with microbiological anaerobic methane oxidation (Reactions S1 to S3).[25] The dissolved Mn and Fe concentrations were statistically lower with higher sulfate and lower methane concentration (Fig. S14), and Fe concentration was lower with smaller distance to coal mine after controlling the confounding effect of topography (Table S4). This was possibly due to that stronger methane oxidation enabled by higher sulfate concentration near the coal mine produced more reduced sulfur (Reaction 2 and 3) which could combine with Mn^{2+} and Fe^{2+} to form the insoluble solid of MnS and FeS. Another explanation could be that the extra sulfate introduced by coal mining would drive methane concentration to below its natural equilibrium level, which reduced the production rate of dissolved Mn and Fe by reaction S1 and S2. Moreover, the dissolved nitrate concentration was positively correlated with sulfate concentration while negatively correlated with methane concentration (Fig. S14). There was abundant agricultural land cover in Region II, and fertilization and animal waste could add

to the groundwater nitrate concentration.[26] One hypothesis for the positive correlation between sulfate and nitrate could be that agricultural activities contributed to the sources of both species through using fertilizer and gypsum ($CaSO_4 \cdot 2H_2O$) soil amendments simultaneously.[27] Lastly in Region II, none of the concentrations of iron, manganese, and nitrate were correlated with distance to O&G well after controlling the confounding effect of topography (Table S4).

$CH_4 + 4MnO_2 + 7H^+ \rightarrow 4Mn^{2+} + HCO_3^- + 5H_2O$ (S1, Mn reduction with methane oxidation[23,25])

$CH_4 + 8Fe(OH)_3 + 15H^+ \rightarrow 8Fe^{2+} + HCO_3^- + 21H_2O$ (S2, Fe reduction with methane oxidation[21,22,25])

$CH_4 + 4NO_3^- \rightarrow 4NO_2^- + HCO_3^- + H_2O + H^+$ (S3, Nitrate reduction with methane oxidation[24,25])

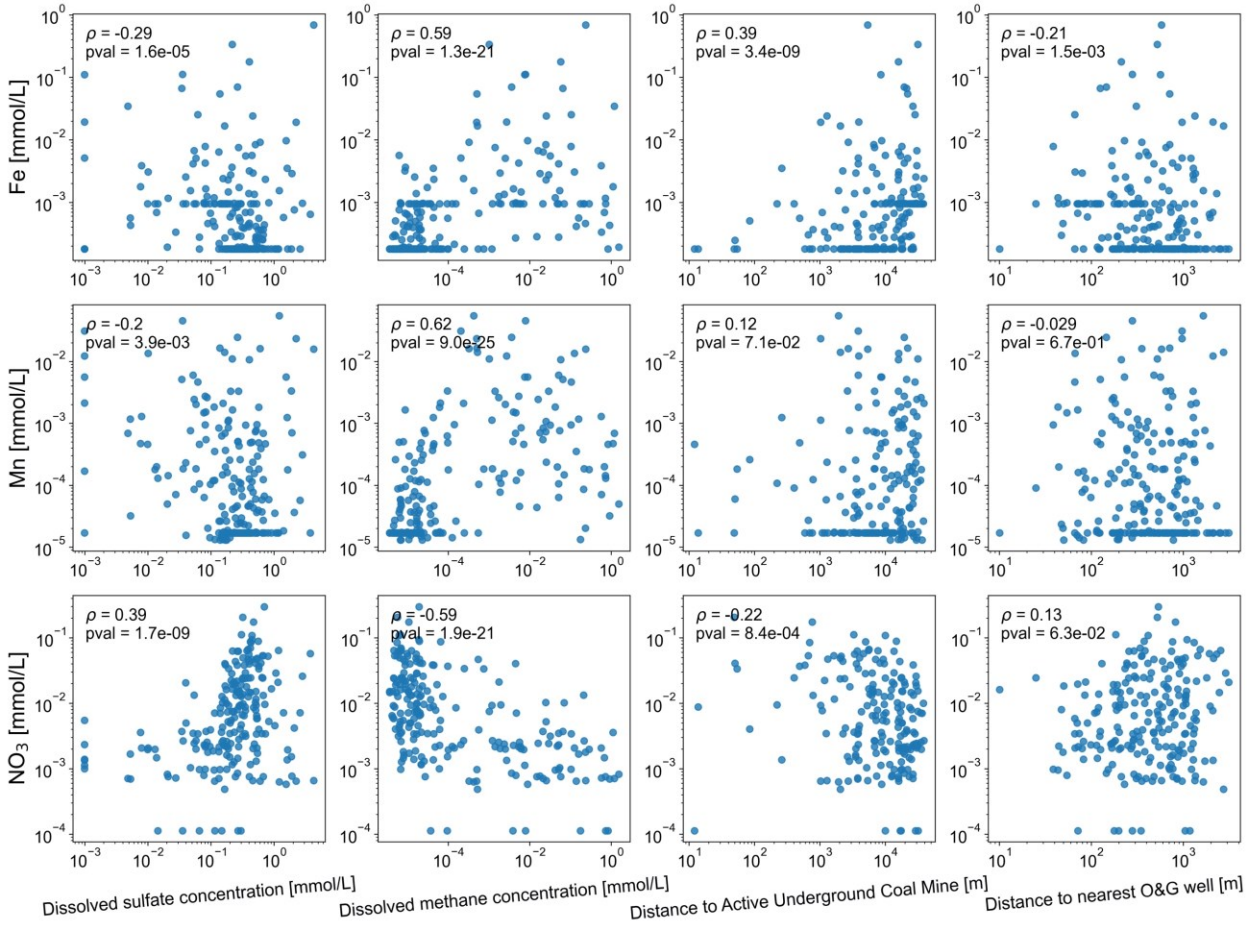

Figure S14. The correlation between other redox agents and sulfate and methane concentration as well as active underground coal mine and O&G spatial metrics among Region II water samples. Subplots on the same row share the same y-axis while those on the same column share the same x-axis. Spearman correlation coefficients (ρ) and p-values are shown on each subplot. The LOD for the measurement of each redox agent could be different between OH samples and WV samples due to separate sampling campaigns.

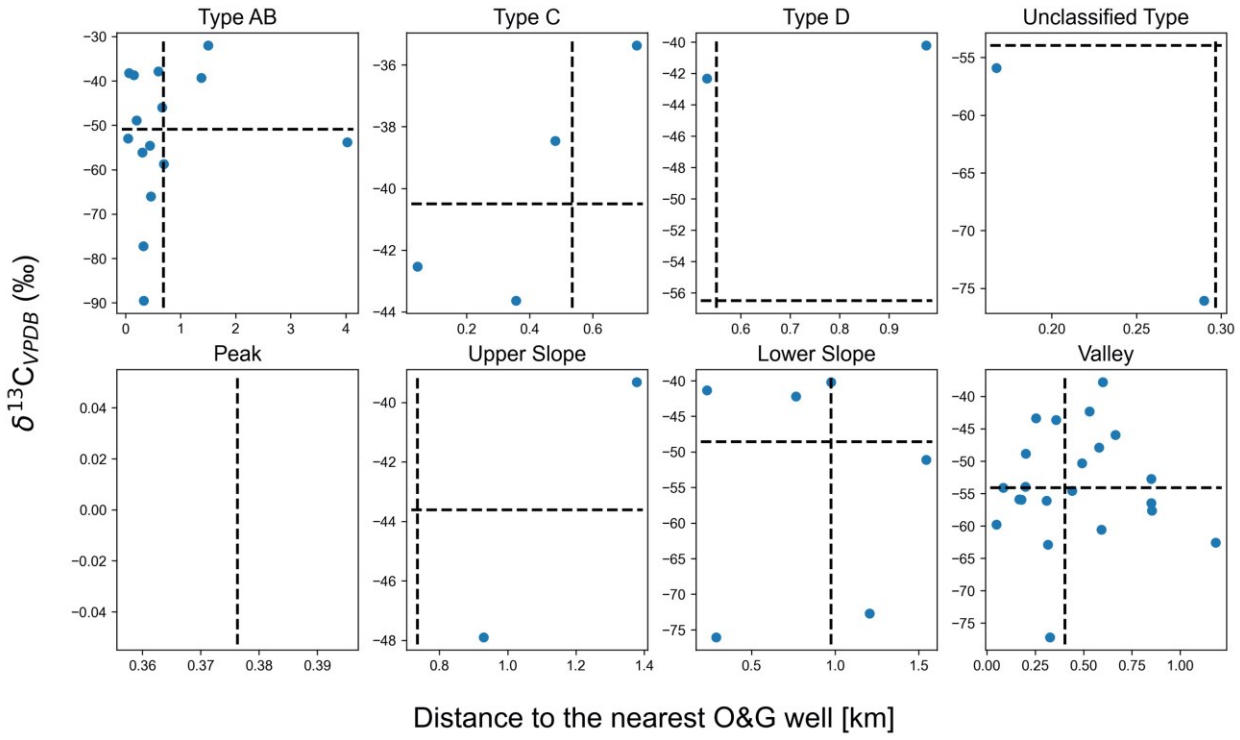

Figure S15. Comparing $\delta^{13}C$ – CH_4 and distance to the nearest O&G well for the outlier data in Fig. 3 and Fig. S8. Subplots on the top row match the four boxes in Fig. S8 while subplots on the lower row match the four boxes in Fig. 3 (the title of each subplot indicating the matching box). The vertical and horizontal dashed lines represent the median values of O&G distance and $\delta^{13}C$ ratio, respectively, within each water type or topography class. Note that only samples with methane concentrations above 0.5 mg/L were selected for $\delta^{13}C$ isotopic analysis.

References

(1) Pennsylvania Department of Environmental Protection. Oil Gas Locations - Conventional https://newdata-padep-1.opendata.arcgis.com/datasets/oil-gas-locations-conventional (accessed Mar 24, 2020).

(2) Pennsylvania Department of Environmental Protection. Oil Gas Locations - Unconventional https://newdata-padep-1.opendata.arcgis.com/datasets/oil-gas-locations-unconventional?geometry=-81.196%2C40.740%2C-74.247%2C42.181 (accessed Mar 24, 2020).

(3) Ohio Department of Natural Resources. Oil and Gas Data https://ohiodnr.gov/discover-and-learn/safety-conservation/about-odnr/oil-gas/oil-gas-resources/featured-content-3 (accessed Feb 1, 2022).

(4) West Virginia Department of Environmental Protection. Oil and Gas Production Data https://dep.wv.gov/oil-and-gas/databaseinfo/Pages/default.aspx (accessed Dec 1, 2020).

(5) Ohio Department of Natural Resources. Mines of Ohio ODNR https://gis.ohiodnr.gov/MapViewer/?config=OhioMines (accessed Feb 1, 2022).

(6) West Virginia Geological and Economic Survey. Coal Bed Mapping Program https://atlas.wvgs.wvnet.edu/arcgis/rest/services/Coal_Web_Mercator/All_Mining_WM/MapServer (accessed Sep 1, 2021).

(7) West Virginia Department of Environmental Protection. Mining and Reclamation Enterprise Data https://data-wvdep.opendata.arcgis.com/datasets/7fd9c7474194428e9150d83bf9b10102_0/explore?location=38.802243%2C-80.350350%2C8.81 (accessed Sep 1, 2021).

(8) Hammond, P. A. The Relationship between Methane Migration and Shale-Gas Well Operations near Dimock, Pennsylvania, USA. *Hydrogeol. J.* **2016**, *24* (2), 503–519. https://doi.org/10.1007/s10040-015-1332-4.

(9) Llewellyn, G. T.; Dorman, F.; Westland, J. L.; Yoxtheimer, D.; Grieve, P.; Sowers, T.; Humston-Fulmer, E.; Brantley, S. L. Evaluating a Groundwater Supply Contamination Incident Attributed to Marcellus Shale Gas Development. *Proc. Natl. Acad. Sci. U. S. A.* **2015**, *112* (20), 6325–6330. https://doi.org/10.1073/pnas.1420279112.

(10) Burruss, R. C.; Laughrey, C. D. Carbon and Hydrogen Isotopic Reversals in Deep Basin Gas: Evidence for Limits to the Stability of Hydrocarbons. *Org. Geochem.* **2010**, *41* (12), 1285–1296. https://doi.org/10.1016/J.ORGGEOCHEM.2010.09.008.

(11) Román-Colón, Y. A.; Ruppert, L. F. *Central Appalachian Basin Natural Gas Database: Distribution, Composition, and Origin of Natural Gases U.S. Geological Survey Open-File Report 2014-1207*; 2014. https://doi.org/10.3133/ofr20141207.

(12) Eltschlager, K. K.; Hawkins, J. W.; Ehler, W. C.; Baldassare, F. J. Technical Measures for the Invetigation and Mitigation of Fugitive Methane Hazards in Areas of Coal Mining, U.S. Department of the Interior, Office of Surface Mining. **2001.**

(13) Warner, N. R.; Jackson, R. B.; Darrah, T. H.; Osborn, S. G.; Down, A.; Zhao, K.; White, A.; Vengosh, A. Geochemical Evidence for Possible Natural Migration of Marcellus Formation Brine to Shallow Aquifers in Pennsylvania. *Proc. Natl. Acad. Sci.* **2012**, *109* (30), 11961–11966. https://doi.org/10.1073/pnas.1121181109.

(14) Mullaney, J. R.; Lorenz, D. L.; Arntson, A. D. *Chloride in Groundwater and Surface*

Water in Areas Underlain by the Glacial Aquifer System, Northern United States Scientific Investigations Report 2009 – 5086; 2009; Vol. 5086.
(15) Wen, T.; Niu, X.; Gonzales, M.; Zheng, G.; Li, Z.; Brantley, S. L. Big Groundwater Data Sets Reveal Possible Rare Contamination Amid Otherwise Improved Water Quality for Some Analytes in a Region of Marcellus Shale Development. *Environ. Sci. Technol.* **2018**, *52* (12), 7149–7159. https://doi.org/10.1021/acs.est.8b01123.
(16) Williams, J. H.; Taylor, L. E.; Low, D. J. Hydrogeology and Groundwater Quality of the Glaciated Valleys of Bradford, Tioga, and Potter Counties, Pennsylvania. *Pennsylvania Geol. Surv. 4th ser. Water Resource Report 68*. **1998**.
(17) Siegel, D. I.; Smith, B.; Perry, E.; Bothun, R.; Hollingsworth, M. Pre-Drilling Water-Quality Data of Groundwater Prior to Shale Gas Drilling in the Appalachian Basin: Analysis of the Chesapeake Energy Corporation Dataset. *Appl. Geochemistry* **2015**, *63*, 37–57. https://doi.org/10.1016/j.apgeochem.2015.06.013.
(18) Jagucki, M. L.; Darner, R. A. *Ground-Water Quality in Geauga County, Ohio—Review of Previous Studies, Status in 1999, and Comparison of 1986 and 1999 Data Water-Resources Investigations Report 01-4160*; 2001.
(19) Poth, C. W. *Occurrence of Brine in Western Pennsylvania: Pennsylvania Geological Survey, 4th Ser., Mineral Resource Report 47*. **1962**.
(20) Sivan, O.; Adler, M.; Pearson, A.; Gelman, F.; Bar-Or, I.; John, S. G.; Eckert, W. Geochemical Evidence for Iron-Mediated Anaerobic Oxidation of Methane. *Limnol. Oceanogr.* **2011**, *56* (4), 1536–1544. https://doi.org/10.4319/lo.2011.56.4.1536.
(21) Egger, M.; Rasigraf, O.; Sapart, C. J.; Jilbert, T.; Jetten, M. S. M.; Röckmann, T.; Van Der Veen, C.; Bânda, N.; Kartal, B.; Ettwig, K. F.; Slomp, C. P. Iron-Mediated Anaerobic Oxidation of Methane in Brackish Coastal Sediments. *Environ. Sci. Technol.* **2015**, *49* (1), 277–283. https://doi.org/10.1021/es503663z.
(22) Bar-Or, I.; Elvert, M.; Eckert, W.; Kushmaro, A.; Vigderovich, H.; Zhu, Q.; Ben-Dov, E.; Sivan, O. Iron-Coupled Anaerobic Oxidation of Methane Performed by a Mixed Bacterial-Archaeal Community Based on Poorly Reactive Minerals. *Environ. Sci. Technol.* **2017**, *51* (21), 12293–12301. https://doi.org/10.1021/acs.est.7b03126.
(23) Beal, E. J.; House, C. H.; Orphan, V. J. Manganese- and Iron-Dependent Marine Methane Oxidation. *Science (80-.).* **2009**, *325* (5937), 184–187. https://doi.org/10.1126/science.1169984.
(24) Haroon, M. F.; Hu, S.; Shi, Y.; Imelfort, M.; Keller, J.; Hugenholtz, P.; Yuan, Z.; Tyson, G. W. Anaerobic Oxidation of Methane Coupled to Nitrate Reduction in a Novel Archaeal Lineage. *Nature* **2013**, *500* (7464), 567–570. https://doi.org/10.1038/nature12375.
(25) Bhattarai, S.; Cassarini, C.; Lens, P. N. L. Physiology and Distribution of Archaeal Methanotrophs That Couple Anaerobic Oxidation of Methane with Sulfate Reduction. *Microbiol. Mol. Biol. Rev.* **2019**, *83* (3). https://doi.org/10.1128/mmbr.00074-18.
(26) Siegel, H. G.; Soriano, M. A.; Clark, C. J.; Johnson, N. P.; Wulsin, H. G.; Deziel, N. C.; Plata, D. L.; Darrah, T. H.; Saiers, J. E. Natural and Anthropogenic Processes Affecting Domestic Groundwater Quality within the Northwestern Appalachian Basin. *Environ. Sci. Technol.* **2022**, *2022*, 13761–13773. https://doi.org/10.1021/acs.est.2c04011.
(27) Jurgens, B. C.; Burow, K. R.; Dalgish, B. A.; Shelton, J. L. *Hydrogeology, Water Chemistry, and Factors Affecting the Transport of Contaminants in the Zone of Contribution of a Public-Supply Well in Modesto, Eastern San Joaquin Valley, California*. *U.S. Geological Survey Scientific Investigations Report 2008–5156*.

2008. http://pubs. usgs.gov/sir/2008/5156

Chapter 4. Prediction of oil and gas well integrity using well construction physical parameters and geospatial metrics

By

[1]Yunpo Li, [1]Jennifer J Zhang, [1]Ethan D Nguyen, [1]Lara Bernard, [1]Kai T McClennen, [1]Michelle J Lei, [1]Lesley L Lambaric, [1]Lindsay McBride, [1]Maria I Alder, [1]Abdurahman Sherif, [1]Sebastian M Quintero, [1]Emily S Zhang, [1]Fabian Yanez-Laguna, [1]Desiree L. Plata

[1]Department of Civil and Environmental Engineering, Massachusetts Institute of Technology, Cambridge, MA 02139

ABSTRACT

The oil and gas (O&G) industry is a major contributor to anthropogenic emissions of methane, a highly potent greenhouse gas. The large number of O&G well pads makes routine inspection or spatiotemporally adequate measurement of methane leaks expensive and sometimes intractable. Machine Learning (ML) algorithms with the ability to predict O&G well integrity issues connected to methane leakage could help prioritize allocation of sensors. For the first time, we manually extracted well characteristics from 1,250 O&G well completion reports in Bradford County, PA, appended geospatial metrics, and used them to predict well integrity issues (i.e., sustained casing pressure and/or casing vent flow) reported by literature. Different ML models (e.g., Random Forrest, XGBoost and Logistic Regression) were compared, and the best model, XGBoost, achieved a 66% F-1 score on test data. Important predictive features were identified by the XGBoost model, such as the length of casings, amount of cement, and well operator. Moreover, the wells with integrity issues were geospatially clustered in our study region. Such clusters could be explained by the clusters of important predictors and topographic variation. Overall, the predictions would help prioritize sensor allocation, improve well design, and choose well location.

Synopsis

This work compiled a new dataset characterizing oil and gas wells and used it to predict integrity issues. Such prediction can guide the prioritized allocation of sensors to detect methane leaks from vulnerable wells.

Introduction

Methane is a powerful greenhouse gas (GHG) with a short average atmospheric lifetime of around 12 years. As a result, methane's warming potential exhibits a time-dependency, where the 20- and 100-year global warming potential (GWPs) are 80 and 30 times higher than the reference case of carbon dioxide.[1] The high, short-term warming effect of methane suggests that its emission reduction can uniquely alter the warming rate of the Earth over the next several decades, where 57% reduction by 2030 translates to 0.5ºC savings by 2100.[2] Indeed, all climate change scenarios that limit global temperature rise to 4°C or less *require* reduction in methane emissions.[3] Methane emissions from oil and gas (O&G) contribute to around 20% of the total anthropogenic emissions,[4] and these emissions are thought to be the most technically feasible and cost-effective opportunity for immediate emissions reduction. Indeed, reducing methane leakage from O&G infrastructure could feasibly recover revenue for the operators, and models estimated that roughly 25% to 50% of the methane emission reduction in the O&G industry could be achieved with negative cost.[5]

A key first step in implementing emission reduction practice from O&G infrastructure is to identify accurately leaking components. For this purpose, various monitoring technologies have been developed to detect fugitive methane emissions.[6,7] Traditionally, manual inspection of well sites with tools such as Optical Gas Imaging have been utilized, and the total cost of survey per site ranged from $100 to $600 USD.[8–10] Considering the large amount of producing O&G wells in the U.S. (roughly one million in 2021[11]), and the number of inspections required (assuming

once per quarter[12]), inspecting all O&G wells manually could require $400M-$2.4B annually. Remote sensing technologies such as satellite and airborne sensors have gained broad interest recently for their ability to scan a large area for methane leakage. However, remote sensing is limited by its scanning frequency (e.g., satellite revisit time ranges from several days to two weeks[13]) and resolution (e.g., 30m[14]) is not sufficient to distinguish methane plumes emitted by wells located close to each other, especially under complex surface meteorological conditions). For example, an intermittent methane emitter was seen only 30% of the time on average in an airborne survey in California.[15] One solution might be deploying sensors such as open-path laser sensors, infra-red cameras, and cavity ring-down spectrometers in close distance to potential emitters and perform continuous monitoring, but the cost of this remains high when deployed over vast infrastructure. As such, identifying a subset of O&G facilities with higher risk of fugitive methane emission would allow prioritization of sensor allocation or inspection to reduce cost, enhance monitoring efficiency, and enable higher chances of meaningfully reducing methane leaks.

Supervised Machine Learning (ML) models could be useful for prioritization of O&G wells vulnerable to fugitive leakage. Currently, large datasets of direct continuous measurement of methane emissions on single O&G well level are lacking or not publicly available. However, large publicly available datasets exist for the inspection results of well integrity failures that could lead to fugitive methane emissions. These datasets also provided multiple historical inspections of the same wells, enhancing their reliability even considering potentially intermittent failures. Therefore, the well integrity inspection results could serve as appropriate proxies of the methane emission risk. The ML models will predict which wells have integrity issues so that they should be given

priority for the close monitoring of methane leaks. Logically, the ability to predict integrity issues would require common characterizations of wells that could be related to such know vulnerabilities. Physical information on well construction, especially casing and cement, would be promising predictor candidates, both because they are plausibly related to integrity failures and because they are known quantities. Lackey et al. used 13 predictors including O&G well parameters such as well depth, depth of surface casing, well drilling density, wellbore deviation, and the percentage of the production casing cemented to fit logistic regression models to predict over-pressurized surface casings among O&G wells in the Wattenberg Test Zone in Colorado.[16] However, this earlier work didn't evaluate the models' prediction performance on a separate dataset not used for training (i.e., test set) and it lacked more detailed physical information of well construction, such as diameter, length, and grade of different casing strings, and type and amount of cement used.

In general, there is a lack of consistency in required or regulated data collection of O&G well physical information among different states, but as a starting point, we explored the utility of Pennsylvania's Exploration and Development Well Information Network (EDWIN) database considering the large growth of O&G wells in the region since 2008. EDWIN maintains completion reports of O&G wells, including detailed physical information regarding casing and cement. Casing and cement make up the functional structures that comprise an O&G well: concentric casings (i.e., tubes) include inner casing inserted inside the outer casing, and the space between casing (i.e., annulus) is sealed with cement. Sometimes, the annular space is uncemented or the cement is faulty (e.g., fractured), which creates a pathway for the upward migration of natural gas from geologic formations or leaky casing.[16–18] Such migrated gas can accumulate in the top part of the annulus beneath a venting valve and gradually increase the annular pressure to

form what is annotated as “sustained casing pressure” (SCP). As the SCP builds up, there is possibility that the annulus gas escapes through a section of annulus not protected by casing or cement. Furthermore, the SCP can be released by open the venting valve on top of the annulus so that natural gas (and possibly trapped liquid) is released to the open air via “casing vent flow” (CVF). Because SCP and CVF are well integrity issues closely related to methane emissions,[16,17] they are regularly monitored by O&G operators in states including Pennsylvania, New Mexico, and Colorado.[17] Further, they may be excellent indicators of methane emission risks, and building ML models to predict SCP and CVF could help prioritize identification and inspection that helps reduce or arrest methane emissions.

In this work, we manually extracted data from EDWIN scanned completion reports so that it was ready for ML training. Note that EDWIN reports are not machine readable, and they are stored as scanned copy of paper forms, and have inconsistencies in the approach for data entry that require human data extraction. Due to the constraints on time and labor, we digitalized well completion information of all O&G wells that had casing and/or cement parameters and were tested for SCP and/or CVF (n=1250) in Bradford County, PA. This county is located in the Northeastern part of Pennsylvania with a high intensity of O&G drilling, and the proportion of wells tested for integrity issues is higher than the state-wide average (77 and 36%, respectively).[17] Additionally, among tested wells in the county, 47% exhibited SCP and/or CVF before 2018, which was higher than the state-wide average of 14%.[17] As such, the abundance of integrity tests and observed integrity issues in Bradford County make it a suitable study region for applying ML methods to predict well integrity issues. Using this dataset, we compared the performance of different ML models to help

guide prioritization of monitoring for potential methane leaks, ultimately supporting methane emission reduction.

Methods

Data collection and processing

The well integrity test results for Pennsylvania O&G wells during 2014 to 2017 were published by Lackey et al.[17] and summarized in a single variable "SCP_and_or_CVF" defined as follows: If the annular pressure exceeds a critical threshold of 50 psi in two consecutive tests or in one test but no following tests were conducted, the pressure was labeled as SCP, and measurable gas or liquid flow from an annulus outside the production casing was labeled as CVF. For an O&G well exhibiting SCP and /or CVF issue at some point during 2014 to 2017, the well was labeled as faulty (SCP_and_or_CVF = 1), otherwise it was labeled as nonfaulty (SCP_and_or_CVF = 0). This label was used as the target variable of the ML prediction task undertaken here. The well construction physical information we used to predict the target variable were extracted from well completion reports from the EDWIN database managed by Pennsylvania Department of Conservation and Natural Resources Bureau of Geological Survey (accessed via an educational subscription;[19]). The completion reports were scanned files (i.e., photocopies of paper reports), and the relevant information (e.g., parameters of casing and cement construction) was extracted manually. For data quality control, a second analyst conducted manual verification and correction of the logged data. Out of the 1,284 wells tested for integrity issues in Bradford County, 1,250 had completion reports containing physical parameters of casing and/or cement in the EDWIN database, and this subset of wells were used as samples for our analysis. The

EDWIN well completion information was paired to the inspection results dataset (including the SCP_and_or_CVF variable) for the 1,250 wells. Note that the completion reports linked cement information to the type of casing (e.g., Conductor, Surface, Intermediate, and Production) outside which the cement was applied. However, other casing parameters were reported in rows ordered by descending casing diameter, without specifying the type of casing. Given such, the casings were grouped into four Ranks based on their diameters (see SI method for details). In addition, geospatial metrics (e.g., distance to the nearest faulty well and count of faulty wells within a certain radius) were constructed to serve as additional predictors. To prevent data leakage, any wells in the test set were excluded from the construction of geospatial metrics (see SI method for details). A summary of all features used for ML training and evaluation was given in Table S1. Among all features except the calculated geospatial features, the median percentage of missing value was 25% (Fig. S1). The data processing was implemented using the "pandas" library of Python, and the geospatial metrics were constructed using the "sklearn.neighbors" module.

Training and evaluation of ML models

The workflow of training and testing ML models (Fig. S2) began by dividing the whole dataset randomly into training dataset (80%) and test dataset (20%) with stratification. A Grid Search technique was used to find the optimal hyperparameters, and with each combination of hyperparameters, the performances of ML models were evaluated using 5-fold cross-validation (CV) on the training dataset. Note that involves splitting the training set into five data bins, and iteratively using each bin as CV-validation set (i.e., where the trained models are evaluated) and the other four bins as CV-training set (where the models are trained). The "F-1 Score" metric was used as the validation score. For each run of cross validation, we built a pipeline consisting

of four steps: data preprocessing, feature scaling, feature selection, and model fitting. First, the data preprocessing step imputed missing values in numeric features using their medians; in the case of categorical values one-hot encoding was employed. Second, each feature was scaled to unit variance by subtracting the mean and dividing by the standard deviation. Third, the ANOVA F values between the features and the target variable were calculated. A certain number (or percentile) of features with the highest F values were selected to stay in the model, and this number (or percentile) was treated as a model hyperparameter being tuned. Fourth, ML models were trained on the selected features and their performances were evaluated by the CV-validation sets, and for each ML model, the best hyperparameters that resulted in the highest mean validation score were selected for that model. Then, we compared all ML models and selected the one with the highest mean score. Lastly, the selected model was evaluated on the test set to produce the test scores, which characterized the model's generalizability on unseen data. The model training and evaluation procedures were implemented using the sklearn library of Python.

Performance metrics of ML models

The performance of ML models on our binary classification task (i.e., whether the well was faulty or not) can be evaluated via several different metrics. Recall is calculated by Equation 1, where positives indicate faulty wells and negatives indicate nonfaulty wells. It equals the number of correctly predicted faulty wells divided by the total number of actually faulty wells. Recall serves as a proxy for the models' ability to identify as many faulty wells as possible. High Recall would transfer to less faulty wells being missed (i.e., false negative), thus minimizing the undetected fugitive methane emissions which could be released from those wells. Precision is

calculated by Equation 2. It equals the number of correctly predicted faulty wells divided by the total number of predicted faulty wells. Functionally, a model with higher precision is less likely to predict faulty wells when they are actually nonfaulty (i.e., false positive). High Precision would lead to fewer resources wasted in conducting high-cost close monitoring of wells without integrity failure (e.g., by placing multiple sensors around the wells). An F-1 score is the harmonic mean of Recall and Precision (Equation 3), and equally values a model's Recall and Precision. The F-1 score was used as the criteria for choosing the best hyperparameters and models.

$$Recall = \frac{True\ Positive}{True\ Positive + False\ Negative}\ (Equation\ 1)$$

$$Precision = \frac{True\ Positive}{True\ Positive + False\ Positive}\ (Equation\ 2)$$

$$F-1\ Score = \frac{2 \times Recall \times Precision}{Recall + Precision}\ (Equation\ 3)$$

Results and discussion

Prediction performance of ML models

Prediction performance of different ML models were compared using 5-fold CV on the training dataset (Fig. 1). We included six ML classification models for the comparison: Random Forrest (RF) and XGBoost (XGB) were tree-based classifiers that are known for good performance on

mixed numeric and categorical predictors. They grow ‘trees’ by repeatedly splitting samples into two ‘branches’ over selected features that minimize sample diversity within each branch. The sequential ‘branching’ over multiple features can also leverage the interaction between features; Logistic Regression (LR) mimics Linear Regression: the log-odds of an event (e.g., well integrity failure) is predicted by a linear combination of predictive features. In addition, a Logistic Regression with Interaction (LR-IA) model was also introduced to add interaction terms of all features (i.e., the multiplication product of each pair of features, including the product of each feature and itself); Support Vector Machine (SVM) uses a decision boundary to separate samples of different labels; and K-Nearest Neighbor (KNN) makes prediction based on the labels of neighbors in the feature space. When all features (i.e., well features from EDWIN database and Lackey et al., as well as calculated geospatial features, Table S1) were used to predict the integrity issues of O&G wells, the mean CV F-1 scores of different models ranged from 62% to 65%. While geospatial features were excluded, the mean F-1 scores ranged from 61% to 65%. Although the scores of different models were similar, the XGB model exhibited a small advantage with 65% F-1 score in both scenarios. Among compared models except KNN, including the geospatial features could slightly increase the mean F-1 scores. Such increase suggested that the faulty statuses of other tested O&G wells in the neighborhood could add useful information for predicting integrity failures, and spatial correlation of O&G well’s faulty status possibly existed in the tested samples.

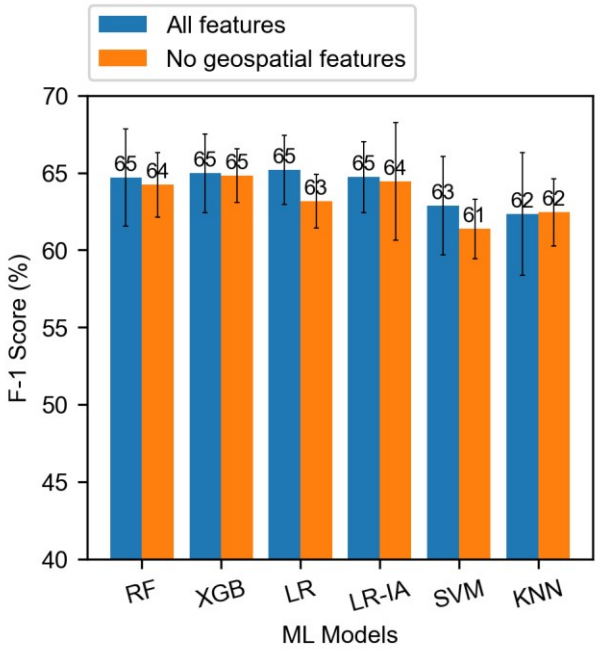

Figure 1. CV F-1 scores of different ML models. The scores of models built on all features and of those built on features excluding the geospatial ones are shown by blue and orange bars, respectively. The mean of F-1 scores in 5-fold CV was represented by the height of each bar, and the standard deviation of F-1 scores was shown as each error bar. Note that the models' hyperparameters had been tuned (i.e., hyperparameters corresponding to the highest mean F-1 score had been selected for each model).

The XGB model was re-trained on the entire training set and used to predict the hold out test set as a final evaluation of its performance (Fig. 2). When using all features, the model predicted 70% of the nonfaulty wells in the test set correctly, and 66% of the faulty wells correctly (Fig. 2A). When excluding geospatial features, 62% of nonfaulty wells were predicted correctly while 65% of the faulty wells were predicted correctly (Fig 2B). Since the model using all features correctly identified more nonfaulty wells and faulty wells than the model excluding geospatial features, its Recall (66%) and Precision (66%) were both higher than the other model (65% and 61%, respectively). As a result, the F-1 score using all features (66%) was higher than that

excluding geospatial features (63%). Importantly, the F-1 scores of XGB model on the hold out test set were similar to their CV F-1 scores, suggesting that the models had good generalizability on unseen data from the same geographical region. This can be very useful since the regional proportions of O&G wells tested for integrity failures were low in the U.S. (36% in Pennsylvania, 25% in Colorado, and 27% in New Mexico[17]), and the faulty statuses of the untested wells in the these regions can become the targets of ML prediction.

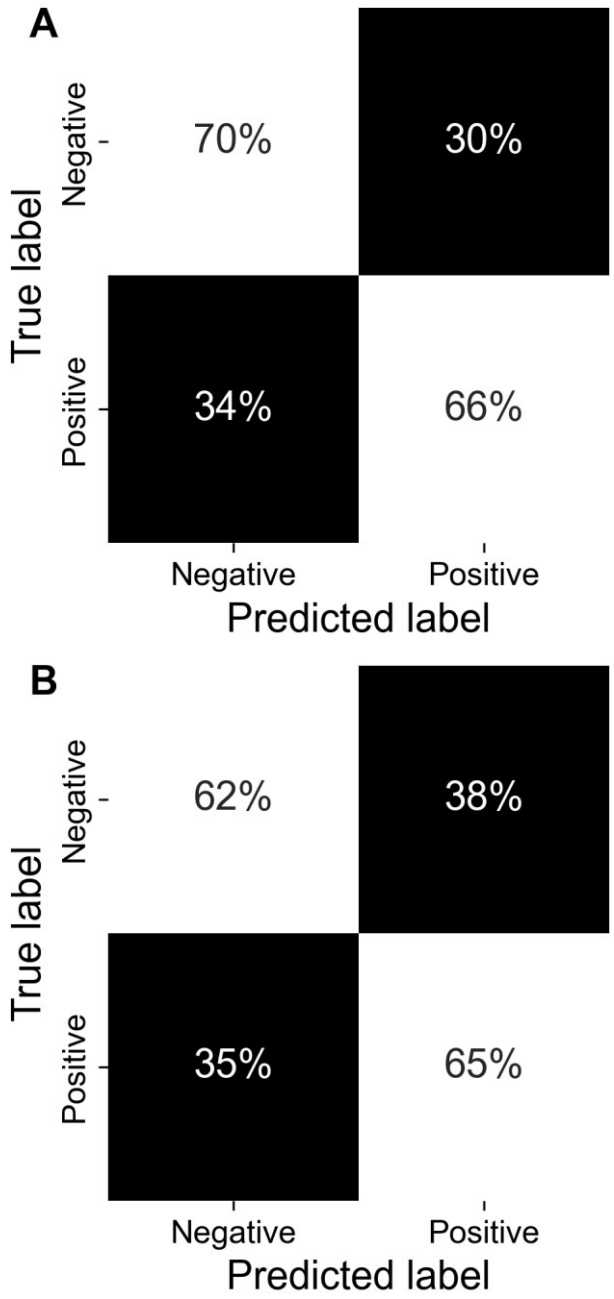

Figure 2. Proportions of test samples predicted as nonfaulty and faulty by the XGB model using (A) all features and (B) all features except the geospatial ones. The percentage values in each row sum up to 100%. The number of nonfaulty and faulty samples in the test set were 132 and 118, respectively. The Recall, Precision, and F-1 Score were 66%, 66%, and 66%, respectively for all features (panel A) and 65%, 61%, and 63%, respectively for all features excluding the geospatial ones (panel B).

Feature importance analysis

SHapley Additive exPlanations (SHAP) value is a useful tool to represent the feature importance in a ML model. The SHAP values of the XGB model were used for demonstrating the importance of the features in this dataset because (i) the XGB model exhibited relatively high F-1 scores (Fig. 1), and (ii) XGB models approximate SHAP values (i.e., TreeSHAP) which are much more tractable to compute compared to regular SHAP values. SHAP values of the XGB models trained on all features (Fig. 3A) and features excluding the geospatial ones (Fig. 3B) were shown. Among the 15 most important features in the first scenario, eight were geospatial features (including longitude and latitude; Fig. 3A). Well integrity issue was associated with smaller distance to the nearest faulty wells and greater distance to the nearest nonfaulty wells. These findings supported the clustering of faulty wells in this dataset and necessitated a spatial correlation analysis to evaluate the clustering.

When features excluding the geospatial ones were used to train the model (Fig. 3B), the amounts in well (i.e., length) of Rank 1, 2, and 3 casings (casing with higher rank has smaller diameter; see SI) were the most important features. O&G wells with smaller lengths of these casings were more likely to be predicted as faulty by the model. Moreover, smaller hole size for Rank 1 casing was linked to faulty well status. Wells with smaller amounts of cement outside the conductor and production casing were also likely to be predicted as Faulty. A hypothesis to explain these observed SHAP values could be that longer casing and larger amount of cement provided better protection to the integrity of O&G wells. When the well was built by a specific operator, C (name anonymized), it was less likely to be predicted as faulty. This operator owned the greatest

number of wells (44% of total), while the 2nd, 3rd, and 4th biggest operators owned 24%, 11%, and 10% of wells, respectively. It was possible that operator C had higher quality standard for building wells or better maintenance practice. Furthermore, wells built at locations with smaller surface elevation were more likely to be predicted as faulty. This suggested that well integrity could be influenced by natural geographical and/or geological features.

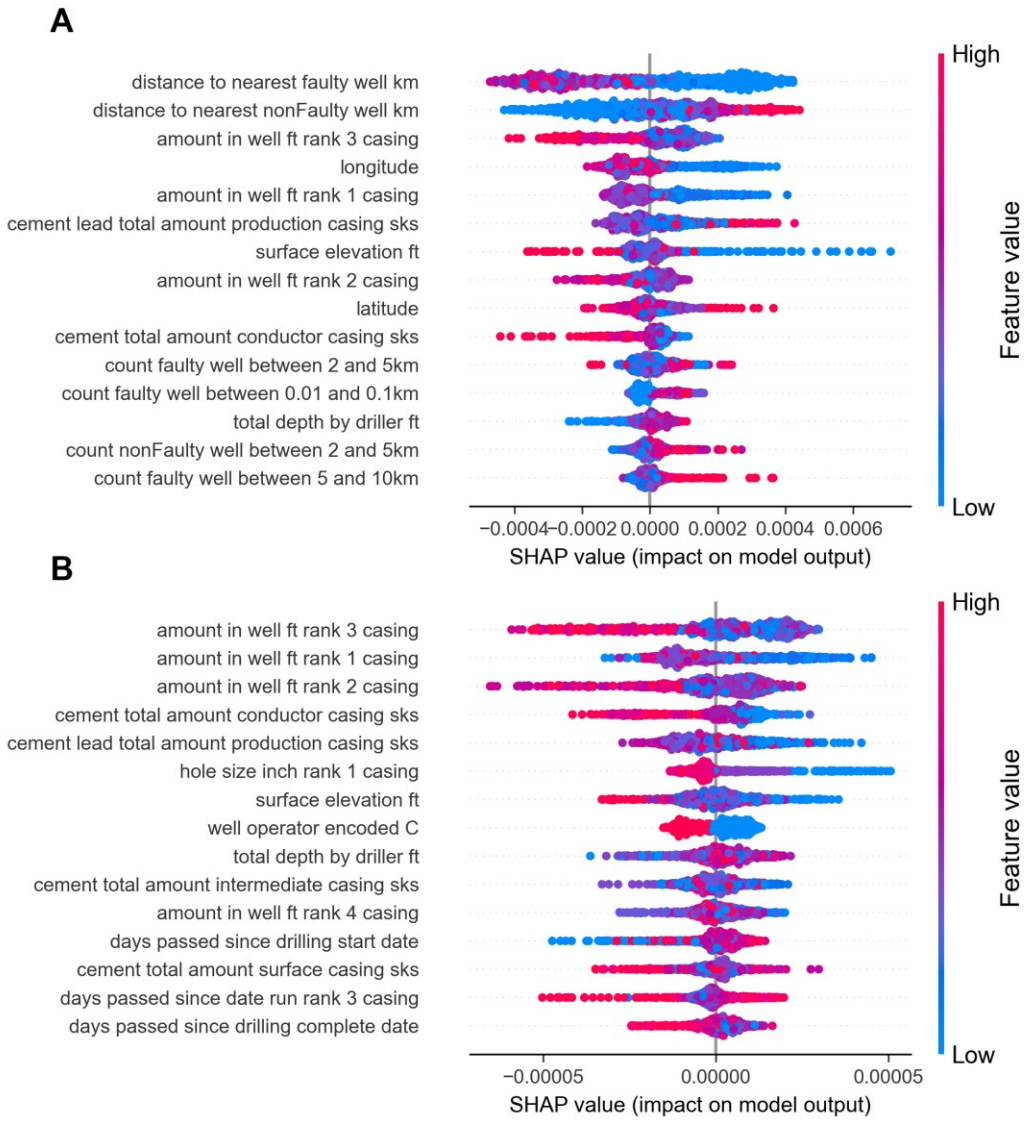

Figure 3. For XGB predictor using (A) all features and (B) all features excluding geospatial ones, the top 15 important features were selected by SHAP values. Samples in the training dataset are shown as dots in each row. The SHAP value of each sample is shown by its horizontal location (x-axis value), with the color scale representing the normalized value of the concerned feature. A SHAP value greater than 0 indicates that the feature value is contributing to the prediction of positive label (i.e., faulty well). The absolute value of SHAP value indicates relative importance of the feature. The features are ordered by descending importance. Note that categorical features were preprocessed using one-hot encoding, which created a binary dummy feature for each class. For example, the feature 'well operator encoded C' took value of one if the operator was C, or zero if the operator was not C.

Geospatial clustering of well integrity issue

The importance of geospatial features in predicting integrity failures would support a probable geospatial clustering of faulty wells within the study region. An overall trend of spatial clustering of faulty wells (i.e., faulty wells located closer to each other than nonfaulty wells) was confirmed by the Join Counts statistic[20–22]: Join Counts for 'black-black' (i.e., faulty well neighboring another faulty well) was 8,410 (simulated p-value = 0.001) compared to its expected mean of 6,406 assuming random spatial distribution. The geospatial distribution of the clusters were shown by the Local Join Counts statistic[23,24] (Fig. 4). This statistic only captured clusters of faulty wells while ignoring any clusters of nonfaulty wells, and larger values indicated higher degrees of clustering between faulty wells (see Fig 4, where the value of the statistic is given by the marker color where the clustering was statistically significant). There were two major clusters of faulty wells on the Western and Eastern side of our study region in Bradford County, PA, and the clustering on the Western side was more substantial than that on the Eastern side (Fig. 4). To understand whether such clustering pattern was driven by the spatial distribution of

important predictive features, the clustering of four important physical features (selected from Fig. 3B) was characterized by Getis and Ord's Gi* statistics.[22,25] Briefly, Getis and Ord's Gi* statistic is a measure of the clustering of high values (warm color) and that of low values (cold color). The Western cluster of faulty wells (Fig. 4) overlapped clusters of low values in Rank 3 casing amount (Fig. S3A), Rank 2 casing amount (weak clustering; Fig. S3C), and cement amount outside conductor casing (Fig. S3D). These findings were consistent with the correlation between faulty well status and smaller amounts of casing and cement indicated by SHAP values (Fig. 3B). However, the Western cluster of faulty wells did not overlap with clusters of smaller amounts of Rank 1 casing (Fig. S3B). In addition, the Eastern cluster of faulty wells, which was less substantial, did not overlap with the clusters of low values in any of these four features. Lastly, the clusters of wells whose operator was not C (Fig. S4, by Local Join Counts) almost perfectly overlapped the Western and Eastern clusters of faulty wells, which emphasized the impact of this specific operator. Overall, the spatial clustering of faulty wells was correlated with the clustering of important predictive features.

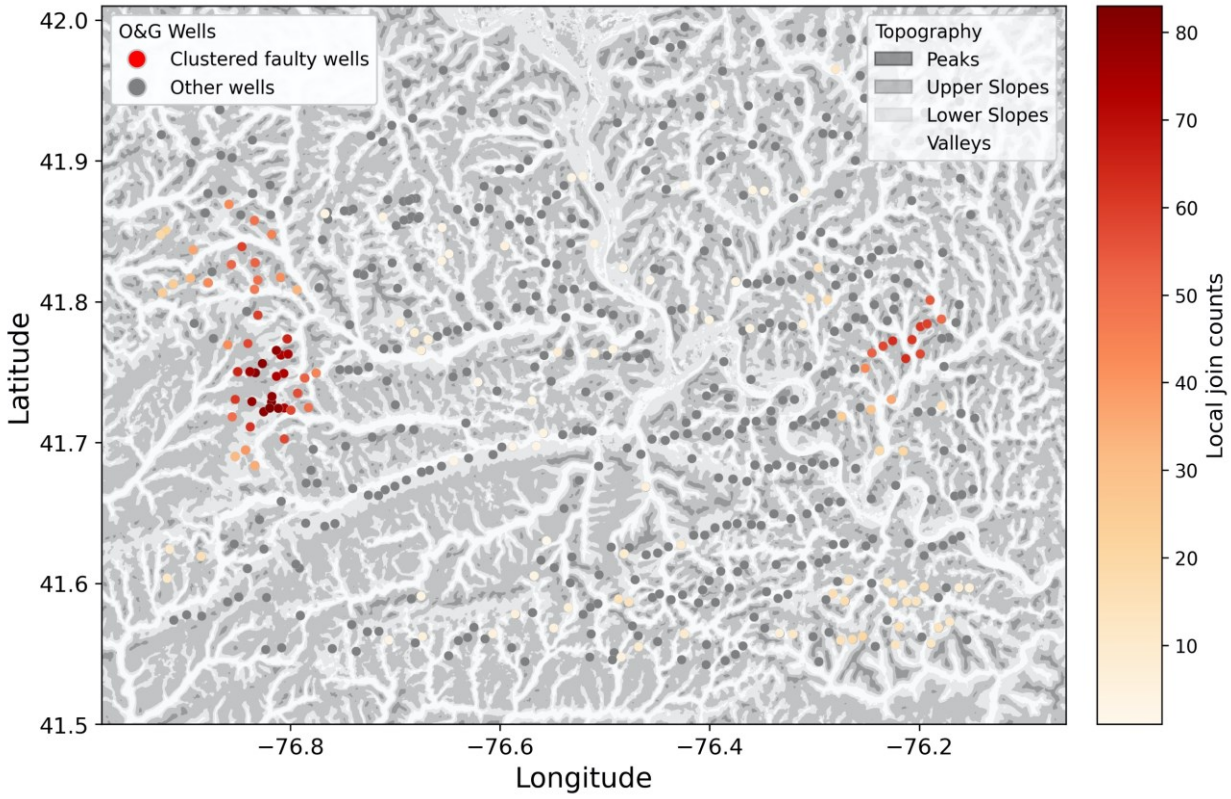

Figure 4. Spatial clustering of faulty wells characterized by the Local Join Counts statistics. Faulty wells that were clustered with statistical significance were shown by warmly colored circles. Warmer color indicated higher degree of clustering. Other wells (i.e., nonfaulty wells, and faulty wells that were not in statistically significant clusters) are shown by grey-colored circles. To calculate the Local Join Counts, the spatial weights were constructed using a distance band equaling the maximum nearest neighbor distance among the wells. Local topography is also represented by color scale, with deeper color indicating higher topographical positions.

It is possible that natural geological factors could also influence the clustering of faulty wells. For example, geological fractures could provide preferential pathways for underground methane migration, and if such methane entered the anulus of O&G wells through faulty casing or cementation, SCP or CVF may arise. Valleys were known to have higher density of geological fractures beneath them due to lithologic weakness and erosion effect,[26–30] and geological folds

(e.g., synclines and anticlines) could also facilitate the development of certain fractures (e.g., joints).[31] In our dataset, the Local Join Counts of faulty wells with significant clustering were higher in topographic lows (i.e., valley and lower slope) than in the topographic highs (i.e., upper slope and peak), and such difference was statistically significant by Welch's ANOVA and Games-Howell post-hoc test (Fig. S5). This suggested that topographic lows could facilitate the clustering of integrity issues, and was consistent with the finding that smaller surface elevation was linked to faulty well status (Fig. 3B). Moreover, multiple geological folds extend across our study region (Fig. S6). The mean distance to the nearest geological fold for faulty wells, nonfaulty wells, and all wells were not statistically different, while clustered faulty wells had statistically larger mean distance to the nearest geologic fold (Welch's ANOVA and Games-Howell post-hoc test; Fig. S7). This suggested that geological folds were unlikely to enhance the clustering of well integrity issues.

Implication

According to the recent data survey conducted in 2021,[17] only a fraction of O&G wells were tested for SCP and/or CVF in three U.S. states (36% in Pennsylvania, 25% in Colorado, and 27% in New Mexico by 2018), and many other states lack any kind of data on such tests. This will certainly change under new legislation, and the untested wells open the opportunity for using ML models to predict well integrity weaknesses in them, potentially allowing for correction prior to catastrophic failure or on a more metered timeframe. In this study, the best performing ML model, XGB, achieved a 66% F-1 score on the hold out test set. The prediction results of well integrity issues can have the following applications: First, these results can guide prioritized

allocation of sensors and other Leak Detection and Repair (LDAR) efforts to monitor methane leaks. Although the predictions of our ML models were not perfectly accurate, such information was already useful for optimizing the monitoring strategy. For example, if the model had a 66% F-1 score, the monitoring team would still place sensors on the wells predicted as nonfaulty, since they knew that a fraction of those wells could be mistakenly predicted. However, they would place a smaller amount of sensors on each of those wells than on each of the wells predicted as faulty. This could decrease the total number of sensors needed than uniformly placing sensors around each well. Prioritized placement of sensors can translate to a lower total cost, better detection, and a more accurate fee structure under the new IRA tax. Second, an improved understanding of how features are correlated with integrity issues can improve guidelines for future well construction. For example, wells with shorter Rank 1, 2, and 3 casings were more likely to be predicted as faulty, and smaller amount of cement outside conductor and production casing were also associated with faulty status. Future well designers should take these into account and improve their strategy to make more reliable wells. In addition, well operator C was linked to lower chance of integrity failure. This emphasized that operators were not equal in terms of maintaining well integrity and such inequality should be noticed by the regulators and or leveraged to promote best practices among the industry. Third, the algorithm and underlying understanding may support identification of poor and strong locations to build new wells. Operators should avoid drilling new wells near existing clusters of faulty wells and choose topographical highlands, as they tended to show a less degree of faulty well clustering.

The implications of this work on regulated data collection are numerous. The difficulty and cost of extracting information from the completion reports can be a major challenge for the large-

scale application of our approach and threatens implementation at scale. For example, in Pennsylvania, most of the completion reports were photocopies of paper documents, and manually extracting information from them would cost a large amount of time and human labor (there are over 150,000 O&G wells in PA by 2018).[17] In addition, the variation in the format of the report (i.e., what fields were included in the tables) was substantial and resulted in large portion of missing values in some features (Table. S1 and Fig. S1). A facile solution would be to enforce the digitalization of information logging using standardized formatting. For example, O&G operators should upload the well completion information by filling out web-based forms or uploading electronic spreadsheets, instead of submitting paper forms. These will make the information immediately available for ML training or statistical analysis and solve many of the issues associated with file-to-file variation. Alternatively, tools can be developed to automatically digitalize the already uploaded photocopies. However, it should be noted that the heterogeneities in the way the forms are filled out required human interpretation in our study. Nevertheless, technologies such as Computer Vision and Natural Language Processing could potentially provide useful solutions if better homogenization or field enforcement was applied. Critically, another substantial challenge regarding data availability is that many states in the US haven't required SCP and/or CVF test or haven't made the test results publicly available. Lackey et al. searched for SCP and/or CVF test records in 33 US states and only found useful publicly available data in Pennsylvania, Colorado, and New Mexico.[17] Therefore, we urge that more US states and nations with O&G production to enforce regular well integrity investigation and publish the results as more data can improve the ML model performance and lead to higher efficiency in monitoring and mitigating O&G methane emissions. Moreover, SCP and/or CVF test was not required for plugged or abandoned wells even in the three data-reporting states.[17] As

wells are transitioned from active to retired, they may continue emitting methane due to integrity failures so tests of these wells should be required under new legislation.

Furthermore, we highlight that Bradford County was dominated by unconventional O&G wells (roughly 95% wells were horizonal or deviated). In other words, this training dataset was biased toward unconventional wells, and this could limit the generalization of the current results. This is particularly true considering unconventional wells exhibited higher frequency of SCP and/or CVF than conventional wells in Pennsylvania and Colorado.[17] Given such, the ML models trained on this Bradford County dataset are most suitable to make predictions in other unconventional well-dominated regions. In the future, when more digitalized well construction data become available in other parts of Pennsylvania or other parts of the world, which covers a more balanced distribution of conventional versus unconventional wells, the ML models can be retrained to improve performance on both well types. Last but not the least, due to the correlational nature of SHAP values (and of ML models), the feature importance demonstrated in this study could only imply correlations between the features and the model output (i.e., faulty status of O&G wells), instead of determining the causal relationship between them. A good strategy would be to modify well designs using these correlations as guidelines (e.g., increasing the length of certain casings) and observe their impacts on well integrity by periodic survey.

Acknowledgment

The authors thank the Pennsylvania Department of Conservation and Natural Resources Bureau of Geological Survey to grant us access to the Exploration and Development Well Information

Network (EDWIN) dataset via educational subscription and the MIT Undergraduate Research Opportunities Program (MIT UROP) and MIT Energy Initiative (MIT EI) for providing funding support to some of the undergraduate authors.

References

(1) Forster, P.; Storelvmo, T.; Armour, K.; Collins, W.; Dufresne, J.-L.; Frame, D.; Lunt, D. J.; Mauritsen, T.; Palmer, M. D.; Watanabe, M.; Wild, M.; Zhang, H. *The Earth's Energy Budget, Climate Feedbacks, and Climate Sensitivity. In Climate Change 2021: The Physical Science Basis. Contribution of Working Group I to the Sixth Assessment Report of the Intergovernmental Panel on Climate Change*; Cambridge, United Kingdom and New York, NY, USA, 2021. https://doi.org/10.1017/9781009157896.009.

(2) Ocko, I. B.; Sun, T.; Shindell, D.; Oppenheimer, M.; Hristov, A. N.; Pacala, S. W.; Mauzerall, D. L.; Xu, Y.; Hamburg, S. P. Acting Rapidly to Deploy Readily Available Methane Mitigation Measures by Sector Can Immediately Slow Global Warming. *Environ. Res. Lett.* **2021**, *16* (5), 054042. https://doi.org/10.1088/1748-9326/abf9c8.

(3) Masson-Delmotte, V.; Zhai, P.; Pirani, A.; Connors, S. L.; Péan, C.; Berger, S.; Caud, N.; Chen, Y.; Goldfarb, L.; Gomis, M. I.; Huang, M.; Leitzell, K.; Lonnoy, E.; Matthews, J. B. R.; Maycock, T. K.; Waterfield, T.; Yelekçi, O.; Yu, R.; Zhou, B. *Summary for Policymakers. In: Climate Change 2021: The Physical Science Basis. Contribution of Working Group I to the Sixth Assessment Report of the Intergovernmental Panel on Climate Change*; 2021. https://doi.org/10.1017/9781009157896.001.

(4) Saunois, M.; Stavert, A.; Poulter, B.; Bousquet, P.; Canadell, J.; Jackson, R.; Raymond, P.; Dlugokencky, E.; Houweling, S.; Patra, P.; Ciais, P.; Arora, V.; Bastviken, D.; Bergamaschi, P.; Blake, D.; Brailsford, G.; Bruhwiler, L.; Carlson, K.; Carrol, M.; Castaldi, S.; Chandra, N.; Crevoisier, C.; Crill, P.; Covey, K.; Curry, C.; Etiope, G.; Frankenberg, C.; Gedney, N.; Hegglin, M.; Höglund-Isaksson, L.; Hugelius, G.; Ishizawa, M.; Ito, A.; Janssens-Maenhout, G.; Jensen, K.; Joos, F.; Kleinen, T.; Krummel, P.; Langenfelds, R.; Laruelle, G.; Liu, L.; Machida, T.; Maksyutov, S.; McDonald, K.; McNorton, J.; Miller, P.; Melton, J.; Morino, I.; Müller, J.; Murguia-Flores, F.; Naik, V.; Niwa, Y.; Noce, S.; O'Doherty, S.; Parker, R.; Peng, C.; Peng, S.; Peters, G.; Prigent, C.; Prinn, R.; Ramonet, M.; Regnier, P.; Riley, W.; Rosentreter, J.; Segers, A.; Simpson, I.; Shi, H.; Smith, S.; Steele, L. P.; Thornton, B.; Tian, H.; Tohjima, Y.; Tubiello, F.; Tsuruta, A.; Viovy, N.; Voulgarakis, A.; Weber, T.; van Weele, M.; van der Werf, G.; Weiss, R.; Worthy, D.; Wunch, D.; Yin, Y.; Yoshida, Y.; Zhang, W.; Zhang, Z.; Zhao, Y.; Zheng, B.; Zhu, Q.; Zhu, Q.; Zhuang, Q. The Global Methane Budget 2000–2017. *Earth Syst. Sci. Data* **2020**, *12* (3), 1561–1623. https://doi.org/10.5194/essd-12-1561-2020.

(5) United Nations Environment Programme and Climate and Clean Air Coalition. *Global Methane Assessment: Benefits and Costs of Mitigating Methane Emissions*; Nairobi, 2021.

(6) Sawyer, W.; Genina, I.; Brenneis, R.; Feng, H.; Li, Y.; Lennon Luo, S.-X. Methane

Emissions and Global Warming: Mitigation Technologies, Policy Ambitions, and Global Efforts. *MIT Sci. Policy Rev.* **2022**, *3*, 73–84. https://doi.org/10.38105/spr.8u4spgvc0e.
(7) Nisbet, E. G.; Fisher, R. E.; Lowry, D.; France, J. L.; Allen, G.; Bakkaloglu, S.; Broderick, T. J.; Cain, M.; Coleman, M.; Fernandez, J.; Forster, G.; Griffiths, P. T.; Iverach, C. P.; Kelly, B. F. J.; Manning, M. R.; Nisbet-Jones, P. B. R.; Pyle, J. A.; Townsend-Small, A.; Al-Shalaan, A.; Warwick, N.; Zazzeri, G. Methane Mitigation: Methods to Reduce Emissions, on the Path to the Paris Agreement. *Reviews of Geophysics*. John Wiley & Sons, Ltd March 1, 2020, p e2019RG000675. https://doi.org/10.1029/2019RG000675.
(8) Environmental Defense Fund. *Finding, Fixing Leaks Is a Cost-Effective Way to Cut Oil and Gas Methane Emissions*; 2016.
(9) Saunier, S.; Haugland, T.; Pederstad, A. *Quantifying Cost-Effectiveness of Systematic Leak Detection and Repair Programs Using Infrared Cameras,* Carbon Limits report CL-13-27; 2014.
(10) Kemp, C. E.; Ravikumar, A. P. New Technologies Can Cost Effectively Reduce Oil and Gas Methane Emissions, but Policies Will Require Careful Design to Establish Mitigation Equivalence. *Environ. Sci. Technol.* **2021**, *55* (13), 9140–9149. https://doi.org/10.1021/acs.est.1c03071.
(11) U.S. Energy Information Administration. US Oil and Gas Wells by Production Rate https://www.eia.gov/petroleum/wells/ (accessed Dec 27, 2022).
(12) U.S. Environmental Protection Agency. *EPA ' s Supplemental Proposal to Reduce Pollution from the Oil and Natural Gas Industry to Fight the Climate Crisis and Protect Public Health: Overview*; 2022.
(13) Sherwin, E. D.; Rutherford, J. S.; Chen, Y.; Aminfard, S.; Kort, E. A.; Jackson, R. B.; Brandt, A. R. Single-Blind Validation of Space-Based Point-Source Detection and Quantification of Onshore Methane Emissions. *Sci. Reports 2023 131* **2023**, *13* (1), 1–10. https://doi.org/10.1038/s41598-023-30761-2.
(14) Liao, F.; Hamburg, S.; Gautam, R. *MethaneSAT: A New Era of Transparency for Methane Measurement*; 2023.
(15) Duren, R. M.; Thorpe, A. K.; Foster, K. T.; Rafiq, T.; Hopkins, F. M.; Yadav, V.; Bue, B. D.; Thompson, D. R.; Conley, S.; Colombi, N. K.; Frankenberg, C.; McCubbin, I. B.; Eastwood, M. L.; Falk, M.; Herner, J. D.; Croes, B. E.; Green, R. O.; Miller, C. E. California's Methane Super-Emitters. *Nature* **2019**, *575* (7781), 180–184. https://doi.org/10.1038/s41586-019-1720-3.
(16) Lackey, G.; Rajaram, H.; Sherwood, O. A.; Burke, T. L.; Ryan, J. N. Surface Casing Pressure As an Indicator of Well Integrity Loss and Stray Gas Migration in the Wattenberg Field, Colorado. *Environ. Sci. Technol.* **2017**, *51* (6), 3567–3574. https://doi.org/10.1021/acs.est.6b06071.
(17) Lackey, G.; Rajaram, H.; Bolander, J.; Sherwood, O. A.; Ryan, J. N.; Shih, C. Y.; Bromhal, G. S.; Dilmore, R. M. Public Data from Three US States Provide New Insights into Well Integrity. *Proc. Natl. Acad. Sci. U. S. A.* **2021**, *118* (14). https://doi.org/10.1073/PNAS.2013894118.
(18) Ingraffe, A. R.; Wells, M. T.; Santoro, R. L.; Shonkoff, S. B. C. Assessment and Risk Analysis of Casing and Cement Impairment in Oil and Gas Wells in Pennsylvania, 2000-2012. *Proc. Natl. Acad. Sci. U. S. A.* **2014**, *111* (30), 10955–10960. https://doi.org/10.1073/pnas.1323422111.

(19) Pennsylvania Department of Conservation and Natural Resources Bureau of Geological Survey. Exploration and Development Well Information Network https://edwin.dcnr.pa.gov/ (accessed May 1, 2023).
(20) Cliff, A. D.; Ord, J. K. *Spatial Processes: Models & Applications*; Pion, 1981.
(21) pysal developers. Exploratory Analysis of Spatial Data: Spatial Autocorrelation https://pysal.org/esda/notebooks/spatialautocorrelation.html (accessed Oct 2, 2023).
(22) Rey, S. J.; Arribas-Bel, D.; Wolf, L. J. *Geographic Data Science with Python*; 2020.
(23) Anselin, L.; Li, X. Operational Local Join Count Statistics for Cluster Detection. *J. Geogr. Syst.* **2019**, *21* (2), 189–210. https://doi.org/10.1007/s10109-019-00299-x.
(24) pysal developers. Local join counts https://pysal.org/esda/notebooks/localjoincounts.html (accessed Oct 2, 2023).
(25) Getis, A.; Ord, J. K. The Analysis of Spatial Association by Use of Distance Statistics. *Geogr. Anal.* **1992**, *24* (3), 189–206. https://doi.org/10.1111/j.1538-4632.1992.tb00261.x.
(26) Ferguson, H. F.; Hamel, J. V. Valley Stress Relief in Flat-Lying Sedimentary Rocks. *Weak rock soft, Fract. Weather. rock. Proc. Symp. Tokyo, Sept. 1981. Vol. 2* **1981**, 1235–1240.
(27) Wyrick, G. G.; Borchers, J. W. Hydrologic Effects of Stress-Relief Fracturing in An Appalachian Valley. *US Geol. Surv. Water Supply Pap.* **1981**. https://doi.org/10.3133/wsp2177.
(28) Mason, G. Structurally Related Migration Of Hydrocarbons in the Central Appalachian Basin of Eastern Ohio. *AAPG Search Discov. Artic. #50733* **2012**.
(29) Taylor, L. E. Groundwater Resources of the Upper Susquehanna River Basin, Pennsylvania. *Pennsylvania Geol. Surv. 4th ser. Water Resource Report 58.* **1984**
(30) Heisig, P. M.; Scott, T.-M. Occurrence of Methane in Groundwater of South-Central New York State, 2012- Systematic Evaluation of a Glaciated Region by Hydrogeologic Setting. *Sci. Investig. Rep.* **2013**, *2013–5190*. https://doi.org/10.3133/sir20135190.
(31) Savage, H. M.; Ryan Shackleton, J.; Cooke, M. L.; Riedel, J. J. Insights into Fold Growth Using Fold-Related Joint Patterns and Mechanical Stratigraphy. *J. Struct. Geol.* **2010**, *32* (10), 1466–1475. https://doi.org/10.1016/j.jsg.2010.09.004.

Supporting information for Chapter 4

Supplementary methods

Details of processing casing and cement information

The EDWIN completion reports usually reported the parameters of each casing in a separate row and ordered the rows by descending casing diameter, but didn't specify the casing type (e.g., Conductor, Surface, Intermediate, and Production) for each row. In order to align the casings of similar diameters from different wells, we grouped the casings into several Ranks according to their diameters. First, we noticed that four pipe sizes (i.e., diameters, in inches) were most common throughout the dataset: 20, 13.375, 9.625, and 5.5. This implied that the diameters of casings followed some industrial standards. We further assigned each casing to one of four Ranks using their diameters in inches: Rank 1 (diameter >= 16), Rank 2 (16 > diameter >= 11.75), Rank 3 (11> diameter >= 7.625), and Rank 4 (7.625 > diameter >= 4.5). The length of the casing increased from Rank 1 to Rank 4. In fact, the diameter ranges of Rank 1 to 4 matched the common diameters of Conductor, Surface, Intermediate, and Production casing, respectively.[1,2]

When the completion reports didn't include a dedicated table for cement information, they often reported cement information under the name 'material behind pipe' in the rows of casing parameters. Specifically, type and amount of 'material behind pipe' were reported in each row. We consolidated such information (e.g., amount of cement behind Rank 1 casing) into the

cement information which was reported together with a casing type (e.g, amount of cement behind Conductor casing). Particularly, we assumed a matching relationship between the casing Rank and casing type, such that we moved 'material behind pipe' of Rank 1 casing to be Conductor casing cement, that of Rank 2 casing to be Surface casing cement, that of Rank 3 casing to be Intermediate casing cement, and that of Rank 4 casing to be Production casing cement.

In most reports, the unit of cement amount was sacks, which can be abbreviated as 'sks' or 'sx'. However, other units were also used. We applied the following unit conversion ratios: one barrel ('BBLs') equals four sacks, one cubic yard ('yds') equals 27 sacks, and one pound ('lbs') equals 0.01 sack.[3–5] In addition, if the type of cement indicated no cement was used (e.g., 'uncemented', 'driven in', or 'screwed in'), the amount of cement was set to be zero. Lastly, the cement outside of production casing consisted of two parts in the majority of reports: lead and tail. For the reports that didn't specify whether the cement was lead or tail (and for material behind Rank 4 casing), we assigned the data to the lead category.

Details of data cleaning and processing

For different types of features, we adopted the following processing approaches: First, date features in the dataset (e.g., drilling start date) were converted to the number of days between that date and a fixed benchmark date, December 31st, 2023, in order to be utilized by ML models. Second, categorical features including thread/weld type of casing, grade of casing, and type of cement could have a large number of possible values (e.g., greater than 20). In such

cases, the one-hot encoder would create an intractable number of dummy columns which greatly expanded the dimension of the feature space and harmed the stability of ML models. However, we noticed that several popular values accounted for most of the samples (e.g., > 90%) and the rest values only had small counts in the dataset. Therefore, we kept the popular values and grouped the rest values into a single class 'other'. Third, some reports gave 'yes or no' answer to whether gas blocking measures were applied for each casing type, while others had long descriptions of the specific measures taken, which were difficult to categorize and to be handled by one-hot encoding. To consolidate these two types of information, we only kept a binary column indicating whether the report had documented gas blocking measures or not, and used it as a predictive feature. Fourth, there were two types of total well depth (i.e., the sum of vertical depth and horizontal depth): the one measured by driller and the one measured by logger, and we used both as predictive features. If the total depth didn't specify which type it belonged to (e.g., it was simply called "total measured depth"), we assumed it was measured by driller.

Details of constructing geospatial metrics to avoid data leakage

The construction of geospatial metrics (e.g., count of faulty/nonfaulty wells within a radius, and distance to the nearest faulty/nonfaulty well) required knowing the faulty statuses of the neighboring wells. However, the dataset was divided into a training set (or Cross-Validation (CV) training set) with known labels (i.e., faulty status) during model training, and a test set (or CV validation set) reserved for evaluating the trained model, whose information was 'invisible' during model training. Given such, the faulty statuses of the wells in the test set should not be used for model training to avoid the so-called 'data leakage'. In this study, the geospatial metrics

were only calculated using the geospatial coordinates and faulty statuses of wells in the training set (or CV training set), excluding any wells in the test set (or CV validation set). For example, when we counted the number of faulty wells in the neighborhood of a given well during model training, we only counted those wells in the training set whose faulty statuses were known to us. And during model evaluation, we also only counted the number of faulty wells in the training set in the neighborhood of each well in the test set (we assumed that each test sample was independent, so it didn't know the location and faulty status of other test samples). The same principle applied to the calculation of distance to the nearest neighboring well.

Topography and geological folds

We constructed four topographical classes (i.e., valley, lower slope, upper slope, and peak) by adapting the classification system of Theobald et al.,[6] which was based on a multi-scale topographic position index (mTPI). The locations of geological folds within our study region were downloaded from Pennsylvania Department of Conservation and Natural Resources.[7] We calculated the distance between O&G wells and geological folds using the distance() method of the GeoPandas module of Python.

Supplementary tables

Table S1. List of feature names, data source, percentage of missing values, and note

	Feature	Data Source	Missing (%)	Note

1	api	EDWIN[8]	0	
2	well_type	EDWIN	2	
3	well_orientation	EDWIN	35	
4	1st_drill_method	EDWIN	7	
5	2nd_drill_method	EDWIN	11	
6	days_passed_since_drilling_start_date	EDWIN	2	
7	days_passed_since_drilling_complete_date	EDWIN	3	
8	ground_water_depth_ft	EDWIN	83	
9	depth_of_deepest_fresh_ground_water_ft	EDWIN	52	
10	true_vertical_depth_ft	EDWIN	67	
11	surface_elevation_ft	EDWIN	2	
12	total_depth_by_driller_ft	EDWIN	3	
13	total_depth_by_logger_ft	EDWIN	68	
14	cement_returned_on_surface_casing	EDWIN	4	
15	cement_returned_on_intermediate_casing	EDWIN	38	
16	cement_type_conductor_casing	EDWIN	24	
17	cement_total_amount_conductor_casing_sks	EDWIN	26	
18	cement_slurry_temperature_fahrenheit_conductor_casing	EDWIN	89	
19	cement_WOC_Hrs_conductor_casing	EDWIN	84	WOC stands for Wait for Cement. It is the time spent "to suspend drilling operations while allowing cement slurries to solidify, harden and

				develop compressive strength".[9]
20	cement_Wt_PPG_conductor_casing	EDWIN	86	Wt_PPG stands for weight in pounds per gallon.
21	cement_Yld_ft3/sk_conductor_casing	EDWIN	87	Yld_ft3/sk stands for yield in cubic feet per sack. It is "the volume occupied by one sack of dry cement after mixing with water and additives to form a slurry of a desired density".[10]
22	gas_block_documented_conductor_casing	EDWIN	0	
23	cement_type_surface_casing	EDWIN	25	
24	cement_total_amount_surface_casing_sks	EDWIN	25	
25	cement_slurry_temperature_fahrenheit_surface_casing	EDWIN	73	
26	cement_WOC_Hrs_surface_casing	EDWIN	68	
27	cement_Wt_PPG_surface_casing	EDWIN	68	
28	cement_Yld_ft3/sk_surface_casing	EDWIN	68	
29	gas_block_documented_surface_casing	EDWIN	0	

30	cement_type_intermediate_casing	EDWIN	6	
31	cement_total_amount_intermediate_casing_sks	EDWIN	6	
32	cement_slurry_temperature_fahrenheit_intermediate_casing	EDWIN	73	
33	cement_WOC_Hrs_intermediate_casing	EDWIN	68	
34	cement_Wt_PPG_intermediate_casing	EDWIN	68	
35	cement_Yld_ft3/sk_intermediate_casing	EDWIN	68	
36	gas_block_documented_intermediate_casing	EDWIN	0	
37	cement_lead_type_production_casing	EDWIN	11	Lead cement is the upper section of cement.
38	cement_tail_type_production_casing	EDWIN	52	Tail cement is the lower section of cement.
39	cement_lead_slurry_temperature_fahrenheit_production_casing	EDWIN	73	
40	cement_tail_slurry_temperature_fahrenheit_production_casing	EDWIN	82	
41	cement_lead_total_amount_production_casing_sks	EDWIN	14	
42	cement_tail_total_amount_production_casing_sks	EDWIN	53	
43	gas_block_documented_lead_production_casing	EDWIN	0	
44	gas_block_documented_tail_production_casing	EDWIN	0	
45	cement_lead_WOC_Hrs_production_casing	EDWIN	73	
46	cement_lead_Wt_PPG_production_casing	EDWIN	69	
47	cement_lead_Yld_ft3/sk_production_casing	EDWIN	69	
48	cement_tail_WOC_Hrs_production_casing	EDWIN	82	
49	cement_tail_Wt_PPG_production_casing	EDWIN	73	

50	cement_tail_Yld_ft3/sk_production_casing	EDWIN	73	
51	well_operator_encoded	EDWIN	1	
52	thread_weld_rank_1_casing	EDWIN	44	
53	grade_casing_tubing_type_rank_1_casing	EDWIN	69	
54	country_of_origin_rank_1_casing	EDWIN	75	
55	Recycled_rank_1_casing	EDWIN	80	
56	hole_size_inch_rank_1_casing	EDWIN	25	
57	pipe_size_inch_rank_1_casing	EDWIN	6	
58	weight_lbs/ft_rank_1_casing	EDWIN	41	
59	amount_in_well_ft_rank_1_casing	EDWIN	6	
60	days_passed_since_date_run_rank_1_casing	EDWIN	8	
61	thread_weld_rank_2_casing	EDWIN	28	
62	grade_casing_tubing_type_rank_2_casing	EDWIN	36	
63	country_of_origin_rank_2_casing	EDWIN	75	
64	Recycled_rank_2_casing	EDWIN	75	
65	hole_size_inch_rank_2_casing	EDWIN	25	
66	pipe_size_inch_rank_2_casing	EDWIN	25	
67	weight_lbs/ft_rank_2_casing	EDWIN	26	
68	amount_in_well_ft_rank_2_casing	EDWIN	25	
69	days_passed_since_date_run_rank_2_casing	EDWIN	25	
70	thread_weld_rank_3_casing	EDWIN	7	
71	grade_casing_tubing_type_rank_3_casing	EDWIN	35	
72	country_of_origin_rank_3_casing	EDWIN	75	
73	Recycled_rank_3_casing	EDWIN	75	
74	hole_size_inch_rank_3_casing	EDWIN	3	
75	pipe_size_inch_rank_3_casing	EDWIN	3	
76	weight_lbs/ft_rank_3_casing	EDWIN	4	

77	amount_in_well_ft_rank_3_casing	EDWIN	4	
78	days_passed_since_date_run_rank_3_casing	EDWIN	4	
79	thread_weld_rank_4_casing	EDWIN	9	
80	grade_casing_tubing_type_rank_4_casing	EDWIN	35	
81	country_of_origin_rank_4_casing	EDWIN	75	
82	Recycled_rank_4_casing	EDWIN	75	
83	hole_size_inch_rank_4_casing	EDWIN	6	
84	pipe_size_inch_rank_4_casing	EDWIN	5	
85	weight_lbs/ft_rank_4_casing	EDWIN	6	
86	amount_in_well_ft_rank_4_casing	EDWIN	6	
87	days_passed_since_date_run_rank_4_casing	EDWIN	6	
88	latitude	Lackey et al.[11]	0	
89	longitude	Lackey et al.	0	
90	well_status	Lackey et al.	0	
91	scp_and_or_cvf	Lackey et al.	0	This is the target variable to be predicted.
92	distance_to_nearest_well_km	Calculated	0	
93	count_well_within_0.005km	Calculated	0	
94	count_well_between_0.005_and_0.01km	Calculated	0	
95	count_well_between_0.01_and_0.1km	Calculated	0	
96	count_well_between_0.1_and_1km	Calculated	0	
97	count_well_between_1_and_2km	Calculated	0	
98	count_well_between_2_and_5km	Calculated	0	

99	count_well_between_5_and_10km	Calculated	0	
100	distance_to_nearest_faulty_well_km	Calculated	0	
101	count_faulty_well_within_0.005km	Calculated	0	
102	count_faulty_well_between_0.005_and_0.01km	Calculated	0	
103	count_faulty_well_between_0.01_and_0.1km	Calculated	0	
104	count_faulty_well_between_0.1_and_1km	Calculated	0	
105	count_faulty_well_between_1_and_2km	Calculated	0	
106	count_faulty_well_between_2_and_5km	Calculated	0	
107	count_faulty_well_between_5_and_10km	Calculated	0	
108	distance_to_nearest_nonFaulty_well_km	Calculated	0	
109	count_nonFaulty_well_within_0.005km	Calculated	0	
110	count_nonFaulty_well_between_0.005_and_0.01km	Calculated	0	
111	count_nonFaulty_well_between_0.01_and_0.1km	Calculated	0	
112	count_nonFaulty_well_between_0.1_and_1km	Calculated	0	
113	count_nonFaulty_well_between_1_and_2km	Calculated	0	
114	count_nonFaulty_well_between_2_and_5km	Calculated	0	
115	count_nonFaulty_well_between_5_and_10km	Calculated	0	

Supplementary figures

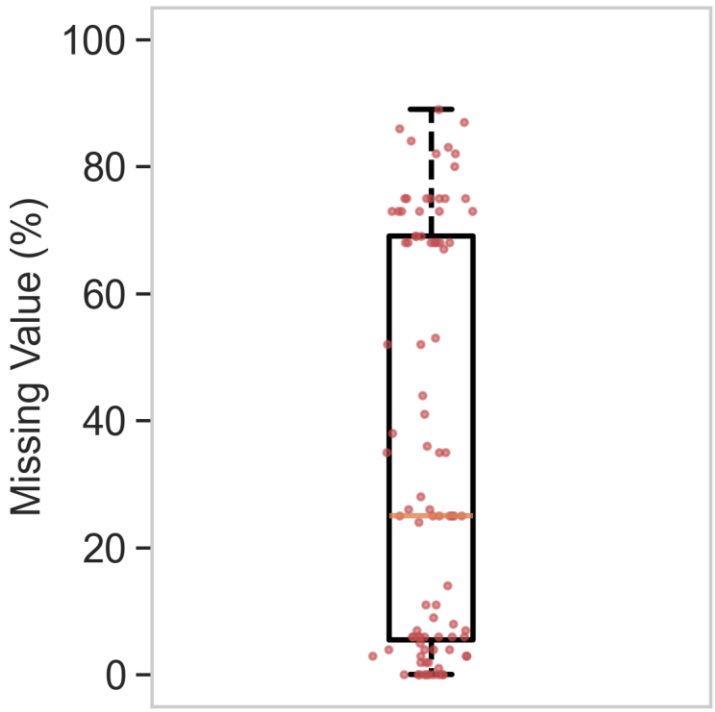

Figure S1. Distribution of the percentage of missing values among features. Calculated geospatial features are excluded. The rectangular box represents the statistical distribution, where the orange horizontal bar gives the median (25%), and the upper and lower edges of the box represent the upper and lower quartiles (69% and 5.5%, respectively). The whiskers indicate variability outside the quartiles. The percentage of missing values for each feature was represented by a red circle.

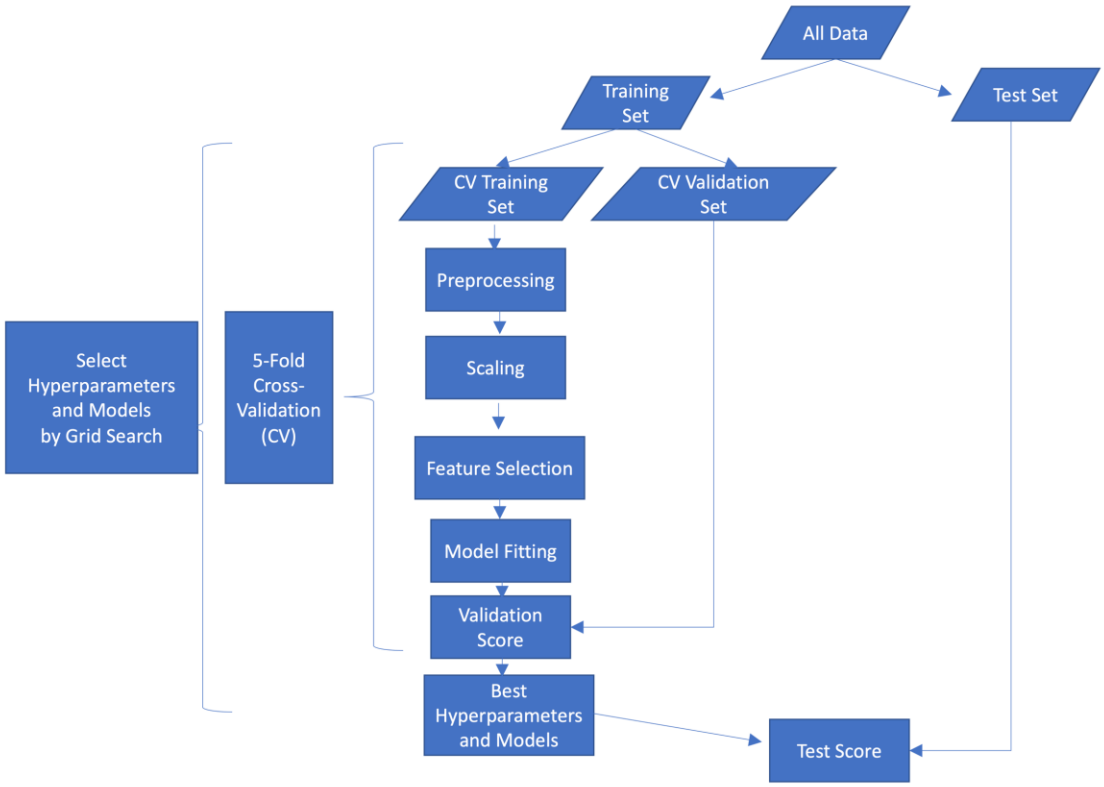

Figure S2. workflow of training and testing machine learning models

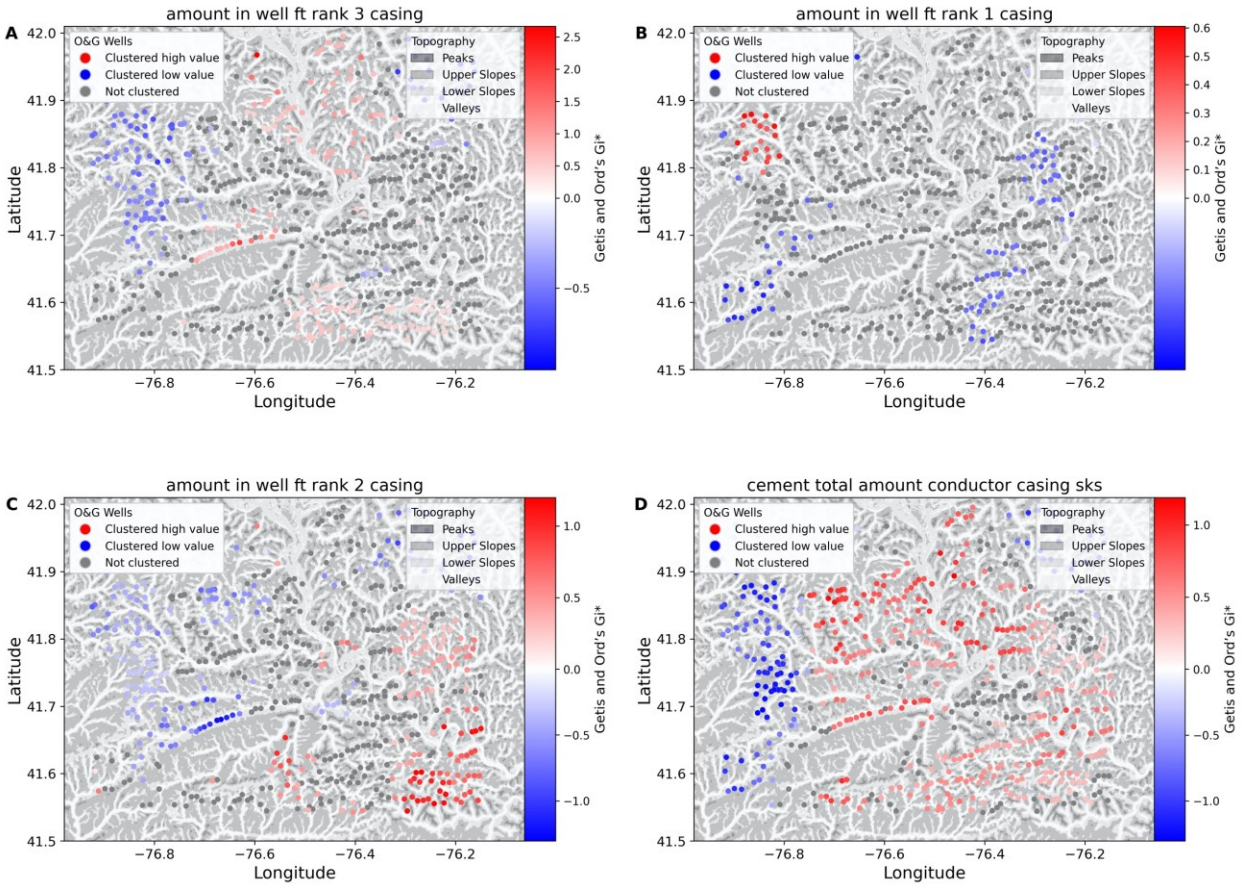

Figure S3. Clusters of high and low values of four important continuous features: (A) amount of Rank 3 casing, (B) amount of Rank 1 casing, (C) amount of Rank 2 casing, and (D) total amount of cement outside conductor casing. The standardized Getis and Ord's Gi* statistics of the features are represented by the color scale: a warmer color indicates clustering of high feature values, while a colder color indicates clustering of low feature values, and wells without statistically significant clustering are colored in grey. Local topography is also represented by color scale, with deeper color indicating higher topographical positions.

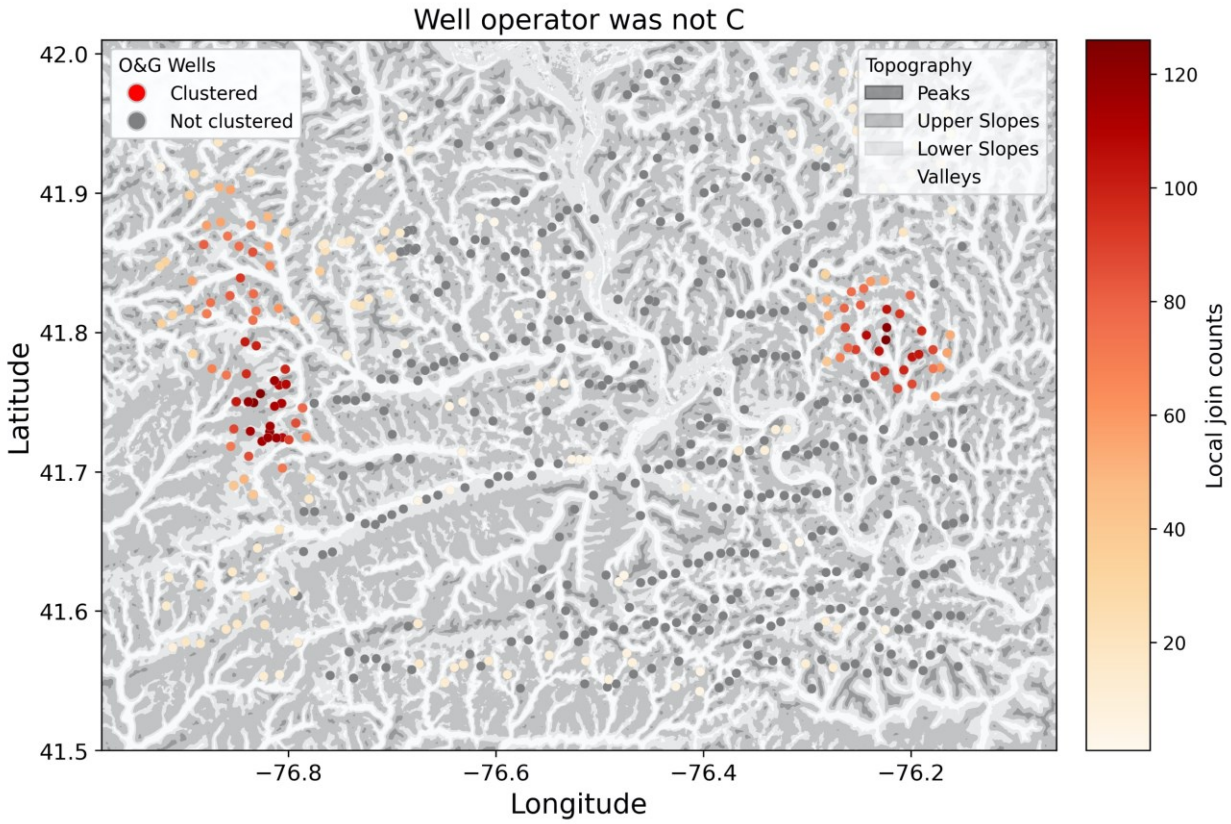

Figure S4. Clustering of wells whose operators were not C. Statistically significant clusters of wells whose operator were not C were shown by warmly-colored circles. Warmer color indicated higher degree of clustering. Other wells (i.e., wells that belonged to operator C, and wells that didn't belong to operator C but were not in statistically significant clusters) are shown by grey-colored circles. To calculate the Local Join Counts, the spatial weights were constructed using a distance band equaling the maximum nearest neighbor distance among the wells. Local topography is also represented by color scale, with deeper color indicating higher topographical positions.

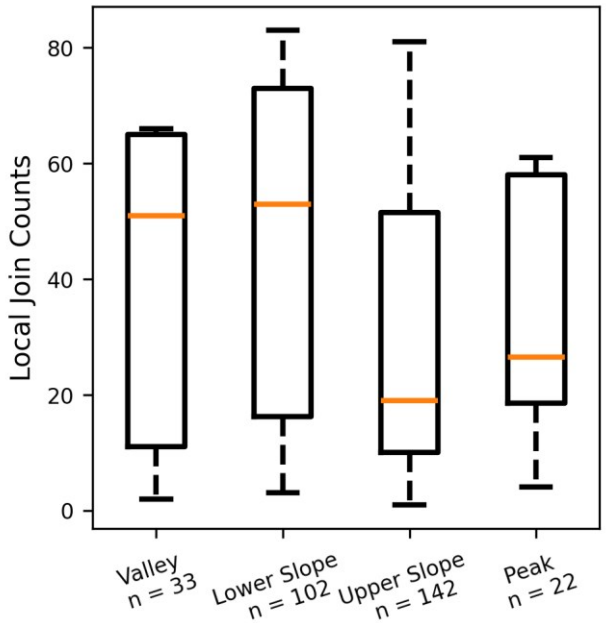

Figure S5. The clustering of faulty wells (represented by Local Join Counts) were more substantial in topographical low-lands. Only wells with statistically significant Local Join Counts were included in the comparison. The orange horizontal bar of each box gives the median, and the upper and lower edges of the box represent the upper and lower quartiles (e.g., 75th and 25th percentile, respectively). The whiskers indicate variability outside the quartiles. The statistically significant difference in the mean Local Join Counts among topographical groups was indicated by Welch's ANOVA test (p-value = 6×10^{-5}) and Games-Howell post-hoc test (pairwise adjusted p-values were significant between Valley and Upper Slope (4×10^{-2}) and between Lower Slope and Upper Slope (1×10^{-5})).

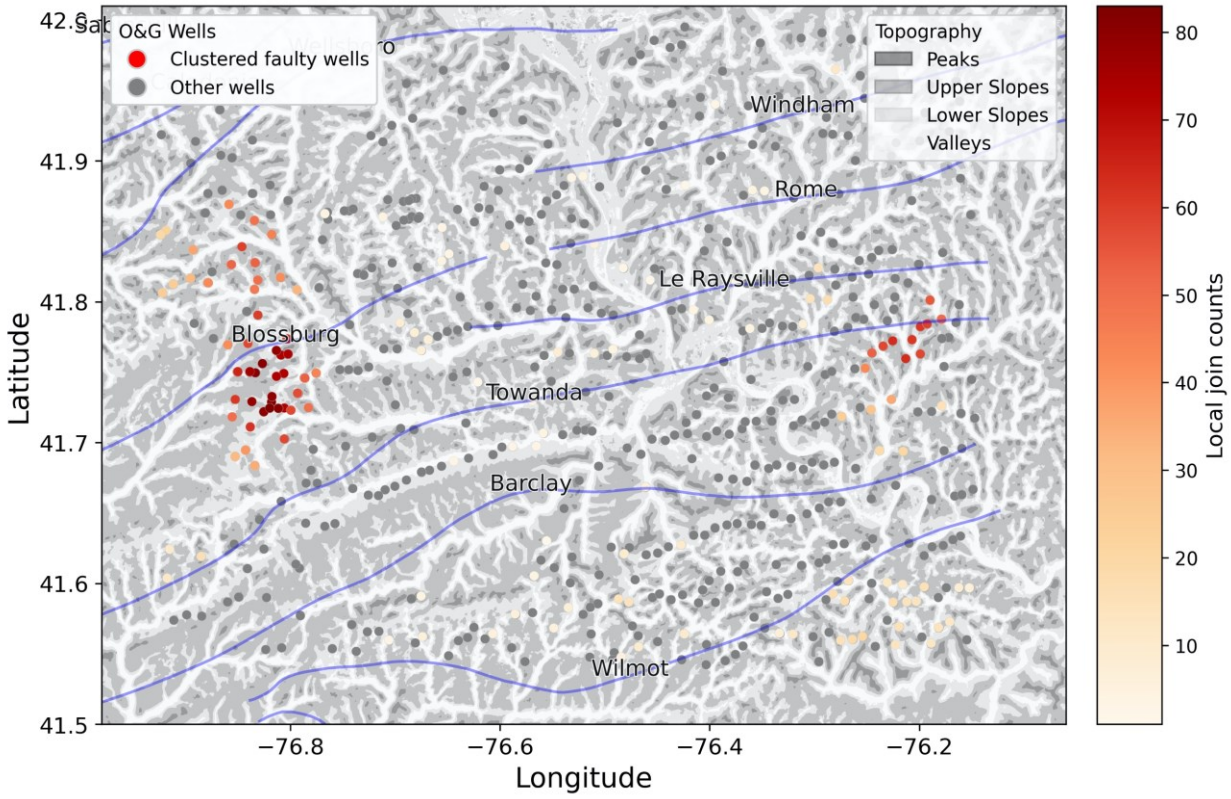

Figure S6. The locations of clustered faulty wells and geological folds in the study region. Faulty wells that were clustered with statistical significance were shown by warmly-colored circles. The color scale indicated degree of clustering. Other wells (i.e., nonfaulty wells, and faulty wells that were not in statistically significant clusters) are shown by grey-colored circles. To calculate the Local Join Counts, the spatial weights were constructed using a distance band equaling the maximum nearest neighbor distance among the wells. The geological folds are shown in blue lines.[7] Local topography is also represented by color scale, with deeper color indicating higher topographical positions.

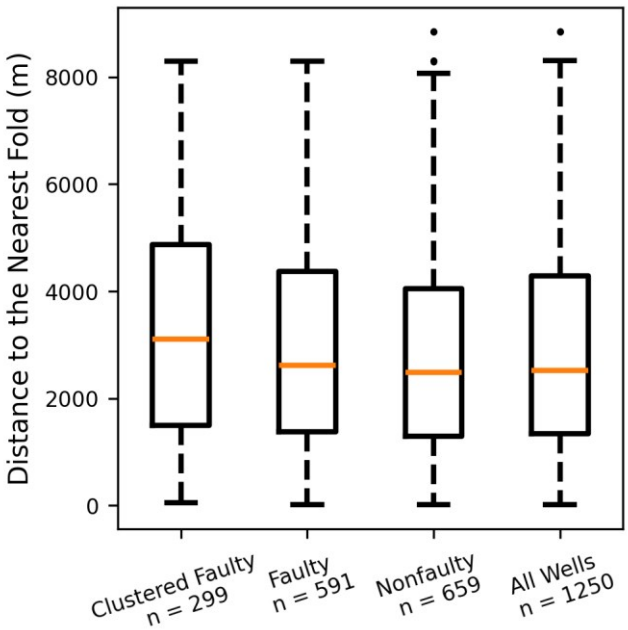

Figure S7. Clustered faulty wells (with statistically significant Local Join Counts) had slightly larger distances to the nearest geological fold compared to faulty wells, nonfaulty wells, and all wells. The orange horizontal bar of each box gives the median, and the upper and lower edges of the box represent the upper and lower quartiles (e.g., 75th and 25th percentile, respectively). The whiskers indicate variability outside the quartiles and individual datum (black dots) are only visible in the extrema outside these ranges. The statistically significant difference in the mean distance to fold among well groups was indicated by Welch's ANOVA test (p-value = 1×10^{-2}) and Games-Howell post-hoc test (pairwise adjusted p-values were significant between clustered faulty wells and all wells (4×10^{-2}) and between clustered faulty wells and Nonfaulty wells (1×10^{-2})).

References

(1) Byrom, T. G. Chapter 3: Casing Depth and Size Determination. In *Casing and Liners for Drilling and Completion*; 2007; pp 77–102. https://doi.org/10.1016/b978-1-933762-06-7.50008-0.

(2) Wu, J. Chapter 2: Casing String and Design. In *Applied Well Cementing Engineering*; Liu,

G., Ed.; Gulf Professional Publishing, 2021; pp 17–67.
(3) Schlumberger Limited. Energy Glossary - Sack https://glossary.slb.com/en/terms/s/sack#:~:text=A unit of measure for,a sack weighs 94 pounds. (accessed Oct 5, 2023).
(4) Zimmerman Industries Inc. Cement Silos https://www.zimmermanindustries.com/cement-silos (accessed Oct 5, 2023).
(5) Wikipedia. Barrel (unit) https://en.wikipedia.org/wiki/Barrel_(unit) (accessed Oct 5, 2023).
(6) Theobald, D. M.; Harrison-Atlas, D.; Monahan, W. B.; Albano, C. M. Ecologically-Relevant Maps of Landforms and Physiographic Diversity for Climate Adaptation Planning. *PLoS One* **2015**, *10* (12), e0143619. https://doi.org/10.1371/journal.pone.0143619.
(7) Pennsylvania Department of Conservation and Natural Resources Bureau of Geological Survey. Pennsylvania Folds https://newdata-dcnr.opendata.arcgis.com/datasets/DCNR::pennsylvania-folds/about (accessed Oct 2, 2023).
(8) Pennsylvania Department of Conservation and Natural Resources Bureau of Geological Survey. Exploration and Development Well Information Network https://edwin.dcnr.pa.gov/ (accessed May 1, 2023).
(9) Schlumberger Limited. Energy Glossary - Wait on cement https://glossary.slb.com/en/terms/w/wait_on_cement (accessed May 1, 2023).
(10) Schlumberger Limited. Energy Glossary - Yield https://glossary.slb.com/en/terms/y/yield (accessed May 1, 2023).
(11) Lackey, G.; Rajaram, H.; Bolander, J.; Sherwood, O. A.; Ryan, J. N.; Shih, C. Y.; Bromhal, G. S.; Dilmore, R. M. Public Data from Three US States Provide New Insights into Well Integrity. *Proc. Natl. Acad. Sci. U. S. A.* **2021**, *118* (14). https://doi.org/10.1073/PNAS.2013894118.

Chapter 5. Methane sensor signal deconvolution - apparatus and preliminary results

By

Yunpo Li

ABSTRACT

Continuous monitoring is a powerful strategy to address the intermittency issue of oil and gas methane emissions. Prototype chemiresistive methane sensors with compact size, low cost, and low energy consumption had been developed for large-scale continuous monitoring. However, such sensors suffer from the interference signals of other gas species such as water vapor. In this chapter, a machine learning (ML) framework is proposed to achieve signal deconvolution for the prototype sensors. An apparatus consisting of mass flow controllers, a gas chamber, and a data logging system was built to collect data for ML model training and testing. In addition, preliminary tests were conducted to study the influences of humidity and gas flow rate on the performance of the sensors. Lastly, ongoing equipment upgrades integrate additional commercial sensors and temperature control systems into the apparatus.

Introduction

To mitigate methane emissions from Oil and Gas (O&G) infrastructures, efficient leakage monitoring tools are desired. Remote sensing instruments (e.g., those mounted on satellites and airplanes) offer a solution to monitor methane leakage in large geographical regions. However, due to the discontinuous nature of remote sensing monitoring, intermittent methane emissions were still not well accounted for and led to an underestimation of the total emission rate. Therefore, continuous monitoring tools are important to fill this gap. Optical sensors are widely used for continuous methane leakage monitoring. Examples of these sensors are infrared cameras, open-path laser detectors, and cavity ring-down spectrometers. However, these sensors

are typically expensive and have intense energy consumption. There are about one million producing O&G wells in the US,[1] and about 14% of them have integrity issues that could lead to methane emissions (based on data from Pennsylvania, Colorado, and New Mexico).[2] Even if only wells with integrity issues are to be continuously monitored (and if these wells can be identified with 100% accuracy), about 140 thousand continuous sensors are still needed assuming each well is monitored by one sensor. Therefore, the expensive optical sensors are not suitable for such a large-scale deployment. Instead, sensors with low cost, low energy consumption, and compact size are better candidates for this task. Recently, Bezdek et al.[3] reported a novel chemiresistive methane sensor based on catalytic methane oxidation. This prototype sensor is printed on a glass substrate 2.5 cm long and 1.5 cm wide, costs less than $10, and can operate using 0.1 mW of energy. Its small size will enable its placement in narrow or confined spaces that cannot be reached by other sensors, and its low cost and low energy consumption will facilitate massive production and deployment. However, this prototype sensor responds not only to methane but also to other interfering species such that it is difficult to separate methane's signal from those of other species. Given such, a signal deconvolution program is needed for this prototype sensor before it can be utilized for real-world methane emission monitoring.

In this chapter, a machine learning (ML) framework is proposed for signal deconvolution of the prototype chemiresistive sensors. A gas chamber was built to collect signals from a sensor array, and the gas concentrations inside the chamber were controlled by mass flow controllers (MFCs). The sensor signals served as predictive features, while the gas concentrations were target variables for ML training and testing. Since the work is still ongoing, this chapter focuses on

introducing the apparatus for collecting ML data as well as the preliminary results characterizing the prototype sensors. Specifically, the influences of relative humidity (RH) and total flow rate on the sensors' ability to detect methane are discussed. Moreover, the ongoing efforts to integrate commercially available MQ-series sensors into the sensor array, and to add temperature control capacity to the apparatus are described. Finally, the future steps of the project and the research implications are briefly discussed.

Material and method

Concept of machine learning for signal deconvolution

The goal of signal deconvolution is to obtain the concentration (i.e., gas phase mixing ratio) of each gas component in the gas mixture (e.g., ambient air polluted by natural gas leakage). The ML models take the signal from each sensor as predictive features, and predict the true gas concentration of each component as target variables. Specifically, if an array of n sensors is used to measure a gas mixture containing m components, the predictive features will be x_1, x_2, …, x_n with x_i being the signal of the ith sensor, and the target variables will be y_1, y_2, …, y_m with y_j being the true concentration of gas component j. In a simplified scenario, we can assume that the underlying relationships between the predictive features and the target variables are linear, and we can use linear regressions to predict the y variables (Eqn. 1). The coefficient k_{ji} represents the contribution of sensor signal x_i on the predicted value of y_j. The coefficients are fitted using a training dataset consisting of data points (x_1, x_2, …, x_n, y_1, y_2, …, y_m). Each data point corresponds to one experiment, where the true gas concentrations y_1 through y_m are manually set

by controlling gas mixing ratios, and the sensor signals x_1 through x_n are recorded. The experiment is repeated for different gas concentrations. Eventually, the trained ML model is evaluated in a held-out test dataset obtained using the same approach. The underlying relationship between the predictive features and the target variables can be nonlinear. In those cases, more complex nonlinear models such as neural networks (Fig. 1) can replace the linear regression model.

Equations 1, using sensor readings to predict true concentrations of gases

$$y_1 = k_{11} \cdot x_1 + k_{12} \cdot x_2 + k_{13} \cdot x_3 + \cdots + k_{1n} \cdot x_n$$

$$y_2 = k_{21} \cdot x_1 + k_{22} \cdot x_2 + k_{23} \cdot x_3 + \cdots + k_{2n} \cdot x_n$$

$$y_3 = k_{31} \cdot x_1 + k_{32} \cdot x_2 + k_{33} \cdot x_3 + \cdots + k_{3n} \cdot x_n$$

$\cdots$

$$y_m = k_{m1} \cdot x_1 + k_{m2} \cdot x_2 + k_{m3} \cdot x_3 + \cdots + k_{mn} \cdot x_n$$

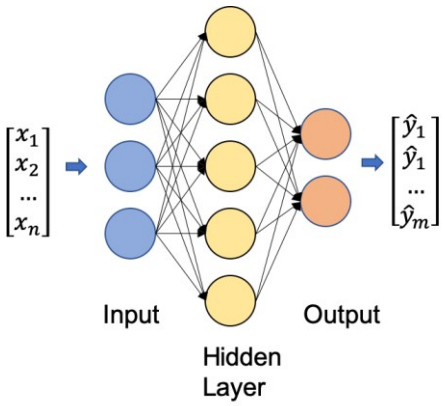

Figure 1. Concept of using advanced machine learning algorithms (e.g., Neural Network) to predict gas concentrations. The input layer, hidden layer, and output layer of the neural network are represented by blue, yellow, and orange circles, respectively.

Sensing material

The method to fabricate the prototype chemiresistive sensors was reported by Bezdek et al.[3] Briefly, single-walled carbon nanotubes (SWCNTs) were combined with poly(4-vinylpyridine) and subsequently with a platinum-polyoxometalate (Pt-POM) catalyst. Such material was deposited between gold electrodes printed on a glass substrate. The Pt-POM catalyzed the oxidation of CH_4 to CH_3OH, HCHO, or CH_3CHO, and this redox process changed the carrier density inside the SWCNT network thus modifying its resistance. The change of resistance then created an electrical signal measured by a potential stat connected to the sensor. Bezdek et al. reported that exposing the sensor to 0.5% methane at room temperature and 10 ± 5% RH could reduce its resistance by about 0.8%.[3] A fabricated sensor device consisted of four sensing channels, which were four individual chemiresistive sensors sharing a common counter-electrode on the same piece of glass substrate. The four sensing channels could undergo different surface treatments so that they would produce distinguishable signals to be utilized by ML prediction (i.e., x_1, x_2, x_3, and x_4 as in Eqn. 1). The size of the device was about 2.5 cm long and 1.5 cm wide, and its material cost was below $10. The sensors could operate at a fixed potential of 0.1 V, thus the power consumption of one device (four channels; the resistance of each greater than 500 Ω) would be smaller than 0.1 mW. The compact size, low cost, and small energy consumption of this prototype device make it suitable for massive deployment to monitor a large number of Oil and Gas (O&G) facilities.

Experimental set-up

The apparatus to collect ML data for signal deconvolution is shown in Fig. 2. On the right-hand side of the apparatus, a Mass Flow Controller Array for Nanostructure Growth Optimization (MANGO) was used to control the flow rate of each gas component. The output gas flow of the first MFC on the right side of MANGO went through a gas bubbler to pick up water vapor and then converged with the output flow of other MFCs to enter a gas chamber in the middle of the set-up. Two prototype chemiresistive sensor devices were installed in a holder platform inside the gas chamber to produce signals responding to the gas concentrations in the chamber. Jumper wires were used to transmit the signals to a potential stat and then to a laptop computer. The effluent gas of the gas chamber was collected by a snorkel. In addition, a hygrometer was used to measure the RH inside the gas chamber. Finally, the prototype sensor devices were stored in a desiccator while not in operation.

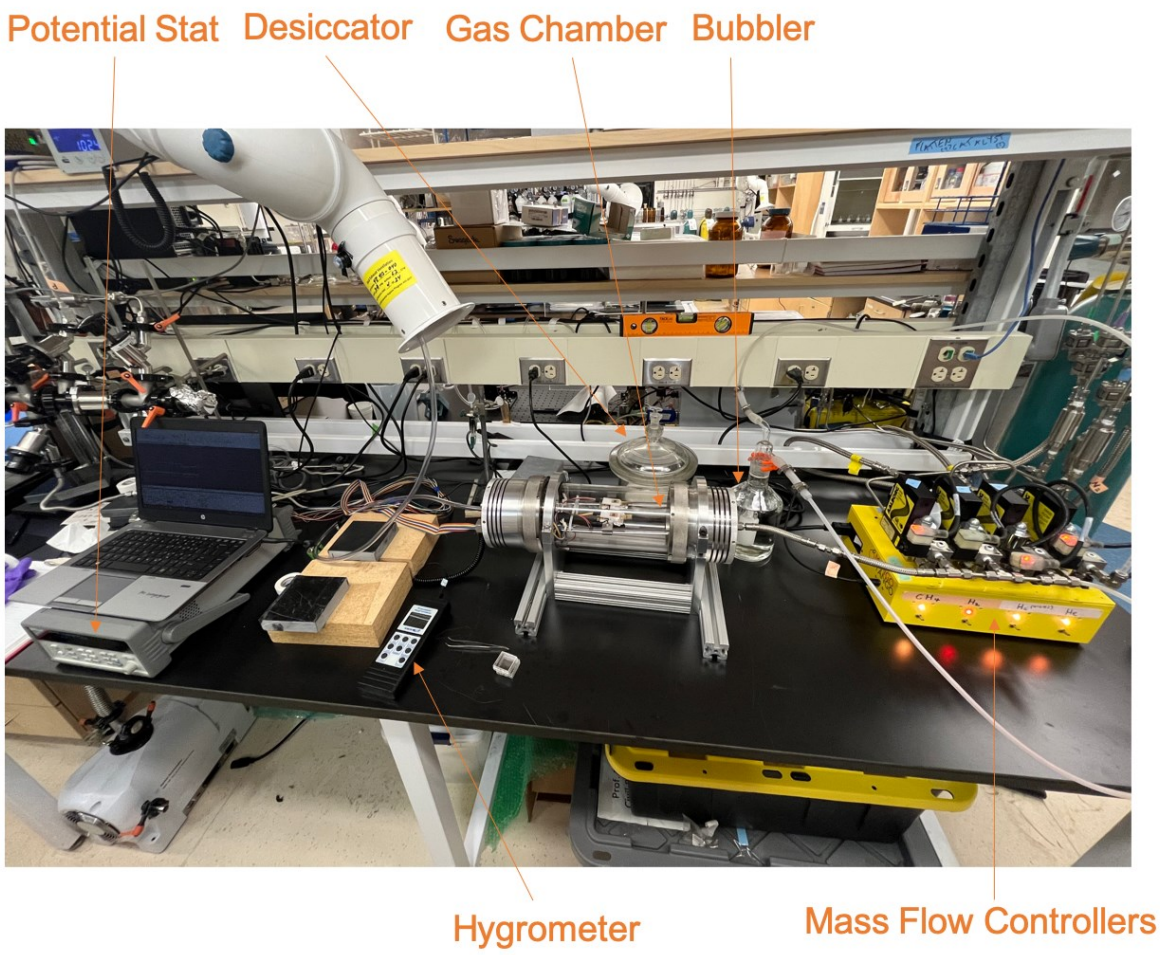

Figure 2. Experimental set-up to collect data for ML signal deconvolution

The MANGO system was designed to control multiple MFCs either manually or automatically through programming. I used four MFCs (Aalborg) with the MANGO system: the first and second one for supplying air, the third one for increasing air flow rate precision, and the fourth one for supplying methane. The first and second MFC both had a maximum flow of 5,000 standard cubic centimeters (sccm) for air. However, the precision of each MFC was 1% of its maximum flow rate, thus they could not change flow rates by any increments smaller than 50 sccm. To improve the precision of the air flow rate, the third MFC had a 69 sccm maximum flow

rate for air (it was originally calibrated for 100 sccm helium; I converted its flow rate using the K-factor ratio between air and helium). For example, a total air flow rate of 1,010 sccm was created by setting the second MFC at 1,000 sccm and the third MFC at 10 sccm. In addition, the fourth MFC had a maximum flow rate of 337 sccm for 10% methane in nitrogen (the MFC was originally calibrated for 500 sccm helium). Lastly, a Totalizer-Input/Output Flow Monitor/Controller (TIO; Aalborg) was paired with each MFC as an additional valve to turn on / off the MFC output gas flow.

The output air flow of the first MFC entered a gas bubbler filled with MilliQ water. The bubbler used a quartz air stone which dispersed the air flow into small bubbles to make them saturated with water vapor. This saturated wet air flow was then converted with the output of the second MFC (dry air). By controlling the flow rate ratio between the first and second MFC, a desired RH level could be set. For example, 2,000 sccm of saturated wet air and 2,000 sccm of dry air could be combined to 4,000 sccm of air with an expected 50% RH. The actual RH of the gas flow was measured by a hygrometer (Traceable) installed inside the gas chamber and used for ML training.

A computer software, Ansari (v2.7.9, Aerogel Technologies, LLC), was used to control the MANGO system. The software could be run in either manual mode or automation mode. In the manual mode, the TIOs were first switched on, and then the desired flow rates were manually set for the MFCs. After the experiment was completed, the flow rates were set back to zero and the TIOs were switched off. In automation mode, a script written in .txt format specified the steps to run the experiment. For example, it could automatically turn on methane gas and set its flow rate

to 100 sccm 30 minutes after the program started, and turn it off after another 10 min. In addition, the steps could be repeated for a desired number of times using a for-loop in the script. Lastly, Ansari generated log files (in .txt format) after the script finished running. One log file documented the timestamps of each action taken (e.g., turning a certain MFC on or off), and another documented the time-series flow rate data of each MFC during the experiment.

Combined gas flow from the MANGO system then entered a gas chamber where the chemiresistive sensors were installed (Fig. 3 and Fig. 4). The chamber consisted of a transparent quartz tube (35.6 cm long, 12 cm inner diameter; Technical Glass Products, Inc.), two aluminum end caps (DPM Solutions Inc.), and a platform for holding the sensors (MIT Machine Shop) mounted on two quartz rods (McMaster-Carr). The inlet gas tubing was connected to the front end cap by an ¼ inch NPT fitting. On the rear end cap, the outlet gas exited the chamber through another ¼ inch NPT fitting, and electrical wires went through either ¼ inch or ½ inch NPT fittings. In a typical experiment, two prototype chemiresistive sensor devices were installed in the chamber (Fig. 4). Each device had five electrodes (four sensing channels and one shared counter electrode) connected to the potential stat via five jumper wires. These jumper wires went through one of the ½" NPT fittings on the rear end cap, and the wire of the hygrometer went through the other ½" fitting. The two ¼" NPT fittings on the rear end cap were reserved for future applications. The gap between the end cap and the quartz tube was sealed by an O-ring (Dash 352 Viton O-ring, McMaster-Carr). The internal volume of the chamber was 4,026 cm^3, and the desired total gas flow rate was set to 4,000 sccm, which resulted in a gas retention time of about one minute. Lastly, the gas chamber was leveraged to about 10 cm above the bench surface by a customized aluminum racket made by the MIT Machine Shop.

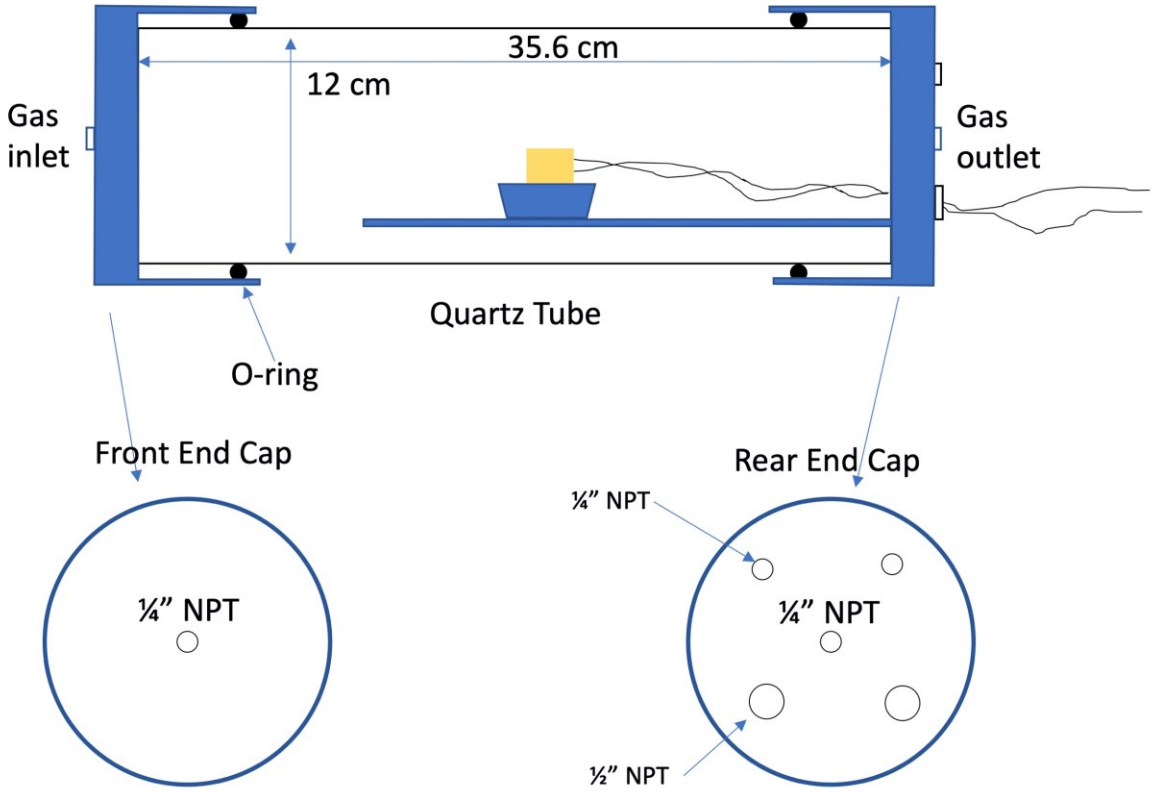

Figure 3. Schematic of the test chamber design

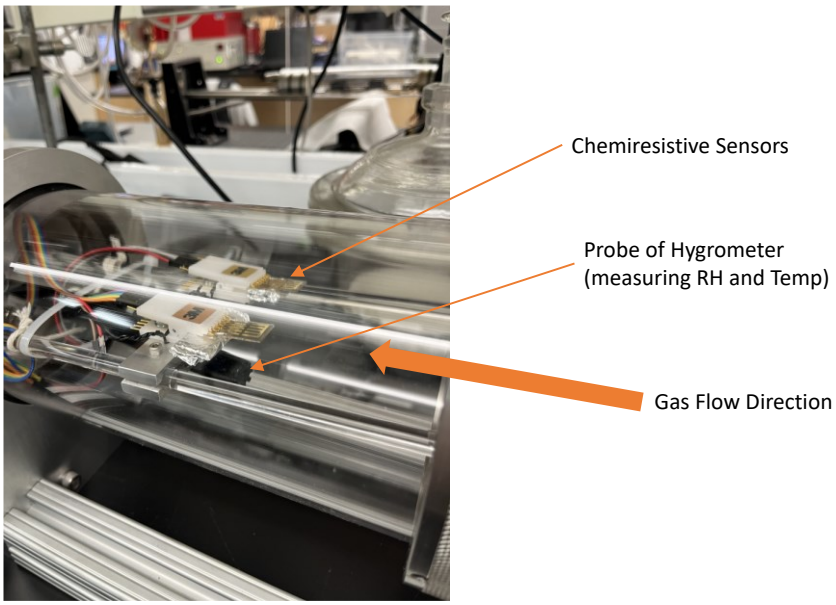

Figure 4. Chemiresistive sensors installed inside the gas chamber

A potential stat (34970a, Agilent Technologies, Inc) was used to continuously measure the resistance of chemiresistive sensors. Upon interacting with methane gas in the gas chamber, the sensors' resistance would change thus forming measurable signals. The sampling frequency of the potential stat was 1 Hz. The signals were recorded by the BenchLink Data Logger 3 (v 4.3) software (Agilent Technologies, Inc), and exported to .csv format. A Python script was used to calculate the percentage change of resistance and visualize the data.

Preliminary sensor test results

Before constructing the ML dataset for sensor signal deconvolution, some preliminary tests were conducted to understand the sensors' tolerance to RH and total flow rate (i.e., the ranges of RH

and flow rate where methane signal could be observed). These ranges would also determine the boundaries of the parameter space of the ML dataset. First, the responses to 0.5% methane (the highest methane concentration tested by Bezdek et al.[3]) were tested at different RH levels for three types of sensors: default chemiresistive sensor reported by Bezdek et al.,[3] chemiresistive sensor coated with Pentypcene dialkoxy (Pentyp),[4] and chemiresistive sensor coated with Spirobifluorene-triptycene (SBF).[5] Pentyp and SBF polymers had good hydrophobicity such that they could potentially discourage water vapor penetration into the SWCNT-Pt-POM sensing material thus improving its RH tolerance. Duplicates of each sensor were tested simultaneously. At 2.5% RH, the resistance of three types of sensors had a sudden decrease immediately after 0.5% methane gas was turned on, and continued to decrease until methane gas was turned off after 10 min (Fig. 5). After the methane gas was turned off, the resistance of the sensors increased but eventually reached a plateau lower than the initial resistance. During the methane exposure experiment, the normalized resistance of the default sensors had the largest decrease (2.2%), followed by the SBF-coated sensor (1.2%) and the Pentyp-coated sensor (1%). These results indicated that (i) all three sensors were responsive to methane with a decrease in resistance, (ii) the change in resistance was reversible when the methane gas was turned off, and (iii) the default sensors had a stronger response than the coated sensors.

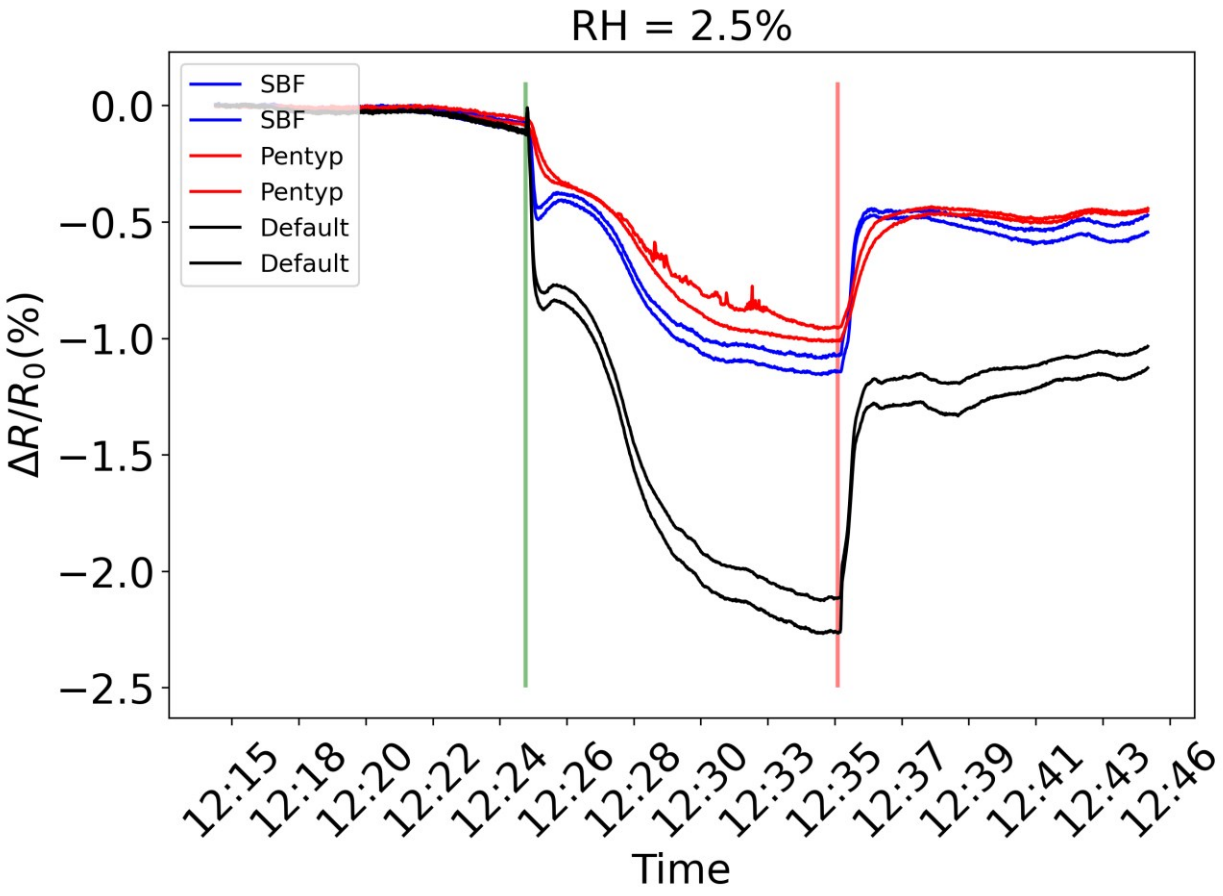

Figure 5. Change in sensors' resistances responsive to 0.5% methane at 2.5% RH. The timing of the onset and offset of methane gas are marked by the green and red vertical line, respectively. The responses of default sensors, sensors coated with Pentyp, and sensors coated with SBF are shown by black, red, and blue curves respectively (duplicate sensors were tested for each sensor type). The resistance baseline (R_0) was chosen at 10 min before the methane onset, and the resistance values were normalized using the baseline ($\Delta R/R_0$; $\Delta R = R - R_0$).

Furthermore, the same sensors were exposed to 0.5% methane at different RH levels (Fig. 6). When RH was lower than 10%, the responses were decreases of resistance among all sensors, and the default sensors had stronger responses than the sensors coated by SBF and Pentyp. Interestingly, when the RH exceeded 10%, the responses transformed into increases in

resistance, and the maximum increases were achieved between 30% and 40% RH. For example, at 37% RH (Fig. 7), the sensors' resistance suddenly increased after the methane gas was turned on, and decreased after it was turned off. The responses of all sensors became weaker after the RH exceeded 40%, and then diminished to zero after RH exceeded 50%. In conclusion, the optimal RH for sensor operation would be 30-40%, and the sensors were intolerant of RH above 50%. This could cause some limitations to the real-world application of these prototype sensors since the morning RH can easily exceed 50% in the US.[6] Therefore, new material designs or strategies should be developed to improve the sensors' tolerance to humidity, and full-scale ML training for signal deconvolution should come after that.

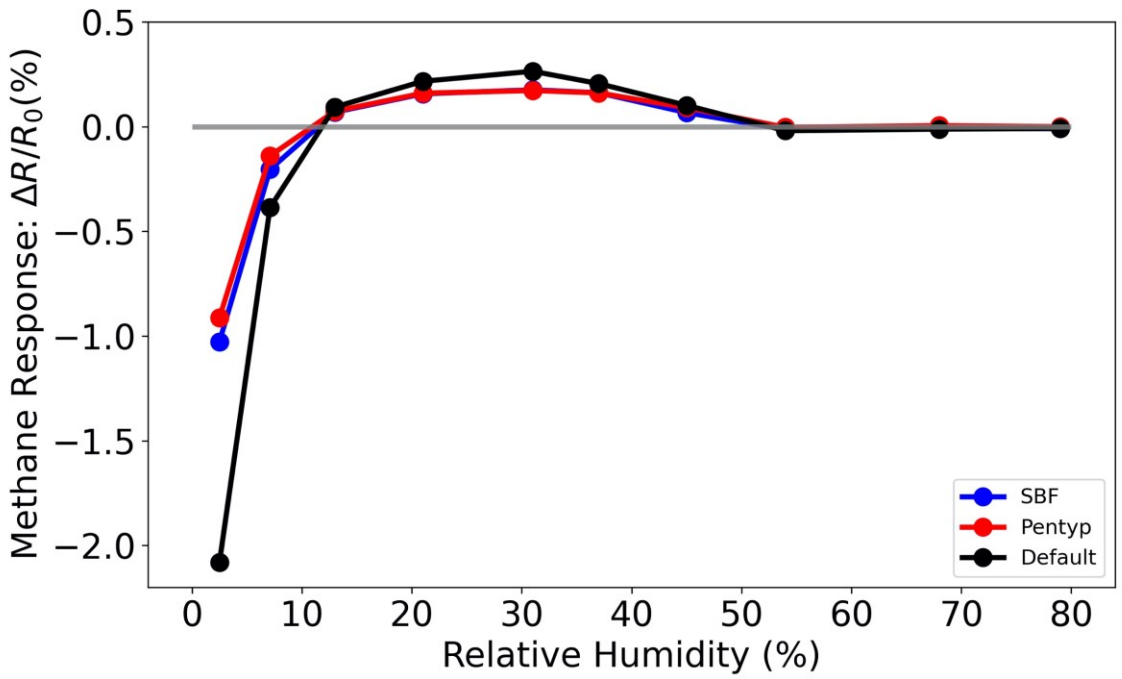

Figure 6. The influence of RH on chemiresistive sensors' responses to 0.5% methane. The baseline resistance (R_0) was the resistance right before methane onset for each methane exposure experiment. The biggest change in resistance between methane onset and offset (ΔR) was then

divided by the baseline resistance ($\Delta R/ R_0$) to characterize the sensor response (y-axis). The responses of default sensors, sensors coated with Pentyp, and sensors coated with SBF are shown by black, red, and blue curve respectively (mean responses of duplicate sensors of each type are shown).

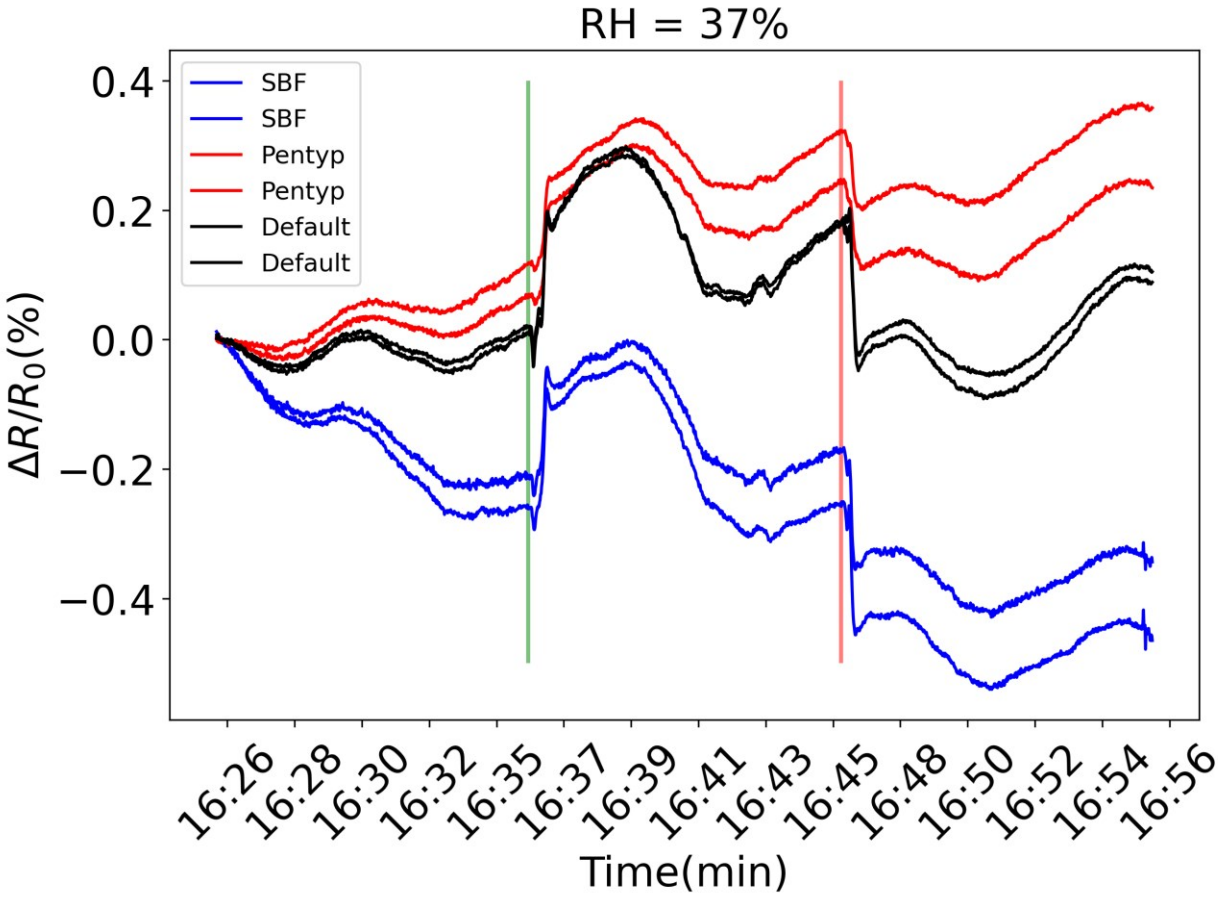

Figure 7. Sensor signals responsive to 0.5% methane at 37% RH. The timing of the onset and offset of methane gas are marked by the green and red vertical line, respectively. The responses of default sensors, sensors coated with Pentyp, and sensors coated with SBF are shown by black, red, and blue curve respectively (duplicate sensors were tested for each type).

In addition to RH, the chemiresistive sensors' sensitivity to methane could also be influenced by the total gas flow rate (Fig. 8). When the total gas flow rate (including air and methane) in the chamber was at 600 sccm, the resistance of all three sensor types decreased when exposed to 0.5% methane, with the SBF-coated sensor showing the biggest resistance change. When the flow rate was raised to 1,000 sccm, the responses were still decreases in resistance but the signal magnitudes were much lower. When the total flow rate was further raised to 2,000 sccm, all sensors stopped responding to methane. These unexpected results suggested that gas flow rate had an impact on the sensors' capability to detect methane. The faster the gas flow rate was, the shorter the gas retention time would be for the test chamber (e.g., a 4,000 sccm flow rate corresponds to a retention time of one minute, while a 600 sccm flow rate corresponds to a retention time of seven minutes). When experiments were run in sequence (e.g., exposure to gas mixture A followed by gas mixture B), a waiting period was needed for the previous composition (A) to be fully replaced by the next composition (B), and this period is determined by the gas retention time (e.g., waiting period equals three times of the retention time). Therefore, a faster total flow rate would translate to a shorter time required to finish the experiments. Future sensor design should improve the sensors' tolerance to higher gas flow rates to reduce the total amount of time required to construct the ML dataset.

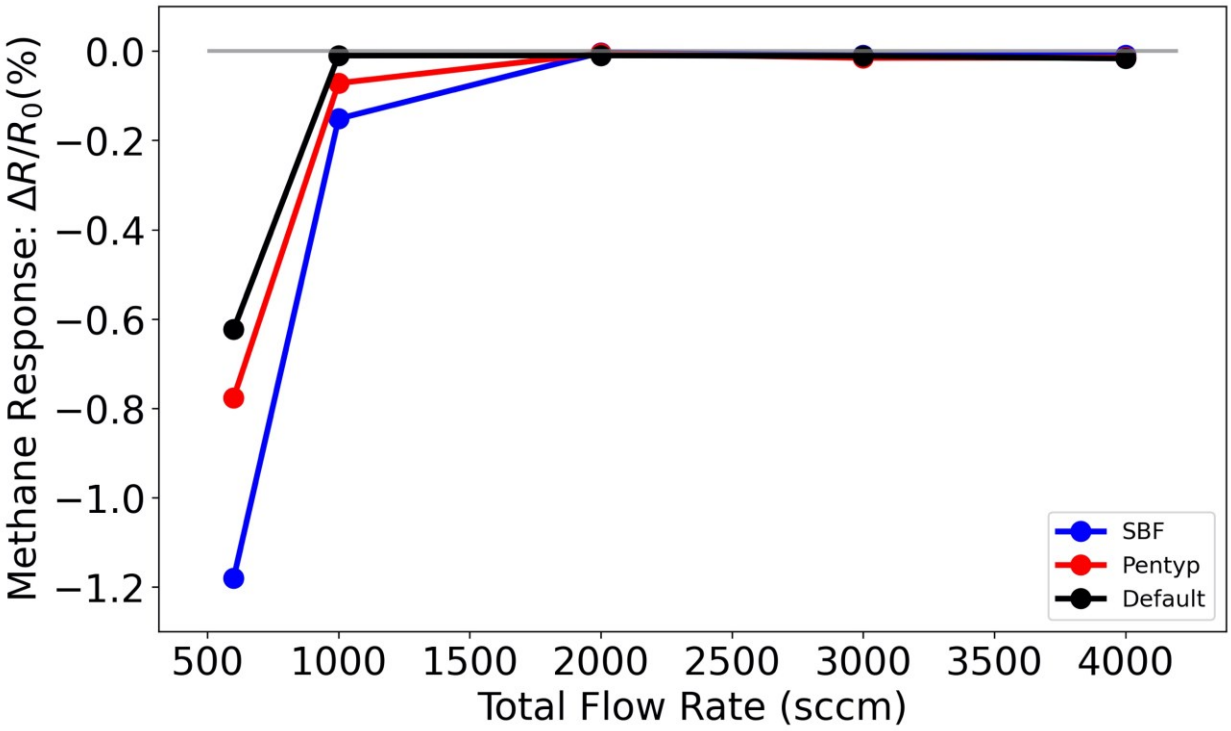

Figure 8. The influence of total flow rate in the gas chamber on chemiresistive sensors' responses to 0.5% methane at <0.5% RH. The responses of default sensors, sensors coated with Pentyp, and sensors coated with SBF are shown by black, red, and blue curves respectively (mean responses of duplicate sensors of each type are shown). The zero response is shown by a grey horizontal line.

Summary and implication of preliminary results

An apparatus consisting of MANGO-MFCs, a gas chamber, and a data logging system was built to collect chemiresistive sensors' signals for given gas concentrations. Before the formal start of data collection for training ML models, the sensors' responses to methane were verified and their tolerances to RH and flow rate were tested. Only if the sensors could operate in an environmentally relevant RH range, it would be meaningful to implement the full-scale ML

signal deconvolution. In other words, since the ML models should be re-trained for different sensor designs, only the final stable version of sensors would be worth full-scale training. Through the preliminary tests, the chemiresistive sensors (default, coated with SBF, and coated with Pentyp) were intolerant of RH greater than 50% and total flow rate greater than 1,000 sccm. Because the environmental RH (e.g., 70%-90%) can easily exceed this operational RH limit, the chemiresistive sensors were not ready for the ML signal deconvolution procedure. Potential solutions to improve the chemiresistive sensors' RH tolerance include (i) new overcoat chemical structures, (ii) surface modification, (iii) surface immobilization of the POM co-oxidant in the Pt-POM catalyst, (iv) alternative co-oxidant, and (v) enclosing the sensors in hydrophobic membrane materials. In parallel to these modifications, commercially available methane sensors could also be tested for (a) their RH tolerance could be better than the prototype sensors, and (b) they could offer a proof-of-concept of the ML signal deconvolution framework. While the sensors' intolerance of flow rate higher than 1,000 sccm was not prohibitive for ML signal deconvolution, it could make data collection much more time-consuming. Therefore, potential improvements to the flow rate tolerance by measures (i) to (v) should also be evaluated.

Ongoing Investigations

One of the ongoing improvements to the apparatus is the integration of commercially available sensors. These sensors use mature technology and have been on the market, so it is reasonable to expect them to function under environmentally relevant conditions, including the RH level. Moreover, these commercial sensors can be used for a proof-of-concept of our ML signal deconvolution framework, while the improvements are being made to the prototype sensors in

parallel. 10 MQ-series sensors were purchased from SparkFun Electronics (Table 1). These sensors are also based on chemiresitive sensing mechanism: metal oxides (e.g., SnO_2) catalyze the oxidation of methane and result in a change of resistance. All of these MQ sensors have compact sizes (with about 20 mm diameter and 25 mm height), so multiple sensors could be tested simultaneously in our gas chamber. Moreover, different MQ sensor models targeted different gas species. For example, MQ-2 targets hydrocarbon and hydrogen, while MQ-131 targets NOx, Cl_2, and O_3. Though some models such as MQ-131 are not explicitly designed to detect methane, due to their catalytic oxidation sensing principle, they are expected to show some degree of methane response. Importantly, different MQ models have different sensitivities toward given gas species (i.e., for gas species i, the fitted coefficients k_{i1}, k_{i2}, …, k_{in} would be distinguishable for sensors 1, 2, …, n), therefore an array of MQ sensors were ideal to solve the ML signal deconvolution problem.

Table 1. Commercial MQ-series sensors[7,8]

Model	**Detection range***	**Reported target species**	**Heating power consumption**	**Preheat time**
MQ-2	5000-20000 ppm methane	Methane, propane, i-butane, hydrogen, Liquefied petroleum gas	< 800mw	> 24 hours

		(LPG), alcohol, smoke		
MQ-3	About 100 - 10,000 ppm methane	Methane, benzine, hexane, carbon monoxide, alcohol, LPG	< 750mw	> 24 hours
MQ-4	200-10000ppm methane	Methane, hydrogen, carbon monoxide, alcohol, smoke, LPG	< 750mw	> 24 hours
MQ-6	200-10000 ppm LPG, iso-butane, propane, and liquified natural gas (LNG)	Methane, carbon monoxide, hydrogen, alcohol, LPG	< 750mw	>24 hours
MQ-7	about 40 - 2,000 ppm methane	Carbon monoxide, hydrogen, LPG, alcohol	about 350 mw	>= 48 hours

MQ-8	about 200 to 10,000 ppm methane	Methane, carbon monoxide, hydrogen, LPG, alcohol	< 800mw	> 24hours
MQ-9	500 -10000ppm methane	Methane, carbon monoxide, LPG	< 340 mw	>= 48 hours
MQ-131	Not reported for methane	Nitrogen oxides, chlorine, ozone	< 1100mw	> 24 hours
MQ-136	Not reported for methane	Carbon monoxide, ammonia, hydrogen sulfide	< 800mw	> 24 hours
MQ-137	Not reported for methane	Ammonia, carbon monoxide, ethanol	< 800mw	> 24 hours

* Some of the detection ranges are concentration ranges used for sensor calibration, thus they don't necessarily infer the sensors' true detection limitation

The MQ sensors can output analog or digital signals through their pins and printed circuit boards (PCBs) were made to extract their signals (Fig. 9). Each PCB could accommodate three MQ sensors on its front side (facing up) and two sensors on its back side (facing down). The PCB also provides a slot on its front side for installing a prototype chemiresistive sensor device, which includes 5 sensors printed on the glass substrate (each sensor has an independent counter-electrode). In gas exposure experiments, two PCBs can be installed in the gas chamber, thus a total of 10 MQ-series sensors and 10 prototype chemiresistive sensors can be tested simultaneously (Fig. 9). The signals of the PCBs are then transmitted to the signal process board and data acquisition board, which are connected to a laptop computer for data logging and processing using the LabVIEW 2023 software.

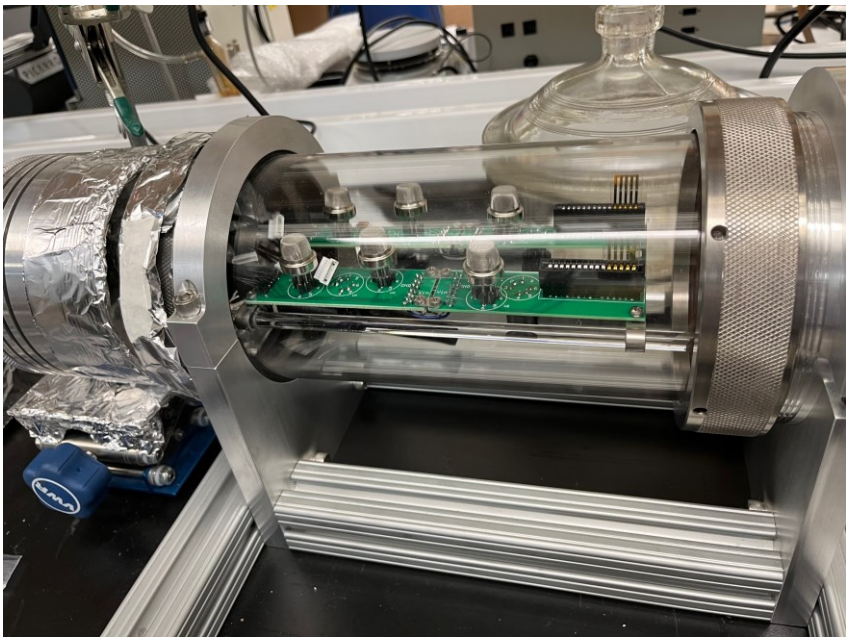

Figure 9. The modified gas chamber to accommodate both prototype chemiresistive sensors and commercial sensors. The process of installing MQ-series commercial sensors and prototype chemiresistive sensors on the PCBs is shown (note that the prototype sensors shown in the

picture were for demonstration only and not the updated design with independent counter electrodes). The front side of the PCB could accommodate three MQ-series sensors and one prototype device of 10 chemiresistive sensors; the back side could accommodate two MQ-series sensors.

Another important ongoing improvement to the experimental apparatus is to enable temperature control. Two separate set-ups will be used for cooling and heating (Fig. 10 and Fig. 11). For cooling, the output gas from the MANGO system goes through a coiled tubing submerged in a water bath and then goes into the gas chamber. The gas chamber and the water bath beaker are wrapped by cooling blankets (FLUX05 Fluxwrap, Powerblanket), which are connected to a circulating chiller to cool the gas inflow and the gas inside the chamber. This system can lower the internal temperature of the chamber from 20 °C to about 5°C. On the other hand, for heating purposes, the cooling blanket around the chamber is substituted for a silicone rubber heating tape with adjustable thermostat control (XtremeFLEX MSTAT, BriskHeat Corporation), and a heating plate (Fisher Scientific) is used to heat the water bath. The temperature inside the chamber can be increased to about 50 °C. This temperature control system can simulate the environmentally relevant temperature range except for Winter temperatures below 5°C. Temperature is an important factor that can alter the sensors' responses to given gas compositions. In future ML model training, the exposure experiment for each gas composition will be repeated for a range of temperatures, and temperature will be used as a separate predictive feature in the ML model.

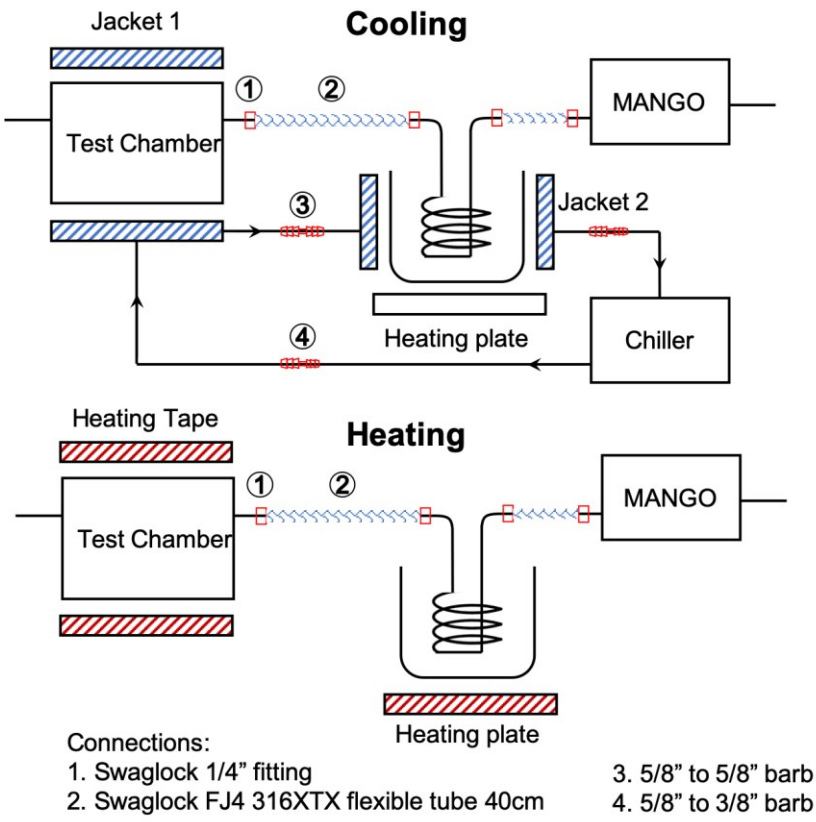

Figure 10. Design diagram of gas temperature control system (minor modifications to the original figure provided by Ruifeng Song**)**

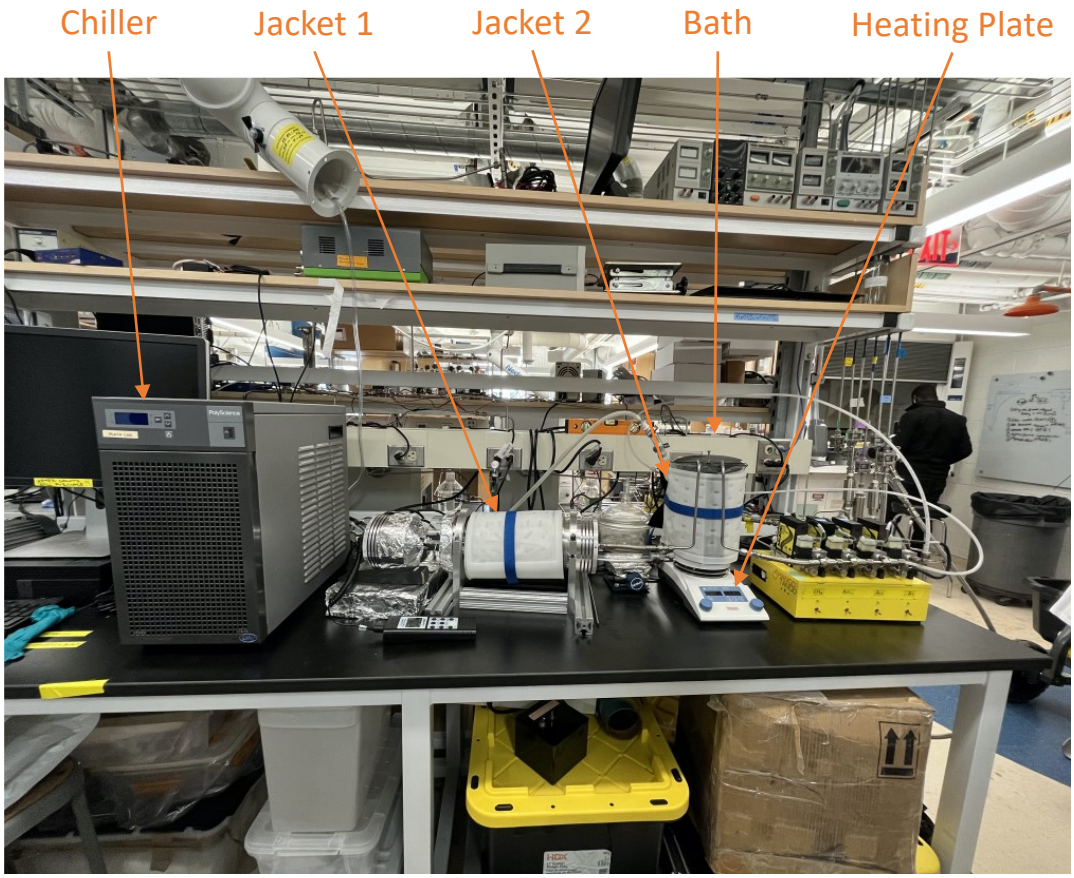

Figure 11. Photo of the gas temperature control system (photo credit: Ruifeng Song)

Future steps for ML signal deconvolution and expected outcomes

Currently, the data logging system and temperature control system are being tested and adjusted. Upon the completion of such preparation, the following steps will be taken to implement ML signal deconvolution: first, the methane responses of MQ-series sensors (and possibly improved prototype chemiresistive sensors as well) will be tested at different RH levels and flow rates. This will imply the tolerance of the new sensor array to RH and flow rate. If the tolerance is satisfying (e.g., RH > 90%; flow rate >= 4,000 sccm), the apparatus can be used for ML dataset

construction. Second, a small parameter space consisting of methane concentration, RH, flow rate, and temperature will be used to construct a preliminary dataset for ML model training and testing. This small training set only requires one MANGO box (with four MFCs) to implement and can serve as a proof-of-concept for the ML signal deconvolution method. The goal is to accurately predict the true methane concentration using the signals of each sensor together with environmental parameters including RH, flow rate, and temperature. Third, based on successful preliminary signal deconvolution experiments, the parameter space will be expanded by including additional MFCs for more interfering gas species, including H_2S, CO, H_2, ethane, and so on. Finally, different ML models will be trained and tested using this expanded dataset and inter-model comparison will be conducted to search for optimal prediction accuracy.

The outcome of this project will be the following: first, a trained ML model that deconvolutes the signals of a methane sensor array. The input of such a model will be the signal of each sensor in the array (i.e., relative changes in their resistance upon gas exposure), and the output will be the predicted concentration of each gas component, including methane and other interfering gas species. Such an ML model will greatly increase the useful information that can be extracted from methane sensors. Without signal deconvolution, the signals of methane sensors essentially reflect a combination of responses to different gas species, and relying on such signals will lead to inaccurate estimation of true methane concentration. However, the ML model would provide a more accurate estimation of methane concentration, which would be useful for the continuous monitoring of gas leakage from O&G facilities and other methane sources, and lead to a better evaluation of the climate impact of these sources. In addition, knowing the concentration of other gas species could have significant public health and safety benefits, for these gases are toxic

(e.g., H_2S and CO) or flammable (e.g., H_2). Second, an apparatus for automatically constructing an ML dataset for signal deconvolution of gas sensors in general. The experimental set-up, including MFCs, gas chamber, and data logging system, can be easily adapted for other compact or portable gas sensors that can be fitted inside the chamber. One of the major advantages of this apparatus is the automatic data collection function: the sequential changes of gas compositions are enabled by the Ansari program, and automatic data logging is enabled by the LabVIEW software. In other words, the users only need to install the sensors in the chamber and start the programs, and then the sequential gas exposure experiments and data logging can be conducted automatically. Such a procedure would largely enhance the efficiency of the signal deconvolution method and prepare it for broad application.

References

(1) U.S. Energy Information Administration. US Oil and Gas Wells by Production Rate https://www.eia.gov/petroleum/wells/ (accessed Dec 27, 2022).

(2) Lackey, G.; Rajaram, H.; Bolander, J.; Sherwood, O. A.; Ryan, J. N.; Shih, C. Y.; Bromhal, G. S.; Dilmore, R. M. Public Data from Three US States Provide New Insights into Well Integrity. *Proc. Natl. Acad. Sci. U. S. A.* **2021**, *118* (14). https://doi.org/10.1073/PNAS.2013894118.

(3) Bezdek, M. J.; Luo, S. X. L.; Ku, K. H.; Swager, T. M. A Chemiresistive Methane Sensor. *Proc. Natl. Acad. Sci. U. S. A.* **2021**, *118* (2), 1–6. https://doi.org/10.1073/pnas.2022515118.

(4) Luo, S. X. L.; Lin, C. J.; Ku, K. H.; Yoshinaga, K.; Swager, T. M. Pentiptycene Polymer/Single-Walled Carbon Nanotube Complexes: Applications in Benzene, Toluene, and o-Xylene Detection. *ACS Nano* **2020**, *14* (6), 7297–7307. https://doi.org/10.1021/acsnano.0c02570.

(5) Guo, S.; Swager, T. M. Versatile Porous Poly(Arylene Ether)s via Pd-Catalyzed C-O Polycondensation. *J. Am. Chem. Soc.* **2021**, *143* (30), 11828–11835. https://doi.org/10.1021/jacs.1c05853.

(6) Current Results weater and science facts. Annual Average Relative Humidity by US State https://www.currentresults.com/Weather/US/annual-average-humidity-by-state.php (accessed Oct 17, 2023).

(7) farmaker47. GitHub Repo: Raspberry-to-assess-food-quality

https://github.com/farmaker47/Raspberry-to-assess-food-quality (accessed Sep 1, 2022).
(8) Robu.In. Gas and Dust Sensor https://robu.in/product-category/sensor-modules/gas-sensor/ (accessed Sep 1, 2022).

Chapter 6. Conclusions, criticisms, and opportunities

By

Yunpo Li

Conclusions

Human-made methane emissions are responsible for about 0.5 °C global temperature rise compared to the 19th century, making it the second largest contributor to climate forcing following carbon dioxide.[1] Reducing anthropogenic methane emissions can be one of the fastest ways to slow down climate change because the global warming potential of methane is 80 times higher than that of carbon dioxide over the next 20 years.[2] Particularly, methane emissions from the Oil and Gas (O&G) industry (22% of total anthropogenic emissions[3]) is considered a 'low hanging fruit' for climate mitigation, since it has high technical feasibility and theoretically recovers revenue for O&G companies. The reduction of O&G methane emissions requires a systematic approach involving evaluating, monitoring, and mitigating the emissions. However, there are still major knowledge gaps and technical difficulties in evaluating and monitoring O&G methane emissions; these threaten to delay emission reduction. First, when this thesis commenced, there was great uncertainty on the O&G methane emission pathway via groundwater systems. A critical question was whether elevated groundwater methane concentration was attributable to O&G development or other anthropogenic sources (e.g., coal mining) and natural sources (e.g., geological migration and methanogenesis). Second, the exceedingly large number of O&G facilities imposes a heavy logistical and economic burden if sufficient monitoring (in space and time) is to be conducted. This could result in shortage of resources for non-selective monitoring of all facilities. In addition, if sensors were distributed evenly among all facilities without knowledge of which facilities have a higher risk of emitting methane, the monitoring efficiency would be low and sensing resources could be wasted. Third, the intermittent nature of methane emissions requires large-scale deployment of low-cost

continuous sensors, but such sensors suffered from signal interferences of gas species other than methane. This thesis addressed these critical challenges by (i) evaluating the impact of O&G extraction on groundwater methane concentration, and explaining how methane migrated and transformed in the underground environment (Chapters 2 and 3); (ii) training ML models to predict O&G well integrity issues related to methane leakage, thus enabling prioritized monitoring (Chapter 4); (iii) building an apparatus to collect data for sensor signal deconvolution using machine learning (Chapter 5). Overall, my thesis deepens the understanding of methane emissions by O&G development and seeks to improve the likelihood of mitigating such contributions.

Summary of thesis contributions

My first research question centered at evaluating the potential methane emission pathway of unconventional oil and gas (UOG) extraction through groundwater systems (**Chapter 2**). If UOG released methane into groundwater aquifers, such methane would be carried by groundwater discharge to surface water bodies, and then enter the atmosphere. Given such, evaluating whether UOG development increased groundwater dissolved methane concentration would be an important first step to evaluate the whole pathway. By analyzing groundwater samples collected from 94 homes in Bradford County, Pennsylvania, I came to the following conclusions: first, dissolved methane concentration was not statistically correlated to the distance to the nearest UOG well, nor was it correlated to the number of UOG wells within a certain distance. Second, the $\delta^{13}C$ and $\delta^{2}H$ isotopic ratios of concentrated groundwater methane did not reflect the signature of shale gas, but instead reflected that of thermogenic methane that likely originated

from Upper Devonian strata. Third, valley topography had the highest groundwater methane concentration. This could have resulted from enhanced permeability by the geological fracture network below the valleys. Lastly, post-drill groundwater methane concentrations showed no systematic increase compared to pre-drill concentrations. Taking these together, I demonstrated that groundwater methane concentration was dominantly influenced by topography-driven natural migration pathways rather than UOG activities in the regional scale. This implied that UOG activities were unlikely to systematically emit methane via the groundwater system in Northeastern Pennsylvania. I further estimated the total rate of methane emission from groundwater discharge and degassing in the study region (approximately 3000 km^2) to be on the order of 2 (or 0.08 – 30) tonnes CH_4 /year, which was much smaller than the regional emission rate from O&G wells (400 tonnes CH_4 /year). Another implication of these findings was that water wells in the valleys were more vulnerable to groundwater methane intrusion than wells in the upper lands (i.e., elevated topologies). Thus, extra safety precautions or prioritized inspection can be undertaken in those locations.

Considering that traditional fossil fuel extraction activities, including conventional oil and gas (COG) and coal mining, overlap UOG extraction in many parts of the US, the influence of these activities on groundwater methane was also evaluated (**Chapter 3**). Groundwater samples from 217 homes in Southeastern Ohio and Northern West Virginia (Region II) were collected to expand the original Northeastern Pennsylvania (Region I) sample set. With the expanded sample set, I made the following discoveries: first, in Region II, dissolved methane concentration was statistically higher when the sample was located closer to the nearest O&G well (i.e., either UOG or COG well). However, such trend was not found in Region I. (Note that the grouping of states

into Region I and II was not an artifact of sampling time, but was systematically tested as a parameter of sensitivity. Also note that the study area of Southeastern Ohio and Northern West Virginia lie in very close proximity). Second, in Region II, the dissolved methane correlation was lower when there was a higher concentration of dissolved sulfate. In addition, higher sulfate concentration was found within closer distance to the nearest active underground coal mine. Third, similar to Region I, topographical lowlands had higher methane concentration in Region II. Interestingly, topography served as a confounding factor behind the correlation between methane concentration and distance to O&G well. Particularly, distance to O&G well became an insignificant predictor of methane concentration after including topography as a second predictor. However, the correlation between methane concentration and sulfate concentration, and the correlation between sulfate concentration and distance to coal mine were robust even when considering the presence of topography as a potential confounder. Fourth, I proposed the following hypotheses to explain the influence of sulfate on methane concentration: coal mining introduced additional sulfate into the groundwater aquifer, and the elevated sulfate concentration inhibited methanogenesis and enhanced anaerobic methane oxidation, therefore reducing the dissolved methane concentration. Overall, I found that the distribution of groundwater methane concentration in Region II was not controlled by O&G extraction, but could be shaped by the interactions between anthropogenic factors (e.g., sulfate released by coal mining) and natural factors (e.g., topographic variation and biogeochemistry processes).

With these findings, the contributions of **Chapter 3** can be summarized as: first, I demonstrated that O&G extraction (both UOG and COG) did not systematically increase groundwater methane concentration in the O&G producing region of Northern Appalachia. This confines the climate

risk associated with O&G groundwater methane emissions. Second, I revealed the influence of geochemical agents on groundwater methane distribution. Particularly, sulfate which likely originated from coal mining, could alter methane concentration through biogeochemical mechanisms. Third, I provided a framework to predict the public safety risk associated with high groundwater dissolved methane concentration. The risk of fire or explosion caused by groundwater dissolved methane could be predicted using the observed correlations between methane concentration and fossil fuel extraction location, topography, and concentrations of sulfate and other geochemical indicators. Governments should prioritize safety inspections over regions with high risk of elevated groundwater methane concentration and educate residents on how to mitigate such risk. Lastly, I demonstrated an example of the importance of confounding factors in environmental studies. Before any conclusions were drawn using observed correlations, researchers should examine whether such correlations were reliable with the presence of potential confounding factors.

The second focus of this thesis is on monitoring O&G methane emissions. One major challenge is to identify a subset of O&G facilities with higher risk of methane emissions, so that prioritized sensor allocation can be achieved to enhance the monitoring efficiency and reduce total cost. I addressed this challenge by predicting well integrity issues related to methane emissions, namely sustained casing pressure (SCP) and/or casing vent flow (CVF), as proxies of emission risk (**Chapter 4**). O&G well completion reports (n=1,250) containing well physical parameters in Bradford County, Pennsylvania, were manually digitalized to serve as the dataset for ML training and evaluation. I found that during cross-validation, all ML models achieved similar F-1 scores (on the 60% level), while the XGBoost model (XGB) was selected as the best model.

Furthermore, the XGB model achieved a good prediction performance (F-1 score = 66%) on the held-out test set which demonstrated good generalizability of the model. Note that this is not a universal finding (i.e., XGB will not be the best model in every application). I leveraged the SHAP values to show the impact of important predictive features on the model outcome. Geospatial features such as distance to the nearest faulty well were among the most important features. Physical features such as casing length and amount of cement contributed to the prediction of faulty status, and whether the well was built by a specific O&G operator also had important impact. Lastly, I observed geospatial clustering of well integrity issues in the study region, and such clustering was correlated to the clustering of important predictors as well as topographic variation.

The main contributions of **Chapter 4** can be summarized as the following: first, the trained ML models provided a tool for guiding prioritized sensor allocation and/or inspection schedule. Remote sensing tools (e.g., satellites and airplanes) can scan relatively large geographical regions for potential methane emissions. For example, the MethaneSAT satellite can scan 90% of the O&G fields in the world using 300 'targets' (i.e., each 'target' is 200 km by 200 km square), but it takes about a week before revisiting each target.[4] This low frequency of revisit would lead to substantial underestimation of emissions due to their intermittent nature. With the help of ML prediction models, the satellite could prioritize 'targets' with higher emission risks and increase their revisit frequencies. This also applies to airplane-based surveys, which could have lower revisit frequency than the satellites. In addition, for other methane sensors and survey methods with lower special coverage, including vehicles, small drones, and hand-held instruments, their total required number would be intractably large if each potential methane

emitter is assigned equal importance without knowing the relative emission risk. Moreover, allocating sensors evenly among a large number of emitters could diffuse the limited resources and reduce the chance of detecting actual methane leaks. Using the results of ML prediction, a larger number of sensors or a higher frequency of inspections can be allocated for high-risk emitters, and a smaller sensor number or a lower inspection frequency for low-risk emitters. This could transfer to a higher probability of capturing methane emissions and/or a smaller total number of sensors and inspections required.

Second, the well construction physical parameters that played important roles in ML prediction can inform better well design and maintenance practice. For example, greater lengths of certain casings were associated with lower risk of integrity issues. Moreover, the fact that certain operators were associated with lower integrity failure risk should raise the attention of regulators or imply that best-practices exist and could be transferred between operators. Third, the observed clustering of well integrity issues suggested that future well drilling should avoid being located near existing clusters to lower the chance of new integrity failures. Lastly, manual digitalization of well completion reports cost enormous time and would be difficult to apply on larger dataset. Thus, it's suggested that future regulators require fully-digitalized data reporting with standardized format (e.g., through web-based forms) to facilitate inspection of the data. Finally, the data should be publicly available and not behind a paywall if maximum benefit and leak prevention strategies are desired.

Once a prioritized sensor allocation strategy is enabled by ML models, the next step is to acquire suitable sensors for continuously monitoring the potential methane emitters. In **Chapter 5**, an

apparatus was built for signal deconvolution of the prototype chemiresistive methane sensors developed by Bezdek et al..[5] The apparatus consisted of mass flow controllers, a gas chamber, a data logging system and other parts. It will be used to construct a complete ML dataset with sensor signals being predictive features and true gas concentrations being target variables. In order to test the readiness of the prototype sensors for data collection, I conducted preliminary experiments to test the sensors' tolerance to humidity and gas flow rate. I found that the sensors stopped responding to methane when relative humidity exceeded 50% and flow rate exceeded 1,000 sccm. Such relative low tolerances suggested that the tested version of prototype sensors was not suitable for full-scale ML data collection, and further improvements were required for the sensor. Meanwhile, commercially available alternative sensors were purchased and integrated to the apparatus, with the goal to improve the tolerances to humidity and flow rate and identify the best possible solution on the market today. In addition, a temperature control system was integrated to the apparatus to simulate various temperatures in the real-world operation environments of the sensors. Because the project is still ongoing, the contributions of **Chapter 5** are mainly on the experimental design and apparatus building. Beside methane sensors, my experimental apparatus can also be adapted for other types of gas sensors which will benefit from ML signal deconvolution. Most importantly, the apparatus is able to collect data in an automatic and sequential manner so that it makes signal deconvolution experiments faster and more convenient. Eventually, the expected outcomes of the work described in this chapter is an array of compact, low-cost, and low-energy consumption sensors which detect methane and co-existing gas species such as water vapor, H_2S, and CO with high accuracy and resolution.

Criticisms and opportunities

This thesis addressed key research challenges in evaluating and monitoring O&G methane emissions. Due to the constraints on time and resources, there are some limitations on the results and implications. However, there are also opportunities for future work to address those limitations and enhance our ability to monitor and mitigate O&G methane emissions. In the groundwater methane analysis (**Chapter 2 & 3**), I proposed several hypotheses on the sulfate-mediated biogeochemical transformation of dissolved methane. Particularly, I hypothesized that sulfate inhibited methanogenesis and enhanced anaerobic methane oxidation. Such mechanisms would involve sulfate reducing bacteria as an important biological agent. Unfortunately, I couldn't verify the presence of this bacteria using our water samples. For the purpose of sample preservation, sodium azide was added to all groundwater samples used for methane analysis, which essentially killed microbes in those samples. Therefore, it was not possible to extract microbes from those water samples and incubate them to search for sulfate-reducing bacteria. Metagenomics could be another tool to analyze the microbial population. However, samples for metagenomic analysis would follow specific protocols (e.g., samples might need to be frozen during transport and storage) and were not collected in the sampling campaigns. Therefore, there was a lack of direct microbiological evidence for the hypothetical biogeochemical processes involving methane and sulfate, although they were supported by the correlation between methane and sulfate concentration, as well as the $\delta^{13}C$ and $\delta^{2}H$ isotopic ratios indicating methane oxidation. Future field studies should consider collecting microbial and metagenomics samples to better understand possible biogeochemical processes affecting groundwater methane. In addition, the microbial methane oxidation and sulfate reduction reactions can also cause

fractionation in the isotopic ratios of relevant chemical compounds, such as $\delta^{34}S - SO_4^{2-}$, $\delta^{18}O - SO_4^{2-}$, and $\delta^{13}C$ – DIC, which could provide additional evidence for the hypotheses. Due to logistic limitations, no water samples were reserved for these additional isotopic analyses in my study, but they should be included in future work as well.

My groundwater methane analyses evaluated the influence of O&G activities on groundwater methane concentration from a systematic and statistical perspective. That said, individual cases of O&G-induced groundwater methane contamination might not be captured by my system-level analysis. A few incidents of O&G induced methane migration in groundwater had been reported in my selected study regions,[6] and the public safety risk posed by these incidents should not be neglected. To address this issue, documents of groundwater quality complaints should be reviewed to search for potential O&G-induced incidents, and sampling of groundwater and soil in close distance to the homes and gas wells will be required. Such investigations can also be conducted by third-party consulting companies hired by the complaining households or the government to determine whether O&G development was responsible for the incidents.

For ML prediction of O&G well integrity issues (**Chapter 4**), Bradford County, PA was chosen as the study region for (i) the proportion of wells tested for integrity issues in the county was higher (77%) than state-wide average (36%) and (ii) the proportion of tested wells with integrity issues (47%) was also higher than state-wide average (14%). However, one limitation associated with this study region was that its O&G well population was biased toward unconventional wells (95% of all wells). Given such, the trained ML models resulted from this study would be most suitable to predict failures in other regions similarly dominated by UOG wells. In the future

when integrity test results become publicly available in other regions with a more balanced percentage between UOG and COG wells (e.g., the OH and WV regions investigated by **Chapter 3**, where the data is not currently available), the ML models will be retrained on the new dataset. Another limitation of the ML models resulted from their correlational nature. Specifically, the SHAP values didn't infer causal relationship between predictive features (i.e., physical parameters) and the target variable (i.e., integrity failure status). Future studies can consider conducting rigorous causal inference using Bayesian models to determine the causes of integrity failures. This effort may require a much larger dataset, which can be obtained by mandatory digitalization of data reporting or digitalization of existing paper reports by computer vision and natural language processing tools.

In Chapter 5, I built the apparatus for signal deconvolution of prototype chemiresistive sensors, and those sensors may someday be deployed in large number to continuously monitor O&G methane emissions (**Chapter 5**). One concern over the ML signal deconvolution methodology is that the trained ML models are specific to the sensors used in training. If the sensor design is modified, the model training process would need to be repeated. This would be less problematic if the sensors' properties (e.g., sensitivity and selectivity to different gases) are consistent across individual sensors of the same model/design, because only one training would be necessary to represent the model/design. However, some degree of variation can be expected between individual sensors of the same model/design. Future research efforts need to convert the variation in individual sensors to well defined uncertainties attached to the ML output (e.g., the predicted methane concentration being a probability distribution rather than a single fixed value).

Closing remarks and looking forward

Reducing methane emissions from O&G infrastructures is one of the fastest ways to slow down climate change over the next few decades. Throughout this thesis, I have evaluated the risk to drinking water in O&G-rich regions and developed methods to better monitor atmospheric methane emissions by predicting emission risk and deconvoluting signals in novel methane sensors. I illustrated that a systematic and interdisciplinary approach can be applied to solve key challenges in controlling O&G methane emissions. By combining the knowledge and tools in geoscience (e.g., gas chromatography, methane isotopes, and topographical analysis), data science (e.g., ML, geospatial analysis, and statistical hypothesis test), and material science (e.g., chemiresistive methane sensors), I was able to deepen the understandings of how methane was emitted to the environment and to develop novel tools for predicting and monitoring methane emissions. An overarching implication of my thesis for future research is that in order to address complex problems like climate change, we need to cross the borders of disciplines and leverage every available tool to create innovative solutions.

Looking forward, there is opportunity for more accurate estimations of O&G methane emission risks through combing the ML prediction results (**Chapter 4**) with real-world measurements by remote sensing tools such as satellite, airplane, and drone. In **Chapter 4**, well integrity issues (i.e., SCP and/or CVF) were used as proxy of methane emission risk. However, the inspections of integrity issues are different from direct measurements of methane leaks, and the direct measurements could serve as an independent verification and enhance the confidence of methane

emission risk estimates. As such, I propose the following approach for future studies: first, ML models can predict integrity issues in O&G facilities using their physical parameters and/or geospatial metrics as predictive features. These prediction results could then be used to construct a prior estimation of the emission risks. Second, remote sensors should be deployed to scan for methane emission plumes among the O&G facilities. The detected methane emissions are used to construct a posterior estimation of the emission risks by inverse modelling. The posterior estimation updates the prior estimation (based on integrity prediction) using the information from direct emission measurements, thus serving as a more accurate estimation. Third, continuing flyovers of the remote sensors will provide new emission measurements that can be used to update the posterior risks. This overcomes the limitation of a single flyover, which is a snap-shot in time and cannot handle intermittent emitters. Lastly, the ML models can be re-trained on the updated posterior risks, and then be applied to new geographical regions where emission risks need to be predicted. From there, the circle of ML prediction and remote sensing measurement can be repeated.

There are several other future research directions that would stem from the work discussed in this thesis: first, a smart methane monitoring framework combining novel sensing technology and artificial intelligence can be developed. Such frame work will utilize a tired-monitoring system consisting of ‘top sensors’ with wide spatial coverage but relatively low spatial and temporal resolution (e.g., satellite and airplane) as well as ‘bottom sensors’ with narrow coverage but high resolution (e.g., stationary sensors). This system will continuously provide emission data to a cloud-based computation platform that optimizes leak fixation strategy and predicts future emissions. In addition to monitoring methane emissions from fossil sources, the smart

monitoring can be leveraged to better understand and quantify emissions from important biogenic sources that have not been well studied. For example, wetland methane emissions are estimated to be approximately 40% of total natural emissions,[3] but such estimation has great uncertainty due to the insufficient number of monitoring stations around the globe. Given such, data fusion efforts can be taken to combine data from various remote sensing and local sensing measurements to fill the gap, and ML algorithms can be leveraged to predict wetland emission rates using ancillary environmental parameters such as temperature, water table depth, and solar radiation.[7,8]In addition, experimental tools, such as gas chromatography, flux chambers, and eddy flux towers, can be used to independently verify the predicted emissions. As another example, emissions from urban wastewater transport and treatment system are poorly understood and quantified. The tiered monitoring system, including vehicle mounted sensors, can be deployed in the cities to detect wastewater emission. Mitigation strategies, such as wastewater aeriation, can be explored to reduce the biogenic methane production by methanogenesis. Overall, the methodologies involved in this thesis can be applied to solve additional exciting problems in the field of methane emission detection and mitigation. Ultimately, this work can inform science and strategies to slow down the pace of climate change.

References

(1) Masson-Delmotte, V.; Zhai, P.; Pirani, A.; Connors, S. L.; Péan, C.; Berger, S.; Caud, N.; Chen, Y.; Goldfarb, L.; Gomis, M. I.; Huang, M.; Leitzell, K.; Lonnoy, E.; Matthews, J. B. R.; Maycock, T. K.; Waterfield, T.; Yelekçi, O.; Yu, R.; Zhou, B. *Summary for Policymakers. In: Climate Change 2021: The Physical Science Basis. Contribution of Working Group I to the Sixth Assessment Report of the Intergovernmental Panel on Climate Change*; 2021. https://doi.org/10.1017/9781009157896.001.

(2) Forster, P.; Storelvmo, T.; Armour, K.; Collins, W.; Dufresne, J.-L.; Frame, D.; Lunt, D. J.; Mauritsen, T.; Palmer, M. D.; Watanabe, M.; Wild, M.; Zhang, H. *The Earth's Energy*

Budget, Climate Feedbacks, and Climate Sensitivity. In Climate Change 2021: The Physical Science Basis. Contribution of Working Group I to the Sixth Assessment Report of the Intergovernmental Panel on Climate Change; Cambridge, United Kingdom and New York, NY, USA, 2021. https://doi.org/10.1017/9781009157896.009.

(3) Saunois, M.; Stavert, A.; Poulter, B.; Bousquet, P.; Canadell, J.; Jackson, R.; Raymond, P.; Dlugokencky, E.; Houweling, S.; Patra, P.; Ciais, P.; Arora, V.; Bastviken, D.; Bergamaschi, P.; Blake, D.; Brailsford, G.; Bruhwiler, L.; Carlson, K.; Carrol, M.; Castaldi, S.; Chandra, N.; Crevoisier, C.; Crill, P.; Covey, K.; Curry, C.; Etiope, G.; Frankenberg, C.; Gedney, N.; Hegglin, M.; Höglund-Isaksson, L.; Hugelius, G.; Ishizawa, M.; Ito, A.; Janssens-Maenhout, G.; Jensen, K.; Joos, F.; Kleinen, T.; Krummel, P.; Langenfelds, R.; Laruelle, G.; Liu, L.; Machida, T.; Maksyutov, S.; McDonald, K.; McNorton, J.; Miller, P.; Melton, J.; Morino, I.; Müller, J.; Murguia-Flores, F.; Naik, V.; Niwa, Y.; Noce, S.; O'Doherty, S.; Parker, R.; Peng, C.; Peng, S.; Peters, G.; Prigent, C.; Prinn, R.; Ramonet, M.; Regnier, P.; Riley, W.; Rosentreter, J.; Segers, A.; Simpson, I.; Shi, H.; Smith, S.; Steele, L. P.; Thornton, B.; Tian, H.; Tohjima, Y.; Tubiello, F.; Tsuruta, A.; Viovy, N.; Voulgarakis, A.; Weber, T.; van Weele, M.; van der Werf, G.; Weiss, R.; Worthy, D.; Wunch, D.; Yin, Y.; Yoshida, Y.; Zhang, W.; Zhang, Z.; Zhao, Y.; Zheng, B.; Zhu, Q.; Zhu, Q.; Zhuang, Q. The Global Methane Budget 2000–2017. *Earth Syst. Sci. Data* **2020**, *12* (3), 1561–1623. https://doi.org/10.5194/essd-12-1561-2020.

(4) Liao, F.; Hamburg, S.; Gautam, R. *MethaneSAT: A New Era of Transparency for Methane Measurement*; 2023.

(5) Bezdek, M. J.; Luo, S. X. L.; Ku, K. H.; Swager, T. M. A Chemiresistive Methane Sensor. *Proc. Natl. Acad. Sci. U. S. A.* **2021**, *118* (2), 1–6. https://doi.org/10.1073/pnas.2022515118.

(6) Llewellyn, G. T.; Dorman, F.; Westland, J. L.; Yoxtheimer, D.; Grieve, P.; Sowers, T.; Humston-Fulmer, E.; Brantley, S. L. Evaluating a Groundwater Supply Contamination Incident Attributed to Marcellus Shale Gas Development. *Proc. Natl. Acad. Sci. U. S. A.* **2015**, *112* (20), 6325–6330. https://doi.org/10.1073/pnas.1420279112.

(7) Wik, M.; Thornton, B. F.; Bastviken, D.; Macintyre, S.; Varner, R. K.; Crill, P. M. Energy Input Is Primary Controller of Methane Bubbling in Subarctic Lakes. *Geophys. Res. Lett.* **2014**, *41* (2), 555–560. https://doi.org/10.1002/2013GL058510.

(8) Knox, S. H.; Jackson, R. B.; Poulter, B.; McNicol, G.; Fluet-Chouinard, E.; Zhang, Z.; Hugelius, G.; Bousquet, P.; Canadell, J. G.; Saunois, M.; Papale, D.; Chu, H.; Keenan, T. F.; Baldocchi, D.; Torn, M. S.; Mammarella, I.; Trotta, C.; Aurela, M.; Bohrer, G.; Campbell, D. I.; Cescatti, A.; Chamberlain, S.; Chen, J.; Chen, W.; Dengel, S.; Desai, A. R.; Euskirchen, E.; Friborg, T.; Gasbarra, D.; Goded, I.; Goeckede, M.; Heimann, M.; Helbig, M.; Hirano, T.; Hollinger, D. Y.; Iwata, H.; Kang, M.; Klatt, J.; Krauss, K. W.; Kutzbach, L.; Lohila, A.; Mitra, B.; Morin, T. H.; Nilsson, M. B.; Niu, S.; Noormets, A.; Oechel, W. C.; Peichl, M.; Peltola, O.; Reba, M. L.; Richardson, A. D.; Runkle, B. R. K.; Ryu, Y.; Sachs, T.; Schäfer, K. V. R.; Schmid, H. P.; Shurpali, N.; Sonnentag, O.; Tang, A. C. I.; Ueyama, M.; Vargas, R.; Vesala, T.; Ward, E. J.; Windham-Myers, L.; Wohlfahrt, G.; Zona, D. FluXNET-CH4 Synthesis Activity Objectives, Observations, and Future Directions. *Bull. Am. Meteorol. Soc.* **2019**, *100* (12), 2607–2632. https://doi.org/10.1175/BAMS-D-18-0268.1.